

Alma Mater Studiorum – Università di Bologna

DOTTORATO DI RICERCA IN

CHIMICA

Ciclo 35

Settore Concorsuale: 03/C1 – CHIMICA ORGANICA

Settore Scientifico Disciplinare: CHIM 06 / CHIMICA ORGANICA

NEW SYNTHESIS AND DERIVATIZATIONS OF PEPTIDOMIMETICS AND
PEPTIDE-CONJUGATES FOR THERANOSTIC APPLICATIONS

Presentata da: Federica Santino

Coordinatore Dottorato

Luca Prodi

Supervisore

Luca Gentilucci

Co-Supervisore

Luca Valgimigli

Esame finale anno 2023

ai miei fratelli, Francesco e Marta

Index

Abstract	5
Introduction	7
Bibliography	9
CHAPTER 1: Green Chemistry for Peptide Synthesis	10
1.1 - Synthesis of NCAs	11
1.2 - Application tests for the use of NCAs in peptide synthesis	13
1.3 - Conclusions	17
1.4 - Experimental procedures	17
1.5 – Bibliography	19
CHAPTER 2: K Opioid Receptor Ligands	22
2.1 - KOR agonists	23
2.2 - Ligand- receptor interactions	28
2.3 - Structural insights in ligand-receptor interactions for KOR agonists	31
2.4 - Design of biased KOR ligands	34
2.5 – Synthesis of KOR selective ligands	35
2.6 – Introduction of 1,2,3-triazole	38
2.7 – Introduction of coumarin	40
2.8 – Conclusions	41
2.9 – Experimental procedures	42
2.10 – Bibliography	56
CHAPTER 3: Peptidomimetic Inhibitors of Lactate Dehydrogenase Enzyme	63
3.1 - LDH-A current inhibitors	65
3.2 - Targeting protein interactions	71
3.3 - Design of peptidomimetics inhibitors	73
3.4 - Synthesis of peptidomimetics inhibitors	75
3.5 - Enzymatic assay	78
3.6 – Conclusions	81
3.7 - Experimental procedures	82
3.8 – Bibliography	88
CHAPTER 4: Nanoparticles for drug delivery	92
4.1 - Silica Nanoparticles	93
4.2 – Design of Non-Toxic Fluorescent Peptide-Coated Silica/PEG NPs	95
4.3 – Synthesis of Non-Toxic Fluorescent Peptide-Coated Silica/PEG NPs	98
4.4 – Experimental procedures	102
4.5 - Colorectal cancer therapy	106
4.6 - Development of multivalent delivery systems for combined therapy	110
4.7 - Synthesis of multivalent platforms	113
4.8 – Conclusion	118
4.9 – Experimental procedure	119
4.10 - Bibliography	129
Final Remarks	133

Abstract

Since the introduction of insulin almost a century ago, the use of peptides as therapeutics has evolved and improved but, even though the number of drugs based on peptide structures is growing every year, for this to happen there is a need to modify the native structure to make it administrable and effective through the design of peptidomimetics.

In the context of a modern green chemistry approach, we firstly tried to substitute the classic peptide synthesis approach with the use of N-carboxyanhydrides in the presence of Hydroxyapatite, a high biocompatible inorganic base. Despite the great results, further developments are necessary for a daily use in laboratory and for our research, we decided to proceed with solid phase or liquid phase synthesis, focusing our attention on selectivity, permeability, and stability as fundamental parameters for creating safe and effective medicines.

In the first chapter, the treatment of pain with the use of opioids is introduced. The abuse and misuse of these kind of potent analgesics, led to the necessity of developing new drugs with less side effects. In fact, nowadays, just MOR selective ligands are approved for medicinal treatment, because they are very potent and able to activate antinociception but unfortunately severe unwanted effects. One solution to this problem, is the development of KOR opioid receptor selective partial agonist, or molecules able of activate G-protein pathway without the recruitment of the β -arrestin. Starting from a previous study, where the introduction of a lactam-like structure in the place of the proline of Endomorphine¹, switched the selectivity from MOR to KOR, we designed and synthesized three different libraries by placing a different trans inducer element to gain the desired selectivity and activity forcing the structure to adopt a linear rather than folded position.

In the second chapter, we focused on lactate dehydrogenase, an enzyme overexpressed when the cells in hypoxia conditions, like in a tumour mass, need to produce energy through the transformation of pyruvate into lactate. We synthesized different cyclic peptidomimetics, designed to be inhibitors, as powerful tool to contrast cancer cells growing. Biological assays produced satisfactory preliminary results, but further studies are necessary for a definitive output.

Finally in the last chapter, the cancer treatment problem is also approached through the design of nanoparticles, self-assembled chemical platforms able to deliver a drug with efficacy and selectivity. We firstly synthesized silica core nanoparticles, built with toxic peptide sequences conjugated through click chemistry with Pluronic acid and then, in collaboration with Miriam Royo's research group, we synthesized multivalent platforms for the simultaneous administration of two of the most widely used drugs for the treatment of advanced colorectal cancer.

Introduction

Since the introduction of insulin almost a century ago¹ the use of peptides as therapeutic has evolved resulting in the approval of more than 80 peptide drugs worldwide. The technology has made substantial progress and has continued to evolve with changes in drug development that bring to the use of synthetic peptide in addition to natural ones.

Therapeutic peptides have found widespread development in medicinal chemistry because they can bind cell surface and trigger intracellular actions with high affinity and specificity although they show less immunogenicity and higher costs^{2,3} compared to classic drugs like small molecules.

In fact, small molecules drugs are known to have low production costs, good permeability and ease oral administration but unfortunately, most of the time, they lack selectivity and their small size also provides them with the characteristic of not being able to interact with large surfaces, like in the protein-protein interaction (PPI),⁴ which is by contrast, an activity well covered by peptide drugs thanks to their large size and flexible backbone.⁵

Despite their great benefits, peptide drugs suffer two major drawbacks represented by poor membrane permeability and lack of in vivo stability conferred by secondary and tertiary structures. The limitation of endogenous peptides provided motivation for researchers to create analogues like peptidomimetics to improve drug properties⁶ and thanks to medicinal chemistry techniques, it is possible to make some adjustments to mimic, stabilize or create a secondary structure that can provide the structure with ideal biological activity, desired properties, and better delivery.⁷

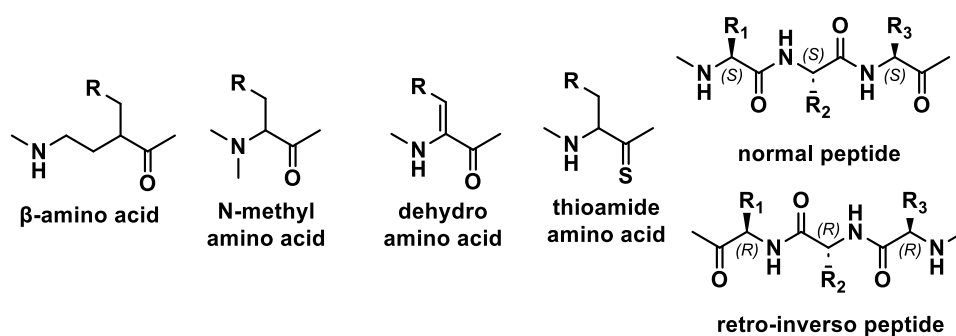


Fig.1 Examples of strategies for peptidomimetic approaches.

These changes include backbone modifications, like the insertion of D-amino acids, methyl amino acids or β -amino acids as effective strategies to extend the plasma half-life, postpone enzymatic degradation and mime β -sheets or β strands. To improve binding affinity and binding selectivity instead, it is recommended to make side chain modifications that include variation in the structure or in the position of the functional group. Furthermore, as already mentioned, it is important to

create a secondary structure to increase stability and permeability.⁸ This important task can be reached with peptide cyclization, like macrolactamization, or by mimicking peptide α -helices.⁹ They are the most common type of secondary structure, and they are formed with intramolecular hydrogen bonds that can be substituted by building cross-link between side chains like lactam bridge, disulfide bonds, or with covalent bond.¹⁰

Synthesis of peptides in most cases is possible with the use of solid phase synthesis, introduced for the first time by Merrifield in 1963.¹¹ This approach has the advantages of allowing quick synthesis of large sequences, which, if desired, can also be automated, with easy purification steps.¹² Unfortunately, it also has high costs due to the large excess of coupling reagents, amino acids and toxic solvents necessary for the synthesis and for this reason, especially when a short to medium peptide is needed, enzyme synthesis or liquid phase synthesis is adopted. Certainly, the latter allows lower costs due to the stoichiometric use of almost all reagents but in contrast, it loses the advantage of easy purification using tedious isolation steps. Furthermore, it must be considered that in both cases, the formation of amide bond is still lacking a general catalytic method therefore the use of benzotriazole derivatives is necessary to provide high coupling efficacy and low racemization with the consequence of having a bad atom economy which worsens due to the forced use of protection and deprotection steps.¹³

Bibliography

- (1) Scott, D. A.; Best, C. H. The Preparation of Insulin. *Ind Eng Chem* **1925**, *17* (3), 238–240. <https://doi.org/10.1021/ie50183a004>.
- (2) Davda, J.; Declerck, P.; Hu-Lieskovan, S.; Hickling, T. P.; Jacobs, I. A.; Chou, J.; Salek-Ardakani, S.; Kraynov, E. Immunogenicity of Immunomodulatory, Antibody-Based, Oncology Therapeutics. *J Immunother Cancer* **2019**, *7* (1), 105. <https://doi.org/10.1186/s40425-019-0586-0>.
- (3) Waldmann, H. Human Monoclonal Antibodies: The Residual Challenge of Antibody Immunogenicity. *Met in Mol Bio* **2014**, *1060*, 1–8. https://doi.org/10.1007/978-1-62703-586-6_1.
- (4) Smith, M. C.; Gestwicki, J. E. Features of Protein–Protein Interactions That Translate into Potent Inhibitors: Topology, Surface Area and Affinity. *Expert Rev Mol Med* **2012**, *14*, e16. <https://doi.org/10.1017/erm.2012.10>.
- (5) Petta, I.; Lievens, S.; Libert, C.; Tavernier, J.; de Bosscher, K. Modulation of Protein–Protein Interactions for the Development of Novel Therapeutics. *Mol Ther* **2016**, *24* (4), 707–718. <https://doi.org/10.1038/mt.2015.214>.
- (6) Di, L. Strategic Approaches to Optimizing Peptide ADME Properties. *AAPS J* **2015**, *17* (1), 134–143. <https://doi.org/10.1208/s12248-014-9687-3>.
- (7) Li, C. Y.; Yap, K.; Swedberg, J. E.; Craik, D. J.; de Veer, S. J. Binding Loop Substitutions in the Cyclic Peptide SFTI-1 Generate Potent and Selective Chymase Inhibitors. *J Med Chem* **2020**, *63* (2), 816–826. <https://doi.org/10.1021/acs.jmedchem.9b01811>.
- (8) Dougherty, P. G.; Wen, J.; Pan, X.; Koley, A.; Ren, J.-G.; Sahni, A.; Basu, R.; Salim, H.; Appiah Kubi, G.; Qian, Z.; Pei, D. Enhancing the Cell Permeability of Stapled Peptides with a Cyclic Cell-Penetrating Peptide. *J Med Chem* **2019**, *62* (22), 10098–10107. <https://doi.org/10.1021/acs.jmedchem.9b00456>.
- (9) Bullock, B. N.; Jochim, A. L.; Arora, P. S. Assessing Helical Protein Interfaces for Inhibitor Design. *J Am Chem Soc* **2011**, *133* (36), 14220–14223. <https://doi.org/10.1021/ja206074j>.
- (10) Wang, L.; Wang, N.; Zhang, W.; Cheng, X.; Yan, Z.; Shao, G.; Wang, X.; Wang, R.; Fu, C. Therapeutic Peptides: Current Applications and Future Directions. *Signal Transduction and Targeted Therapy*. Springer Nature December 1, 2022. <https://doi.org/10.1038/s41392-022-00904-4>.
- (11) Merrifield, R. B. Solid Phase Peptide Synthesis. I. The Synthesis of a Tetrapeptide. *J Am Chem Soc* **1963**, *85* (14), 2149–2154. <https://doi.org/10.1021/ja00897a025>.
- (12) Gentilucci, L.; Tolomelli, A.; Squassabia, F. *Peptides and Peptidomimetics in Medicine, Surgery and Biotechnology*. *Curr. Med. Chem.* **2006**, *13*, 2449 – 2466. doi: 10.2174/09298670677935041
- (13) Isidro-Llobet, A.; Kenworthy, M. N.; Mukherjee, S.; Kopach, M. E.; Wegner, K.; Gallou, F.; Smith, A. G.; Roschangar, F. Sustainability Challenges in Peptide Synthesis and Purification: From R&D to Production. *J Org Chem* **2019**, *84* (8), 4615–4628. <https://doi.org/10.1021/acs.joc.8b03001>.

CHAPTER 1

Green Chemistry for peptide synthesis

With the aim of providing a viable alternative to the classic method of peptide synthesis in a green chemistry perspective, we decided to reconsider the use of N-carboxyanhydrides (NCAs), generated for the first time by Leuchs in 1906¹ using phosgene and firstly coupled with amino acids in 1966². We also wanted to take advantages of mechanochemical activation for the substantial reduction of the amount of solvent employed. In fact, this kind of approach, virtually allows to operate under solvent-free conditions³ with the complete preservation of the stereochemistry⁴, particularly important aspect in the chemistry of the peptides, often sensitive to epimerization. In many cases, to improve the yield and decrease the reaction time, small number of solvents can be added, resulting in liquid-assisted grinding condition (LAG).⁵

In terms of atom economy, unprotected NCAs represent the most convenient amino acid derivative to perform peptide synthesis, because they are designed to protect the α -amino group and activate the carboxy group of an amino acid at the same time and all the molecular bulk remains inside the product. Unfortunately, they are also prone to polymerization in a neutral or acidic environment, due to the decarboxylation of the intermediate carbamic acid and hence the reaction conditions to the synthesis must be carefully controlled.⁶

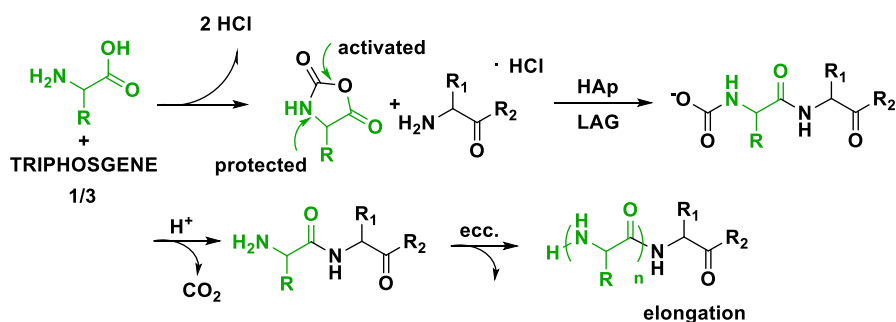


Fig.1 Mechanism of action of N-carboxyanhydrides

Hence, the reaction conditions to the synthesis of a dipeptide must be strictly controlled and, in our work, we tried different approaches in order to identify the one that would provide the best result. The original Hirschmann's NCA process involved the batch reaction of α -amino carboxylates with solid NCAs in 1M sodium borate buffer. The pH was maintained at 10.2 by addition of 6M KOH. Hirschmann recognized the need for high shear mixing to rapidly disperse the highly reactive solid NCA. To solve this practical aspect, solid NCA was added portion wise to the reaction into a kitchen blender, and temperature was kept at 0°C by adding ice into the shake.⁷

Several modifications of this original procedure have been proposed, including the use of organic acids and bases. NCAs were also utilized in solid phase peptide synthesis on PEG-based ChemMatrix® resins under controlled aqueous conditions and thanks to this procedure, a sufficient yield and purity of short peptide amide was produced, without the need of coupling reagents or protecting groups.⁸

A more recent study analyzed in details the mechanisms, the kinetics, and the many parameters, like the stirring, the fluid velocity, the particle shape and size, the temperature, and the pH, of the coupling reactions in the liquid boundary layer and bulk solution during dissolution of the solid NCA, responsible for dimerization or polymerization, or by-product formation.⁹ This comprehensive study underline the importance of controlling the reaction conditions to prevent side reactions and led to the construction of a continuous flow stirred tank reactor designed to control, within a narrow range, operating conditions that favor the reaction of NCA with an amino acid and minimize side reactions.

Unfortunately, the complex control of the reaction parameters necessary to avoid polymerization strongly diminishes the practical utility of NCAs in peptide synthesis. As a matter of fact, NCAs are more frequently utilized for the fabrication of high molecular weight polypeptides via ring-opening polymerization.^{10,11} In order to definitively prevent the risk of polymerization, but at the disadvantage of atom economy, Fuller et al. proposed *N*-protection of NCAs with Boc or Fmoc to give UNCAs.¹² and recently, Lamaty and coworkers, utilized UNCAs counterparts in the presence of NaHCO₃, for the solvent-free preparation of dipeptides, into a steel high-frequency ball-mill.¹³ The same authors also improved the previously reported procedure by adding minimal amounts of environmentally benign solvents. Subsequently, Juaristi et al. successfully utilized *N*-Boc-UNCAs derived from β-amino acids to perform the solvent-free coupling with different α- and β-amino ester hydrochlorides under ball-milling activation.¹⁴

1.1 – Synthesis of NCAs

In this context, we reconsidered the reaction of unprotected NCAs for peptide synthesis in liquid assisted grinding (LAG) conditions in amalgam with nanocrystalline hydroxyapatite (HAp)¹⁵, a common form of calcium phosphate (Ca₁₀(PO₄)₆(OH)₂), highly biocompatible thanks to the structural similarity to the mineral phase of bone tissues.

Furthermore, because of its great features that include high affinity for amino acids, low solubility, high stability, and relatively weak basic character, it can prevent unwanted reactions by stabilizing

the intermediate carbamic acid.¹⁶ It could also be reused without substantial loss of efficacy after easy regeneration and precipitation from ethanol.

Unfortunately, different studies suggest that the properties of Hap, strictly depends on the methods of preparation thus also preventing its use as nanomaterials and its applications in biological field.¹⁷ Apart from pay attention to the preparation of Hap, initially, we also explored the reaction conditions for optimization using as the model partners D-Val-OMe HCl and the NCA of Trp (TrpNCA). The latter was prepared by means of a modified version of the Fuchs-Farthing method,¹⁸ that consist in combine a limp mixture of the amino acid with one third of $\text{OC}(\text{OCCl}_3)_2$ (triphosgene) under MW irradiation while gently blowing with nitrogen.¹⁹ Triphosgene was used because, though included in the hazardous compounds (GHS05, GHS06), is regarded as a convenient alternative to phosgene, provided that it was properly handled²⁰ and it is really useful for the introduction of a carbonyl group.

Not only the preparation of the Hap affects the good result of the reaction, but it appears that, also several authors pointed at the purity and the crystallinity of the NCAs as fundamental issues for increasing the quality of their reactions.^{21–25} In fact, typically, NCAs contain traces of water, acid, acid chlorides, or isocyanates and the presence of these minute impurities can cause problems by promoting side reactions.

Because initially, as already mentioned, the reaction conditions were explored for optimization using as the model partners D-Val-OMe HCl and the NCA of Trp, we decided to deeply explore this aspect by using diverse batches of TrpNCA isolated according to alternative protocols that resulted in diverse crystalline forms of the samples. TrpNCA-A¹⁹, isolated by precipitation from THF and hexane, showed disordered aggregates with no regular morphology and dimensions, which may be presumably due to the fast phase separation. In contrast, TrpNCA-B²⁴ and TrpNCA-C, obtained with repeated crystallization from THF and hexane upon slow decrease in solubility at low temperature, presented well-defined separate crystals with different morphologies. The resulting samples were analyzed by ¹H NMR spectroscopy, which confirmed the higher purity of TrpNCA-B and TrpNCA-C. Accordingly, we also decided to analyze the NCA powders as obtained by the diverse protocols according with the procedure indicated by Schäfer and collaborators.²¹ Although this method does not provide structural information, sharp peaks characteristic for a crystalline phase are indicative of the crystalline state of the NCAs. The Powder X-ray diffraction patterns of the diverse samples of NCA are shown in the following figure where it is possible to distinguish the three preparations by color and where the TrpNCA-A is red, the TrpNCA-B is in green, and TrpNCA-C is in blue.

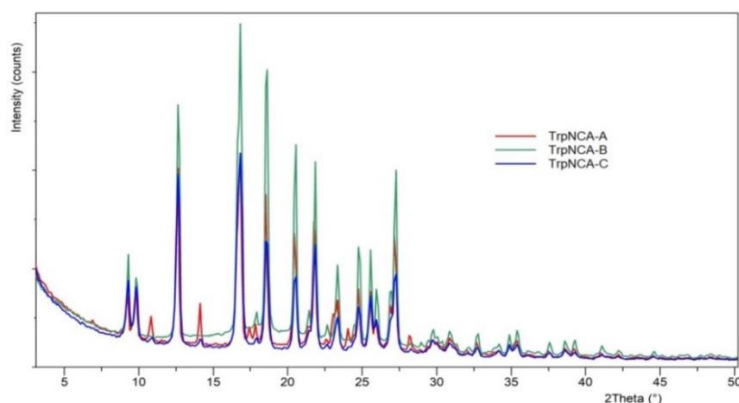


Fig. 2 Powder X-ray diffraction patterns of TrpNCA isolated by precipitation (TrpNCA-A, red), *Errore. Il segnalibro non è definito.* by the Semple's procedure (TrpNCA-B, green),²⁵ and by Semple's procedure/crystallization upon slow decrease of solubility (TrpNCA-C, blue).

The crystal shapes of the NCA prepared by the three protocols were also analyzed by SEM and the comparison of the images confirmed the diverse crystalline forms of the samples. TrpNCA-A, isolated by precipitation, showed disordered aggregates with no regular morphology and dimensions, which may be presumably due to the fast phase separation. In contrast, TrpNCA-B and TrpNCA-C presented well-defined separate crystals with different morphologies.

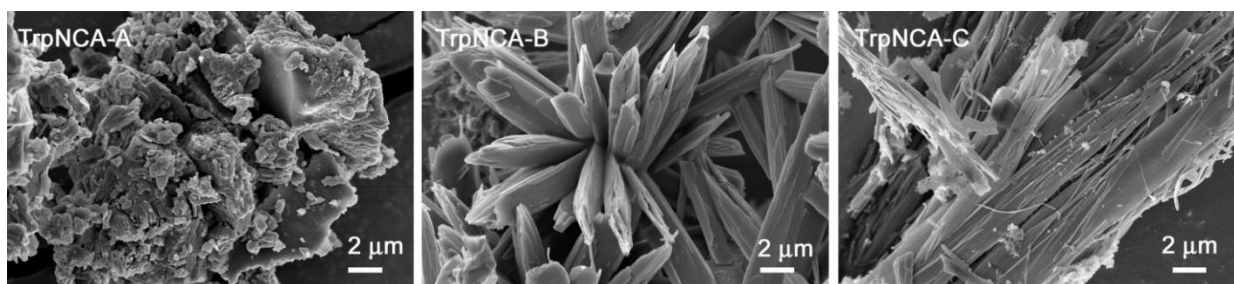


Fig. 3. Scanning electron microscopy of TrpNCA-A, TrpNCA-B, TrpNCA-C showing alternative structures.

In particular, TrpNCA-B displayed rod-like particles composed by smaller aligned crystals elongated along a preferential direction; the rod-like particles were arranged from a common center to form spherulites. TrpNCA-C instead, sample obtained through crystallization by slow decrease of solubility, was composed of long and flexible needle-like crystals with a very high length/width ratio.

1.2 – Application tests for the use of NCAs in peptide synthesis

In a set preliminary experiment, a sample of TrpNCA from each batch A-C (50 mg) was made to react with 1 equiv. of D-Val-OMe HCl in the presence of HAp (100 mg). The mixture was grinded into a low-frequency planetary ball mill, consisting of an agate jar equipped with three balls of the same material. The milling system (jar and balls) was precooled at +3°C into a regular fridge²⁶ to avoid excessive heating of the system and to increase the homogeneity of the mixture, the reaction was

conducted in liquid-assisted grinding (LAG) conditions, hence in the presence of a minimal amount (0.1 mL) of solvent. Green solvents, as γ -valerolactone (GVL)^{27–29}, were preferred during the tests to choose which solvent was most suitable.

After 30 min, the milling was stopped, the mixture was diluted with ethanol, and the suspension was separated by centrifugation in order to recover the HAp crystals, which being of inorganic nature, are insoluble in this solvent, unlike the product and the starting materials. In the event that residual carbamate intermediates were present, the collected organic layers were treated with 1M HCl in ethanol (50 μ L),²⁶ and stirred for 30 min at RT. The solvent was removed at reduced pressure, and the resulting dipeptide-HCl salt was triturated with EtOAc. The residue was then acetylated with an excess of Ac₂O in a mixture of dioxane and saturated aqueous solution of NaHCO₃. We opted for this extra derivatization step for the convenience of the analysis of the mixtures, which was thereafter performed by RP HPLC in neutral conditions.

Table 1. LAG of the NCAs and the amino ester/amide partners (HCl salts) in the presence of HAp and a green solvent. The crude reaction mixtures were acetylated prior to analysis.

	NCA	Amm	Base (x) ^a	Solvent (y) ^b	Ac-3 (%) ^c	Ac-4 (%) ^c	Ac-5 (%) ^c	Ac-1 (%) ^c
1	TrpNCA-A	D-Val-OMe	HAp (2)	GVL (2)	65	24	6	traces
2	TrpNCA-B	D-Val-OMe	HAp (2)	GVL (2)	79	12	5	Nd
3	TrpNCA-C	D-Val-OMe	HAp (2)	GVL (2)	76	15	6	Nd
4	TrpNCA-B	D-Val-OMe	HAp (4)	GVL (4)	93	traces	Nd	Nd
5	TrpNCA-B	D-Val-OMe	HAp (4)	EtOH (4)	80	8	traces	Nd
6	TrpNCA-B	D-Val-OMe	HAp (4)	DMSO (4)	92	traces	traces	Nd
7	TrpNCA-B	D-Val-OMe	Cs ₂ CO ₃ (4)	GVL (4)	80	12	4	traces
8	TrpNCA-B	D-Val-OMe	Al ₂ O ₃ (4)	GVL (4)	82	10	traces	traces
9	TrpNCA-B	D-Val-OMe	Cs ₂ CO ₃ (4)	DMSO (4)	84	5	traces	Nd
10	TrpNCA-B	D-Val-OMe	Al(OH) ₃ (4)	GVL (4)	78	10	traces	traces
11	TrpNCA-B	D-Val-OMe	carbonate buffer pH 8 (8)		83	9	traces	traces
12	TrpNCA-B	D-Val-OMe	HAp ^d (4)	GVL (4)	88 ^e	traces	traces	Nd
13	TrpNCA-B	Phe-NH ₂	HAp (4)	GVL (4)	90	5	Nd	Nd
14	AlaNCA	Phe-OEt	HAp (4)	GVL (4)	91	traces	Nd	traces
15	LeuNCA	Phe-OEt	HAp (4)	GVL (4)	90	6	traces	Nd
16	Lys(Cbz)NCA	Gly-OEt	HAp (4)	GVL (4)	86	traces	traces	traces
17	GluNCA	Phe-OEt	HAp (4)	GVL (4)	92	traces	Nd	Nd
18	TrpNCA	Pro-OBn	HAp (4)	GVL/0.2	98	Nd	Nd	Nd
19	TyrNCA	Phe-OEt	HAp (4)	GVL (4)	90	7	Nd	Nd
20	PheNCA	Met-OMe	HAp (4)	GVL (4)	94	traces	Nd	Nd
21	PhgNCA	D-Val-OMe	HAp (4)	GVL (4)	93 ^f	5 ^g	traces	Nd

^ax = mg HAp/mg NCA. ^by = μ L solvent/mg NCA. ^cDetermined by RP HPLC. ^dReutilized for up to 5 overall cycles. ^eAnalysis of the 5th cycle. ^f92:8 Ac-Phg-D-Val-OMe/Ac-D-Phg-D-Val-OMe. ^gMixture of diastereoisomers. Traces, \leq 4%. Nd=not detected.

As we can see in the previous table, where all the results are reported, the RP HPLC analyses of the acetylated reaction mixtures confirmed that in all cases the conversion was almost quantitative but with different results depending on the type of NCA.

In fact, for the reaction of TrpNCA-A, reported in the first entry, the mass analysis confirmed the presence of the dipeptide Ac-Trp-D-Val-OMe as the major product (65%) but accompanied by a significant amount of the tripeptide Ac-(Trp)₂-D-Val-OMe (24%), and even of the tetrapeptide Ac-(Trp)₃-D-Val-OMe. The acetylated reactant Ac-D-Val-OMe was also detected. Besides, the reaction gave rise to the formation of a number of minor by-products, possibly arising from decomposition and/or reactions of the NCA. Better results were observed in the reactions of TrpNCA-B or TrpNCA-C (entry 2 and 3), under the same conditions described above, plausibly due to their higher purity as compared to TrpNCA-A. Interestingly, the best results were observed with TrpNCA-B. After acetylation, the analysis of the reaction revealed a higher yield of the dipeptide (79%), and reduced amounts of the acetylated reagent Ac-D-Val-OMe, of the tripeptide, and of the other by-products, while TrpNCA-C gave slightly inferior results.

The dependence of NCA reactivity in LAG conditions on a combination of purity and crystallinity was not completely unexpected. In fact, as already mentioned, Schäfer et al. analyzed batch of NCAs obtained by different methods to underline different crystalline state, and consequent purity, linked to their reactivity. They indeed observed that highly crystalline NCA monomers gave higher mw chains by nucleophilic ring-opening polymerization.²¹ Furthermore, Kanazawa et al. analyzed the crystal structure of amino acid NCAs by X-ray analysis to explain the reactivity in the solid state. Reproducibility could not be warranted in the polymerization of amino acid NCAs even when highly purified NCA crystals were used and so the reactivity in the solid state was considered to depend also on crystal structure and density.³⁰

To corroborate these theories, we repeated the reaction with TrpNCA-B using this time a double amount of HAp (200 mg) and solvent (0.2 mL). These new conditions, inserted in entry 4, allowed to further increase the yield of principal product, being the amounts of by-products almost negligible, plausibly due to an improved mixing of the reagents in the mill and a more homogeneous dough.

We also wanted to test the actual efficacy of the solvent and we replace GVL with other solvents, obtaining interesting and diverse results. While EtOH gave the desired dipeptide in modest yield and purity (Entry 5), DMSO gave a result comparable to GVL (entry 6). Even though not included among the prominent green solvents, DMSO is regarded as an acceptable greener alternative for

hazardous dipolar aprotic such as DMF.³¹ However, due to the superior classification in the green solvent lists, and the comparable results, GLV was designed as the solvent of choice.

Subsequently, using the TrpNCA-B/GVL combination under the best-performing conditions, HAp was replaced in the model reaction by other inorganic bases,^{32,33} as we can see from entry 7 to entry 11, where Cs_2CO_3 , Al_2O_3 , $\text{Al}(\text{OH})_3$ and carbonate buffer, were tested in LAG conditions; in all cases, the reaction gave comparatively inferior results.

After each reaction, the mineral HAp powder was recovered almost quantitatively by centrifugation, then it was cleaned up by washes with EtOH, and dried for 6 h at 50 °C. The powder was reutilized for 4 further reactions cycles of the reaction between TrpNCA and D-Val-OMe, giving comparable results (Entry 12). The X-ray diffraction analysis (Figure 4A) of recovered HAp showed the same patterns as the pristine powder, and TEM (Figure 4B) confirmed that the nanocrystals maintained the original shape and dimensions.³⁴

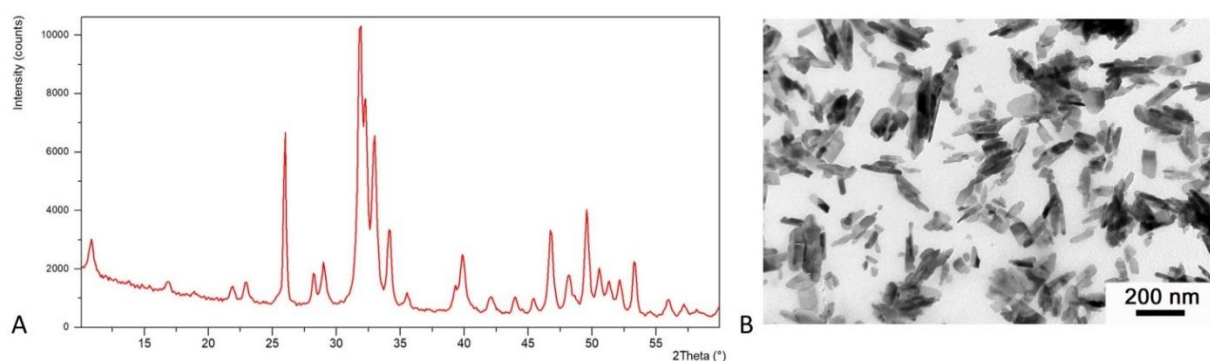


Fig. 4 Characterization of HAp nanocrystals after five cycles of peptide bond formation. (A) Powder X-ray diffraction patterns. (B) TEM image.

To confirm the amino acid scope of the procedure, the conditions reported in entry 4 were exploited for the preparation of various dipeptides by reaction of amino amides or esters with diverse NCAs, prepared in turn by MW activation, and subsequently isolated according to the Semple's protocol (B).²⁵ In all cases, after acetylation the coupling reactions gave results comparable to that of TrpNCA as reported in Entry 4 (Entries 13-21). Notably, the NCAs of Glu (entry 17) and Tyr (entry 19) have been utilized without protection at the side chain. The reaction between TrpNCA and Pro-OBn gave an outstanding 98% conversion to dipeptide (entry 19). Possibly, the almost complete lack of by-products arising from NCA polymerization can be correlated to the higher nucleophilicity of the pyrrolidine ring of Pro-OBn respect to the primary amine of the dipeptide product H-Trp-Pro-OBn.³⁵ In general, the peptide-forming reactions discussed above proceeded without appreciable epimerization, as determined on the basis of RP HPLC/ESI MS analyses, which is in line with observations reported in the literature. Errore. Il segnalibro non è definito.,Errore. Il segnalibro non è definito.,Errore. Il

segnalibro non è definito.,Errore. Il segnalibro non è definito. To assess the potential epimerisation of sensitive amino acids, the reaction was repeated on the racemisation vulnerable residue phenylglycine (Phg).³⁶L-PhgNCA was prepared according to the literature,³⁷ and utilized for reaction with D-Val-OMe under the usual conditions (entry 21). After acetylation, the analysis of the mixture revealed an amount of dipeptide in line with the other NCAs (93%), albeit in the form of a 92:8 mixture of the diastereoisomers Ac-Phg-D-Val-OMe / Ac-D-Phg-D-Val-OMe, while the tripeptide was also detected in traces as mixture of diastereoisomers Ac-(L/D-Phg)₂-D-Val-OMe.

1.3 - Conclusions

In conclusion, the protocol discussed herein represents a convenient method for the synthesis of oligopeptides, coherent to the principles of Green Chemistry because the use of NCAs allowed to avoid the recourse to protecting and activating agents and the reactions were conducted by grinding the reagents with the aid of a minimal amount of the green solvent GVL. The only solvents utilized in large amount were EtOH and EtOAc, ranked as “recommended” in the solvent selection guides.^{Errore. Il segnalibro non è definito.,Errore. Il segnalibro non è definito.} On the other hand, an excess of HAp powder was utilized as base. However, this fully biocompatible base was easily recycled and reutilized, making the entire process convenient. HAp has also proved to be more efficient as compared to other inorganic bases in preventing NCA polymerization, generally regarded as the fundamental caveat to the use of NCAs for peptide synthesis. Interestingly, the analyses of diverse batches of NCA suggested that NCA purity and crystalline form significantly influenced the outcome of the reactions in terms of dipeptide versus polymer and by-products formation.

Despite these great preliminary results, subsequent tests are necessary to make the procedure truly feasible in the laboratory, and we decided to proceed with the synthesis of peptidomimetics, which we will analyse in the following chapters, using classical methods.

1.4 - Experimental Procedure

General information

All commercially available reagents purchased from Merck (Darmstadt, Germany) were used without further purification. The synthetic procedures under MW irradiation were performed with a Microwave Labstation for Synthesis (Micro-SYNTH, Bergamo, BG, IT) equipped with a built-in ATC-FO advanced fiber-optic automatic temperature control. Ball milling was carried out in a low-

frequency PlanetaryMill Pulverisette (Fritsch GmbH, Idar-Oberstein, Germany), mounting an agate jar ($\phi = 7.5$ cm) equipped with three balls of the same material ($\phi = 2.0$ cm). Purities were assessed by analytical reverse phase high-performance liquid chromatography (RP HPLC) on a 1100 series apparatus (Agilent, CA, USA), using a XSelect Peptide CSH C18 column (Waters, Milford, MA, USA), 4.6 mm \times 100 mm, 130 Å, 3.5 μ m; DAD 210 nm; mobile phase: from 8:2 water/CH₃CN to 2:8 water/CH₃CN, in 8 min, at a flow rate of 0.5 ml min⁻¹, followed by 10 min at the same composition. ESI-MS was done on a MS single quadrupole HP 1100 MSD detector (Agilent). UPLC analysis was performed on an Acquity UPLC H-Class Plus apparatus, using a Acquity C18 BEH column, 1.7 μ m and 2.1 \times 100 mm; mobile phase: from 3:1 H₂O/0.1% HCO₂H//CH₃CN/0.1% HCO₂H to 1:1 H₂O/0.1% HCO₂H //CH₃CN/0.1% HCO₂H, in 1.5 min at a flow rate of 0.5 mL/min, followed by 1.0 min at the same composition, then to 1:4 H₂O/0.1% HCO₂H//CH₃CN/0.1% HCO₂H in 0.5 min, followed by 1.0 min at the same composition. High resolution mass spectrometry (HRMS) was performed with a Xevo G2XS QTof apparatus. ¹H NMR was performed at 400 MHz on a Varian Gemini 400 (Agilent) in 5 mm tubes in DMSO-d₆ at rt; chemical shifts are reported as δ values relative to residual H peak (δ H = 2.50 ppm). NCAs morphology was observed using a Zeiss Leo1530 Gemini field-emission scanning electron microscope (SEM) equipped with InLens detector and operating at 5kV. Samples were sputter coated with gold before observation. Powder X-ray diffraction patterns were recorded using a PANalytical-X'Pert PRO powder diffractometer (Malvern Panalytical-Spectris, Egham, UK) equipped with a fast X'Celerator (Malvern Panalytical-Spectris) detector ($\lambda = 0.154$ nm, 40 mA, 40 kV). For phase identification, the 2θ range was investigated from 10 to 60 $2\theta^\circ$ with a step size of 0.1° and time/step of 100 s.

General synthesis for peptide bond formation

The NCA (0.2 mmol) was mixed with the amino partner.HCl (0.2 mmol), HAp powder (100 mg) and γ -valerolactone (GVL) (0.2 mL). The mixture was milled at 10 Hz frequency into agate jar equipped with three balls. The milling system (jar and balls) was precooled at +3°C into a regular fridge. After 30 min, milling was stopped, the mixture was diluted with ethanol (5 mL), and the suspension was separated by centrifugation. The HAp crystals were washed twice with ethanol (5 mL) and collected by centrifuge and dried at 50°C for 6h. The collected organic layers were treated with 1M HCl in ethanol (50 μ L), and stirred for 30 min at RT, the solvent was removed at reduced pressure, and the resulting dipeptide.HCl salt was triturated with EtOAc.

1.5 - Bibliography

- (1) Leuchs, H. Ueber Die Glycin-carbonsäure. *Berichte der deutschen chemischen Gesellschaft* **1906**, *39* (1), 857–861. <https://doi.org/10.1002/cber.190603901133>.
- (2) Denkewalter, R. G.; Schwam, H.; Strachan, R. G.; Beesley, T. E.; Veber, D. F.; Schoenewaldt, E. F.; Barkemeyer, H.; Paleveda, W. J.; Jacob, T. A.; Hirschmann, R. The Controlled Synthesis of Peptides in Aqueous Medium. I. The Use of α -Amino Acid N-Carboxyanhydrides. *J Am Chem Soc* **1966**, *88* (13), 3163–3164. <https://doi.org/10.1021/ja00965a069>.
- (3) Bolm, C.; Hernández, J. G. From Synthesis of Amino Acids and Peptides to Enzymatic Catalysis: A Bottom-Up Approach in Mechanochemistry. *Chem Sus Chem* **2018**, *11* (9), 1410–1420. <https://doi.org/10.1002/cssc.201800113>.
- (4) Yeboue, Y.; Jean, M.; Subra, G.; Martinez, J.; Lamaty, F.; Métro, T.-X. Epimerization-Free C-Term Activation of Peptide Fragments by Ball Milling. *Org Lett* **2021**, *23* (3), 631–635. <https://doi.org/10.1021/acs.orglett.0c03209>.
- (5) Porte, V.; Thioly, M.; Pigoux, T.; Métro, T.; Martinez, J.; Lamaty, F. Peptide Mechanosynthesis by Direct Coupling of N-Protected α -Amino Acids with Amino Esters. *European J Org Chem* **2016**, *2016* (21), 3505–3508. <https://doi.org/10.1002/ejoc.201600617>.
- (6) Jolley, K. E.; Nye, W.; González Niño, C.; Kapur, N.; Rabion, A.; Rossen, K.; Blacker, A. J. Highly Productive Continuous Flow Synthesis of Di- and Tripeptides in Water. *Org Process Res Dev* **2017**, *21* (10), 1557–1565. <https://doi.org/10.1021/acs.oprd.7b00214>.
- (7) Denkewalter, R. G.; Schwam, H.; Strachan, R. G.; Beesley, T. E.; Veber, D. F.; Schoenewaldt, E. F.; Barkemeyer, H.; Paleveda, W. J.; Jacob, T. A.; Hirschmann, R. The Controlled Synthesis of Peptides in Aqueous Medium. I. The Use of α -Amino Acid N-Carboxyanhydrides. *J Am Chem Soc* **1966**, *88* (13), 3163–3164. <https://doi.org/10.1021/ja00965a069>.
- (8) de Marco, R.; Tolomelli, A.; Greco, A.; Gentilucci, L. Controlled Solid Phase Peptide Bond Formation Using N-Carboxyanhydrides and PEG Resins in Water. *ACS Sustain Chem Eng* **2013**, *1* (6), 566–569. <https://doi.org/10.1021/sc400058r>.
- (9) Jolley, K. E.; Nye, W.; González Niño, C.; Kapur, N.; Rabion, A.; Rossen, K.; Blacker, A. J. Highly Productive Continuous Flow Synthesis of Di- and Tripeptides in Water. *Org Process Res Dev* **2017**, *21* (10), 1557–1565. <https://doi.org/10.1021/acs.oprd.7b00214>.
- (10) Song, Z.; Fu, H.; Wang, J.; Hui, J.; Xue, T.; Pacheco, L. A.; Yan, H.; Baumgartner, R.; Wang, Z.; Xia, Y.; Wang, X.; Yin, L.; Chen, C.; Rodríguez-López, J.; Ferguson, A. L.; Lin, Y.; Cheng, J. Synthesis of Polypeptides via Bioinspired Polymerization of in Situ Purified N-Carboxyanhydrides. *Proc Natl Acad Sci* **2019**, *116* (22), 10658–10663. <https://doi.org/10.1073/pnas.1901442116>.
- (11) Kanazawa, H.; Inada, A.; Kawana, N. Re-Examination of the Reactivity Of N-Carboxy Amino Acid Anhydrides 1. Polymerisation of Amino Acid NCAs in Acetonitrile and in the Solid State in Hexane. *Macromol Symp* **2006**, *242* (1), 104–112. <https://doi.org/10.1002/masy.200651016>.
- (12) Fuller, W. D.; Cohen, M. P.; Shabankareh, M.; Blair, R. K.; Goodman, M.; Naider, F. R. Urethane Protected Amino Acid N-Carboxyanhydrides and Their Use in Peptide Synthesis. *J Am Chem Soc* **1990**, *112* (20), 7414–7416. <https://doi.org/10.1021/ja00176a063>.

- (13) Bonnamour, J.; Métro, T.-X.; Martinez, J.; Lamaty, F. Environmentally Benign Peptide Synthesis Using Liquid-Assisted Ball-Milling: Application to the Synthesis of Leu-Enkephalin. *Green Chem* **2013**, *15* (5), 1116. <https://doi.org/10.1039/c3gc40302e>.
- (14) Hernández, J. G.; Juaristi, E. Green Synthesis of α,β - and β,β -Dipeptides under Solvent-Free Conditions. *J Org Chem* **2010**, *75* (21), 7107–7111. <https://doi.org/10.1021/jo101159a>.
- (15) Santino, F.; Petruzzelli, R.; Zhao, J.; Boanini, E.; Gentilucci, L. Peptide Bond Formation Using Unprotected N-Carboxyanhydrides under Green Chemistry Conditions. *Sustain Chem Pharm* **2021**, *24*, 100540. <https://doi.org/10.1016/j.scp.2021.100540>.
- (16) Kanazawa, H.; Inada, A.; Kawana, N. Re-Examination of the Reactivity Of N-Carboxy Amino Acid Anhydrides 1. Polymerisation of Amino Acid NCAs in Acetonitrile and in the Solid State in Hexane. *Macromol Symp* **2006**, *242* (1), 104–112. <https://doi.org/10.1002/masy.200651016>.
- (17) Bigi, A.; Boanini, E. Functionalized Biomimetic Calcium Phosphates for Bone Tissue Repair. *J Appl Biomater Funct Mater* **2017**, *15* (4), e313–e325. <https://doi.org/10.5301/jabfm.5000367>.
- (18) Wilder, R.; Mobashery, S. The Use of Triphosgene in Preparation of N-Carboxy .Alpha.-Amino Acid Anhydrides. *J Org Chem* **1992**, *57* (9), 2755–2756. <https://doi.org/10.1021/jo00035a044>.
- (19) de Marco, R.; Tolomelli, A.; Greco, A.; Gentilucci, L. Controlled Solid Phase Peptide Bond Formation Using N -Carboxyanhydrides and PEG Resins in Water. *ACS Sustain Chem Eng* **2013**, *1* (6), 566–569. <https://doi.org/10.1021/sc400058r>.
- (20) Cotarca, L.; Geller, T.; Répási, J. Bis(Trichloromethyl)Carbonate (BTC, Triphosgene): A Safer Alternative to Phosgene? *Org Process Res Dev* **2017**, *21* (9), 1439–1446. <https://doi.org/10.1021/acs.oprd.7b00220>.
- (21) Schäfer, O.; Schollmeyer, D.; Birke, A.; Holm, R.; Johann, K.; Muhl, C.; Seidl, C.; Weber, B.; Barz, M. Investigation of α -Amino Acid N-Carboxyanhydrides by X-Ray Diffraction for Controlled Ring-Opening Polymerization. *Tetrahedron Lett* **2019**, *60* (3), 272–275. <https://doi.org/10.1016/j.tetlet.2018.12.028>.
- (22) Song, Z.; Fu, H.; Wang, J.; Hui, J.; Xue, T.; Pacheco, L. A.; Yan, H.; Baumgartner, R.; Wang, Z.; Xia, Y.; Wang, X.; Yin, L.; Chen, C.; Rodríguez-López, J.; Ferguson, A. L.; Lin, Y.; Cheng, J. Synthesis of Polypeptides via Bioinspired Polymerization of in Situ Purified N -Carboxyanhydrides. *Proc Natl Acad Sci* **2019**, *116* (22), 10658–10663. <https://doi.org/10.1073/pnas.1901442116>.
- (23) Kramer, J. R.; Deming, T. J. General Method for Purification of α -Amino Acid- N -Carboxyanhydrides Using Flash Chromatography. *Biomacromolecules* **2010**, *11* (12), 3668–3672. <https://doi.org/10.1021/bm101123k>.
- (24) Otake, Y.; Nakamura, H.; Fuse, S. Rapid and Mild Synthesis of Amino Acid N - Carboxy Anhydrides: Basic-to-Acidic Flash Switching in a Microflow Reactor. *Angew Chem Int Ed* **2018**, *57* (35), 11389–11393. <https://doi.org/10.1002/anie.201803549>.
- (25) Semple, J. E.; Sullivan, B.; Sill, K. N. Large-Scale Synthesis of α -Amino Acid-N-Carboxyanhydrides. *Synth Commun* **2017**, *47* (1), 53–61. <https://doi.org/10.1080/00397911.2016.1249289>.
- (26) Denkwalter, R. G.; Schwam, H.; Strachan, R. G.; Beesley, T. E.; Veber, D. F.; Schoenewaldt, E. F.; Barkemeyer, H.; Paleveda, W. J.; Jacob, T. A.; Hirschmann, R. The Controlled Synthesis of Peptides in Aqueous Medium. I. The Use of α -Amino Acid N-Carboxyanhydrides. *J Am Chem Soc* **1966**, *88* (13), 3163–3164. <https://doi.org/10.1021/ja00965a069>.
- (27) Pawlas, J.; Rasmussen, J. H. ReGreen SPPS: Enabling Circular Chemistry in Environmentally Sensible Solid-Phase Peptide Synthesis. *Green Chem* **2019**, *21* (21), 5990–5998. <https://doi.org/10.1039/C9GC02775K>.

- (28) Ferrazzano, L.; Corbisiero, D.; Martelli, G.; Tolomelli, A.; Viola, A.; Ricci, A.; Cabri, W. Green Solvent Mixtures for Solid-Phase Peptide Synthesis: A Dimethylformamide-Free Highly Efficient Synthesis of Pharmaceutical-Grade Peptides. *ACS Sustain Chem Eng* **2019**, *7* (15), 12867–12877. <https://doi.org/10.1021/acssuschemeng.9b01766>.
- (29) Jessop, P. G. Searching for Green Solvents. *Green Chem* **2011**, *13* (6), 1391. <https://doi.org/10.1039/c0gc00797h>.
- (30) Kanazawa, H.; Inada, A.; Kawana, N. Re-Examination of the Reactivity of N-Carboxy Amino Acid Anhydrides 1. Polymerisation of Amino Acid NCAs in Acetonitrile and in the Solid State in Hexane. *Macromol Symp* **2006**, *242* (1), 104–112. <https://doi.org/10.1002/masy.200651016>.
- (31) Prat, D.; Wells, A.; Hayler, J.; Sneddon, H.; McElroy, C. R.; Abou-Shehada, S.; Dunn, P. J. CHEM21 Selection Guide of Classical- and Less Classical-Solvents. *Green Chem* **2016**, *18* (1), 288–296. <https://doi.org/10.1039/C5GC01008J>.
- (32) Landeros, J. M.; Juaristi, E. Mechanochemical Synthesis of Dipeptides Using Mg-Al Hydrotalcite as Activating Agent under Solvent-Free Reaction Conditions. *European J Org Chem* **2017**, *2017* (3), 687–694. <https://doi.org/10.1002/ejoc.201601276>.
- (33) Bonnamour, J.; Métro, T.-X.; Martinez, J.; Lamaty, F. Environmentally Benign Peptide Synthesis Using Liquid-Assisted Ball-Milling: Application to the Synthesis of Leu-Enkephalin. *Green Chem* **2013**, *15* (5), 1116. <https://doi.org/10.1039/c3gc40302e>.
- (34) Anselmi, M.; Stavole, P.; Boanini, E.; Bigi, A.; Juaristi, E.; Gentilucci, L. Green Synthesis of Bioactive Oligopeptides Promoted by Recyclable Nanocrystalline Hydroxyapatite. *Future Med Chem* **2020**, *12* (6), 479–491. <https://doi.org/10.4155/fmc-2019-0320>.
- (35) Kanzian, T.; Nigst, T. A.; Maier, A.; Pichl, S.; Mayr, H. Nucleophilic Reactivities of Primary and Secondary Amines in Acetonitrile. *Eur J Org Chem* **2009**, *2009* (36), 6379–6385. <https://doi.org/10.1002/ejoc.200900925>.
- (36) Liang, C.; Behnam, M. A. M.; Sundermann, T. R.; Klein, C. D. Phenylglycine Racemization in Fmoc-Based Solid-Phase Peptide Synthesis: Stereochemical Stability Is Achieved by Choice of Reaction Conditions. *Tetrahedron Lett* **2017**, *58* (24), 2325–2329. <https://doi.org/10.1016/j.tetlet.2017.04.047>.
- (37) Milo, A.; Neumann, R. An Achiral Manganese Salen Catalyst Encapsulated in a Peptidic Phosphonate Homochiral Solid for the Enantioselective Formation of Diols by Consecutive Epoxidation and Hydration Reactions. *Chem Comm* **2011**, *47* (9), 2535. <https://doi.org/10.1039/c0cc04205f>.

CHAPTER 2

K opioid receptor ligands

Opioids receptors are G-protein-coupled receptors (GPCR) and they are part of the superfamily of seven transmembrane spanning receptors (7TM). Being a very large family, receptors capable of modulating many neuronal and hormonal responses are responsible for antinociception and analgesic action in general, but as they are present in both central and peripheral nervous system, depending on the receptor subtype their action results in different effects.

Since the discovery of opioids binding sites in 1950s¹ numerous pharmacological studies have followed, leading to the identification of four opioids receptor subtypes. MOR (μ for morphine), the first one to be isolated and the most studied, capable of provoking a great analgesic action but with it also numerous side effects like addiction, respiratory depression and reduced gastrointestinal mobility; KOR (κ for ketocyclazocine) an antipruritic also capable of analgesic action but causing less severe unwanted effects like dysphoria and anhedonia; DOR (δ for deference, because it was first identified by executing the electrically stimulated mouse vas deference) the only one unable of analgesic action but with interesting anxiolytic and antidepressant functions and NOR (initially called ORL-1, or nociception/orphanin FQ receptor) particularly linked to emotional behaviour, has generated interest in recent years as a possible alternative to treating pain without causing side effects. In fact, since the isolation of morphine in 1805² as the most active component of opium, pharmaceutical companies have developed a wide variety of painkillers and currently most of them are MOR agonist. Over the last two decades, opioids overdoses have dramatically increased, particularly in north America³, as a result of misuse and over prescription for pain relief. This opioid crisis has encouraged interest in developing better opioids to treat pain.

In this context, selective KOR activation has attracted a lot of attention. Not only its activation produces a high antinociception effect with low abuse potential, but KOR selective ligands could also be used as a powerful weapon for the treatment of abuse conditions, pruritis, multiple sclerosis and immune mediated disease.⁴

Nevertheless, despite their great potential, no KOR agonists are currently used for the therapeutic treatment of pain in humans, mostly due to the relevant side effects but a lot of efforts are being made for the development of safer analgesics.

2.1 - KOR agonists

The endogenous ligand of KOR are dynorphins⁵, discovered in the late 1980s when the gene PDYN encoding peptide precursor preprodynorphin⁶, was isolated. Since then, a lot of natural, naturally derived, and synthetic KOR selective ligand have been isolated and tested.

The κ receptor owes its name to ketocyclazocine, the first selective KOR ligand⁷, which elicited analgesia and sedation and belongs to the benzomorphans class, obtained by morphine skeleton reduction. Despite ketocyclazocine resulted to be less potent than morphine, Benzomorphans were studied for many years for their interesting mixed KOR agonist/MOR antagonist profile, but their clinical development was precluded because they also induce respiratory depression and other side effects.

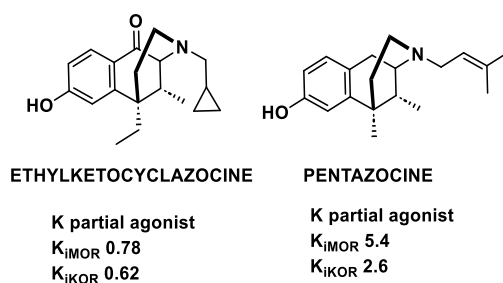


Fig.1 Structures and K_i values (expressed in nM) of ketocyclazocine and pentazocine.

Another morphine derivative though, Pentazocine is still under investigation, and recent studies showed that it was more potent in activating p38 MAPK mediated by h-KOR than the rat KOR and it also resulted to be a potent promoter of β -arrestin 2 recruitment⁸. Studies on Pentazocine also led to the identification of Bremazocine as a potent KOR agonist. Despite its activity profile, it doesn't seem to elicit morphine-like adverse actions, and it was thought, it could be used for its analgesic and diuretic activity. Its psychotomimetic side effects, however, have curbed its use as a therapeutic, not eliminating the possibility of its use in the treatment of addictions⁹.

Another important class of KOR-selective ligands are the Arylacetamide derivatives, described for the first time in 1982¹⁰. Among them, U50,488 emerged for novel structure, potency, and selectivity, with analgesic, antipruritic, and other effects. Unfortunately, U50,488 and its subsequent derivatives showed all the side effects correlated to the activation of KOR, and also a modest permeability of the Blood Brain Barrier (BBB).

Subsequent studies on Arylacetamides led to the discovery of Asimadoline that was found to inhibit nociception via activation of KORs expressed on the peripheral endings of nociceptors in the colon, suggesting a peripherally restricted action which might be useful for a variety of painful conditions in the viscera.

With the attempt to further improve the structure of U50,488, a spiroester was added to the cyclohexane ring, leading to a special branch of the Arylacetamide family, of which U69593 was the precursor. U69593 produced antinociception without affecting GIT mobility, suggesting, in contrast to Asimadoline, a central but not a peripheral activity.

Further modifications lead to Spiradoline (U62-066) and Enadoline (CI-977), molecules capable of crossing the BBB with reasonable efficacy with an analgesic potency comparable with morphine, with reduced respiratory depression¹¹. Unfortunately, they still have dose related central effects like anhedonia, dysphoria, and hallucination-like effect so it was impossible to carry on further clinical investigations¹².

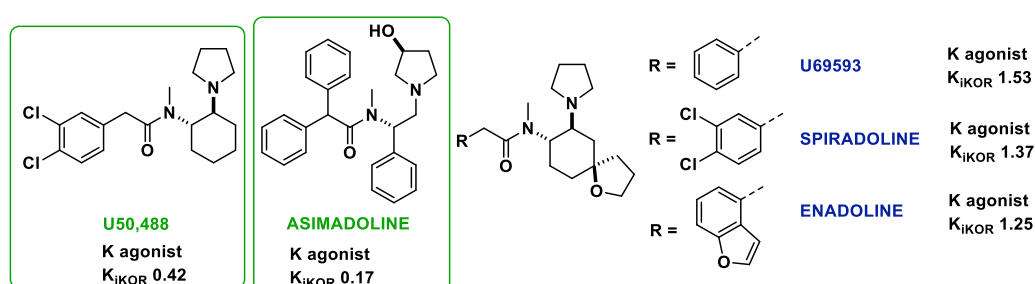


Fig. 2 Examples of Arylacetamide KOR agonists with related K_i values expressed in nM.

As a result of two different screenings, in 2013 Zhou et al. discovered two new classes of KOR selective agonists: triazoles and isoquinolines¹³. Both showed high binding affinity with a preferential activation of G-protein and minimal effect on β -arrestin recruitment and downstream ERK1/2 activation.

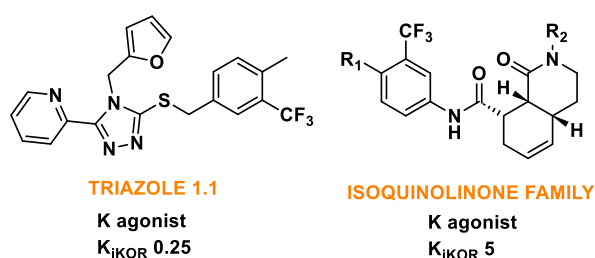


Fig. 3 Structures of triazoles and isoquinolines with related K_i values expressed in nM.

Further studies revealed that triazole is able to induce antinociception, without altering locomotion nor provoking dysphoria or aversion. Triazole 1.1 retained the antinociceptive and antipruritic efficacies of conventional KOR agonists, yet it did not induce sedation or reductions in dopamine release in vivo, nor did it produce dysphoria as determined by intracranial self-stimulation in rats¹⁴. In 1978 Diphenethylamines were firstly described, as potentially anti-Parkinson's drug¹⁵. The first synthesized molecule was RU24213, which was followed, through extensive studies, by diverse libraries of molecule with suitable modification of substituent to increase KOR affinity, selectivity,

agonist potency and efficacy.^{16,17}

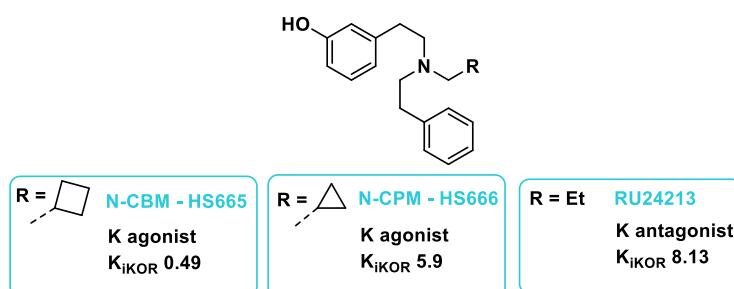


Fig.4 Structures and relative K_i values (expressed in nM) of Diphenethylamines.

Considering the inclusion in recent years of fluorine in drug candidates, in 2017 Erli et al. expanded the SAR studies on the original series and demonstrated that some analogues gained subnanomolar affinity and excellent KOR selectivity, acting as full or partial agonists or as antagonists¹⁵.

Salvinorins, on the other hand, are the only κ -selective small molecules of natural origin. Salvinorin A (SalA) is a terpenoid isolated in 1982 by Ortega et al. from *Salvia Divinorum*, an herbal plant native to the SW region of Mexico¹⁸. Two years later, Valdes et al. extracted Salvinorin B¹⁹ and in 2001 also Salvinorin C²⁰. These compounds resulted to be selective KOR agonists with analgesic and hallucinogen effects and immediately rouse interest because of their lack of structural similarity to the other psychotomimetic substances. Indeed, unlike the conventional opioid ligands, salvinorins do not contain any nitrogen atoms.

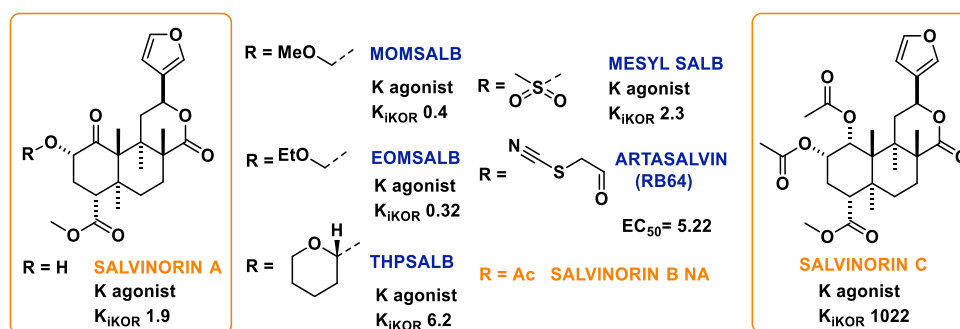


Fig. 5 Salvinorins family structures with related K_i values expressed in nM.

Unfortunately, these natural molecules suffered from short half-life and rapid onset of action, therefore a large number of analogues was prepared to improve the pharmacokinetics profile, generally by modifying the positions at C2, C4 of furan ring but unfortunately this did not translate to increased brain residence time even if they seem to have a biased G-protein activity and to be very effective for reduce cocaine primed – induced reinstatement.^{21,22}

In addition to many small molecules, some of which have just been mentioned, peptides and peptidomimetics can also be selective towards the κ receptor.

Dynorphin is the endogenous 17-mer neuropeptide ligand of KOR. Other peptides with KOR activity

have been identified in fungi and invertebrates and several others have been obtained by chemical synthesis²³. Native peptides such as dynorphin have the potential to powerfully activate opioid receptors but their clinical use is hampered by poor pharmacokinetic properties. Consequently, starting from the native sequences, a variety of peptidomimetics was designed in the perspective to increase enzymatic stability and bioavailability^{24,25}.

Several research groups designed oligopeptides comprising D-amino acid, and these studies yielded molecules which appeared suitable for assessment peripherally acting analgesics. Most of these oligopeptides shared a common N-terminal D-Phe-D-Phe^{5,26–28} including Difelikefalin like CR845, an all-D-amino acid tetrapeptide developed by Cara Therapeutics with high selectivity for KOR that has been shown to be effective in the treatment of chronic pruritus²⁹ and post-operative pain after abdominal surgery³⁰. Unfortunately, due to its hydrophilic properties, transport across the blood–brain barrier is limited, and its intravenous delivery remains a key obstacle for its widespread use.

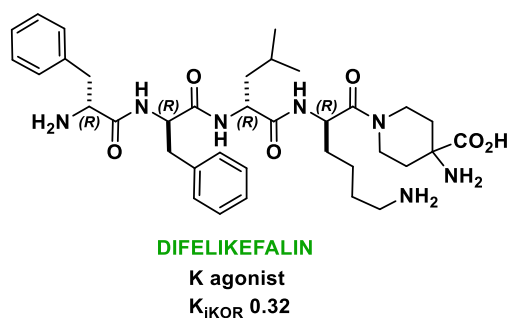


Fig. 6 Structure of CR845 a peptidomimetic KOR agonists with related K_i value.

Bedini et al. synthesized a mini-library of diastereomeric and constrained analogues of the endogenous, highly selective MOR agonist Endomorphin-1 (EM1)^{31,32}, H-Tyr-Pro-Trp-PheNH₂ by introducing a β^2 -homo-Freidinger lactam-like scaffolds in position 2³³. The 5-(aminomethyl) oxazolidinone-2,4-dione (Amo) scaffolds were obtained by side chain cyclization of isoserine-Trp³⁴. Intriguingly, the all-(S) configured H-Tyr-Amo-Trp-PheNH₂ displayed high KOR affinity (K_i 9.8 nM) and high selectivity with a partial agonist profile.

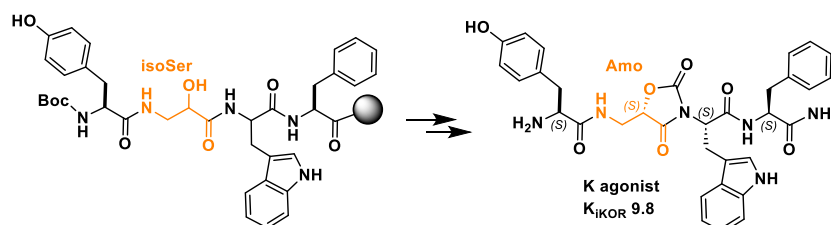


Fig. 7 Structure of selective K ligand obtained from EM1.

In the tail-immersion test, the peptidomimetic determined a relevant analgesic effect (20 mg/kg, ip: 60% MPE at 15 min, and still 42% MPE at 30 min), and the effects were counteracted by the pre-

emptive administration of the KOR selective antagonist nor-BNI, thus confirming also *in vivo* a KOR-mediated activity.

In 2004, Saito et al. isolated from the fermentation broth of the fungus *Ctenomyces serratus* ATCC15502 the cyclotetrapeptide c[Phe-D-Pro-Phe-Trp] known as CJ-15,208 with a modestly selective KOR/MOR activity³⁵. Following numerous biological tests, it was confirmed its antagonist behaviour and furthermore the Ala-scan highlighted the importance of the residues Phe³ and Trp⁴; indeed, c[Ala-D-Pro-Phe-Trp] showed low nanomolar affinity for KOR and MOR, while the other Ala derivatives suffered a substantial loss in binding affinity³⁶.

Numerous studies have followed by making changes in the original structure but all of the derivatives of CJ-15,208 maintained the same mixed KOR > MOR affinity profile, albeit with different K_i values, and did not exhibit any agonist activity *in vitro*.

Unexpectedly, *in vivo* tests showed contrasting activities when compared to the parent peptides: as expected, c[Phe-D-Pro-Phe-D-Trp] behaved as a KOR antagonist also *in vivo* and prevented the stress-induced reinstatement of extinguished cocaine-seeking behavior³⁷, but, the natural isomer CJ-15,208, exhibited robust antinociceptive activity in the warm-water tail withdrawal test following icv administration, it was found to be orally active and appeared to penetrate the BBB^{38–40}. Intriguingly, also the Ala analog c[Ala-D-Pro-Phe-D-Trp] produced potent OR-mediated antinociception *in vivo*⁴¹.

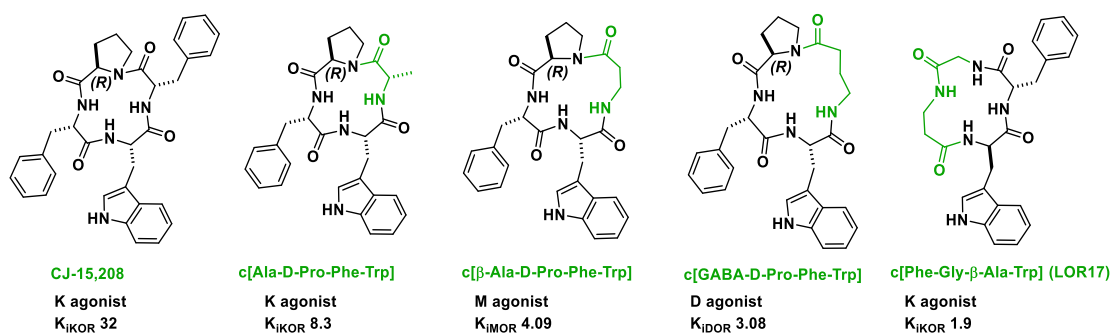


Fig. 8 CJ-15,208 and some relevant derivatives with related K_i values expressed in nM.

The structures of CJ-15,208 and all its derivatives appear clearly correlated to that of c[Phe-Gly-Tyr-D-Pro-D-Trp]⁴², a cyclopentapeptide (CPP) discovered independently from CJ-15,208, designed as a cyclic analogue of the EM1. The CPP was found to be a MOR ligand (K_i 10^{-8} M), partial agonist in the cAMP functional assay and after systemic administration, it produced antinociception in a mouse model of visceral pain, while the parent EM1 was completely ineffective⁴³. The introduction of different substituents at the indole of D-Trp influenced BBB permeability, allowing a measurable MOR-mediated central antinociception in the mouse warm-water tail withdrawal test after

administration⁴⁴.

These Trp-containing macrocycles are clearly alternative respect the classic opioid peptides, as they lack in the protonable amino group of Tyr1, commonly regarded as the fundamental “message” pharmacophore^{45,46}. Despite the close structural similarities, the two families of opioid peptides showed distinct receptor selectivity and in vivo activity and this assumption led to presume a correlation between bioactivity and 3D displays of the pharmacophores, which depend in turn on ring size, stereochemistry, and secondary structures.

More recently, the same authors designed and synthesized the analogue c[Phe-Gly-β-Ala-D-Trp] (LOR17). The peptide showed a KOR selective agonist activity in different cell models with nM affinity (K_i 1.19 nM)⁴⁷ and also, in contrast to U50,488, LOR17 displayed functional selectivity toward G-protein signaling and provoked antinociceptive/antihypersensitivity effects in different in vivo models, including neuropathy by oxaliplatin.

2.2 - Ligand- receptor interactions

When a GPCR is activated by an agonist, its action is to activate $G\alpha$ and $G\beta\gamma$ subunits to initiate a signalling and provoke the phosphorylation with consequent desensitization and internalization process. The activation of GPCRs also include the recruitment of β -arrestins that are considered signalling molecules in their own right.⁴⁸

GPCR mediated signalling is dependent on the conformation of the receptor. That means that agonists are defined for their abilities to shift the inactive conformation towards the one that promotes signalling. Because a receptor has a three-dimensional structure, it is also possible to have a shift just in one area with no change in the others, and this is the case of biased agonists. In fact, a biased signalling refers to the ability of a ligand to activate only one preferential pathway and for GPCRs, this subset activation means that it is either the β -arrestin mediated signalling or $G\alpha$ and $G\beta\gamma$ events but not both of them. Because traditionally, when a ligand is studied, just the $G\alpha$ - $G\beta\gamma$ mediated events are examined, when an agonist only activates the β -arrestin pathway results to be an antagonists otherwise, when it activates just G-protein is called biased agonists and in the last decades the development of this kind of molecules has been the leading trend in opioid fields to reach benign drugs with reduced side effects.⁴⁹

The first G protein biased opioid ligand reported in the literature with limited β -arrestin recruitment was the MOR ligand (R)-TRV130 (oliceridine)⁵⁰ that seemed to elicit potent antinociception in vivo without inhibiting GIT transit or causing respiratory depression⁵¹. Unfortunately, TRV130 initially

failed in clinical trials⁵² due to side effects comparable to that of morphine, but recently it was reconsidered and approved for moderate and severe pain in adults.⁵³ After TRV130, other G-protein biased agonists have been identified, like the MOR ligand PZM21 which was discovered by in-silico screening⁵⁴ and was proposed as an analgesic with unprecedented profile and reduced side effects in the hot-plate assay, but not in the tail-flick test.

Interestingly, experiments with a non-phosphorylatable version of MOR knock-out-mice⁵⁵ showed that total abolishment of β -arrestin binding improved analgesia, reduced tolerance, but worsened other opioid side effects so doubts began to be cast on the practical usefulness of biased agonism in MOR.^{56,57}

Although most biased agonists at MOR have failed so far as therapeutics into the market, functional selectivity at KOR is still considered interesting and potentially promising. There is evidence that KOR signaling through G-protein pathways (including adenylyl cyclase inhibition and early ERK1/2 phosphorylation) mediates the antinociceptive and anti-pruritic effects of KOR agonists, whereas β -arrestin-2-dependent signaling (including p38MAPK activation) mediates the dysphoric effects as well as sedation and motor incoordination⁵⁸.

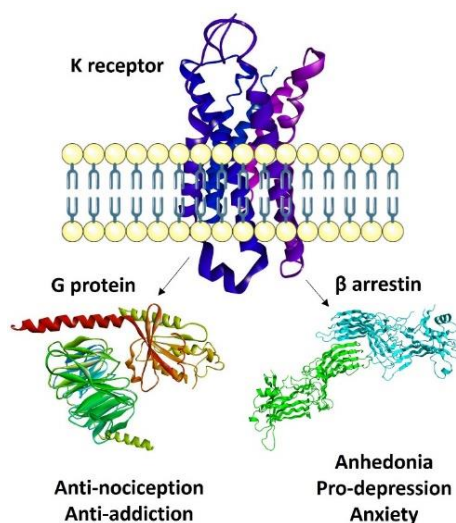


Fig. 9 Activation and linked effects of G-protein and β -arrestin.

The 1-pyrazole methyl ester MPC1 was shown to elicit KOR-mediated antinociception without sedation, constipation, or motor impairment in different models of inflammatory and neuropathic pain⁵⁹ and, as mentioned before many research group have also focused their attention on biased agonism in search for new KOR ligands^{13,15,17,60} and all their results support the idea that functionally selective KOR agonists may activate G protein-mediated signaling, to produce antinociception, over β -arrestin 2-dependent induction of p38MAPK, which preferentially contributes to adverse effects.

The alternative profiles just mentioned can actually also be explained with the drug efficacy of the molecules. In fact, signaling bias can also be linked to a partial agonist profile, and thus be provoked by a good therapeutic index but low efficacy, stimulus amplification and receptor reserve^{56,61}. In other words, KOR partial agonists may allow an analgesic response to be produced at dosages lower than those required to produce the adverse effects. A G-protein-dependent output (e.g.: inhibition of cAMP accumulation) encompasses high amplification, while arrestin recruitment at the receptor has little or no amplification.

Partial agonists may hold potential for the treatment of depression, mood disorders, psychiatric comorbidity, and specific drug addictions. Besides, some partial KOR agonists display anti-inflammatory and neuroprotective effects, and they suppress the rewarding effects of opioids and cocaine. Such compounds may restore homeostatic control of dopaminergic function underlying mood and reward and may also diminish severity of relapse/re-escalation. Furthermore, they could also be beneficial in promoting more prolonged abstinence, as well as decreasing the severity of relapse episodes. Mixed agonists/partial agonists/antagonists at different OR subtypes are employed to treat alcohol dependence and cocaine craving⁶². As for KOR antagonists, these are already used to treat opioid dependence and withdrawal^{63,64}.

Unfortunately, owing to lack of KOR>MOR selectivity in known ligands, these therapeutic opportunities have been not clinically exploited, so far. In this respect, it is worth to mention the peptide Tyr-Amo-Trp-PheNH₂. This peptide was a selective ligand of KOR with nanomolar affinity and behaved as a partial agonist in the functional test, since it inhibited forskolin-induced cAMP accumulation in HEK cells stably expressing hKOR, with IC₅₀ 0.22 nM and E_{max} 40%, as compared to U50,488 (IC₅₀ 1.2 nM and E_{max} 90%). When 1 μM of the peptide was administered together with U50,488, 40% inhibition of forskolin-induced cAMP accumulation was observed and U50,488 concentration-response curve was shifted rightward, thus, confirming a partial agonist activity for the peptide³³.

As mentioned before, KOR agonists do not induce euphoria/addiction, respiratory depression, or GIT transit inhibition and therefore, they were initially viewed as an attractive alternative strategy to design potent and safer analgesics. Indeed, small-molecules KOR agonists of the first generation, were orally active, brain penetrating, and lacked morphine-like side effects, but unfortunately, these molecules also displayed unwanted neuropsychiatric effects, such as sedation and dysphoria. Therefore, subsequent studies have been conducted to achieve analgesia without triggering the side effects and it was realised that also peripheral KORs are able to induce analgesia particularly after

tissue injury and inflammation, and because they avoid CNS penetration, they don't allow the arising of unwanted effects.

Asimadoline was the first molecule to enter clinical trials with the hopes that it might treat peripheral pain. In fact, it appears to inhibit nociception via activation of KORs expressed on the peripheral endings of colonic nociceptors, suggesting a peripherally restricted KOR agonist might be useful treatment for a variety of visceral pain conditions including irritable bowel syndrome (IBS)⁶⁵. Unfortunately, asimadoline still produced central adverse effects and also hyperalgesia in non-visceral postoperative pain.

The goal to avoid penetration across BBB to reduce central effect⁶⁶, could be easily achieved through structural modifications leading to decreases in lipophilicity for example by switching to peptide-base compounds. Indeed, peptides are known to have limited ability to cross BBB⁶⁷. This opportunity yielded peptidic KOR ligands such as the all-D configured sequence Difelikefalin (CR845)^{29,30}, which compared with many other opioids, exhibits a minimal effect on the CNS and does not cause respiratory depression or sedation, somnolence or paresthesia, and not even euphoric effect. Because of its many benefits, in 2021, Difelikefalin was approved by the Food and Drug Administration (FDA) and in 2022 by European Medicines Agency (EMA) as a first drug for the treatment of CKD-aP in adult, hemodialysis patients.

It is important to mention however that, in contrast to linear peptides, cyclic peptides might show some ability to cross the BBB^{24,25}. For instance, the macrolactam peptide LOR17, already mentioned, was a full KOR agonist with significant antinociception both in the acetic acid-induced writhing assay and in the warm water tail-withdrawal assay, when administered in the same range of doses, thus, suggesting that LOR17 may distribute to the CNS⁴⁷.

2.3 - Structural insights in ligand-receptor interactions for KOR agonists

MOR, DOR, and KOR, exhibit remarkably conserved amino acid sequences, with a 70% sequence identity in their seven transmembrane domains, particularly in the orthosteric binding pocket. However, KOR is different from the other opioid receptors in terms of tissue expression patterns, functional properties, and side effect profile upon activation. A detailed analysis of the inactive and active-state structures revealed structural determinants that can be exploited for specificity⁶⁸. In particular KOR binding pocket is comparatively much narrower and deeper and partially capped by the ECL2 β -hairpin, the region between TM2-TM3 of KOR is more hydrophobic and has a number non-conserved "address" residues⁶⁹.

A breakthrough in the GPCRs field was the disclosure of the crystal structure of a truncated version of human KOR, in complex with the selective antagonist JD_{Tic} at 2.9Å resolution.

T4L phage lysozyme was inserted to replace highly mobile intracellular loop 3 (ICL3), hence stabilizing overall KOR structure⁷⁰ and the receptor was crystallized in a cholesterol-doped monoolein lipidic cubic mesophase. The JD_{Tic}-KOR complex shows the ligand in a V-shaped conformation into the bottom of the binding cleft, stabilized by salt bridges, polar and hydrophobic interactions with the receptor. The protonated amines in both piperidine and isoquinoline moieties of the ligand form ionic bonds with Asp138(3.32) carboxylate (in brackets, the Ballesteros–Weinstein nomenclature).

The hydroxy group at position 6 of isoquinoline scaffold forms a hydrogen bond with conserved crystallographic water, mediating an interaction with H291(6.52), while the other phenoxy group interacts with structured water mediating a contact with V118(2.63). Besides, JD_{Tic} interacts with four residues in the binding pocket that differ in other closely related ORs, i.e., Val 108(2.53), Val 118(2.63), Ile 294(6.55), and Tyr 312(7.35).

In 2018, information on KOR was greatly expanded by the determination of an active-state crystal structure of KOR in complex with the potent morphinan agonist MP1104 and the nanobody Nb39⁷¹. The shape of MP1104 partially overlaps with the isoquinoline moiety of JD_{Tic} and also forms a similar salt-bridge to the Asp138(3.32). The MP1104-KOR complex is characterized by a ~10% contraction in the volume of the orthosteric site as compared to antagonist-bound inactive state, and a slightly deeper binding of the agonist ligand, likely connected to conformational changes in Met142(3.36) and Trp287(6.48).

Similarly, to other GPCRs, the active structure of KOR differs from the inactive one by a ~10Å outward movement in the intracellular end of TM6 and a ~3Å inward movement of TM7. The structure of the complex was utilized for molecular docking of other several other important KOR ligands sharing epoxymorphinan scaffold, including guanidinonaltrindoles (5'-GNTI, 6'-GNTI), and all compounds maintained a similar binding pose.

Despite the progress made in these important studies, a deep knowledge of KOR specificities is fundamental for the identification and development of subtype-selective agonists and antagonists. Starting from the inactive and active models of the receptor, several research groups have envisaged *in silico* virtual ligand screening to identify novel lead compounds^{72–75}. In general, the effort led to the identification of active KOR ligands characterized by high diversity of bioactive poses among the diverse ligands.

Following this approach, Zheng et al exploited the crystal structure of JDTic-KOR for a virtual screening campaign aimed at identifying new chemotypes of KOR ligands. After optimization of the receptor model, the screening of millions of commercially available compounds gave a bunch of hits in submicromolar affinity range, including compd. 81, a potent Gi biased agonist for KOR with minimal β -arrestin recruitment⁶⁰.

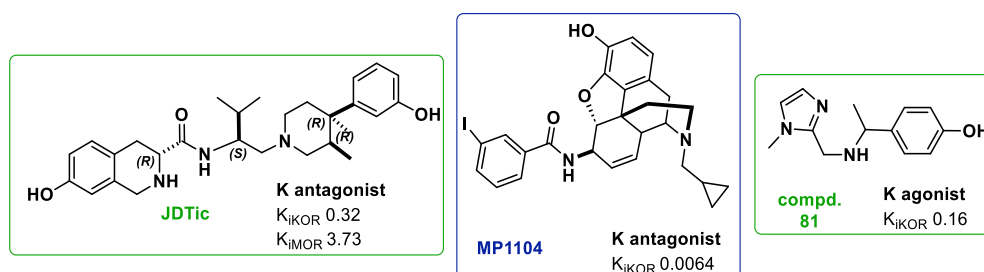


Fig. 10 Structures of KOR ligands used for structural studies: JDTic, MP1104 and comp. 81.

This kind of virtual approach was also used for molecule already mentioned and studied for a better understanding of their behavior. Guerrieri et al. for example, performed docking studies for diphenethylamines, and the simulations predicted that the interaction of the ligand to the hydrophobic pocket formed by Val108, Ile316 and Tyr320 influenced ligand binding. Moreover, the phenolic 3-OH group allowed the stabilizing interaction with His291. The docking was fundamental for structural modification, because predicted that bulky N-substituents increased selectivity and affinity, and the introduction of a second hydroxyl group in position 3' resulted in the identification of potent KOR partial agonists⁷⁶.

Even De Marco et al. used molecular modeling and docking analysis to shed light into the bioactive structure of their EM1 analogue³³. Molecular docking computations in the X-ray structure of the active conformation of KOR (PDB ID: 6B73) supported the role of Amo in orienting the pharmacophores for optimal receptor fitting. Together with the C-terminal portion, the scaffold itself appeared to belong to the “address” of the ligand, being responsible of interactions with residues which are not conserved across the other ORs.

The protonated amine of Tyr¹ forms the salt bridge with Asp138(3.32) carboxylate, while the phenolic side chain shows interactions with Tyr320 and Trp287. Albeit not totally unusual for KOR ligands⁷⁷, Tyr¹ appeared to adopt a disposition alternative to that of tetrahydroisoquinoline ring of JDTic⁷⁰ and to the tyramine portion of MP1104⁷¹.

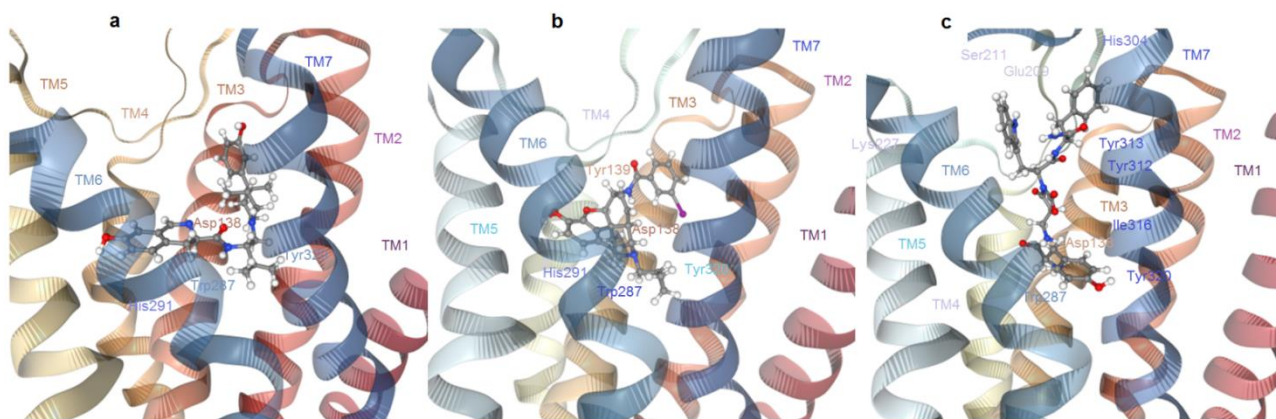


Fig. 11 Comparison of the ligand-receptor complexes as extracted from (a) the X-ray crystal structures of antagonist JD1c-KOR (inactive), (b) of agonist MP1104-KOR (active) and (c) docked structure of Tyr-Amo-Trp-PheNH₂-KOR (active) (Figure obtained with PacDOCK web server⁷⁸).

2.4 - Design of biased KOR ligands

As for MOR, starting from the ligand-receptor models discussed above, some research groups were able to identify structural specificities to rationally design functionally selective KOR agonists. Very recently, Uprety et al. studied the biased behavior at MOR and KOR of diverse analogues of the unbiased morphinan MP1104 by means of a combination of SAR studies, receptor mutagenesis and molecular docking.⁷⁹

These studies led to identify sub-pockets of the orthosteric site as the hot spots for functional selectivity. Ligands capable to place morphinan-amidophenyl “address” in contact with the TM2-TM3 transmembrane domains were shown to maintain balanced G-protein and arrestin signaling, while morphinan derivatives directing the amidophenyl group towards the TM5-ECL2 region specifically led to the recruitment of G protein. The differences between KOR and MOR were explained in terms of the different composition of their TM2/TM3 sub-pockets, which accommodate the hydrophobic amidophenyl arm of the ligands. This sub-pocket is more hydrophobic in KOR due to the presence of the non-conserved V118(2.63) residue and a conformational change in the conserved Q115(2.60) residue.

Based on the above analysis, the authors proposed that a rational design of MP1204 analogs that are G protein biased at MOR or KOR would require a switch of amidophenyl arm from the TM2-TM3 sub-pocket to the TM5-ECL2 one for both receptors. To verify this conjecture, polar or charged substituents were introduced at the amidophenyl to disfavor the interactions at the hydrophobic TM2-TM3 pocket of KOR, while basic moieties were introduced for improving the interactions toward the TM5-ECL2 pocket, since the latter includes acidic residues Asp223(5.35) and Glu209(ECL2).

The conclusions of those studies were in part confirmed by the docking analyses of Tyr-Amo-Trp-PheNH₂ in KOR. In fact, in the bioactive conformation the C-terminal address section of the peptide made interactions with residues of EL2 (Glu209, Ser211, Leu212), and of TM7 (Tyr313, Tyr312), with His304(EL3), and with Lys227(TM5), while having no interaction with TM2-TM3.

2.5 – Synthesis of KOR selective ligands

Taking all this information into account, we decided to design a small library of compounds starting from the structure and the encouraging results of modified EM1.³³

We decided to replace the lactam like scaffold with diverse oxopirrolidine heterocycles that could be obtained by the cyclization of the side chain of an amino acid and could retain the proline like profile that forced the conformation to switch from cis to trans and gain the KOR selectivity.

We therefore introduced in the place of the proline of EM1, serine, glutamic acid and diamino propionic acid to obtain a heterocycle containing an oxygen, a carbon, and an amine in addition to the alpha-carbonyl amine respectively.

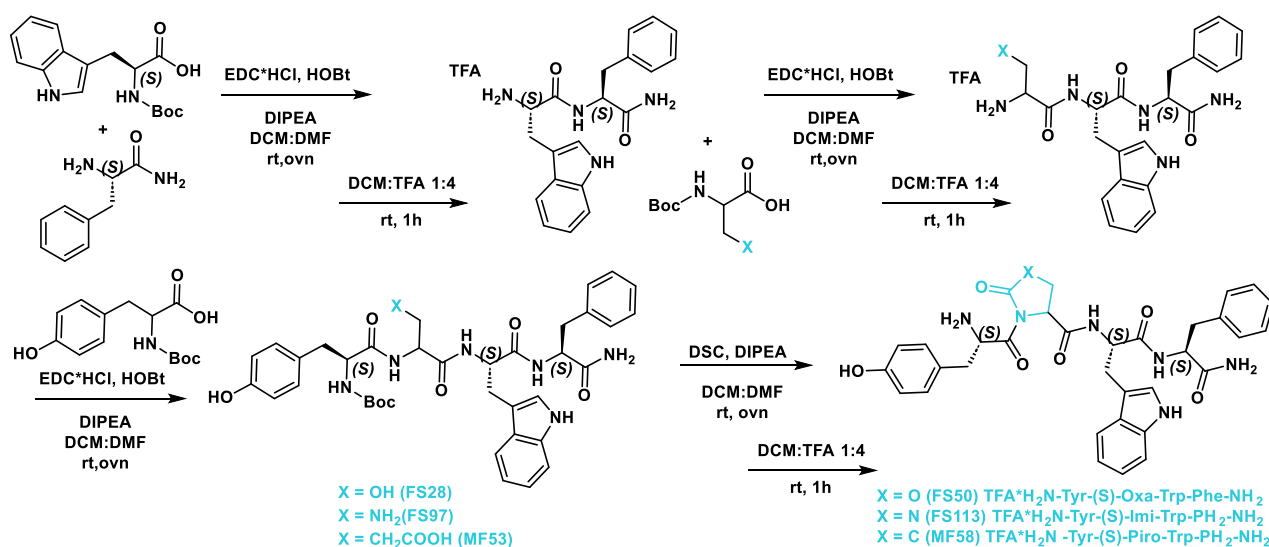


Fig.12 Synthesis of L-stereochemistry library of pseudoproline.

Once it was synthesized the peptidic sequence with liquid phase conditions, the cyclization was performed as last synthetic steps in presence of DIPEA and DSC (N,N-Disuccinimidyl carbonate), a carbonate able to link together the alpha amine and the heteroatom of the side chain and guarantee a good yield of cyclization.

After the purification, all the final products were analysed with mono and bi dimensional NMR in order to verify the presence of the extended structure and the trans bond formation.

We also decided to introduce a cysteine and deeply study the presence of sulphur and the formation of thiazolidines. In fact, this structure has attracted a lot of interest because of its potential as therapeutic agent and as intracellular delivery system for cysteine⁸⁰, fundamental in the synthesis of the glutathione, a potent antioxidant.

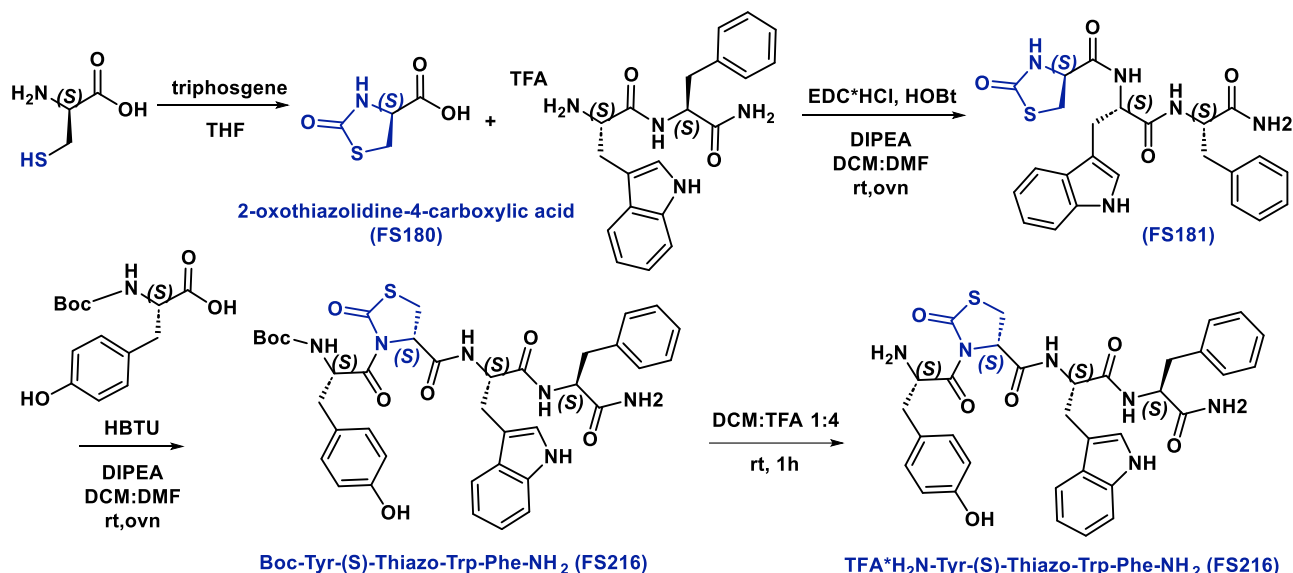


Fig. 13 Synthesis of thiazolidine derivative in the L-Stereochemistry library of pseudoprolines.

Because of the great instability of the cysteine, this analogue had to be synthesized starting from the heterocycle. Once we obtained the oxothiazolidine by means of the reaction with triphosgene, we reacted the acid that was readily available with the diamino acids portion, and then forced the amide of the heterocycle to couple with tyrosine using HBTU.

Once the L-stereochemistry compounds of the library were all completed, we decided to invert the stereocentre of the pseudoprolines, following the studies already mentioned on this subject²⁸ that the insertion of an inverted stereocentre improves the *in vivo* characteristics of the drug and the selectivity.

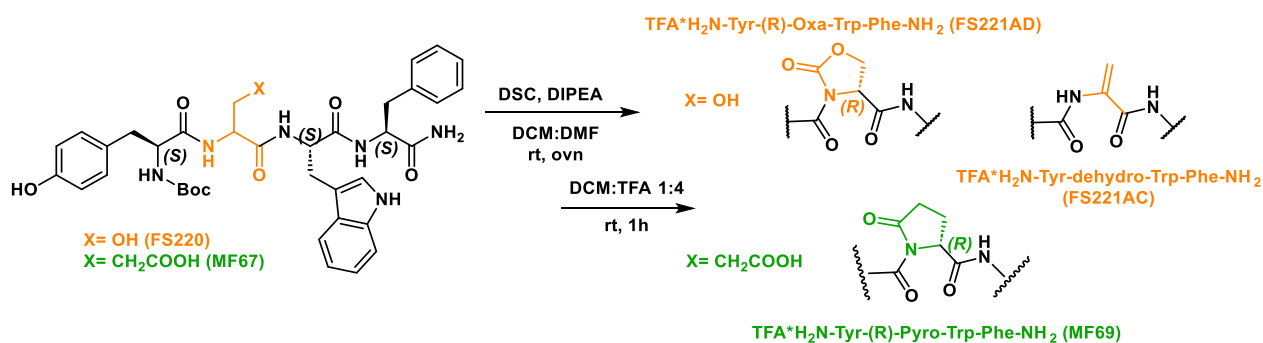


Fig. 14 Synthesis of D-stereochemistry analogues with serine and glutamic acid.

The introduction and the final cyclization of the analogue with D-serine and D-glutamic acid proceeded exploiting the same synthetic steps of the L-counterparts. Nonetheless, we discovered

that the insertion of a different stereocentre brings instability to the final structure and in the case of D-serine, we were able to isolate together with the desired product, the dehydroalanine product, result from the decarboxylation of the oxazolidinone. This behaviour is actually theorised for all heterocycles of this type⁸¹, with both stereochemistry, and it is especially used in solid-phase peptide synthesis as a cleavage strategy. The other compounds, however, were found to be very stable, whereas this last one gave elimination product at a different point from the theorised one, not at the amide position but at the alpha carbonyl one.

The D-cysteine compound instead was found to be completely unstable and after a couple of hours from the formation of the final product, the amide of the thiazolidine eliminate the tyrosine.

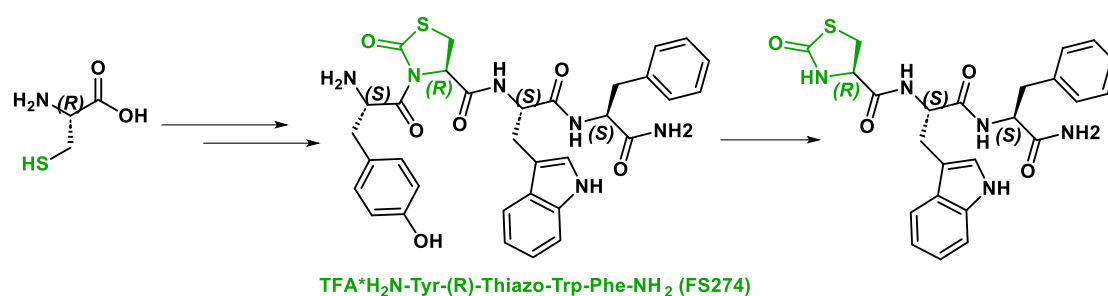


Fig. 15 Attempt introduction of D-cysteine inside the sequence with related instability.

D-amino propionic acid is very difficult to obtain, and it is not commercially available unless prohibitive prices. To synthesize this moiety, we took advantages of the Hoffmann's rearrangement of the primary amide of glutamine that in the presence of PIDA (Diacetoxyiodo)benzene resulted in the formation of a primary amine.

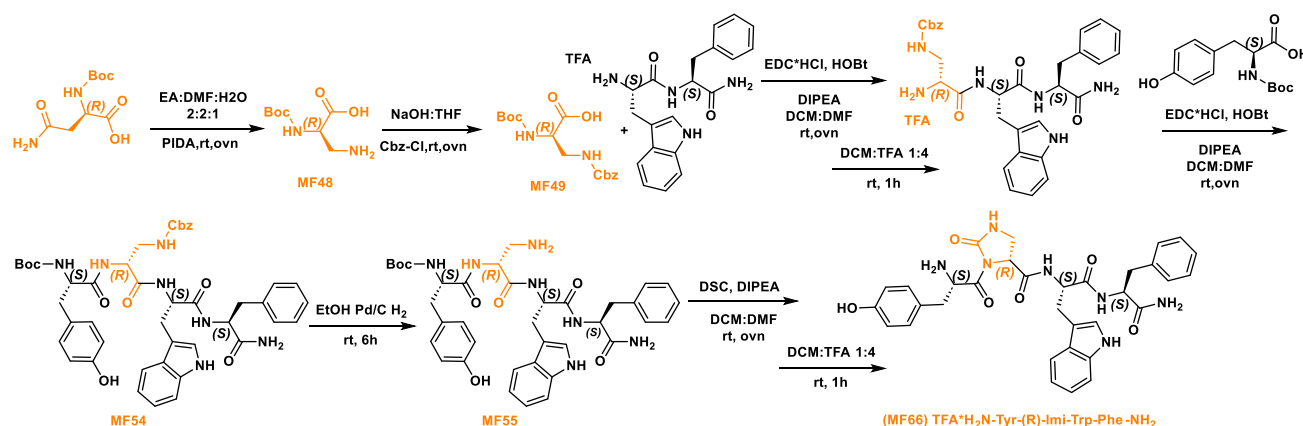


Fig. 16 Synthetic steps for the synthesis of D- Imidazolidinone compound.

The D-amino propionic acid synthesized it was then coupled with the amino acids necessary for the formation of the right sequence, and cyclization was performed as last synthetic steps after the removal of benzyl chloroformate protecting group from the side chain.

2.6 – Introduction of 1,2,3-triazole

Considering that the presence of heteroatoms is one of the factors most influencing the reactivity of compounds, we thought of replacing proline with 1,2,3-triazole synthesized with a Cu(I)-catalyzed Huisgen 1,3-dipolar cycloaddition better known as Click reaction⁸². This kind of Huisgen reaction, as described by Sharpless, is modular, give high yield, generate only inoffensive byproducts that can be easily removed, and it is stereospecific. Furthermore, it has simple reaction conditions and simple product isolation and because of that it could be broadly used especially in peptide-based drug discovery as a potent tool to increase stability⁸³.

In fact, this kind of scaffold is being increasingly used in modern drug development as a bioisostere replacement of amide bond moiety of peptides and because of its possibility to form CH- π interactions that can strongly modify biological interactions.⁸⁴ The physicochemical similarities between the 1,2,3 triazole and a peptide bond includes the distance between substituents that is 3.8-3.9 Å in amides and 5.0–5.1 Å in 1,2,3-triazoles and the dipole moment that is almost the same (4 Debye in amide, 5 Debye in 1,2,3-triazole). Furthermore, the 1,2,3-triazole rings, with sp²-hybridized nitrogen atoms N (2) and N (3), can function as weak hydrogen-bond acceptors as well as a donor similar to amide because of the strong dipole moment that polarized the C (5) proton and can align with that of the other amides in a solid secondary structure.

In addition to being used as surrogates of amide, 1,4 disubstituent they also have been proved by Horne and collaborators⁸⁵ to fix trans amide bonds configuration, characteristic that in our case can be exploited, as already tried with pseudoproline, to obtain a more stretched structure that will be more selective towards the KOR receptor.

The two partners required for a click reaction are an azide and a terminal alkyne. We decided to modify the acid portion of tyrosine to obtain the terminal alkyne by synthesising the desired ester or amide using propargyl amine or propargyl alcohol.

In order to reduce the synthetic steps and make the synthetic route more convenient, although not very well described, it was decided to synthesise the azide portion directly on the already coupled amino acids and not on the single tryptophan. To do this, the diazotransfer reagent imidazole-1-sulfonyl azide was previously synthesised in hydrochloride salt form, so as to be stable and perfectly manageable. This intermediate was then reacted with the acidic diamine under basic conditions and in the presence of copper sulphate and the reaction results in excellent yields without changing the stereochemistry of the compound.

Once the alkyne and the azide moiety were obtained as pure product, it was possible to get them react with the Click reaction. Instead of using the classic Sharpless's conditions involving the formation in situ of the active catalyst Cu(I) from Cu (II) salts using sodium ascorbate as reducing agents, we decided to place directly a Cu(I) salt in presence of DIPEA, that helps the solubilization in organic solvent. Because we didn't use an organic basic solvent, we also added 2,6 lutidine as it is proven to produce the minimum amount of side products in the presence of amino acids.⁸⁶

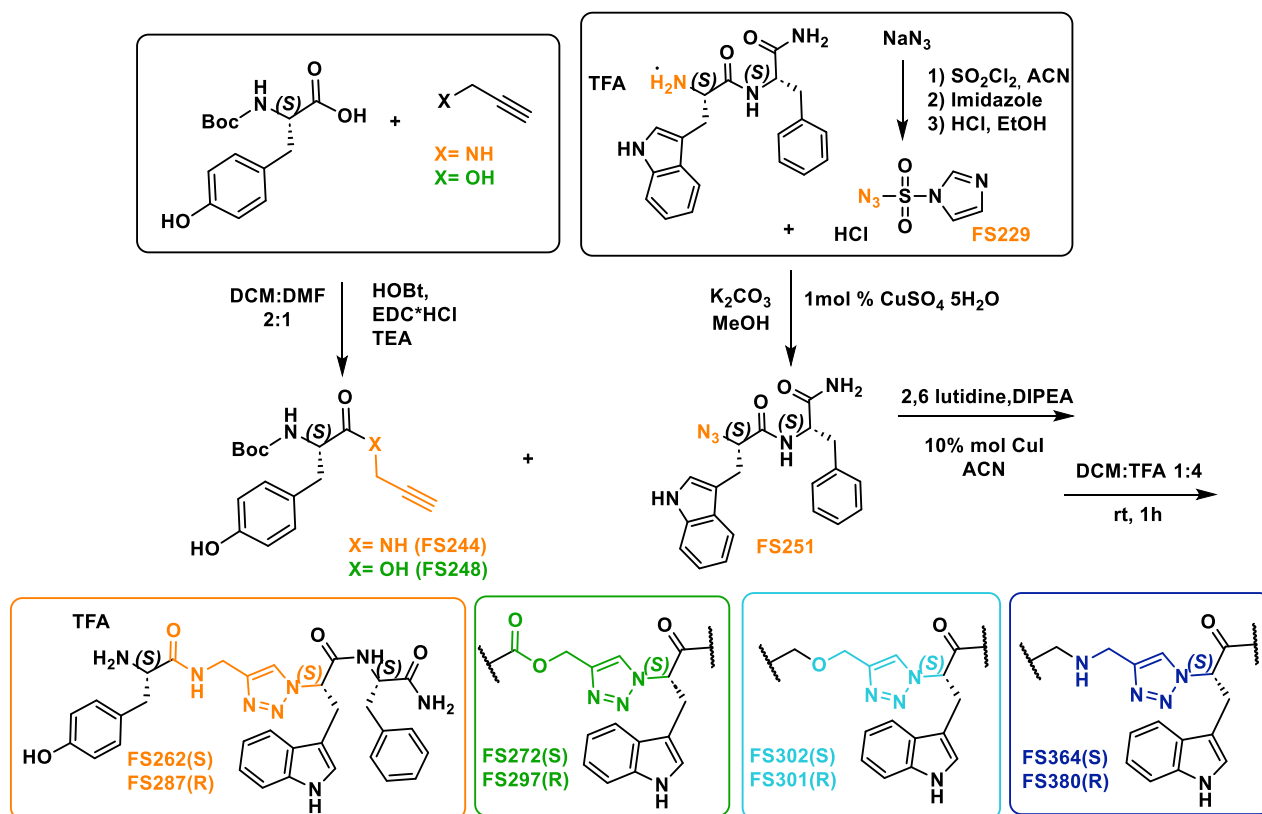


Fig.17 Synthetic scheme of Click Reaction analogues.

After having obtained the first two compounds where the triazole was linked to the tyrosine with an amide and an ester, we decide to also reduce these two functional groups and thus change the possible interactions within the receptor pocket and the stability, especially in the case of the ester which is easily hydrolysed.

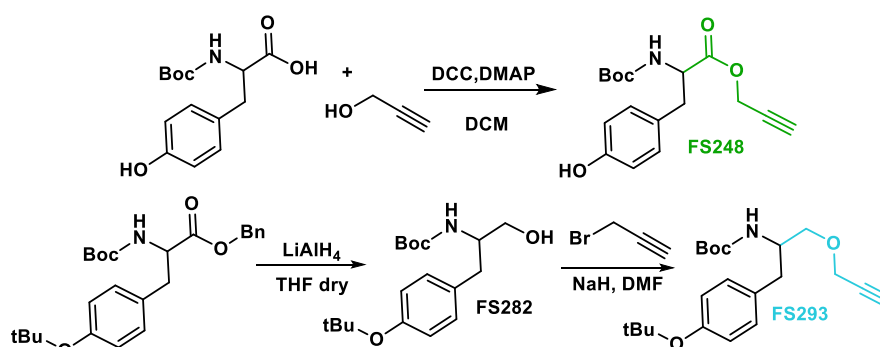


Fig.18 Synthetic steps for ester and ether derivatives.

For the formation of the ether, we couldn't directly use the ester previously synthesized so as not to risk the reduction of alkynic function, which is also sensitive to the action of LiAlH_4 . We then synthesised a benzyl ester and used this as a substrate for reduction to alcohol, which in turn was allowed to react with propargyl bromide to obtain the desired product. We also use the same benzyl ester as substrate for the synthesis of the amine of the tyrosine. For this purpose, instead of using LiAlH_4 , we used DIBAL-H at a controlled temperature to achieve reduction to aldehyde and, and then performed reductive amination with propargyl amine.

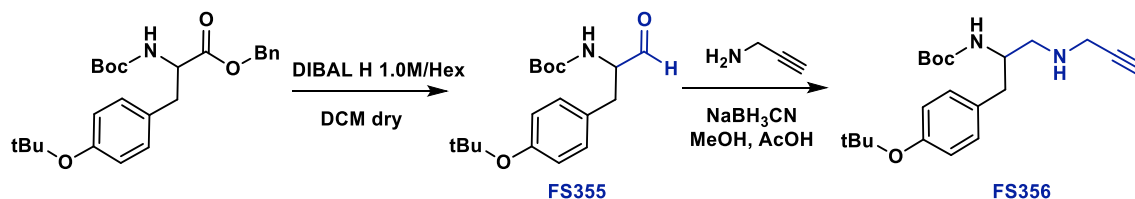


Fig.19 Reduction of Tyrosine to achieve the double amine derivative.

This intermediate will completely disrupt the interaction within the receptor because the acceptor hydrogen-bonding point, a function previously performed by the carbonyl due to the presence of oxygen, will be totally absent and a donor hydrogen-bonding point will be inserted instead.

2.7 – Introduction of coumarin

As previously mentioned, there are not many natural products with the characteristic of being active and selective towards the KOR receptor, but one of these is Salvinorin, and with the aim of mimicking its structure, we decided to include coumarin in our sequence instead of tyrosine. Coumarins are easy to synthesize and are also known to perform many biological functions and to be useful pharmacophores for UV-VIS analyses.

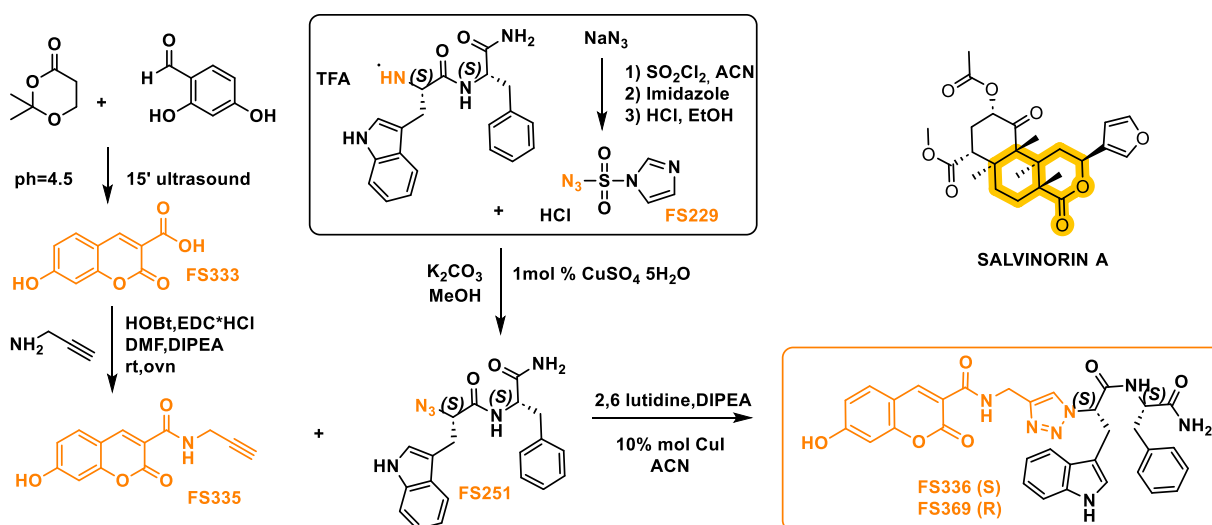


Fig.20 Synthetic steps for the introduction of coumarin inside the desired sequence.

We decided to synthesize the 7-hydroxycoumarin-3-carboxylic acid in order to have a structure easy to conjugate with the rest of the molecule. The carboxylic in fact, can be easily modified in order to obtain an amide or an ester. For this library, introduce again the terminal alkyne moiety because we didn't want to make any further changes apart from the substitution of tyrosine, so we decide to maintain the triazole structure before the tryptophane and the phenylalanine amide.

The synthesis of 7-hydroxycoumarin-3-carboxylic acid was carried out by sonicating Meldrum's acid and 2,4-dihydroxybenzaldehyde in the presence of a 4.5 pH buffer. After a few minutes, the phosphorescent yellow product is precipitated and easily recovered by filtration. A normal coupling reaction can be performed over this intermediate with the desired amine to obtain the alkyne moiety, for the synthesis of the ester derivative instead the other functional group must be considered and the coumarin must be previously treated with SOCl_2 in toluene in order to enhance the reactivity of the carboxyl acid, and then make it react with propargyl alcohol to obtain the desired product.



Fig.21 Synthesis of the ester derivative of 7-hydroxycoumarin-3-carboxylic acid.

After the two alkynes moiety were obtained, they have been made to react with the azide portion as previously described. Once again, the stereocentre of the tryptophane was changed for both final products in order to obtain four derivatives and start a little library of compounds. The idea is to continue this library with the reduction of the carboxylic acid in position three of the coumarin and produce similar, perfectly comparable, compounds to the previous library. Unfortunately, a synthetic route that takes into account the co-presence in coumarin's structure of so many functional groups sensitive to the action of reducing agents has yet to be devised.

2.8 – Conclusions

Following a careful analysis carried out on the k selective agonist discovered until now, the research group was able to modify the structure of the Endomorphine-1 with the introduction of a lactam like scaffold in place of the proline, that switch the selectivity from MOR to KOR. Starting from this encouraging result, we design and synthesize three libraries of compounds with the aim of introduce a trans conformation inductor moiety to tackle the k selectivity. In the first library we introduced four different amino acids in position three and we performed a cyclization on their side chain to

form a pseudoproline heterocycle. In the second library instead, we completely removed an amino acid with the introduction of a triazole on the behave of a peptidic bond and in the last library we introduce a coumarin scaffold instead of the tyrosine with the attempt to mime the structure of salvinorin, a well-known natural κ selective agonist. All the compounds were furthermore synthesized with the inverted stereocentre of the tryptophane to give more stability of all structures. Binding tests and functional assays are still ongoing, and we are still waiting for the result for further investigations.

2.9 – Experimental procedures

General information

All purchased reagents were used without further purifications. RP HPLC: Agilent 1100 series apparatus, with a RP column Phenomenex mod. Gemini 3 μ C18 110 Å 100 \times 3.0 mm, stationary phase octadecyl carbon chain-bonded silica with trimethylsilyl end-capping, fully porous organo-silica solid support, particle size 3 μ m, pore size 110 Å, length 100 mm, internal diameter 3 mm, DAD 210 and 254 nm, mobile phase from 8:2 to 1:9 water/CH₃CN, in 20 min, at a flow rate of 0.5 mL/min, followed by 10 min at the same composition.

Semipreparative RP-HPLC: Agilent 1100 series, RP column Waters XSelect Peptide CSHTM C18 OBDTM Prep Column 19 \times 150 mm 5 μ m, stationary phase octadecyl carbon chain bonded silica, double endcapped, particle size 7 μ m, pore size 130 Å, length 150 mm, internal diameter 19 mm, DAD 210 nm; mobile phase from H₂O/ CH₃CN (8:2) to CH₃CN (100%) in 10 min at a flow rate of 10 mL/min.

¹H-NMR (400 MHz) and ¹³C-NMR (101 MHz) spectroscopies were performed on a Varian Gemini 400 MHz instrument using the solvents CDCl₃, or DMSO-d₆. Chemical shifts (δ) are expressed in ppm and referenced to the appropriate NMR solvent peak(s). The following abbreviations are used to indicate multiplicity: s: singlet, d: doublet, t: triplet, m: multiplet.

Water suppression was achieved by the PRESAT procedure implemented in Varian. Proton resonance assignment was accomplished through gCOSY. VT 1H NMR experiments were recorded over the range of 298–348 K; temperature calibration was done with the ethylene glycol OHCH_n chemical shift separation method. 2D ROESY experiments were done at rt, phase-sensitive mode, spin-locking field (γb_2) = 2000 Hz, mixing time = 250 ms; spectra were processed in the hypercomplex approach; peaks were calibrated on solvent. Only ROESY-derived constraints were included in the restrained molecular dynamics (MD). Cross-peak intensities were ranked and associated to the distances (Å): very strong = 2.3, strong = 2.6, medium = 3.0, weak = 5.0. The

intensities of the cross peaks arising from protons separated by known distances (e.g., geminal) were found to match with these associations, but were discarded.

General synthesis of solution peptide synthesis

The general procedure is as follows: a mixture of Boc-amino acid (0.3 mmol) and 1-Hydroxybenzotriazole hydrate (HOBt*H₂O) (1.2 eq., 0.36 mmol) was stirred in 5mL of 3:1 DCM/DMF at rt, and after 10 minutes, the amino ester counterpart (1 eq., 0.3 mmol), N-Ethyl-N'-(3-dimethylaminopropyl) carbodiimide hydrochloride (EDC*HCl) (1.2 eq., 0.36 mmol) and triethylamine (TEA) (3 eq., 0.9 mmol) were added in sequence and the reaction was allowed to stir at room temperature. After 6 hours the solvent was removed, the residue was diluted with ethyl acetate and extracted with HCl 0.5M (2x), saturated NaHCO₃ (2x) and brine (1x). The organic phase was dried over MgSO₄, filtered, and evaporated under vacuum. The intermediate crude peptide sequences, obtained in quantitative yield, were analysed by RP HPLC, and used without further purifications.

Boc deprotection was accomplished by stirring the crude peptides in 1:3 TFA/DCM for 1 hour. Then the mixture was concentrated at reduce pressure and the crude triturated in Et₂Ox2. The peptide-TFA salts precipitate and were used without further purification for the next coupling.

Benzyl ester deprotection was accomplished by stirring the crude peptides in a mixture of EtOH with 10% of Pd/C overnight under hydrogen atmosphere at a pressure of 1atm. The catalyst was removed by filtration though celite and washed with methanol and DCM. The product was recollected and concentrated under vacuum.

General procedure for side-chain cyclization in solution

The general procedure is as follows: the peptide sequence with the free functional group ready to react was dissolved in a solution 3:1 DCM: DMF. N,N'-Disuccinimidyl carbonate (DSC) (2eq.) and DIPEA (2eq.) were added and the reaction was allowed to stir at room temperature for four hours. The solvent was then removed, and the residue was diluted with ethyl acetate and extracted with HCl 0.5M (2x), saturated NaHCO₃ (2x) and brine (1x). The organic phase was dried over MgSO₄, filtered, and evaporated under vacuum. The residue was purified by semipreparative RP HPLC on a C18 column with an isocratic program of 45% H₂O/ 55% ACN of 10 minutes at a flow rate of 10 mL/min and purity was confirmed by RP HPLC.

Boc deprotection of Tyrosine was always performed at the end following the general procedure.

TFA*H₂N-Tyr-(S)-Oxa-Trp-Phe-NH₂ (FS50)

Cyclization of FS28 (50 mg, 0.071 mmol), according to the general procedure, gave FS50 (46.6 mg, 0.06mmol, Y=100%). Purification was performed using a RP semipreparative with ACN and H₂O as solvents and the pure product was obtained as a white solid (8.3 mg, 0.01 mmol, Y=20%). The Boc protection was removed before the final characterization.

¹H NMR (DMSO-d₆, 400MHz): δ 10.84 (s,1H), 9.4 (s, 1H), 8.58-8.56 (d, 1H), 8.19 – 8.17 (m, 2H), 7.60 – 7.58 (d, 1H), 7.36 – 7.31 (m, 2H), 7.22 – 7.02 (m, 11H), 6.99 – 6.96 (m, 2H), 6.74 – 6.72 (d, 2H), 5.023 – 4.99 (dd, 1H), 4.94 – 4.92 (dd, 1H), 4.68 – 4.63 (t, 1H), 4.57 – 4.52 (ddd, 1H), 4.48 – 4.43 (ddd, 1H), 4.21 – 4.18 (dd, 1H), 3.20 – 3.17 (dd, 1H), 3.09 – 3.04 (dd,1H), 3.01 – 2.97 (dd,1H), 2.94 – 2.88(dd, 1H), 2.83 – 2.78 (dd, 1H), 2.72 – 2.65 (dd, 1H); **¹³C NMR :** δ 172.62, 170.35, 168.73, 167.34, 156.80, 152.90, 137.71, 136.03, 130.52, 129.24, 129.21, 128.02, 127.96, 127.34, 126.19, 124.32, 123.71, 120.88, 118.45, 118.35, 115.57, 111.25, 109.56, 109.37, 80.52, 77.93, 66.72, 55.19, 53.90, 53.59, 37.69; **HPLC-MS:** [M+1] = 727, [M+1-Boc] = 627, [2M+Na] = 1476

TFA*H₂N-Tyr-(S)-Imi-Trp-Phe-NH₂ (FS113)

Cyclization of FS97 (114 mg, 0.2 mmol), according to the general procedure, gave FS113 (56.8 mg, 0.08mmol, Y=40%). Purification was performed using a RP semipreparative with ACN and H₂O as solvents and the pure product was obtained as a white solid (7.8 mg, 0.01 mmol, Y= 12.5%). The Boc protection was removed before characterization.

¹H NMR (DMSO-d₆, 400MHz): δ 10.81 (s,1H), 9.36 (s,1H), 8.44 – 8.42 (d,1H), 8.13 (s,1H), 8.08 – 8.06 (d, 1H), 8.02 (s,2H), 7.60 – 7.58 (d, 1H), 7.33 – 7.31 (d, 1H), 7.28 (s,1H), 7.24 – 7.18 (m,4H), 7.16 – 7.14 (d, 2H), 7.12 – 7.07 (t, 2H), 7.06 – 6.98 (t , 1H), 6.72 – 6.70 (d, 2H), 5.05 (s, 1H), 4.87 – 4.83 (ddd, 1H), 4.55 – 4.49 (ddd, 1H), 4.46 – 4.41 (ddd, 1H), 3.66 – 3.61 (t, 1H), 3.22 – 3.19 (dd, 1H), 3.13 – 3.08 (dd, 1H), 3.01 – 2.96 (dd, 1H), 2.94 – 2.91 (dd, 1H), 2.83 – 2.76 (m, 2H), 2.66 – 2.63 (m , 1H); **¹³C NMR :** δ 172.98, 171.25, 158.70, 144.83, 138.18, 136.62, 135.42, 131.11, 129.76, 128.45, 127.72, 118.81, 115.90, 109.98, 93.14, 91.10, 84.46, 72.50, 69.17, 68.43, 53.89, 36.92; **HPLC-MS:** [M+1] = 726, [M+1-Boc] = 626, [2M+Na] = 1475

2-oxothiazolidine-4-carboxylic acid (FS180)

Cysteine (500mg, 4.11 mmol) was dissolved in 12.3 mL of NaOH 1M and at 0°C triphosgene (1.2g, 4.11 mmol) dissolved in 8.2 mL of dioxane, was slowly added. The reaction was allowed to stir at room temperature for three hours. The solvent was removed under vacuum and the residue is

washed with hot ACN. The solvent is filtrate and evaporated to give the pure product as a transparent oil (327.8 mg, 2.21 mmol, Y= 54%).

¹H NMR (DMSO-d₆, 400MHz): δ 8.435 (s,1H), 4.409 – 4.376 (dd, 1H), 3.74 – 3.69 (dd, 1H), 3.46 – 3.43 (dd, 1H); **HPLC-MS:** [M+1] = 149

TFA*H₂N-Tyr-(S)-Thiazo-Trp-Phe-NH₂ (FS216)

The general procedure of coupling reaction in solution on compound FS181 (50mg, 0.1 mmol) with the use of HBTU ad coupling reagent instead of HOBT*H₂O and EDC*HCl gave compound FS216 (59.44 mg, 0.08mmol). Purification was performed using a RP semipreparative with ACN and H₂O as solvents and the pure product was obtained as a white solid (6.3 mg, 0.008 mmol, Y= 11%). The Boc protection was removed before characterization.

¹H NMR (DMSO-d₆, 400MHz): δ 10.78 (s,1H), 9.29 (s,1H), 8.55 – 8.53 (d, 1H), 8.14 – 8.09 (m, 4H), 7.59 – 7.57 (d, 1H), 7.31 – 7.28 (m, 3H), 7.22 – 7.13 (m, 8H), 7.11 – 7.02 (m, 7H), 6.98 – 6.94 (t, 2H), 6.71 – 6.68 (d, 2H), 5.24 – 5.21 (ddd, 1H), 4.89 – 4.81 (m, 1H), 4.55 – 4.51 (dd, 1H), 4.47 – 4.42 (dd, 1H), 3.82 – 3.77 (dd, 1H), 3.25 – 3.21 (dd, 1H), 3.12 – 3.04 (m, 2H), 3.0 – 2.9 (m, 3H), 2.83 – 2.78 (dd, 1H), 2.65 – 2.6 (m, 1H); **¹³C NMR :** δ 175.2, 174.9, 171.7, 165.3, 155.7, 136.5, 130.2, 129.5, 128.3, 127.7, 125.9, 123, 121.7, 119.7, 118.8, 115.6, 11.1, 109.7, 59.4, 54.8, 51.02, 38.7, 37.1, 35.8, 27.9; **HPLC-MS:** [M+1] = 644

TFA*H₂N-Tyr-Piro-Trp-Phe-NH₂ (MF58)

Cyclization of MF53 (70 mg, 0.094 mmol), according to the general procedure, gave MF58 (64,2 mg, 0.09 mmol, Y=100%). Purification was performed using a RP semipreparative with ACN and H₂O as solvents and the pure product was obtained as a white solid (20 mg, 0.02 mmol, Y=31%). The Boc protection was removed before the final characterization.

¹H NMR (DMSO-d₆, 400MHz): δ 10.81 (s,1H), 9.38 (s, 1H), 8.48-8.46 (d, 1H), 8.09 (s,1H), 7.98 – 7.96 (d, 1H), 7.60 – 7.58 (d, 1H), 7.32 – 7.30 (d, 1H), 7.28 – 7.25 (s, 1H), 7.16 – 7.24 (m, 5H), 7.13 – 7.11 (d, 1H), 7.08 – 7.06 (m, 2H), 6.99 – 6.96 (m, 1H), 6.74 – 6.72 (d, 2H), 6.53 (s, 1H), 5.023 – 4.99 (dd, 1H), 4.84 – 4.82 (dd, 1H), 4.48 – 4.47 (dd, 1H), 3.11 – 3.09 (dd,1H), 3.07 – 3.05 (dd, 1H), 3.01 – 2.97 (dd,1H), 2.94 – 2.88(dd, 1H), 2.83 – 2.78 (m, 2H), 2.62 – 2.59 (dd, 1H), 2.58 – 2.56 (dd, 1H), 2.3 – 2.28 (m, 1H), 1.87 – 1.85 (m,1H); **¹³C NMR :** δ 175.7, 175.2, 174.9, 171.7, 171.1, 155.7, 136.6, 130.2, 129.3, 128.8, 127.6, 127.4, 125.9, 123, 121.7, 119.8, 118.6, 115.8, 111.1, 109.7, 59.5, 59.4, 52.6, 51.1, 38.6, 37.3, 30.7, 27.9, 23.2; **HPLC-MS:** [M+1] = 725, [2M+Na] = 1471.

TFA*H₂N-Tyr-(R)-Oxa-Trp-Phe-NH₂ (FS221AD) and TFA*H₂N-Tyr-dehydro-Trp-Phe-NH₂ (FS221AC)

Cyclization of FS220 (65.7 mg, 0.09 mmol), according to the general procedure, gave FS221 (62.3 mg, 0.08mmol, Y=95%). Purification was performed using a RP semipreparative with ACN and H₂O as solvents and the pure product was obtained as a white solid (9.4 mg, 0.01 mmol, Y=16.2%). Since the product is unstable, from the mass spectrum it was observed a partial degradation in dehydroalanine. The purification was performed again before the Boc deprotection and final characterization to obtain the two pure products (FS221AD 0.6mg, FS221AC 0.7mg).

¹H NMR FS221AD (DMSO-d₆, 400MHz): δ 10.81 (s,1H), 9.36 (s,1H), 8.55 – 8.52 (d, 1H), 8.24 – 8.22 (d, 1H), 7.60 – 7.58 (d,1H), 7.41 (s, 1H), 7.33 – 7.18 (m, 4H), 7.11 – 6.94 (m, 7H), 6.71 – 6.68 (d,2H), 4.93 – 4.87 (m, 1H), 4.64 – 4.59 (m, 2H), 4.50 – 4.45 (ddd, 1H), 4.23 – 4.19 (t, 1H), 3.47 – 3.43 (dd, 2H), 3.18 – 2.95 (m , 4H); **HPLC-MS:** [M+1] = 627.

¹H NMR FS221AC (DMSO-d₆, 400MHz): δ 10.77 (s,1H), 9.31 – 9.30 (d, 1H), 8.43 – 8.41 (d, 1H), 8.05 – 8.03 (d, 1H), 7.65 – 7.63 (d, 1H), 7.27 – 7.14 (m, 4H), 7.11 – 6.95 (m, 7H), 6.69 – 6.66 (d,2H), 6.16 (s,1H), 5.49 (s,1H), 4.78 – 4.76 (dd, 1H), 4.51 – 4.46 (dd, 1H), 4.40 – 4.38 (dd, 1H), 3.73 – 3.68 (dd, 1H), 2.91 – 2.72 (m, 6H); **HPLC-MS:** [M+1] = 584.

TFA*H₂N-Tyr-(R)-Pyro-Trp-Phe-NH₂ (MF69)

Cyclization of MF67 (170 mg, 0.23 mmol), according to the general procedure, gave MF69 (140 mg, 0.19 mmol, Y=84%). Purification was performed using a RP semipreparative with ACN and H₂O as solvents and the pure product was obtained as a white solid (10 mg, 0.01 mmol, Y=7%). The Boc protection was removed before the final characterization.

¹H NMR (DMSO-d₆, 400MHz): δ 10.79 (s,1H), 8.36 (s,1H), 8.4 – 8.38 (d,1H), 8.09 – 8.07 (d,1H), 7.59 – 7.57 (d,1H), 7.42 (s,1H), 7.20 – 7.32 (m,5H), 6.98 – 7.07 (m, 4H), 6.97 – 6.94 (d, 2H), 6.93 – 6.91 (d,2H), 6.70 – 6.68 (d,2H), 4.64 (m,1H), 4.58 – 4.56 (dd,1H), 4.48 – 4.46 (m,1H), 4.07 – 4.05 (m,1H), 3.17 – 3.14 (dd,1H), 3.02 – 3.0 (dd,1H), 2.87 – 2.85 (m,1H), 2.83 – 2.81 (dd,1H), 2.80 – 2.78 (m, 1H), 2.73 – 2.7 (m,1H), 2.21 – 1.98 (m,1H), 1.93 – 1.89 (m,1H), 1.24 – 1.21 (m,1H); **HPLC-MS:** [M+1] = 725, [2M+Na] = 1471

TFA*H₂N-Tyr-(R)-Imi-Trp-Phe-NH₂ (MF66)

Cyclization of MF55 (58 mg, 0.08 mmol), according to the general procedure, gave MF60 (57 mg, 0.07mmol, Y= 77.6%). Purification was performed using a RP semipreparative with ACN and H₂O as solvents and the pure product was obtained as a white solid (7.8 mg, 0.01 mmol, Y= 12.5%). The Boc

protection was removed before characterization of the final product MF66.

¹H NMR (DMSO-d₆, 400MHz): δ 10.8 (s,1H), 9.36 (s,1H), 8.44 – 8.42 (d,1H), 8.12 (s,1H), 8.08 – 8.06 (d, 1H), 7.93 (s,1H), 7.60 – 7.58 (d, 1H), 7.43 (s,1H), 7.33 – 7.31 (d, 1H), 7.28 – 7.25 (m,5H), 7.06 – 7.04 (dd, 2H), 7.02 – 6.99 (d, 2H), 6.98 – 6.96 (dd, 1H), 6.69 – 6.67 (d, 2H), 6.52 (s, 1H), 5.11 (s, 1H), 4.67 – 4.64 (dd, 1H), 4.55 – 4.49 (dd, 1H), 4.46 – 4.41 (dd, 1H), 3.38 – 3.36 (dd, 1H), 3.14 – 3.11 (dd, 1H), 3.04 – 3.03 (dd, 1H), 3.01 – 2.98 (dd, 1H), 2.84 – 2.82 (dd, 1H), 2.81 – 2.79 (m, 2H), 2.78 – 2.75 (dd, 1H), 2.44 – 2.42 (dd,1H); **¹³C NMR :** δ 172.98, 171.25, 158.70, 144.83, 138.18, 136.62, 135.42, 131.11, 129.76, 128.45, 127.72, 118.81, 115.90, 109.98, 93.14, 91.10, 84.46, 72.50, 69.17, 68.43, 53.89, 36.92; **HPLC-MS:** [M+1] = 725.4, [M+1-Boc] = 625.4, [M+Na] = 747.4

1H-imidazole-1-sulfonyl azide (FS229)

Sulfonyl chloride (5mmol, 405μL) was added dropwise to an ice-cooled suspension of NaN₃ (5mmol, 325 mg) in 5 mL of acetonitrile. The solution was allowed to reach room temperature and stirred overnight. The day after, the reaction was brought at 0°C again and imidazole (2eq., 10mmol, 680mg) was slowly added. The reaction is allowed to reach room temperature and stirred for three hours. The mixture is diluted with 10mL of EtOAc and extracted with H₂O (2x 10mL) and NaHCO₃ sat (2x 10mL). The organic phase was dried over MgSO₄ and filtered. A solution of HCl in EtOH (obtained by the drop-wise addition of AcCl (1.5 eq., 533.3 μL) to ice-cooled dry ethanol (2 mL)) was added dropwise to the filtrate with stirring, the mixture chilled in an ice-bath, filtered and the filter cake washed with EtOAc to give the product as colourless needles. (1.5mmol, 317.3 mg, Y=30%).

¹H NMR (D₂O, 400MHz): δ 7.68 (dd, 1 H), 8.09 (dd, 1 H), 9.53 (dd); **¹³C NMR:** δ 120.8, 123.4, 138.3.

Tert-butyl (3-(4-hydroxyphenyl)-1-oxo-1-(prop-2-yn-1-ylamino)propan-2-yl)carbamate (FS244)

The product was obtained following the general coupling in solution procedure (0.5 mmol, Y=quant).

¹H NMR (DMSO-d₆, 400MHz): δ 9.14 (s, 1H), 8.32 – 8.3 (t, 1H), 7.02 – 7.00 (d, 2H), 6.8 – 6.77 (d, 1H), 6.63 – 6.61 (d, 2H), 4.06 – 3.99 (ddd, 1H), 3.85 – 3.84 (d, 2H), 3.11 – 3.10 (t, 1H), 2.80 – 2.76 (dd, 1H), 2.62 – 2.56 (dd, 1H), 1.29 (s, 9H); **HPLC-MS:** [M+1] = 319, [M+1-Boc] = 219, [M+Na] = 342

prop-2-yn-1-yl (tert-butoxycarbonyl)tyrosinate (FS248)

DCC (1.5 eq., 83.34 mg) was added to an ice cooled solution of BocTyr(OBz)OH (0.26 mmol, 100mg) and propargyl alcohol (2eq., 31.35 μL) in 5 mL of DCM. After 5 minutes DMAP (0.4 eq., 12.7 mg) was added, and the reaction was allowed to stir at room temperature overnight. The day after water

was added and the crude product is extracted with 10% of MeOH. The mixture is purified with flash chromatography using EtOAc: Exane (2:8) as solvents to give the pure product (0.1mmol, Y= 40%).

¹H NMR (DMSO-d₆, 400MHz): δ 7.41 – 7.28 (m,5H), 7.06 – 7.04 (d, 2H), 6.89 – 6.87 (d,2H), 5.01 (s, 2H), 4.6 – 4.52 (d, 1H), 3.22 – 3.14 (m, 1H), 3.09 – 2.98 (m, 2H), 2.47 – 2.45 (t, 1H), 1.94 – 1.96 (m, 1H), 1.75 – 1.68 (m,1H), 1.4 (s, 9H); **HPLC-MS:** [M+1] = 410, [M+1-Boc] = 310, [M+Na] = 433

N₃-Trp-Phe-NH₂ (FS251)

FS229 (1.2eq., 0.64 mmol, 135.12 mg) is added to a suspension of TFA*H₂N-Trp-Phe-NH₂ (0.54 mmol, 250 mg), K₂CO₃ (2eq., 1.07 mmol, 148.93 mg) and 1mol% of CuSO₄*H₂O (0.0054 mmol, 1.34 mg) in 3mL of MeOH. The reaction was allowed to stir at room temperature for seven hours and monitored with TLC. The solvent was removed, the residue is diluted with 5mL of HCl 1M and extracted with EtOAc (3x 5mL). The organic phase was recollected and dried over MgSO₄, filtered, and evaporated under vacuum to give the pure product as a pale-yellow solid (0.5mmol, Y=100%).

HPLC-MS: [M+1] = 377, [M+Na] = 399

(S)-2-amino-N-(((S)-1-(((S)-1-amino-1-oxo-3-phenylpropan-2-yl)amino)-3-(1H-indol-3-yl)-1-oxopropan-2-yl)-1H-1,2,3-triazol-4-yl)methyl)-3-(4-hydroxyphenyl)propanamide (FS262)

FS255 (0.18mmol, 70mg) and FS244 (0.18mmol, 60mg) are dissolved in 2mL of ACN under argon atmosphere. DIPEA (2eq., 0.37 mmol, 65μL), 2,6 lutidine (2eq., 0.37 mmol, 45 μL) and last of all 10% Cul (0.02 mmol, 3.8 mg) were added to the solution and the reaction was allowed to stir under inert atmosphere at room temperature overnight. Then the solvent was removed, the residue was dissolved in 5mL of HCl 1M and extracted with EtOAc (3x 5mL). The organic phase was recollected and dried over MgSO₄, filtered, and evaporated under vacuum to give the pure product as a pale-yellow solid (0.15 mmol, Y=83%). Purification was performed using a RP semipreparative with ACN and H₂O as solvents and the pure product was obtained as a white solid (34.5 mg, 0.05 mmol, Y= 33.2%). The Boc protection was removed before characterization of the final product FS262.

¹H NMR (DMSO-d₆, 400MHz): δ 10.74 (s,1H), 9.32 (s,1H), 8.85 – 8.79 (m, 2H), 8.03 (s, 2H), 7.91 (s,1H), 7.62 – 7.60 (d, 1H), 7.48 (s, 1H), 7.25 – 7.23 (d, 1H), 7.14 – 7.10 (m, 4H), 7.03 – 6.93 (m, 4H), 6.877 – 6.872 (d, 1H), 6.68 – 6.65 (d, 2H), 5.76 – 5.72 (dd, 1H), 4.48 – 4.43 (ddd, 1H), 4.41 – 4.36 (dd, 1H), 4.25 – 4.20 (dd, 1H), 3.9 – 3.82 (m, 1H), 3.5 – 3.44 (m, 2H), 3.04 – 2.99 (dd, 1H), 2.97 – 2.92 (dd, 1H), 2.83 – 2.76 (m, 2H); **¹³C NMR:** δ 172.72, 168.39, 168.09, 156.98, 143.43, 137.96, 136.36, 130.86, 129.48, 128.44, 127.24, 126.65, 125.22, 124.02, 122.45, 121.50, 118.78, 115.79, 111.79, 109.99, 108.83, 65.33, 63.16, 54.49, 54.24, 38.06, 36.74, 15.59; **HPLC-MS:** [M+1] = 695.

(1-(1-((1-amino-1-oxo-3-phenylpropan-2-yl)amino)-3-(1H-indol-3-yl)-1-oxopropan-2-yl)-1H-1,2,3-triazol-4-yl)methyl tyrosinate (FS272)

The same procedure described for FS262 was performed on FS248 for the synthesis of FS268 as a crude product (168.9 mg, 0.21 mmol, Y= 97 %). Purification was performed using a RP semipreparative with ACN and H₂O as solvents and the pure product was obtained as a white solid (17.8 mg, 0.02 mmol, Y= 11 %). The benzyl and the Boc protection were removed in this order before characterization of the final product FS272.

¹H NMR (DMSO-d₆, 400MHz): δ 10.78 (s, 1H), 9.42 (s, 1H), 8.91 – 8.89 (d, 1H), 8.16 (s, 1H), 7.65 – 7.63 (d, 1H), 7.53 (s, 1H), 7.27 – 7.26 (d, 1H), 7.17 – 7.08 (m, 3H), 7.05 – 7.01 (t, 1H), 6.98 – 6.91 (m, 3H), 6.69 – 6.67 (d, 2H), 5.77 – 5.73 (dd, 1H), 5.21 – 5.06 (dd, 2H), 4.47 – 4.42 (ddd, 1H), 4.20 – 4.17 (t, 1H), 3.10 – 3.04 (dd, 1H), 3.03 – 2.91 (m, 3H), 2.80 – 2.75 (dd, 1H); **¹³C NMR:** δ 172.75, 169.38, 167.93, 157.09, 140.64, 137.93, 136.36, 130.93, 129.46, 128.42, 127.20, 126.64, 124.77, 124.54, 124.15, 121.49, 118.79, 115.87, 108.71, 75.01, 72.87, 63.31, 54.49, 53.81, 46.13, 35.65, 17.66, 17.38, 17.34, 9.0; **HPLC-MS:** [M+1] = 595, [M+Na] = 617

(S)-2-amino-N-((1-((R)-1-((S)-1-amino-1-oxo-3-phenylpropan-2-yl)amino)-3-(1H-indol-3-yl)-1-oxopropan-2-yl)-1H-1,2,3-triazol-4-yl)methyl)-3-(4-hydroxyphenyl)propenamide (FS287)

The same procedure described for FS262 was performed on the (d)-Trp analogue of FS251 (N₃-(D)-Trp-Phe-NH₂ (FS285)) for the synthesis of MSP71B as a crude product (150 mg, 0.21 mmol, Y= 97 %). Purification was performed using a RP semipreparative with ACN and H₂O as solvents and the pure product was obtained as a white solid (49 mg, 0.07 mmol, Y= 34 %). The Boc protection was removed before characterization of the final product FS287.

¹H NMR (DMSO-d₆, 400MHz): δ 10.756 – 10.751 (d, 1H), 9.34 (s, 1H), 8.98 – 8.96 (d, 1H), 8.84 – 8.81 (t, 1H), 8.09 (s, 1H), 8.06 (s, 1H), 7.65 – 7.63 (d, 1H), 7.59 (s, 1H), 7.29 – 7.28 (d, 1H), 7.24 – 7.17 (m, 5H), 7.12 (s, 1H), 7.08 – 7.06 (dd, 1H), 7.04 – 7.03 (dd, 1H), 7.015 – 6.99 (d, 2H), 6.81 – 6.80 (d, 1H), 6.70 – 6.68 (d, 2H), 5.75 – 5.72 (dd, 1H), 4.54 – 4.49 (ddd, 1H), 4.39 – 4.34 (d, 1H), 4.28 – 4.23 (d, 1H), 3.87 (s, 1H), 3.21 – 3.14 (dd, 1H), 3.05 – 2.93 (m, 3H), 2.82 – 2.72 (m, 2H); **¹³C NMR:** δ 172.91, 168.33, 167.92, 156.96, 143.42, 138.01, 136.37, 130.86, 129.71, 128.45, 127.18, 126.77, 125.19, 124.11, 122.63, 121.49, 118.92, 118.80, 115.78, 111.76, 108.74, 65.33, 63.27, 54.21, 54.14, 38.42, 36.70, 34.74, 29.02, 17.24, 17.23, 15.59; **HPLC-MS:** [M+1] = 595, [M+Na] = 617

(1-((R)-1-(((S)-1-amino-1-oxo-3-phenylpropan-2-yl)amino)-3-(1H-indol-3-yl)-1-oxopropan-2-yl)-1H-1,2,3-triazol-4-yl)methyl L-tyrosinate (FS297)

The same procedure described for FS262 was performed on FS248 and the (d)-Trp analogue of FS251 (N₃-(D)-Trp-Phe-NH₂ (FS285)) for the synthesis of FS288 as a crude product (55 mg, 0.07 mmol, Y= 78 %). Purification was performed using a RP semipreparative with ACN and H₂O as solvents and the pure product was obtained as a white solid (31 mg, 0.04 mmol, Y= 56 %). The benzyl and the Boc protection were removed in this order before characterization of the final product FS297.

¹H NMR (DMSO-d₆, 400MHz): δ 10.72 (s, 1H), 9.37 (s,1H), 9.00 – 8.98 (d, 1H), 8.29 (s, 1H), 7.63 – 7.61 (d, 1H), 7.59 (s, 1H), 7.25 – 7.20 (m, 3H), 7.19 – 7.12 (m, 2H), 7.09 (s, 1H), 7.06 – 6.97 (m, 3H), 6.94 – 6.92 (d, 2H), 6.78 – 6.77 (d, 1H), 6.65 – 6.63 (d, 2H), 5.75 – 5.71 (dd, 1H), 5.20 – 5.08 (dd, 2H), 4.52 – 4.46 (ddd, 1H), 4.17 – 4.14 (t, 1H), 3.16 – 3.12 (dd, 1H), 3.00 – 2.97 (m, 2H), 2.90 – 2.88 (d, 2H), 2.75 – 2.69 (dd, 1H); **¹³C NMR:** δ 172.93, 169.51, 167.85, 157.05, 140.80, 138.05, 136.37, 130.91, 129.72, 128.46, 127.15, 126.78, 124.89, 124.66, 124.22, 121.47, 118.92, 118.79, 115.85, 111.77, 110.18, 108.62, 63.66, 59.13, 54.22, 53.88, 35.91, 28.95, 16.43; **HPLC-MS:** [M+1] = 687.

tert-butyl (1-(4-(tert-butoxy)phenyl)-3-hydroxypropan-2-yl)carbamate (FS282)

BocTyr(OtBu)oBn (0.68mmol, 292.9 mg) is dissolved in 4mL of THF dry under argon atmosphere. The reaction is cooled at 0°C and LiAlH₄ (3 eq., 2.04mmol, 77.42mg) is slowly added. After 10 minutes the reaction is allowed to reach room temperature and it is stirred for one hour. Quenching is made with 5mL of KOH 10% and the product is extracted with EtOAc (3x5mL) The organic phase was recollected and dried over MgSO₄, filtered, and evaporated under vacuum to give the product (0.55 mmol, Y=80%). The crude product is purified with a flash chromatography using a solution of Exane:EtOAc 6:4 as eluent (0.3 mmol, Y=51%). **HPLC-MS:** [M+1] = 324.

tert-butyl (1-(4-(tert-butoxy)phenyl)-3-(prop-2-yn-1-yloxy)propan-2-yl)carbamate (FS293)

FS282 (0.27 mmol, 90 mg) in 2mL of DMF was added dropwise in a precooled suspension of NaH (2.1 eq., 0.58 mmol, 14 mg) in 2mL of DMF. Propargyl bromide (0.27 mmol, 25 μL) was added and the reaction was allowed to stir at room temperature for three hours. H₂O was added for quenching and the solvent evaporated. The residue was dissolved in 5mL of EtOAc and extracted with HCl 1M (3x 5mL). The organic phase was recollected and dried over MgSO₄, filtered, and evaporated under vacuum to give the pure product as a white solid (0.17 mmol, Y=63%).

HPLC-MS: [M+1] = 362.

(S)-N-((S)-1-amino-1-oxo-3-phenylpropan-2-yl)-2-(4-(((S)-2-amino-3-(4-hydroxyphenyl)propoxy)methyl)-1H-1,2,3-triazol-1-yl)-3-(1H-indol-3-yl)propenamide (FS302)

The same procedure described for FS262 was performed on FS293 for the synthesis of FS296 as a crude product (59 mg, 0.08 mmol, Y= 100 %). Purification was performed using a RP semipreparative with ACN and H₂O as solvents and the pure product was obtained as a white solid (10.8 mg, 0.01 mmol, Y= 18 %). The tBu and the Boc protection were removed together before characterization of the final product FS302.

¹H NMR (DMSO-d₆, 400MHz): δ 10.78 (s, 1H), 9.34 (s, 1H), 8.88 – 8.86 (d, 1H), 8.13 (s, 1H), 7.9 (s, 1H), 7.66 – 7.64 (d, 1H), 7.53 (s, 1H), 7.29 – 7.27 (d, 1H), 7.19 – 6.95 (m, 10H), 6.92 (s, 1H), 6.72 – 6.70 (d, 2H), 5.77 – 5.73 (dd, 1H), 4.49 – 4.44 (m, 1H), 3.49 – 3.37 (m, 4H), 3.03 – 2.67 (m, 5H); ¹³C NMR: δ 173.54, 168.91, 157.54, 143.94, 138.79, 137.17, 131.44, 130.29, 129.24, 128.04, 127.11, 124.72, 122.30, 119.56, 116.65, 112.92, 109.66, 69.91, 66.14, 63.98, 55.69, 52.56, 35.91, 32.08, 29.65, 17.43, 16.40; HPLC-MS: [M+1] = 582, [M+Na] = 604

(R)-N-((S)-1-amino-1-oxo-3-phenylpropan-2-yl)-2-(4-(((S)-2-amino-3-(4-hydroxyphenyl)propoxy)methyl)-1H-1,2,3-triazol-1-yl)-3-(1H-indol-3-yl)propenamide (FS301)

The same procedure described for FS302 was performed with the (d)-Trp analogue of FS251 (N₃-(D)-Trp-Phe-NH₂ (FS285)) for the synthesis of FS294 as a crude product (54 mg, 0.07 mmol, Y= 100 %). Purification was performed using a RP semipreparative with ACN and H₂O as solvents and the pure product was obtained as a white solid (8.1 mg, 0.01 mmol, Y= 14 %). The tBu and the Boc protection were removed together before characterization of the final product FS301.

¹H NMR (DMSO-d₆, 400MHz): δ 10.73 (s, 1H), 9.33 (s, 1H), 9.02 – 9.00 (d, 1H), 8.29 (s, 1H), 7.89 (s, 2H), 7.66 – 7.64 (d, 1H), 7.62 (s, 1H), 7.29 (s, 1H), 7.27 – 6.99 (m, 7H), 6.69 (s, 1H), 6.71 – 6.69 (dd, 2H), 5.77 – 5.73 (dd, 1H), 4.51 – 4.43 (m, 3H), 3.50 – 3.47 (m, 2H), 3.21 – 3.14 (dd, 1H), 3.05 – 2.99 (m, 2H), 2.78 – 2.62 (m, 3H); ¹³C NMR: δ 172.98, 167.99, 156.71, 143.10, 138.07, 136.35, 130.62, 129.72, 128.46, 127.16, 126.29, 124.04, 121.99, 121.29, 118.47, 115.83, 111.59, 108.73, 70.20, 68.51, 65.06, 63.97, 53.89, 52.21, 35.51, 29.26, 16.52.; HPLC-MS: [M+1] = 593.

tert-butyl (1-(4-(tert-butoxy)phenyl)-3-oxopropan-2-yl)carbamate (FS355)

Boc-Tyr-(tBu)-OBn (0.89 mmol, 380.4 mg) was dissolved in 5mL of DCM dry and DIBAL-H (1.0M in hexane) (2.2 eq., 3mL) was slowly added at -78°C. The solution is allowed to stir for three hours and then it was quenched with 1mL of ETOH. 2mL of saturated solution of Rochelle salts were added

and the reaction was allowed to stir at room temperature overnight. The next day the aqueous phase was extracted with EtOAc (3x 8mL), all the organic phases were recollected and extracted once with brine, dried over MgSO₄, filtered, and evaporated under vacuum to give the product (0.80 mmol, Y=94%).

¹H NMR (DMSO-d₆, 400MHz): δ 9.50 (s, 1H), 7.20 – 7.17 (m, 1H), 7.00 – 6.94 (d, 2H), 6.83 – 6.80 (d, 2H), 2.97 – 2.92 (m, 1H), 2.67 – 2.66 (d, 1H), 2.31 (s, 1H), 1.33 (s, 9H), 1.23 (s, 9H); **HPLC-MS:** [M+1] = 314.

tert-butyl (1-(4-(tert-butoxy)phenyl)-3-(prop-2-yn-1-ylamino)propan-2-yl)carbamate (FS356)

Propargylamine (1.2 eq., 1.068 mmol, 70 μL) was dissolved in 10mL of MeOH, acetic acid was added (100 μL) and the reaction was allowed to stir for 5 minutes. FS355 was added slowly followed by NaBH₃CN and the reaction was allowed to stir overnight. The day after the solvent was removed, the residue was dissolved in 10 mL of EtOAc and extracted with brine (3x 10mL). All the organic phases were recollected, dried over MgSO₄, filtered, and evaporated under vacuum. The product was purified with flash chromatography using as solvents EtOAc and Exane (6:4) (0.31 mmol, 112 mg, Y = 35%)

¹H NMR (DMSO-d₆, 400MHz): δ 7.00 – 6.99 (d, 2H), 6.81 – 6.79 (d, 2H), 4.71 – 4.69 (d, 1H), 3.79 (s 1H), 3.36 – 3.28 (dd, 2H), 2.69 – 2.59 (m, 3H), 2.08 (s, 1H), 1.33 (s, 9H), 1.23 (s, 9H); **HPLC-MS:** [M+1] = 361.

(S)-N-((S)-1-amino-1-oxo-3-phenylpropan-2-yl)-2-(4-(((S)-2-amino-3-(4-hydroxyphenyl)propyl)amino)methyl)-1H-1,2,3-triazol-1-yl)-3-(1H-indol-3-yl)propenamide (FS364)

FS251 (0.18mmol, 70mg) and FS356 (0.18mmol, 64.8 mg) are dissolved in 2mL of ACN under argon atmosphere. DIPEA (2eq., 0.37 mmol, 65μL), 2,6 lutidine (2eq., 0.37 mmol, 45 μL) and last of all 10% Cul (0.02 mmol, 3.8 mg) were added to the solution and the reaction was allowed to stir under inert atmosphere at room temperature overnight. The day after, the solvent was removed, and purification was performed directly using a RP semipreparative with ACN and H₂O as solvents. The pure product was obtained as a brown oil (17.9 mg, 0.02 mmol, Y= 13.5 %). The tBu and the Boc protection were removed together before characterization of the final product FS364.

¹H NMR (DMSO-d₆, 400MHz): δ 10.79 (s, 1H), 8.94 – 8.92 (d, 1H), 8.19 (s, 1H), 7.64 – 7.62 (d, 1H), 7.53 (s, 1H), 7.26 – 7.24 (d, 1H), 7.24 – 6.91 (m, 11H), 6.71 – 6.69 (d, 2H), 5.81 – 5.77 (dd, 1H), 4.45 – 4.40 (ddd, 1H), 4.22 – 4.13 (dd, 2H), 3.62 – 3.5 (m, 1H), 3.36 – 3.33 (m, 2H), 3.16 – 3.06 (m, 2H),

3.00 – 2.96 (dd, 1H), 2.78 – 2.73 (m, 3H); $^{13}\text{C NMR}$: δ 172.71, 167.90, 157.05, 156.80, 137.97, 136.43, 136.35, 130.78, 130.70, 129.50, 129.46, 128.44, 128.40, 127.24, 127.18, 126.66, 125.43, 124.71, 124.13, 121.55, 118.82, 115.99, 115.87, 111.83, 108.59, 65.34, 63.27, 54.58, 50.08, 48.55, 42.60, 38.09, 36.04, 28.89, 15.59; **HPLC-MS**: $[M+1] = 581$

(R)-N-((S)-1-amino-1-oxo-3-phenylpropan-2-yl)-2-(4-(((S)-2-amino-3-(4-hydroxyphenyl)propyl)amino)methyl)-1H-1,2,3-triazol-1-yl)-3-(1H-indol-3-yl)propenamide (FS380)

The same procedure described for FS364 was performed with the (d)-Trp analogue of FS251 (N_3 - (D)-Trp-Phe-NH₂ (FS285)) for the synthesis of FS380 as a crude product. Purification was performed directly using a RP semipreparative with ACN and H₂O as solvents and the pure product was obtained as a white solid (9.5 mg, 0.01 mmol, Y= 14 %). The tBu and the Boc protection were removed together before characterization of the final product.

$^1\text{H NMR}$ (DMSO-d₆, 400MHz): δ 10.73 (s, 1H), 9.33 (s, 1H), 7.28 – 7.22 (m, 9H), 7.03 – 7.01 (d, 2H), 7.00 (s, 1H), 6.81 – 6.79 (d, 2H), 6.64 (s, 1H), 6.19 – 6.16 (t, 1H), 4.87 (s, 2H), 4.81 – 4.79 (t, 1H), 4.73 (s, 1H), 3.93 – 3.88 (d, 2H), 3.56 – 3.52 (dd, 1H), 3.32 – 3.28 (dd, 1H), 3.14 – 3.11 (dd, 1H), 2.97 – 2.91 (m, 3H), 2.70 – 2.67 (ddd, 1H), 2.55 – 2.51 (dd, 1H), 1.52 (s, 1H), 1.12 – 1.07 (d, 2H); $^{13}\text{C NMR}$: δ 172.98, 167.99, 156.71, 143.10, 138.07, 136.35, 130.62, 129.72, 128.46, 127.16, 126.29, 124.04, 121.99, 121.29, 118.47, 115.83, 111.59, 108.73, 70.20, 68.51, 65.06, 63.97, 53.89, 52.21, 35.51, 29.26, 16.52; **HPLC-MS**: $[M+1] = 593$.

7-hydroxycoumarin-3-carboxylic acid (FS333)

Meldrum's acid (1.01 eq., 2.92 mmol, 421.57 mg) and 2,4-dihydroxybenzaldehyde (2.89 mmol, 400 mg) were suspended in 10mL of 4.5 pH buffer. The suspension was irradiated with ultrasound for 15 minutes and the pure product precipitated and was filtrated (2.17 mmol, 447.7 mg, Y= 45%).

$^1\text{H NMR}$ (DMSO-d₆, 400MHz): δ 14.9 (s,1H), 10.4 (s,1H), 8.52 (s, 1H), 7.51 – 7.49 (d, 1H), 6.81 – 6.79 (d, 1H), 6.74 (s, 1H); $^{13}\text{C NMR}$: δ 166.2, 158.1, 157.3, 155.7, 148.5, 130.2, 118.3, 112.6, 110.5, 102.4; **HPLC-MS**: $[M+1] = 207$, $[M+\text{Na}] = 229$

7-hydroxycoumarin-N-(prop-2-yn-1-yl)-3-carboxamide (FS335)

The same procedure described for FS244 was performed with FS333 to obtain FS335 as pure product (0.39 mmol, 94.8 mg, Y = 85%).

$^1\text{H NMR}$ (DMSO-d₆, 400MHz): δ 11.08 (s, 1H), 8.87 – 8.84 (t, 1H), 8.80 (s, 1H), 7.83 – 7.81 (d, 1H),

6.89 – 6.86 (dd, 1H), 6.80 (s, 1H), 4.11 – 4.09 (dd, 2H), 3.14 – 3.13 (t, 1H); ¹³C NMR: δ 162.97, 162.15, 160.87, 155.81, 130.69, 129.89, 116.90, 113.88, 112.30, 102.54, 76.30, 71.85, 30.64; HPLC-MS: [M+1] = 207, [M+Na] = 229.

N-((1-((S)-1-(((S)-1-amino-1-oxo-3-phenylpropan-2-yl)amino)-3-(1H-indol-3-yl)-1-oxopropan-2-yl)-1H-1,2,3-triazol-4-yl)methyl)-7-hydroxy-2-oxo-2H-chromene-3-carboxamide (FS336)

The same procedure described for FS262 was performed on F335 for the synthesis of FS336 as a crude product (159.6 mg, 0.25 mmol, Y = 100 %). Purification was performed with precipitation in MeOH to obtain the pure product as a white solid (28.9 mg, 0.04 mmol, Y= 18.6 %).

¹H NMR (DMSO-d₆, 400MHz): δ 11.07 (s, 1H), 10.76 (s, 1H), 9.02 – 8.99 (t, 1H), 8.83 (s, 1H), 8.80 – 8.78 (d, 1H), 7.99 (s, 1H), 7.84 – 7.82 (d, 1H), 7.62 – 7.60 (d, 1H), 7.50 (s, 1H), 7.27 – 7.25 (d, 1H), 7.14 – 7.08 (m, 5H), 7.009 – 6.96 (dd, 1H), 6.94 – 6.90 (dd, 1H), 6.86 – 6.84 (m, 2H), 6.817 – 6.811 (d, 1H), 5.70 – 5.66 (dd, 1H), 4.52 – 4.51 (d, 2H), 4.49 – 4.43 (ddd, 1H), 3.44 – 3.40 (m, 2H), 3.02 – 2.97 (dd, 1H), 2.79 – 2.74 (dd, 1H); ¹³C NMR: δ 172.71, 167.96, 164.13, 161.91, 161.44, 156.75, 148.68, 137.85, 136.32, 132.49, 129.41, 128.38, 127.25, 126.57, 124.06, 121.41, 118.81, 118.73, 114.79, 113.86, 111.75, 111.55, 108.87, 102.24, 63.66, 54.32, 49.02, 38.03, 35.16, 17.46; HPLC-MS: [M+1] = 620.

N-((1-((R)-1-(((S)-1-amino-1-oxo-3-phenylpropan-2-yl)amino)-3-(1H-indol-3-yl)-1-oxopropan-2-yl)-1H-1,2,3-triazol-4-yl)methyl)-7-hydroxy-2-oxo-2H-chromene-3-carboxamide (FS373)

The same procedure described for FS262 was performed with the (d)-Trp analogue of FS251 (N₃-(D)-Trp-Phe-NH₂ (FS285)) for the synthesis of FS369 as a crude product (47 mg, 0.08 mmol, Y = 43 %). Purification was performed with precipitation in MeOH to obtain the pure product as a white solid (28.9 mg, 0.04 mmol, Y= 50 %).

¹H NMR (DMSO-d₆, 400MHz): δ 11.07 (s, 1H), 10.76 (s, 1H), 9.02 – 8.99 (t, 1H), 8.83 (s, 1H), 8.80 – 8.78 (d, 1H), 7.99 (s, 1H), 7.84 – 7.82 (d, 1H), 7.62 – 7.60 (d, 1H), 7.50 (s, 1H), 7.27 – 7.25 (d, 1H), 7.14 – 7.08 (m, 5H), 7.009 – 6.96 (dd, 1H), 6.94 – 6.90 (dd, 1H), 6.86 – 6.84 (m, 2H), 6.817 – 6.811 (d, 1H), 5.70 – 5.66 (dd, 1H), 4.52 – 4.51 (d, 2H), 4.49 – 4.43 (ddd, 1H), 3.44 – 3.40 (m, 2H), 3.02 – 2.97 (dd, 1H), 2.79 – 2.74 (dd, 1H); ¹³C NMR: δ 172.71, 167.96, 164.13, 161.91, 161.44, 156.75, 148.68, 137.85, 136.32, 132.49, 129.41, 128.38, 127.25, 126.57, 124.06, 121.41, 118.81, 118.73, 114.79, 113.86, 111.75, 111.55, 108.87, 102.24, 63.66, 54.32, 49.02, 38.03, 35.16, 17.46; HPLC-MS: [M+1] = 620.

7-hydroxycoumarin-N-(prop-2-yn-1-yl)-3-carboxylate (FS339)

FS333 (0.48 mmol, 100mg) was added to a flask with 8mL of thionyl chloride, and the mixture was allowed to stir under reflux for two hours. The solvent was removed, the residue was dissolved in 5mL of toluene and propargyl alcohol (1eq., 30 μ L) was added dropwise and the reaction was allowed to stir under reflux overnight. The day after the residue was removed, the mixture was diluted with EtOAc and extracted with HCl 0.5M (2x), saturated NaHCO₃ (2x) and brine (1x). The organic phase was dried over MgSO₄, filtered, and evaporated under vacuum to obtain the pure product as a brown solid (0.48 mmol, Y = 100%).

¹H NMR (DMSO-d₆, 400MHz): δ 11.08 (s, 1H), 8.38 (s, 1H), 7.49– 7.47 (d, 1H), 6.74 – 6.73 (dd, 1H), 6.72 (s, 1H), 5.129 – 5.123 (dd, 2H), 3.14 – 3.13 (t, 1H); **¹³C NMR:** δ 163.07, 160.87, 159.07, 155.81, 130.69, 129.37, 113.88, 112.49, 112.30, 102.54, 79.75, 78.06, 56.53; **HPLC-MS:** [M+1] = 245, [M+Na] = 268.

(1-((R)-1-(((S)-1-amino-1-oxo-3-phenylpropan-2-yl)amino)-3-(1H-indol-3-yl)-1-oxopropan-2-yl)-1H-1,2,3-triazol-4-yl)methyl 7-hydroxy-2-oxo-2H-chromene-3-carboxylate (FS342)

The same procedure described for FS262 was performed with the (d)-Trp analogue of FS251 (N₃-(D)-Trp-Phe-NH₂ (FS285)) for the synthesis of FS342 as a crude product (47 mg, 0.08 mmol, Y = 43 %). Purification was performed directly using a RP semipreparative with ACN and H₂O as solvents and the pure product was obtained as a white solid (13 mg, 0.02 mmol, Y= 25 %)

¹H NMR (DMSO-d₆, 400MHz): δ 10.67 (s, 1H), 8.98 – 8.96 (d, 1H), 8.60 (s, 1H), 8.32 (s, 1H), 7.72 – 7.70 (d, 1H), 7.63 – 7.61 (d, 1H), 7.56 (s, 1H), 7.23 – 6.94 (m, 7H), 6.69 – 6.76 (m, 2H), 6.67 – 6.66 (d, 1H), 6.48 (s, 1H), 5.71 – 5.67 (dd, 1H), 5.22 (s, 1H), 4.53 – 4.47 (ddd, 1H), 3.18 – 3.12 (m, 2H), 3.00 – 2.97 (m, 2H), 2.75 – 2.69 (dd, 1H); **¹³C NMR:** δ 172.84, 167.86, 162.87, 158.43, 156.70, 150.10, 141.65, 138.08, 136.32, 132.69, 129.72, 128.46, 127.16, 126.76, 124.26, 121.60, 118.74, 111.73, 110.88, 108.65, 102.23, 63.67, 58.11, 53.89; **HPLC-MS:** [M+1] = 621.

2.10 - Bibliography

- (1) Beckett, A. H.; Casy, A. F. Synthetic Analgesics: Stereochemical Considerations. *JPP* **2011**, *6* (1), 986–1001. <https://doi.org/10.1111/j.2042-7158.1954.tb11033.x>.
- (2) Brownstein, M. J. A Brief History of Opiates, Opioid Peptides, and Opioid Receptors. *Proc Natl Acad Sci* **1993**, *90* (12), 5391–5393. <https://doi.org/10.1073/pnas.90.12.5391>.
- (3) Kolodny, A.; Courtwright, D. T.; Hwang, C. S.; Kreiner, P.; Eadie, J. L.; Clark, T. W.; Alexander, G. C. The Prescription Opioid and Heroin Crisis: A Public Health Approach to an Epidemic of Addiction. *Annu Rev Public Health* **2015**, *36* (1), 559–574. <https://doi.org/10.1146/annurev-publhealth-031914-122957>.
- (4) Santino, F.; Gentilucci, L. Design of κ -Opioid Receptor Agonists for the Development of Potential Treatments of Pain with Reduced Side Effects. *Molecules* **2023**, *28* (1), 346. <https://doi.org/10.3390/molecules28010346>.
- (5) Chavkin, C. Dynorphin—Still an Extraordinarily Potent Opioid Peptide. *Mol Pharmacol* **2013**, *83* (4), 729–736. <https://doi.org/10.1124/mol.112.083337>.
- (6) Kieffer, B. L.; Gavériaux-Ruff, C. Exploring the Opioid System by Gene Knockout. *Prog Neurobiol* **2002**, *66* (5), 285–306. [https://doi.org/10.1016/S0301-0082\(02\)00008-4](https://doi.org/10.1016/S0301-0082(02)00008-4).
- (7) Martin, W. R.; Martin, W. R.; Eades, C. G.; Thompson, J. A.; Huppler, R. E.; Gilbert, P. E. The effects of morphine- and nalorphine- like drugs in the nondependent and morphine-dependent chronic spinal dog *J Pharmacol Exp Ther* **1976**, *197*, 517- 532
- (8) Schattauer, S. S.; Kuhar, J. R.; Song, A.; Chavkin, C. Nalfurafine Is a G-Protein Biased Agonist Having Significantly Greater Bias at the Human than Rodent Form of the Kappa Opioid Receptor. *Cell Signal* **2017**, *32*, 59–65. <https://doi.org/10.1016/j.cellsig.2017.01.016>.
- (9) Dortch-Carnes, J.; Potter, D. E. Bremazocine: A κ -Opioid Agonist with Potent Analgesic and Other Pharmacologic Properties. *CNS Drug Rev* **2006**, *11* (2), 195–212. <https://doi.org/10.1111/j.1527-3458.2005.tb00270.x>.
- (10) Szmuszkovicz, J.; von Voigtlander, P. F. Benzeneacetamide Amines: Structurally Novel Non-m.Mu. Opioids. *J Med Chem* **1982**, *25* (10), 1125–1126. <https://doi.org/10.1021/jm00352a005>.
- (11) Spetea, M.; Schmidhammer, H. Kappa Opioid Receptor Ligands and Pharmacology: Diphenethylamines, a Class of Structurally Distinct, Selective Kappa Opioid Ligands. In *Handbook of Experimental Pharmacology*; Springer Science and Business Media Deutschland GmbH, 2022; Vol. 271, pp 163–195. https://doi.org/10.1007/164_2020_431.
- (12) Faouzi, A.; Varga, B. R.; Majumdar, S. Biased Opioid Ligands. *Molecules*. MDPI AG September 1, 2020. <https://doi.org/10.3390/molecules25184257>.
- (13) Zhou, L.; Lovell, K. M.; Frankowski, K. J.; Slauson, S. R.; Phillips, A. M.; Streicher, J. M.; Stahl, E.; Schmid, C. L.; Hodde, P.; Madoux, F.; Cameron, M. D.; Prisinzano, T. E.; Aubé, J.; Bohn, L. M. Development of Functionally Selective, Small Molecule Agonists at Kappa Opioid Receptors. *J Bio Chem* **2013**, *288* (51), 36703–36716. <https://doi.org/10.1074/jbc.M113.504381>.
- (14) Brust, T. F.; Morgenweck, J.; Kim, S. A.; Rose, J. H.; Locke, J. L.; Schmid, C. L.; Zhou, L.; Stahl, E. L.; Cameron, M. D.; Scarry, S. M.; Aubé, J.; Jones, S. R.; Martin, T. J.; Bohn, L. M. Biased Agonists of the Kappa Opioid Receptor Suppress Pain and Itch without Causing Sedation or Dysphoria. *Sci Signal* **2016**, *9* (456). <https://doi.org/10.1126/scisignal.aai8441>.

- (15) Erli, F.; Guerrieri, E.; ben Haddou, T.; Lantero, A.; Mairegger, M.; Schmidhammer, H.; Spetea, M. Highly Potent and Selective New Diphenethylamines Interacting with the κ -Opioid Receptor: Synthesis, Pharmacology, and Structure-Activity Relationships. *J Med Chem* **2017**, *60* (17), 7579–7590. <https://doi.org/10.1021/acs.jmedchem.7b00981>.
- (16) Spetea, M.; Eans, S. O.; Ganno, M. L.; Lantero, A.; Mairegger, M.; Toll, L.; Schmidhammer, H.; McLaughlin, J. P. Selective κ Receptor Partial Agonist HS666 Produces Potent Antinociception without Inducing Aversion after i.c.v. Administration in Mice. *Br J Pharmacol* **2017**, *174* (15), 2444–2456. <https://doi.org/10.1111/bph.13854>.
- (17) Spetea, M.; Berzetei-Gurske, I. P.; Guerrieri, E.; Schmidhammer, H. Discovery and Pharmacological Evaluation of a Diphenethylamine Derivative (HS665), a Highly Potent and Selective κ Opioid Receptor Agonist. *J Med Chem* **2012**, *55* (22), 10302–10306. <https://doi.org/10.1021/jm301258w>.
- (18) Ortega, A.; Blount, J. F.; Manchand, P. S. Salvinorin, a New Trans-Neoclerodane Diterpene from *Salvia Divinorum* (Labiatae). *J Chem Soc Perkin 1* **1982**, 2505. <https://doi.org/10.1039/p19820002505>.
- (19) Valdes, L. J.; Butler, W. M.; Hatfield, G. M.; Paul, A. G.; Koreeda, M. Divinorin A, a Psychotropic Terpenoid, and Divinorin B from the Hallucinogenic Mexican Mint *Salvia Divinorum*. *J Org Chem* **1984**, *49* (24), 4716–4720. <https://doi.org/10.1021/jo00198a026>.
- (20) Valdés, L. J.; Chang, H. M.; Visger, D. C.; Koreeda, M. Salvinorin C, a New Neoclerodane Diterpene from a Bioactive Fraction of the Hallucinogenic Mexican Mint *Salvia Divinorum*. *Org Lett* **2001**, *3* (24), 3935–3937. <https://doi.org/10.1021/ol016820d>.
- (21) Roach, J. J.; Shenvi, R. A. A Review of Salvinorin Analogs and Their Kappa-Opioid Receptor Activity. *Bioorg Med Chem Lett* **2018**, *28* (9), 1436–1445. <https://doi.org/10.1016/j.bmcl.2018.03.029>.
- (22) Morani, A. S.; Ewald, A.; Prevatt-Smith, K. M.; Prisinzano, T. E.; Kivell, B. M. The 2-Methoxy Methyl Analogue of Salvinorin A Attenuates Cocaine-Induced Drug Seeking and Sucrose Reinforcements in Rats. *Eur J Pharmacol* **2013**, *720* (1–3), 69–76. <https://doi.org/10.1016/j.ejphar.2013.10.050>.
- (23) Aldrich, J. v.; McLaughlin, J. P. Peptide Kappa Opioid Receptor Ligands: Potential for Drug Development. *AAPS J* **2009**, *11* (2), 312–322. <https://doi.org/10.1208/s12248-009-9105-4>.
- (24) Gentilucci, L. *New Trends in the Development of Opioid Peptide Analogues as Advanced Remedies for Pain Relief*; 2004; Vol. 4.
- (25) Gentilucci, L.; de Marco, R.; Cerisoli, L. *Chemical Modifications Designed to Improve Peptide Stability: Incorporation of Non-Natural Amino Acids, Pseudo-Peptide Bonds, and Cyclization*; 2010; Vol. 16.
- (26) Schlechtingen, G.; DeHaven, R. N.; Daubert, J. D.; Cassel, J. A.; Chung, N. N.; Schiller, P. W.; Taulane, J. P.; Goodman, M. Structure-Activity Relationships of Dynorphin a Analogues Modified in the Address Sequence. *J Med Chem* **2003**, *46* (11), 2104–2109. <https://doi.org/10.1021/jm020125+>.
- (27) Vanderah, T. W.; Schteingart, C. D.; Trojnar, J.; Junien, J.-L.; Lai, J.; Riviere, P. J.-M. FE200041 (d-Phe-d-Phe-d-Nle-d-Arg-NH₂): A Peripheral Efficacious κ Opioid Agonist with Unprecedented Selectivity. *J Pharmacol Exp Ther* **2004**, *310* (1), 326–333. <https://doi.org/10.1124/jpet.104.065391>.
- (28) Vanderah, T. W.; Largent-Milnes, T.; Lai, J.; Porreca, F.; Houghten, R. A.; Menzaghi, F.; Wisniewski, K.; Stalewski, J.; Sueiras-Diaz, J.; Galyean, R.; Schteingart, C.; Junien, J.-L.; Trojnar, J.; Rivière, P. J.-M. Novel D-Amino Acid Tetrapeptides Produce Potent Antinociception by Selectively Acting at Peripheral κ -Opioid Receptors. *Eur J Pharmacol* **2008**, *583* (1), 62–72. <https://doi.org/10.1016/j.ejphar.2008.01.011>.

- (29) Fugal, J.; Serpa, S. M. Difelikefalin: A New κ -Opioid Receptor Agonist for the Treatment of Hemodialysis-Dependent Chronic Kidney Disease–Associated Pruritus. *Ann Pharmacother* **2022**, 106002802211158. <https://doi.org/10.1177/10600280221115889>.
- (30) Kutlu Yalcin, E.; Araujo-Duran, J.; Turan, A. Emerging Drugs for the Treatment of Postsurgical Pain. *Expert Opin Emerg Drugs* **2021**, 26 (4), 371–384. <https://doi.org/10.1080/14728214.2021.2009799>.
- (31) Fichna, J.; Janecka, A.; Costentin, J.; do Rego, J.-C. The Endomorphin System and Its Evolving Neurophysiological Role. *Pharmacol Rev* **2007**, 59 (1), 88–123. <https://doi.org/10.1124/pr.59.1.3>.
- (32) Harrison, C.; McNulty, S.; Smart, D.; Rowbotham, D. J.; Grandy, D. K.; Devi, L. A.; Lambert, D. G. The Effects of Endomorphin-1 and Endomorphin-2 in CHO Cells Expressing Recombinant μ -Opioid Receptors and SH-SY5Y Cells. *Br J Pharmacol* **1999**, 128 (2), 472–478. <https://doi.org/10.1038/sj.bjp.0702798>.
- (33) de Marco, R.; Bedini, A.; Spampinato, S.; Comellini, L.; Zhao, J.; Artali, R.; Gentilucci, L. Constraining Endomorphin-1 by β , α -Hybrid Dipeptide/Heterocycle Scaffolds: Identification of a Novel κ -Opioid Receptor Selective Partial Agonist. *J Med Chem* **2018**, 61 (13), 5751–5757. <https://doi.org/10.1021/acs.jmedchem.8b00296>.
- (34) Greco, A.; Tani, S.; De Marco, R.; Gentilucci, L. Synthesis and Analysis of the Conformational Preferences of 5-Aminomethyloxazolidine-2,4-Dione Scaffolds: First Examples of β^2 - and $\beta^{2,2}$ -Homo-Freidinger Lactam Analogues. *Chemistry - A European Journal* **2014**, 20 (41), 13390–13404. <https://doi.org/10.1002/chem.201402519>.
- (35) SAITO, T.; HIRAI, H.; KIM, Y.-J.; KOJIMA, Y.; MATSUNAGA, Y.; NISHIDA, H.; SAKAKIBARA, T.; SUGA, O.; SUJAKU, T.; KOJIMA, N. CJ-15,208, a Novel Kappa Opioid Receptor Antagonist from a Fungus, *Ctenomyces Serratus* ATCC15502. *J Antibiot (Tokyo)* **2002**, 55 (10), 847–854. <https://doi.org/10.7164/antibiotics.55.847>.
- (36) Aldrich, J. v.; Kulkarni, S. S.; Senadheera, S. N.; Ross, N. C.; Reilley, K. J.; Eans, S. O.; Ganno, M. L.; Murray, T. F.; McLaughlin, J. P. Unexpected Opioid Activity Profiles of Analogues of the Novel Peptide Kappa Opioid Receptor Ligand CJ-15,208. *ChemMedChem* **2011**, 6 (9), 1739–1745. <https://doi.org/10.1002/cmdc.201100113>.
- (37) Ross, N. C.; Reilley, K. J.; Murray, T. F.; Aldrich, J. v.; McLaughlin, J. P. Novel Opioid Cyclic Tetrapeptides: Trp Isomers of CJ-15,208 Exhibit Distinct Opioid Receptor Agonism and Short-Acting κ Opioid Receptor Antagonism. *Br J Pharmacol* **2012**, 165 (4b), 1097–1108. <https://doi.org/10.1111/j.1476-5381.2011.01544.x>.
- (38) Eans, S. O.; Ganno, M. L.; Reilley, K. J.; Patkar, K. A.; Senadheera, S. N.; Aldrich, J. v.; McLaughlin, J. P. The Macrocyclic Tetrapeptide [D-Trp]CJ-15,208 Produces Short-Acting κ Opioid Receptor Antagonism in the CNS after Oral Administration. *Br J Pharmacol* **2013**, 169 (2), 426–436. <https://doi.org/10.1111/bph.12132>.
- (39) Aldrich, J. v.; Senadheera, S. N.; Ross, N. C.; Ganno, M. L.; Eans, S. O.; McLaughlin, J. P. The Macrocyclic Peptide Natural Product CJ-15,208 Is Orally Active and Prevents Reinstatement of Extinguished Cocaine-Seeking Behavior. *J Nat Prod* **2013**, 76 (3), 433–438. <https://doi.org/10.1021/np300697k>.
- (40) Brice-Tutt, A. C.; Senadheera, S. N.; Ganno, M. L.; Eans, S. O.; Khaliq, T.; Murray, T. F.; McLaughlin, J. P.; Aldrich, J. v. Phenylalanine Stereoisomers of CJ-15,208 and [d-Trp]CJ-15,208 Exhibit Distinctly Different Opioid Activity Profiles. *Molecules* **2020**, 25 (17), 3999. <https://doi.org/10.3390/molecules25173999>.
- (41) Aldrich, J. v.; Senadheera, S. N.; Ross, N. C.; Reilley, K. A.; Ganno, M. L.; Eans, S. E.; Murray, T. F.; McLaughlin, J. P. Alanine Analogues of [D-Trp]CJ-15,208: Novel Opioid Activity Profiles and Prevention of Drug- and Stress-Induced Reinstatement of Cocaine-Seeking Behaviour. *Br J Pharmacol* **2014**, 171 (13), 3212–3222. <https://doi.org/10.1111/bph.12664>.

- (42) Cardillo, G.; Gentilucci, L.; Tolomelli, A.; Spinosa, R.; Calienni, M.; Qasem, A. R.; Spampinato, S. Synthesis and Evaluation of the Affinity toward μ -Opioid Receptors of Atypical, Lipophilic Ligands Based on the Sequence c[-Tyr-Pro-Trp-Phe-Gly-]. *J Med Chem* **2004**, *47* (21), 5198–5203. <https://doi.org/10.1021/jm0498811>.
- (43) Bedini, A.; Baiula, M.; Gentilucci, L.; Tolomelli, A.; de Marco, R.; Spampinato, S. Peripheral Antinociceptive Effects of the Cyclic Endomorphin-1 Analog c[YpwFG] in a Mouse Visceral Pain Model. *Peptides (N.Y.)* **2010**, *31* (11), 2135–2140. <https://doi.org/10.1016/j.peptides.2010.08.005>.
- (44) de Marco, R.; Bedini, A.; Spampinato, S.; Gentilucci, L. Synthesis of Tripeptides Containing D-Trp Substituted at the Indole Ring, Assessment of Opioid Receptor Binding and in Vivo Central Antinociception. *J Med Chem* **2014**, *57* (15), 6861–6866. <https://doi.org/10.1021/jm5002925>.
- (45) Gentilucci, L.; Squassabia, F.; Artali, R. *Re-Discussion of the Importance of Ionic Interactions in Stabilizing Ligand-Opioid Receptor Complex and in Activating Signal Transduction*; 2007; Vol. 8.
- (46) Gentilucci, L.; Tolomelli, A.; de Marco, R.; Artali, R. *Molecular Docking of Opiates and Opioid Peptides, a Tool for the Design of Selective Agonists and Antagonists, and for the Investigation of Atypical Ligand-Receptor Interactions*; 2012; Vol. 19.
- (47) Bedini, A.; di Cesare Mannelli, L.; Micheli, L.; Baiula, M.; Vaca, G.; de Marco, R.; Gentilucci, L.; Ghelardini, C.; Spampinato, S. Functional Selectivity and Antinociceptive Effects of a Novel KOPr Agonist. *Front Pharmacol* **2020**, *11*. <https://doi.org/10.3389/fphar.2020.00188>.
- (48) Andresen, B. T. *A Pharmacological Primer of Biased Agonism*; 2011.
- (49) Kenakin, T.; Christopoulos, A. Signalling Bias in New Drug Discovery: Detection, Quantification and Therapeutic Impact. *Nat Rev Drug Discov* **2013**, *12* (3), 205–216. <https://doi.org/10.1038/nrd3954>.
- (50) Chen, X.-T.; Pitis, P.; Liu, G.; Yuan, C.; Gotchev, D.; Cowan, C. L.; Rominger, D. H.; Koblisch, M.; DeWire, S. M.; Crombie, A. L.; Violin, J. D.; Yamashita, D. S. Structure–Activity Relationships and Discovery of a G Protein Biased μ Opioid Receptor Ligand, [(3-Methoxythiophen-2-Yl)Methyl]({2-[(9 R)-9-(Pyridin-2-Yl)-6-Oxaspiro-[4.5]Decan-9-Yl]Ethyl})Amine (TRV130), for the Treatment of Acute Severe Pain. *J Med Chem* **2013**, *56* (20), 8019–8031. <https://doi.org/10.1021/jm4010829>.
- (51) DeWire, S. M.; Yamashita, D. S.; Rominger, D. H.; Liu, G.; Cowan, C. L.; Graczyk, T. M.; Chen, X.-T.; Pitis, P. M.; Gotchev, D.; Yuan, C.; Koblisch, M.; Lark, M. W.; Violin, J. D. A G Protein-Biased Ligand at the μ -Opioid Receptor Is Potently Analgesic with Reduced Gastrointestinal and Respiratory Dysfunction Compared with Morphine. *J Pharmacol Exp Ther* **2013**, *344* (3), 708–717. <https://doi.org/10.1124/jpet.112.201616>.
- (52) Soergel, D. G.; Ann Subach, R.; Sadler, B.; Connell, J.; Marion, A. S.; Cowan, C. L.; Violin, J. D.; Lark, M. W. First Clinical Experience with TRV130: Pharmacokinetics and Pharmacodynamics in Healthy Volunteers. *Journal Clinical Pharmacol* **2014**, *54* (3), 351–357. <https://doi.org/10.1002/jcph.207>.
- (53) Lambert, D.; Calo, G. Approval of Oliceridine (TRV130) for Intravenous Use in Moderate to Severe Pain in Adults. *Br J Anaesth* **2020**, *125* (6), e473–e474. <https://doi.org/10.1016/j.bja.2020.09.021>.
- (54) Manglik, A.; Lin, H.; Aryal, D. K.; McCorvy, J. D.; Dengler, D.; Corder, G.; Levit, A.; Kling, R. C.; Bernat, V.; Hübner, H.; Huang, X.-P.; Sassano, M. F.; Giguère, P. M.; Löber, S.; da Duan; Scherrer, G.; Kobilka, B. K.; Gmeiner, P.; Roth, B. L.; Shoichet, B. K. Structure-Based Discovery of Opioid Analgesics with Reduced Side Effects. *Nature* **2016**, *537* (7619), 185–190. <https://doi.org/10.1038/nature19112>.
- (55) Kliewer, A.; Schmiedel, F.; Sianati, S.; Bailey, A.; Bateman, J. T.; Levitt, E. S.; Williams, J. T.; Christie, M. J.; Schulz, S. Phosphorylation-Deficient G-Protein-Biased μ -Opioid Receptors Improve Analgesia and Diminish

- Tolerance but Worsen Opioid Side Effects. *Nat Commun* **2019**, *10* (1), 367. <https://doi.org/10.1038/s41467-018-08162-1>.
- (56) Conibear, A. E.; Kelly, E. A Biased View of μ -Opioid Receptors? *Mol Pharmacol* **2019**, *96* (5), 542–549. <https://doi.org/10.1124/mol.119.115956>.
- (57) Gillis, A.; Gondin, A. B.; Kliewer, A.; Sanchez, J.; Lim, H. D.; Alamein, C.; Manandhar, P.; Santiago, M.; Fritzwanker, S.; Schmiedel, F.; Katte, T. A.; Reekie, T.; Grimsey, N. L.; Kassiou, M.; Kellam, B.; Krasel, C.; Halls, M. L.; Connor, M.; Lane, J. R.; Schulz, S.; Christie, M. J.; Canals, M. Low Intrinsic Efficacy for G Protein Activation Can Explain the Improved Side Effect Profiles of New Opioid Agonists. *Sci Signal* **2020**, *13* (625). <https://doi.org/10.1126/scisignal.aaz3140>.
- (58) Mores, K. L.; Cummins, B. R.; Cassell, R. J.; van Rijn, R. M. A Review of the Therapeutic Potential of Recently Developed G Protein-Biased Kappa Agonists. *Front Pharmacol* **2019**, *10*. <https://doi.org/10.3389/fphar.2019.00407>.
- (59) Trevisan, G.; Rossato, M. F.; Walker, C. I. B.; Oliveira, S. M.; Rosa, F.; Tonello, R.; Silva, C. R.; Machado, P.; Boligon, A. A.; Martins, M. A. P.; Zanatta, N.; Bonacorso, H. G.; Athayde, M. L.; Rubin, M. A.; Calixto, J. B.; Ferreira, J. A Novel, Potent, Oral Active and Safe Antinociceptive Pyrazole Targeting Kappa Opioid Receptors. *Neuropharmacology* **2013**, *73*, 261–273. <https://doi.org/10.1016/j.neuropharm.2013.06.011>.
- (60) Zheng, Z.; Huang, X.-P.; Mangano, T. J.; Zou, R.; Chen, X.; Zaidi, S. A.; Roth, B. L.; Stevens, R. C.; Katritch, V. Structure-Based Discovery of New Antagonist and Biased Agonist Chemotypes for the Kappa Opioid Receptor. *J Med Chem* **2017**, *60* (7), 3070–3081. <https://doi.org/10.1021/acs.jmedchem.7b00109>.
- (61) Azevedo Neto, J.; Costanzini, A.; de Giorgio, R.; Lambert, D. G.; Ruzza, C.; Calò, G. Biased versus Partial Agonism in the Search for Safer Opioid Analgesics. *Molecules* **2020**, *25* (17), 3870. <https://doi.org/10.3390/molecules25173870>.
- (62) BIDLACK, J. M.; McLAUGHLIN, J. P.; WENTLAND, M. P. Partial Opioids: Medications for the Treatment of Pain and Drug Abuse. *Ann N Y Acad Sci* **2006**, *909* (1), 1–11. <https://doi.org/10.1111/j.1749-6632.2000.tb06672.x>.
- (63) Aldrich, J. v.; McLaughlin, J. P. Opioid Peptides: Potential for Drug Development. *Drug Discovery Today: Technologies*. Elsevier Ltd 2012. <https://doi.org/10.1016/j.ddtec.2011.07.007>.
- (64) Aldrich, J. v.; Patkar, K. A.; McLaughlin, J. P. Zyklophin, a Systemically Active Selective Kappa Opioid Receptor Peptide Antagonist with Short Duration of Action. *Proc Natl Acad Sci* **2009**, *106* (43), 18396–18401. <https://doi.org/10.1073/pnas.0910180106>.
- (65) Mangel, A. W.; Williams, V. S. Asimadoline in the Treatment of Irritable Bowel Syndrome. *Expert Opin Investig Drugs* **2010**, *19* (10), 1257–1264. <https://doi.org/10.1517/13543784.2010.515209>.
- (66) Beck, T. C.; Dix, T. A. Targeting Peripheral κ -Opioid Receptors for the Non-Addictive Treatment of Pain. *Future Drug Discov* **2019**, *1* (2). <https://doi.org/10.4155/fdd-2019-0022>.
- (67) Gentilucci, L.; Tolomelli, A.; Squassabia, F. *Peptides and Peptidomimetics in Medicine, Surgery and Biotechnology*; 2006; Vol. 13.
- (68) Zaidi, S. A.; Katritch, V. Structural Characterization of KOR Inactive and Active States for 3D Pharmacology and Drug Discovery; 2021; pp 41–64. https://doi.org/10.1007/164_2021_461.
- (69) Ferré, G.; Czaplicki, G.; Demange, P.; Milon, A. Structure and Dynamics of Dynorphin Peptide and Its Receptor; 2019; pp 17–47. <https://doi.org/10.1016/bs.vh.2019.05.006>.

- (70) Wu, H.; Wacker, D.; Mileni, M.; Katritch, V.; Han, G. W.; Vardy, E.; Liu, W.; Thompson, A. A.; Huang, X.-P.; Carroll, F. I.; Mascarella, S. W.; Westkaemper, R. B.; Mosier, P. D.; Roth, B. L.; Cherezov, V.; Stevens, R. C. Structure of the Human κ -Opioid Receptor in Complex with JD1c. *Nature* **2012**, *485* (7398), 327–332. <https://doi.org/10.1038/nature10939>.
- (71) Che, T.; Majumdar, S.; Zaidi, S. A.; Ondachi, P.; McCorvy, J. D.; Wang, S.; Mosier, P. D.; Uprety, R.; Vardy, E.; Krumm, B. E.; Han, G. W.; Lee, M.-Y.; Pardon, E.; Steyaert, J.; Huang, X.-P.; Strachan, R. T.; Tribo, A. R.; Pasternak, G. W.; Carroll, F. I.; Stevens, R. C.; Cherezov, V.; Katritch, V.; Wacker, D.; Roth, B. L. Structure of the Nanobody-Stabilized Active State of the Kappa Opioid Receptor. *Cell* **2018**, *172* (1–2), 55–67.e15. <https://doi.org/10.1016/j.cell.2017.12.011>.
- (72) Puls, K.; Schmidhammer, H.; Wolber, G.; Spetea, M. Mechanistic Characterization of the Pharmacological Profile of HS-731, a Peripherally Acting Opioid Analgesic, at the μ -, δ -, κ -Opioid and Nociceptin Receptors. *Molecules* **2022**, *27* (3), 919. <https://doi.org/10.3390/molecules27030919>.
- (73) Mehr-un-Nisa; Munawar, M. A.; Rankin, D.; Hruby, V. J.; Porreca, F.; Lee, Y. S. C-Terminal Modified Enkephalin-like Tetrapeptides with Enhanced Affinities at the Kappa Opioid Receptor and Monoamine Transporters. *Bioorg Med Chem* **2021**, *51*, 116509. <https://doi.org/10.1016/j.bmc.2021.116509>.
- (74) Yadav, V. D.; Kumar, L.; Kumari, P.; Kumar, S.; Singh, M.; Siddiqi, M. I.; Yadav, P. N.; Batra, S. Synthesis and Assessment of Fused B-Carboline Derivatives as Kappa Opioid Receptor Agonists. *ChemMedChem* **2021**, *16* (12), 1917–1926. <https://doi.org/10.1002/cmdc.202100029>.
- (75) Stefanucci, A.; Iobbi, V.; della Valle, A.; Scioli, G.; Pieretti, S.; Minosi, P.; Mirzaie, S.; Novellino, E.; Mollica, A. In Silico Identification of Tripeptides as Lead Compounds for the Design of KOR Ligands. *Molecules* **2021**, *26* (16), 4767. <https://doi.org/10.3390/molecules26164767>.
- (76) Guerrieri, E.; Bermudez, M.; Wolber, G.; Berzetei-Gurske, I. P.; Schmidhammer, H.; Spetea, M. Structural Determinants of Diphenethylamines for Interaction with the κ Opioid Receptor: Synthesis, Pharmacology and Molecular Modeling Studies. *Bioorg Med Chem Lett* **2016**, *26* (19), 4769–4774. <https://doi.org/10.1016/j.bmcl.2016.08.031>.
- (77) Wtorek, K.; Ghidini, A.; Gentilucci, L.; Adamska-Bartłomiejczyk, A.; Piekilna-Ciesielska, J.; Ruzza, C.; Sturaro, C.; Calò, G.; Pieretti, S.; Kluczyk, A.; McDonald, J.; Lambert, D. G.; Janecka, A. Synthesis, Biological Activity and Molecular Docking of Chimeric Peptides Targeting Opioid and NOP Receptors. *Int J Mol Sci* **2022**, *23* (20), 12700. <https://doi.org/10.3390/ijms232012700>.
- (78) Carbone, J.; Ghidini, A.; Romano, A.; Gentilucci, L.; Musiani, F. PacDOCK: A Web Server for Positional Distance-Based and Interaction-Based Analysis of Docking Results. *Molecules* **2022**, *27* (20), 6884. <https://doi.org/10.3390/molecules27206884>.
- (79) Uprety, R.; Che, T.; Zaidi, S. A.; Grinnell, S. G.; Varga, B. R.; Faouzi, A.; Slocum, S. T.; Allaoa, A.; Varadi, A.; Nelson, M.; Bernhard, S. M.; Kulko, E.; le Rouzic, V.; Eans, S. O.; Simons, C. A.; Hunkele, A.; Subrath, J.; Pan, Y. X.; Javitch, J. A.; McLaughlin, J. P.; Roth, B. L.; Pasternak, G. W.; Katritch, V.; Majumdar, S. Controlling Opioid Receptor Functional Selectivity by Targeting Distinct Subpockets of the Orthosteric Site. *Elife* **2021**, *10*. <https://doi.org/10.7554/eLife.56519>.
- (80) Oiry, J.; Puy, J. Y.; Mialocq, P.; Clayette, P.; Fretier, P.; Jaccard, P.; Dereuddre-Bosquet, N.; Dormont, D.; Imbach, J. L. Synthesis and in Vitro Anti-HIV Activity in Human Monocyte-Derived Macrophages of 2-Oxothiazolidine-4(R)-Carboxylic Acid Derivatives. *J Med Chem* **1999**, *42* (23), 4733–4740. <https://doi.org/10.1021/jm980289j>.

- (81) Elashal, H. E.; Cohen, R. D.; Elashal, H. E.; Raj, M. Oxazolidinone-Mediated Sequence Determination of One-Bead One-Compound Cyclic Peptide Libraries. *Org Lett* **2018**, *20* (8), 2374–2377. <https://doi.org/10.1021/acs.orglett.8b00717>.
- (82) Rostovtsev, V. v.; Green, L. G.; Fokin, V. v.; Sharpless, K. B. A Stepwise Huisgen Cycloaddition Process: Copper(I)-Catalyzed Regioselective “Ligation” of Azides and Terminal Alkynes. *Angew Chem Int Ed Engl* **2002**, *41* (14), 2596–2599. [https://doi.org/10.1002/1521-3773\(20020715\)41:14<2596:AID-ANIE2596>3.0.CO;2-4](https://doi.org/10.1002/1521-3773(20020715)41:14<2596:AID-ANIE2596>3.0.CO;2-4).
- (83) Li, H.; Aneja, R.; Chaiken, I. Click Chemistry in Peptide-Based Drug Design. *Molecules*. August 2013, pp 9797–9817. <https://doi.org/10.3390/molecules18089797>.
- (84) Icik, E.; Jolly, A.; Löffler, P.; Agelidis, N.; Bugdayci, B.; Altevogt, L.; Bilitewski, U.; Baro, A.; Laschat, S. Synthesis and Biological Evaluation of a Library of AGE-Related Amino Acid Triazole Crosslinkers. *Eur J Org Chem* **2020**, *2020* (33), 5368–5379. <https://doi.org/10.1002/ejoc.202000811>.
- (85) Horne, W. S.; Olsen, C. A.; Beierle, J. M.; Montero, A.; Ghadiri, M. R. Probing the Bioactive Conformation of an Archetypal Natural Product HDAC Inhibitor with Conformational Homogeneous Triazole-Modified Cyclic Tetrapeptides. *Angew Chem Int Ed Engl* **2009**, *48* (26), 4718–4724. <https://doi.org/10.1002/anie.200805900>.
- (86) Hein, C. D.; Liu, X.-M.; Wang, D. Click Chemistry, A Powerful Tool for Pharmaceutical Sciences. *Pharm Res* **2008**, *25* (10), 2216–2230. <https://doi.org/10.1007/s11095-008-9616-1>.

CHAPTER 3

Peptidomimetic Inhibitors of Lactate Dehydrogenase Enzyme

Lactate dehydrogenase (LDH) is a common enzyme that can be found in all living cells and belongs to the oxidoreductase class, important for the anaerobic metabolic pathway. Its role is the catalytic reversible conversion of lactate to pyruvate with the reduction of NAD⁺ to NADH and vice versa.¹

LDH was discovered to be composed of two main subunits known as M monomer and H monomer, that pair into tetramers forming five different variants. The different isoforms are called isozymes and are named from LDH-1 to LDH-5 with various expression in distinct tissue: LDH-1 has four H subunit (4H), and it is the most present in heart tissue; LDH-2 has one M and three H (1M3H) and is mainly found in reticuloendothelial system and in red blood cells; LDH-3 has a symmetric two M and two H subunits (2M2H) and it is found in lungs; LDH-4 has one H and three M subunits (3M1H) and is the most present in kidneys and LDH-5 has all M subunits (4M) and can be found in skeletal muscles and in liver.²

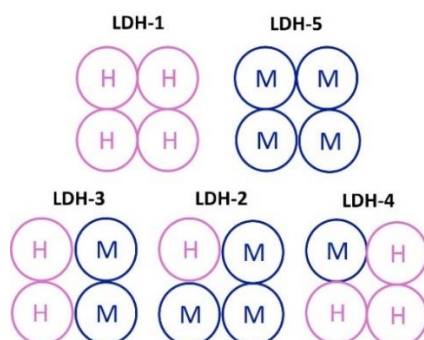


Fig.1 Subunits and composition of the five LDH isoforms.

Despite the five isozymes are structurally very similar, they have distinct kinetic properties that result in slightly different interaction within the active site between the present amino acids. The genes that produce LDH are LDH-A, B, and C that encode the L-isomers of the enzyme and so use and produce the L enantiomeric form of lactate, and LDH-D that encode the D-isomer. The LDH-A subunit has a net negative charge that makes it have greater affinity towards pyruvate, thus converting pyruvate to lactate and NADH to NAD⁺, while LDHB has a net positive charge resulting in having the opposite affinity then towards lactate and the consequent preferential conversion of lactate to pyruvate and NAD⁺ to NADH.

In the enzyme's substrate-binding pocket is placed the active side, the same one for both the subunits that contained highly conserved aminoacidic sequence, like His-193, present in all the

animals, as well as Asp-168, Arg-171, Thr-246 and Arg-106.³ Although the active site is the same, in the tertiary structure, the alanine of the M chain is replaced with glutamine in the H chain. The difference of charge and polarity provides different chemical properties occurring in the ability of the H subunit to bind faster but with a fivefold reduced catalytic activity.

As mentioned before, LDH is one of the enzymes whose purpose is to catalyse the reversible conversion of pyruvate to lactate with H transfer using NADH mainly in the cytosol of human cells. In fact, this enzyme is primarily implicated in the anaerobic glucose metabolism, that is when oxygen is lacking or almost absent.⁴

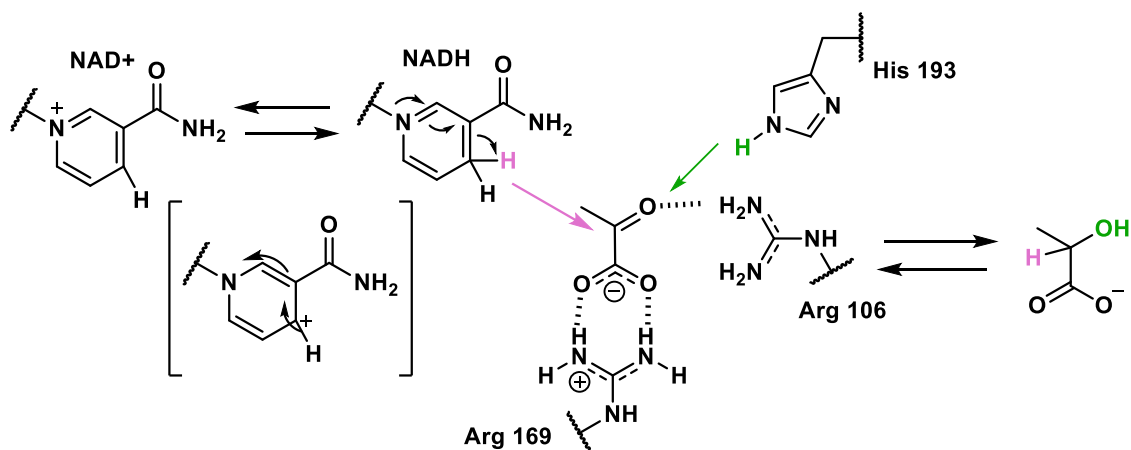


Fig. 2 Catalytic conversion of pyruvate into lactate inside the enzyme.

In one direction of this thermodynamically favoured reaction, pyruvate is reduced producing lactate while NADH is oxidized to NAD⁺. Inside the active site, the mechanism involves a hydride transfer from the dihydropyridine portion of the NADH to the ketone carbonyl of the pyruvate, while the other portion of the molecule is engaged in hydrogen bonds with Arg 169, followed by the prompt transfer of a proton by His 193. Arg 106 also stabilize the substrate with the formation of a hydrogen bond with the ketone carbonyl before the participation of the histidine.⁵

The cellular metabolism, where the aim is the production of ATP (adenosine triphosphate) for energy storage, is characterized by the transformation of D-glucose into pyruvate. When the oxygen is present, the pyruvate is decarboxylated by mitochondria and converted to AcetylCo-A, but when instead the oxygen is not present, the pyruvate is transformed into lactate through lactic fermentation to decrease NADH concentration, toxic in high level.

In cancer cells, fast and uncontrol grow due to high ATP consume, leads to a condition of hypoxia due to compressions and obstructions of blood vessels from which the cells draw oxygen and nourishment. Under these conditions, cells remain with an accumulation of reduced cofactors (NADH) and therefore, to continue to exploit glycolysis as the fastest way of synthesis of ATP, an

overexpression of the enzyme LDH is necessary allowing to restore the oxidized cofactors (NAD⁺). The main consequence of this process is the increase in the concentration of lactic acid, which acidifying the surrounding environment and facilitates tumor invasion and metastasis.

In particular, the isoform that is most involved in cancer tissues is LDH-5 because it has a high conversion rate of pyruvate to lactate under hypoxia conditions, thanks to the presence of four “M” monomer units. This overexpression has several implications in cancer genesis, metastasis formation and cancer proliferation. In fact, LDH-5 activates octamer-binding transcription factor 4 (Oct-4), involved in self-renewal of embryonic stem cells, and responsible of determining cancer cell phenotype and also it inhibits apoptosis since it favours several antiapoptotic proteins expression. Metastasis formation is strictly connected to LDH-5 overexpression since it stimulates proteins involved in extracellular matrix degradation, it promotes immunosuppression, and it inhibits cytotoxic response carried out by the immune system against cancer cells.⁶

The low oxygen pressure in neoplastic tissue has further and relevant consequence since it enables tumour resistance to chemotherapy. Neoplastic tissues proliferate far away from blood vessel and thus they cannot be easily reached from circulating drugs. Moreover, the anaerobic environment inhibits reactive oxygen species (ROS) activity-based drugs. O₂ radicals seriously damage DNA, causing double helix denaturation and stable organic peroxides formation, thus fatal chromosome aberration occurs. Although this damage could be fixed by thiolic group of N-acetylcysteine, under normal oxygen pressure it could be consider irreversible. In cancer cell the low oxygen pressure makes easier to repair this damage and resistance to ROS chemotherapeutics is observed.

Considering its link with cancer cells proliferation, LDH-5 is a promising target in cancer therapy⁷ since the lowering of its activity directly affects the growth and development of the tumour tissue. If its activity within the tumour were to be stopped completely, glycolysis alone would not be able to satisfy the large energy requirement and cell proliferation would be much less rapid and more easily treatable.⁸

3.1 - LDH-A current inhibitors

Considering its importance in cancer proliferation⁹, interfere with LDH-A activity or biosynthesis has become an important goal for cancer treatment and for overcoming resistance in cancer therapy, because it appears to cause significant reduction of the tumour area.¹⁰One way to achieve this important result is the development of small organic molecules as inhibitors of this specific isoform. Initially, these small molecules were identified as part of a larger study as antimalarial drugs, by

targeting *Plasmodium falciparum* LDH (pfLDH), which is essential for the survival of the malaria parasite. Unfortunately, however, they did not prove particularly effective for this purpose because they were not selective but, on the contrary, they showed some activity towards LDH-5.¹¹

Since then, oxamate has been considered as a reference for further inhibitors. It is a pyruvate structural isostere showing a high affinity for pyruvate binding pockets ($K_I = 94.4 \mu\text{M}$) but not a great selectivity nor a great permeation capacity. Structural modification has been carried out by Yu and coworkers¹² to reach different N-monosubstituted oxamic acids, but none of them appears to fulfill clinical trials parameters.

Extensive research has been carried out and X-ray crystal studies reveal that there is a larger, cofactor binding domain, and a smaller mixed α/β substrate binding domain, each of which compromise different aminoacidic residue. Analyses of NADH-LDH-oxamate were essential for a deep knowledge of the receptor pocket where it result that oxamate interacts with residue Gln99, Arg105, Asn137, Arg168, His192, and Thr247 via hydrogen-bonding, whereas Leu164 and Ala237 are engaged in hydrophobic contacts. Furthermore, the side chain of Arg168 interacts with the carboxylate group of the ligand.¹³ A different ternary complex represented by NADH-LDH-pyruvate, also showed similar kinds of interaction, and confirmed the importance of Arg169, Thr248, and His193.¹⁴ These cocrystal structures studies were able to improve the rational design of chemicals compounds and a great improvement has been made by Genetec corporation with previously the development of 2-thio-6-oxo-1,6-dihydropyrimidines and then of 2-amino-5-aryl-pyrazines-based compounds¹⁵ where the major pharmacophores are the carboxylic acid groups that can interact through H-bonds with the protonated His 192. Furthermore the 2-amino pyrazine ring acts as a donor-acceptor H- bond motif and the methyl group at the C-6 position of the benzoic acid improves the binding with hydrophobic interaction.

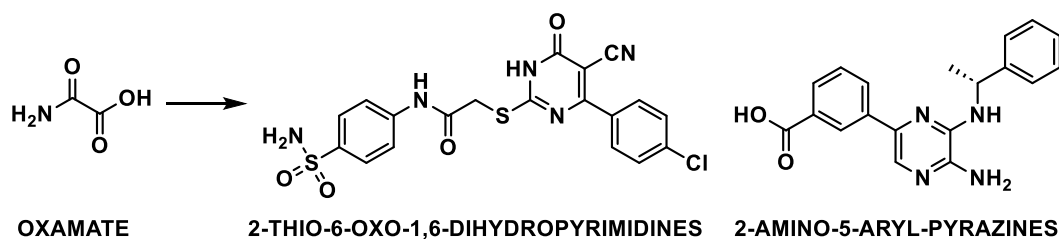


Fig.3 Oxamate and structures of its first derivatives.

The initial pharmacology interest in gossypol arises because of its spermicidal activity but further on it shows the ability to inhibit LDH isoforms in a NADH competitive manner (LDH5 $K_i = 1.9 \mu\text{M}$, LDH1 $K_i = 1.4 \mu\text{M}$).¹⁶ It is a natural disesquiterpene originally isolated from a specific kind of cotton seed, where it acts together with other active substances, as natural antiparasitic and antiviral.¹⁷ It

exists in two enantiomeric forms, where the R form resulted to be more potent than the S isomer, due to the rotation around the 2-2' carbon-carbon single bond that link together the two naphthalene units. Although it displays promising pharmacological activities, it failed all the clinical trials because of its high toxicity: in fact, the two aldehyde groups and the catechol hydroxyl group are a danger because of their sensibility and ease in generating toxic metabolites.¹⁸ To avoid the formation of the Schiff's base between the aldehydic group of the molecule and the free amino group of the side chain of the lysine residue of the active site, derivatives have been developed with the intention of replacing the carboxyl group of the aldehyde and decreasing the toxicity but progress in clinical trials of these products is still limited by the presence of the catechol moiety.¹⁹

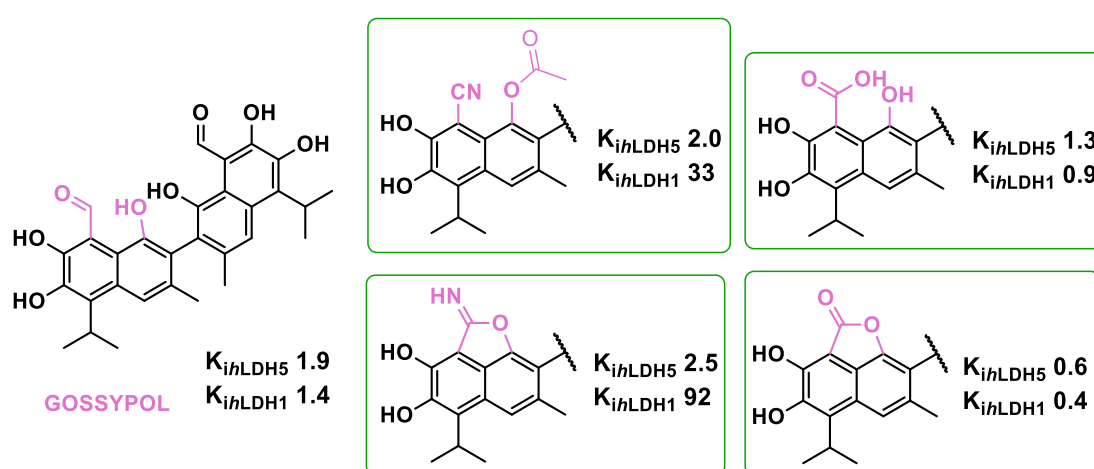


Fig.4 Structures and K_i values (expressed in nM) of gossypol and its derivatives.

With the aim of maintaining the biological activity and improving the selectivity, various changes have been made to the gossypol structure up to the 8-deoxyhemigossylic acid and its derivatives developed with different substitutions in position 4 and 7.²⁰ These studies were very important to discover that just one half of the reference structure is necessary to gain the selectivity and the inhibitory activity for LDH5. In fact, the first compound of the library, displayed more selectivity for LDH5 than LDH1 whereas the corresponding dimer was completely nonselective and indeed improved the activity only against LDH1. Among all the compounds synthesized, just FX11 was identified as the most selective and with the best inhibitory activity. Although it was initially designed as an antimalarial agent, it was considered a potential anticancer lead candidate because of its ability to reduce ATP levels and cellular lactate production, induce oxidative stress resulting with the suppression of the tumour progression thanks to the NADH competition in human lymphoma and pancreatic cancer. Nevertheless, the catechol portion continues to prevent its full approval for therapeutic treatment.

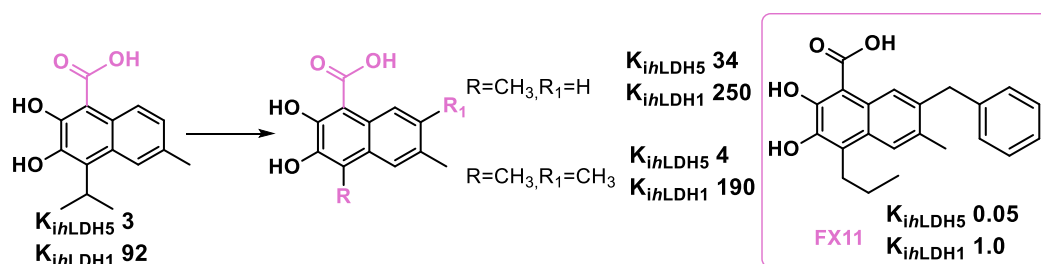


Fig.5 Structures and K_i values (expressed in nM) of 2,3-Dihydroxynaphthoic acid derivatives.

Besides gossypol, other polyphenolic scaffolds have been extracted from nature. In particular, Wang and collaborators²¹ extracted from *Spatholobus suberectus*, an aquatic Leguminosae, epigallocatechin that showed significant inhibition of breast cancer development and without being selective for a specific isoform form was considered a lead compound for anticancer development. Even Galloflavin²², a tricyclic flavone-like molecule, showed significant inhibition activity but no selectivity for LDH5 isomer. In fact, it is able to completely block the activity of both LDH5 and LDH1, exhibiting a K_i value of 5.46 μM vs pyruvate and 56.0 μM vs NADH in hLDH5 compared to $K_i = 15.1 \mu\text{M}$ vs Pyruvate and 23.2 μM vs NADH in LDH1, but unlike the previously described compound, it also showed a low cytotoxicity in healthy cells.

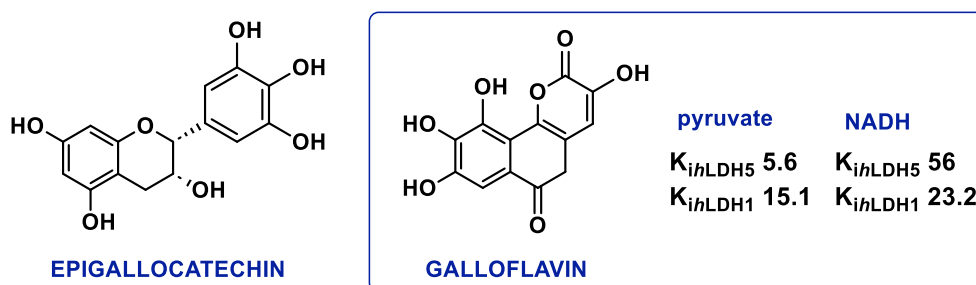


Fig.6 Structures and K_i values (expressed in μM) of polyphenolic flavone-based hLDH5 inhibitors.

A class of new inhibitors of both NADH and pyruvate was discovered in the N-hydroxyindole molecules (NHIs).¹⁴ In this library the central indole scaffold contains a hydroxyl group on the nitrogen atom and a carboxyl group in the adjacent position 2. Positions 4,5 and 6 of the aromatic rings have been suitably modified with different functional groups^{23,24} to increase selectivity as much as possible while the OH and the COOH have been identified, thank to structure activity studies, as pharmacophores because of their structural similarity of the natural substrate of LDH, and thus remained unchanged in the most efficient molecules of the library. The SAR studies of all the compounds, apart from confirming the pharmacophore activity, underline the importance of an aromatic substitution in position 6 and an additional presence of an electron-withdrawing group, like a trifluoromethyl, to enhance the selectivity and the potency. The glucose conjugation²⁵ from the OH group on the nitrogen atom also, showed a better permeability proving sufficient efficacy in

reducing lactate production and compromising cell proliferation.

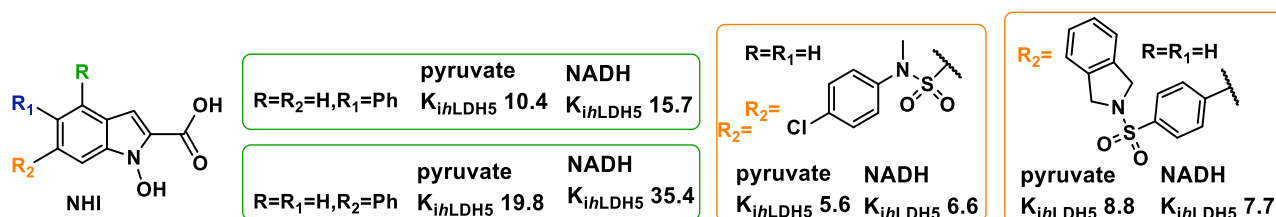


Fig.7 Structures and K_i values (expressed in μM) of N-Hydroxyindole scaffold-based hLDH5 inhibitors.

Molecular modelling studies showed that the carboxylic group interacts with the Arg 169 with the formation of a salt bridge and with Thr 248 with hydrogen bond. The interaction is also enhanced by the formation of additional hydrogen bonds by the hydroxyl group on nitrogen with Thr 248 and His 193. From these studies the aromatic group seems to be lying inside the lipophilic pocket covering part of the cofactor binding site.¹⁴

Other bicyclic aromatic compounds that appeared to have inhibitory activity for LDH are the quinoline and quinolone-based compounds where in the reference compounds, the central scaffold is substituted in position 4 by a hydroxyl group, and in position 2 or 3 by a carboxylic group, synthesized for the first time in 1972 from Baker and Bramhall.^{26–28}

Since then, these molecules have served as starting point for the elaboration of new drugs, until in 2012 GSK^{29,30} reported potent LDH inhibitors consisting of a central quinoline scaffold where position 3 is substituted by an amide or sulphonamide group, position 4 is conjugated through an amine with an aromatic ring containing a carboxyl moiety and position 7 is linked with different aromatic or heteroaromatic rings. Some of these compounds resulted to be very active and displayed in different cell types increased oxygen consumption rate and ROS activity, reduce glucose consumption and inhibition of cell proliferation. From crystal structures they appear to be competitive just for NADH and not for pyruvate and they seem to penetrate cellular membrane because of the high protein binding of the compounds. Unfortunately, their pharmacokinetics properties are still too weak for further in vivo experiments, and modification are necessary.

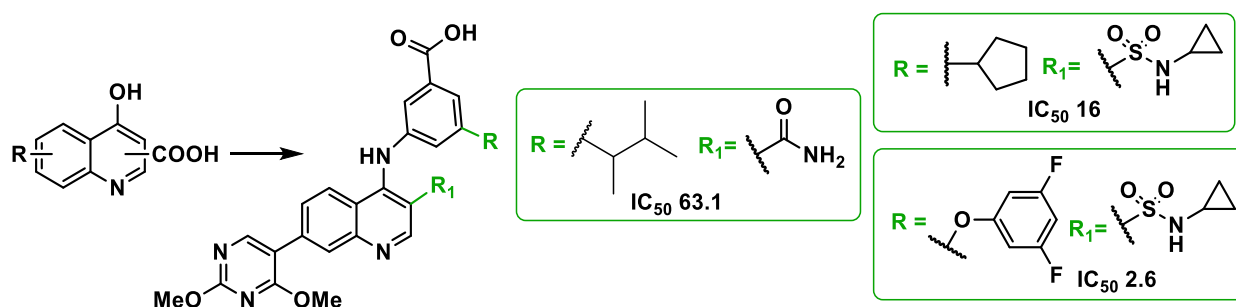


Fig.8 Structures and IC_{50} values (expressed in nM) of Quinoline scaffold-based hLDH5 inhibitors.

Some classes of compound were also designed containing a sulphur moiety. The representative

molecule of the dihydropyridine series³¹, didn't demonstrate selectivity and with the aim of improving this aspect, several analogues were synthesized by changing the sulphonamide nature or the substituents on the phenyl ring. These changes underline how the p-sulphonamide group in the aniline ring and the cyano group in the central scaffold, have a fundamental role in the LDH5 selectivity and inhibitory activity. Furthermore, it appears that also the chirality is very important to modulate the solubility in aqueous media and the cell permeability.³²

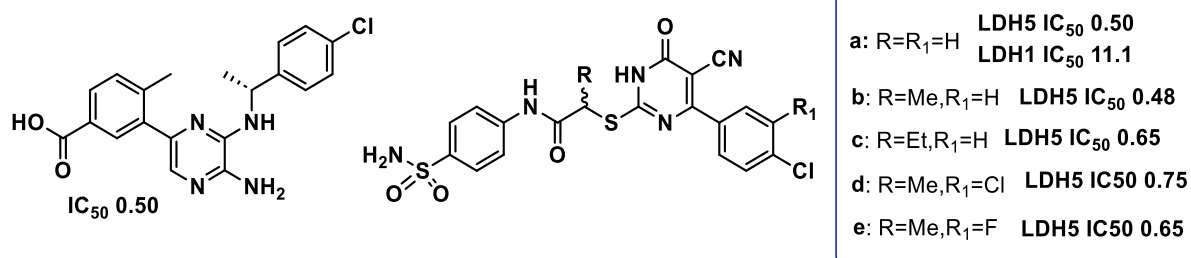


Fig.9 Structures and IC₅₀ values (in μM) of Dihydropyrimidine and pyrazine-based hLDH5 inhibitors

The solubility issue was solved with the synthesis of the dihydropyrone derivatives^{33,34}, that in fact demonstrate high solubility in physiological condition, high plasma-protein binding, and lipophilicity. The interactions seem to be stabilized by the hydrogen bond between the carbonyl group and His 192 and also with Asp 165 and more importantly by the bidentate hydrogen bond between the thioether and Arg 168. From these compounds, following the screening approach, it was possible the identification of cyclohex-2-enone derivatives that showed a marked selectivity towards LDH5. This result can be rationalized with the observation that the enol moiety mimics the carboxylate moiety of the oxamate and interacts with Arg 168, while this interaction is stabilized with the hydrogen bond between the ketone and the His 192 and Asp 137. For this latter series of compounds, too, solubility is such that they can be well administered orally but, unfortunately, their efficacy seems to be lacking.

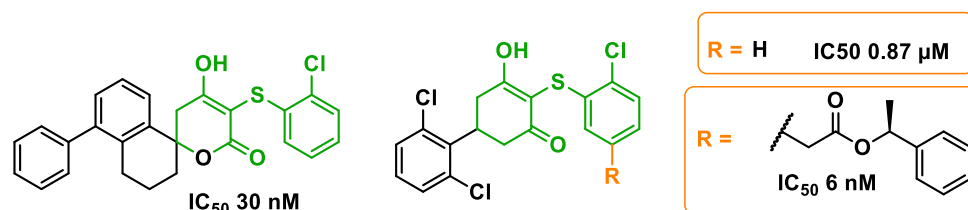


Fig.10 Structures and IC₅₀ values of dihydropyrone and cyclohex-2-enone derivatives.

All the compounds previously described can act as pyruvate or as NADH competitors and it is not sure if the molecule is more efficient acting one way or the other. In 2010 for the first time³⁵, chimeric inhibitors were synthesized and the whole binding pocket was supposed to be covered by their structure where substrate and cofactor mimic portion were present together in the same

molecule. Glycolic acid-NADH conjugate was the first one designed with the glycolic acid linked through the reduced nicotinamide ring, it displayed a strong LDH inhibition activity and cardioprotective effect which unfortunately couldn't be clinically used because of the poor permeability. Later, using the click chemistry³⁶, a bis(indolyl)-maleimide moiety was conjugated with a triazole ring with a carboxylate using various alkyl or aryl alkyl chains. Considering the sodium oxamate as reference compound, the products synthesized appear to have more inhibition activity. Further changes were made by Astrazeneca with the introduction of a diacid malonate scaffold and by ARIAD³⁷ with the use of a flexible polyhydroxyl linker.

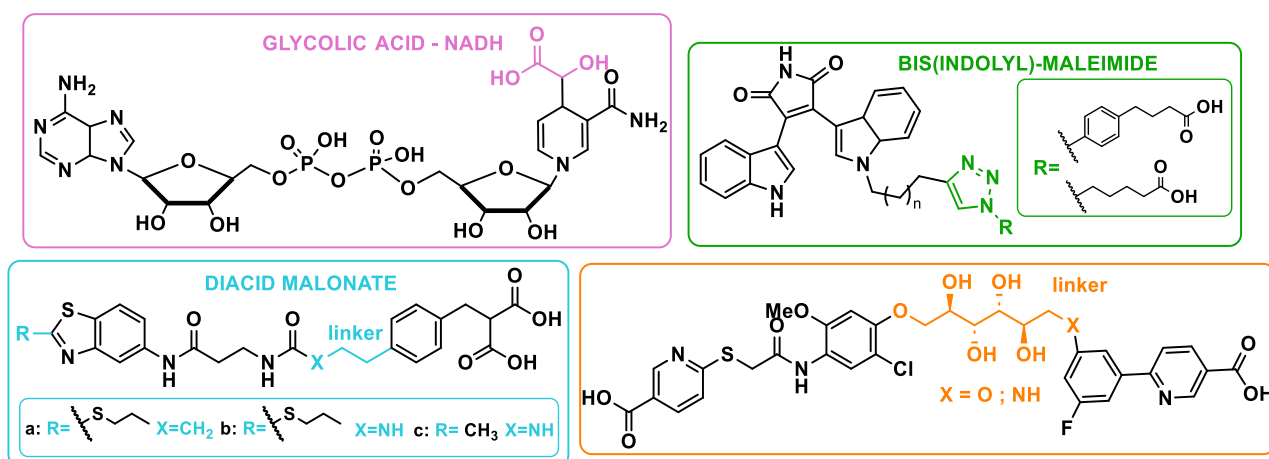


Fig.11 Structures and of chimeric bifunctional-type inhibitors.

Despite all these attempts, the develop of a new efficient therapy to destroy tumour cells without damaging the healthy tissue is still a challenging task. All these approaches described so far consider the use of small molecules and taking into account all their behaviour and crystal structures analysed, in our research group we decided to exploit the protein-protein interaction and design a peptidomimetic type structure.

3.2 - Targeting protein interactions

It is well known that proteins hold several biological functions, and they usually have one or more binding partners thus protein-protein interactions are essential for the correct activity of the cellular machinery. Proteins interact by their interfaces: each interface belongs to an independent polypeptidic chain where some residues, identified by Ala-scan and called "hot spots", give a larger contribute to the binding.³⁸ They are also organized in clusters known as hot regions, where they are tightly packed but not always through a linear surface. In fact, the protein surface is rich in pockets, crevices, and indentations which have a high complementarity with the partner surface.³⁹

Jafary and collaborators⁴⁰ were the first one to identify the LDH hot region in the two dimers involving the residues 5-17 of the N-terminal chain and the residues 293-305 of the C-terminal chain.

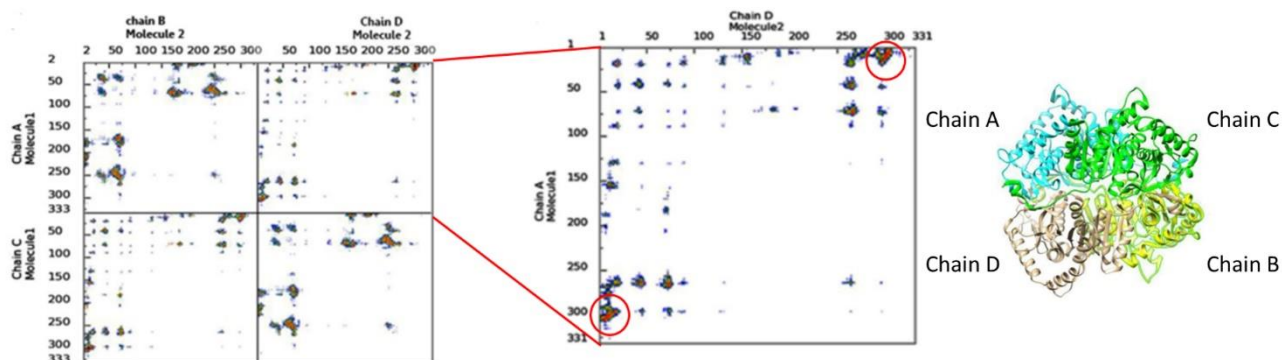


Fig.12 3D structure of the tetramers and Hot region of the dimers.

Several hydrogen bonds involving amide groups in the backbone have been predicted between Gln296, Asn297, Ser300 and Leu302 (C-terminal region of one subunit) with Gln16, Glu14, Leu11, Asn10 and Tyr 9 (N-terminal arm of the other subunit). Lateral chain of Lys304 and Asp301 establish strong H-bonds respectively with Asp5 and Asn10. Hydrophobic contacts involve both backbone and lateral chain, the most significant one regard Gln296-Gln19, Ile299-Leu11 and Leu302-Ile8.

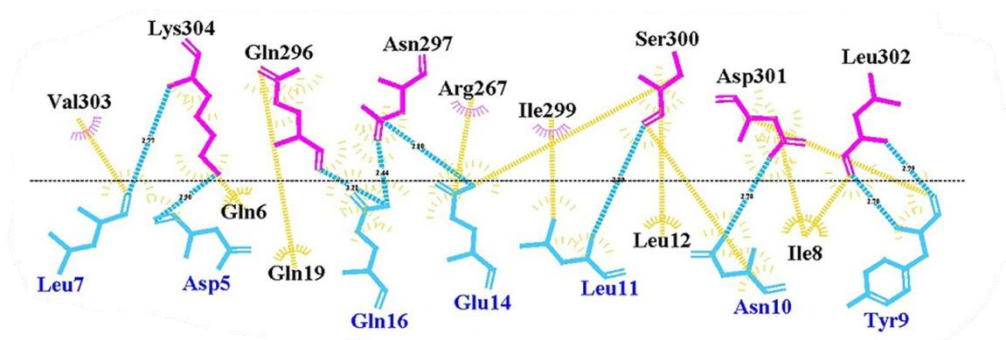


Fig.13 2D of the interaction between the dimers where H-b are in blue and Hydroph. Inter. are in yellow.

They identified several suitable linear inhibitors, among which the most promising resulted to be the sequence IYNLLK, able to increase the percentage of dimers and showing interesting inhibition activity. Furthermore, Henriques's research group⁴¹ explored the region of interaction between residues from 6 to 20 in the N-terminal arm of one subunit and the residues from 297 to 305 in the C-terminal region of its binding partner that are arranged in a β -strand. Interestingly, short linear peptides, designed as mimic of N- or C-terminus or predicted by Rosetta simulation, did not show inhibition which instead was observed when sequences mimicking the C-terminal strand were grafted into a β -strand scaffold.

LDH-B tetramerization inhibition were also investigated.⁴² LDH-A and LDH-B have highly conserved residues along in the N-terminal region, thus, inhibitors targeting that region would disassemble

without selectivity. The targeted region in this case is composed of the first 19 residues of the N-terminal, which are organised in a small helix, a short loop, and a β -strand. Linear peptides of different lengths did not show again inhibition activity, while a stapled octapeptide, mimicking the small α -helix sequence, had promising results. Stapling was achieved with the introduction of two Cys residue, in position 1 and 4 of the chain, and cross linking them by α,α' -dibromo-*m*-xylene.

3.3 - Design of peptidomimetics inhibitors

Considering the previous works and the studies over the hot region of the LDH we decided to pick up a specific region of contact between the subunits and we focused our attention on the C-terminal portion, in the segment ranging from residues Ile 299 to Leu 302.

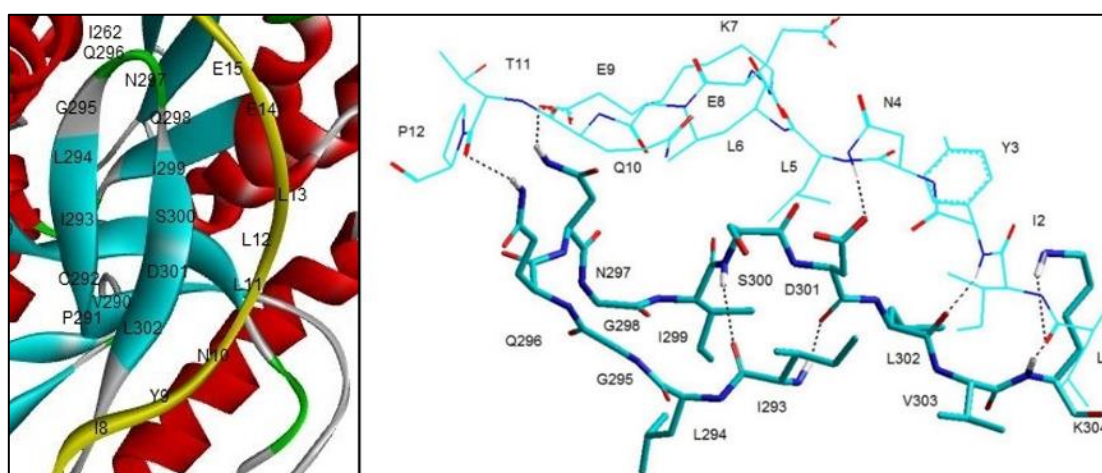


Fig.14 Magnification of the area of contact between the subunits.

As it could be seen from the image, these four amino acids form a small fold and we initially decided to exploit this folding to create a peptidomimetic, which contains the same amino acidic residues, and which would respect the appropriate residue distances by recreating the conformation present in the receptor with a rigid structure. This approach increases the probability that the synthetic product has at least the same affinity of the C-terminal chain to the residues present in the N-terminal chain. At the beginning, two cyclic peptidomimetics were designed, with the same residue apart from the length of the linker: in fact, after observing the structure in x-rays and carrying out some molecular dynamic simulations, we decided to mime Ile with the introduction of D-allo and to also invert the stereocentre of the Leu by incorporating D-Leu. From the simulations appears that these changes induce a better spatial orientation, and they are likely to give the peptide increased resistance to metabolism at the time they will have to express their function. The ring closure remains uncertain, which is why we decided to synthesize two homologues that differ

only by one carbon in linker length; in one structure we choose to insert γ -amino butyric acid, and in the other β -alanine and obtain two very similar and promising options.

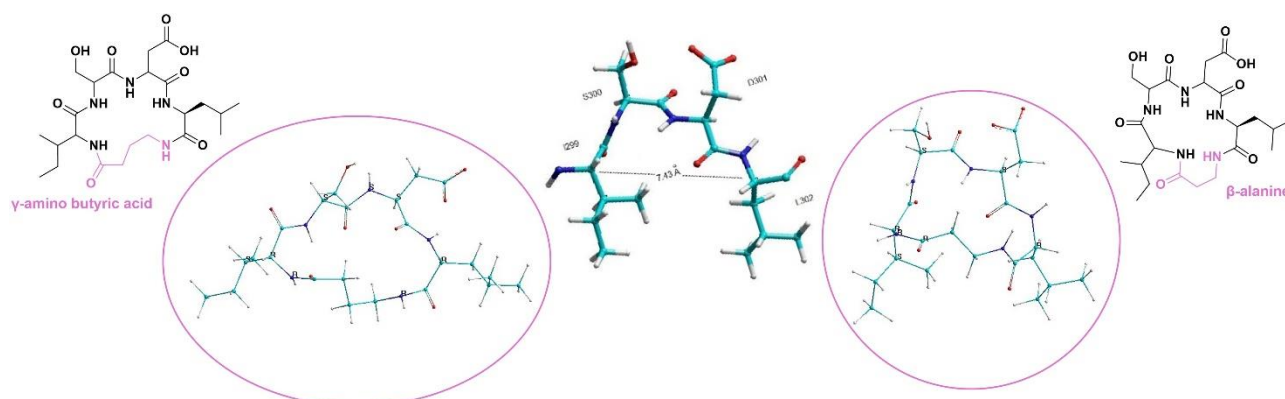


Fig.15 3D structure of the region 299-302 of the LDH enzyme and of the two peptidomimetics.

A deeply analysis of the chosen fragment makes one realise that in addition to mimicking the central part of the portion, where one ring is naturally generated, the entire fraction can be easily mimicked by generating two rings joined at the centre. The rational design undertaken to draw the two loops involves the retainment of hot spot residues like Gln296, Asp301, Leu 302 and the replacement of “secondary” ones, which have a marginal role in subunits association, with selected residues to accomplish macrolactamization. For this reason, iso-Aspartic acid, bonded by the β -carboxylic group, replaced Gly298 in the first turn, while Lysine substitute Ile299 in the second turn. Although Ile299 is a hot spot, the strong hydrophobic contact with Leu may be assured by the methylenic side chain of Lysine.

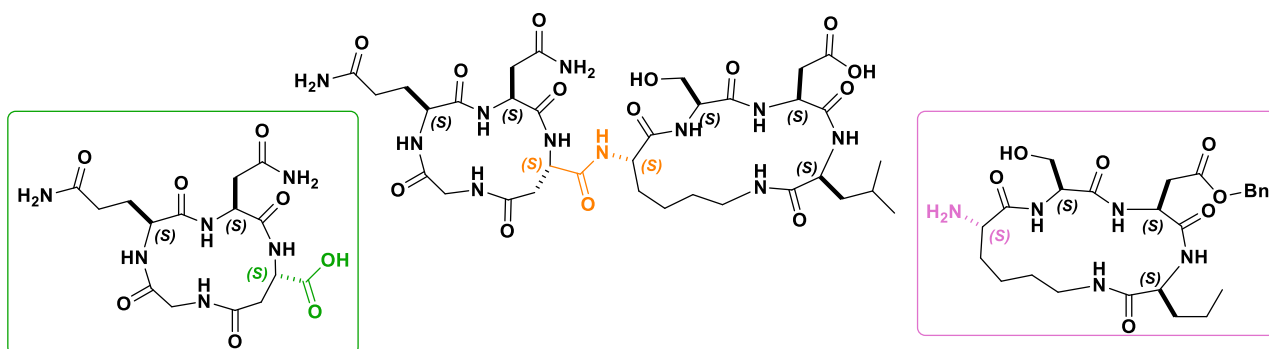


Fig.16 Structure of the second peptidomimetic also show in its divided rings.

To obtain the desired final structure two independent rings were designed and constructed in the solid phase by inserting amino acids with appropriately protected side chains with orthogonal groups. We therefore have synthesized the linear sequence for each of the two portions and performed the cyclization in order to obtain the two cyclic peptides. In this phase the reactive functional group present and not required for the formation of the ring were left protected and

deprotected just after the formation and purification of the products. At this point, the synthesis of the final loop was obtained in high dilution condition in the presence of the two rings previously formed and appropriate coupling agents.

3.4 - Synthesis of peptidomimetics inhibitors

As mentioned above, the synthesis has been conducted in solid phase regarding the production of the linear peptide precursor at first, and then after the cleavage, the cyclization in high dilution condition in liquid phase was performed.

Although all the necessary purification steps have been meticulously carried out, after several attempts, it was decided to insert D-alle as the last amino acid in the peptide chain since it is synthesized and therefore could have some impurities that can interfere with peptide growth. However, the most critical solid phase synthesis step remains the attack of the first amino acid to the resin because it is crucial for the success of the whole synthesis and to obtain a high yield at the end of the process.

Different type of resins has been used depending on the type of protective groups to be taken into account during synthesis. The resin that has been used for the synthesis of the linear precursors MSP56, MSP 89, peptide 1 and peptide 3 is the 2-Chlorotrityl, for the precursor peptide 2 was used the Wang resin and for the synthesis of the precursor peptide 6 the Rink amide resin.

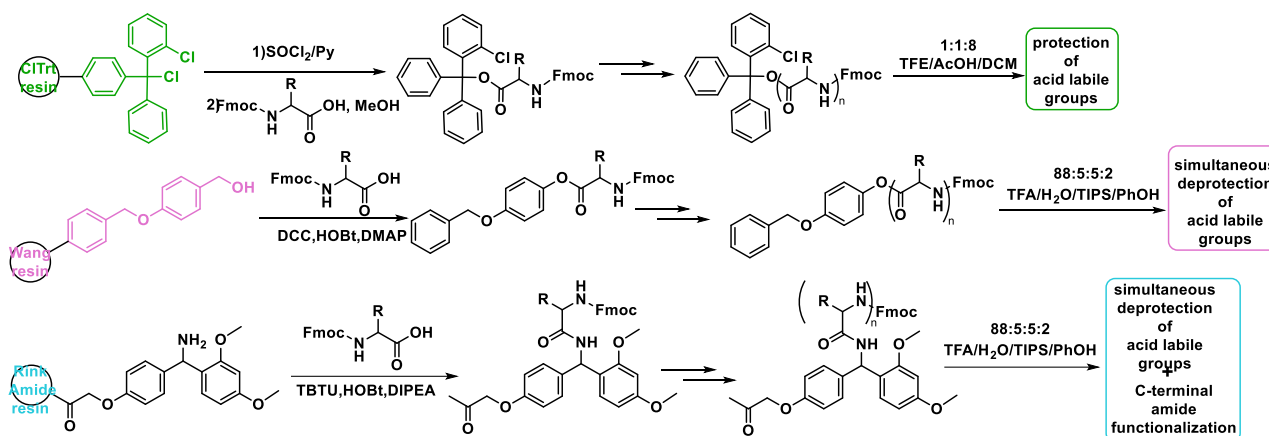
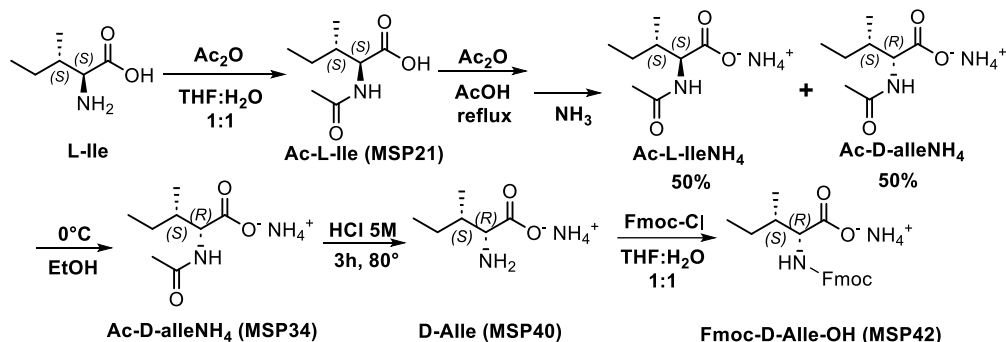


Fig.17 Kind of resins used for the solid-phase synthesis of peptide linear sequence.

The 2-Chlorotrityl resin, in particular, allows the use of protected Fmoc/tBu amino acids, that are the ones used in this project. 2-chlorotrityl resin is very sensitive to moisture that hydrolyses reactive groups at the surface of the resin to the corresponding alcohol. To accomplish a good yield, a treatment with SOCl_2 and pyridine were recommended to re-activate the resin. The cleavage of the peptide from the ClTrt resin occurs in the presence of acid, but because of the mild conditions,

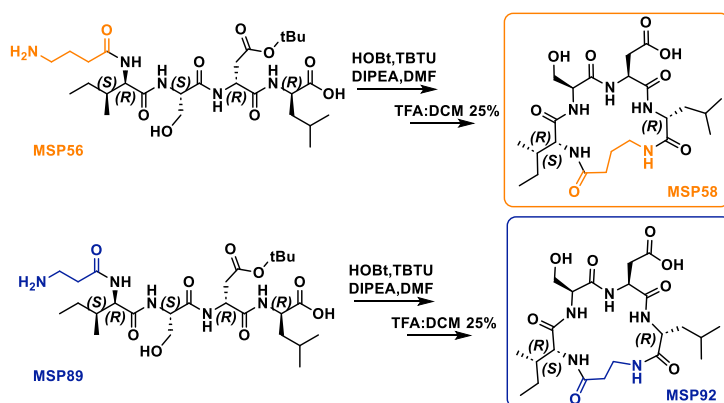
the acid labile groups remain protected. In this way it is possible to carry out all the steps of synthesis and deprotection of the peptide chain in basic conditions, without worrying that the lateral protective groups.

As already mentioned, we firstly focused our attention on the synthesis of the Fmoc-D-Alle-OH without which it would be impossible to carry on with the synthesis of the complete sequence.



The procedure known in the literature was followed, according to which the free amine must first be protected with acetic anhydride, which is then racemized to 50% by adding acetic acid. The transformation of the product into ammonium salts, makes separation with cold ethanol possible and the subsequent deprotection of the acyl group and protection with Fmoc, leads to the synthesis of the amino acid required for solid-phase synthesis.

Once the peptide sequence was completed and cleaved from the resin, the cyclization of the linear peptide precursor was performed in the liquid phase.



A syringe pump was used for the process, which allowed the reagent to be inserted into the reaction environment very slowly and so works under conditions of extreme dilution to decrease favoring the intramolecular reaction.

Finally, after purification of the neutral products with the preparative HPLC, the synthesis was concluded with the deprotection of the tert-butyl group from the side chain of aspartate operating under acidic conditions with 25% of trifluoroacetic acid (TFA).

Once the first two compounds were completed, we started the synthesis of the linear peptides necessary for the formation of the bigger ring. As mentioned before, the resins used were different depending on the protecting group present and on the requirements for the final cyclization.

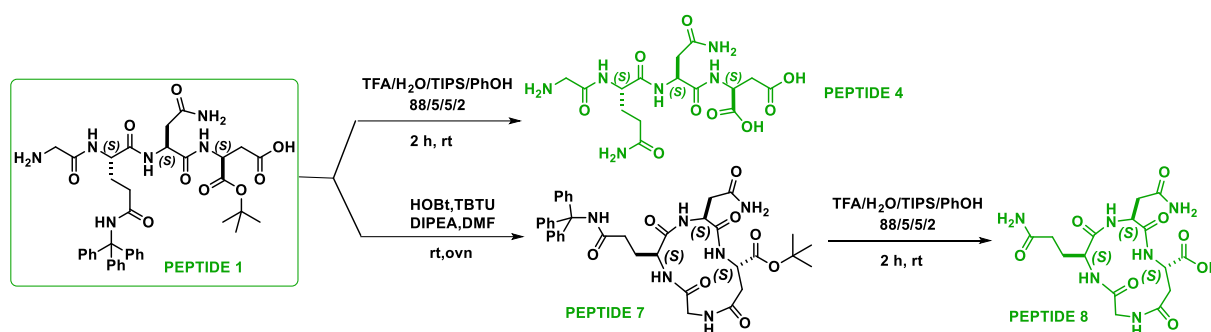


Fig.20 Schematic synthesis from peptide 1 to the final cyclic structure of peptide 8.

For peptide 1, where *-tBu* protection was present on the α -carboxylic group and that must be conserved in order to perform a chemo selective head-to-tail cyclization, a 2-chlorotrityl resin was chosen to obtain a protected peptide, since mild acidic conditions were required for cleavage, as already described. Part of the linear product was treated under acid conditions which led to the formation of peptide 4 that was tested independently for biological assays, the rest was used for the cyclization and formation of cyclic peptide 7 which undergoes acid deprotection to obtain peptide 8 as the final product.

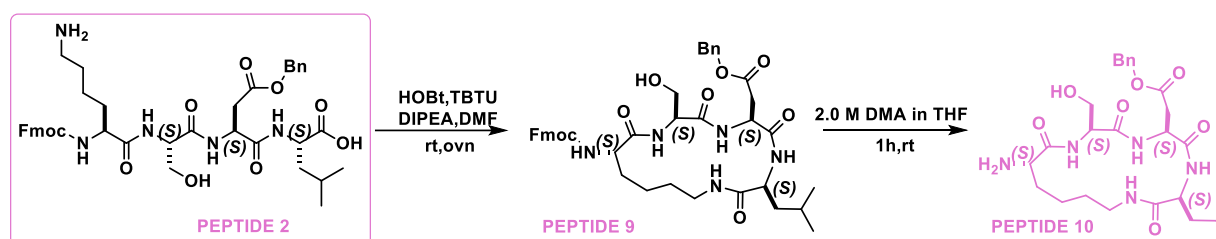


Fig.21 Schematic synthesis from peptide 2 to the final cyclic structure of peptide 10.

Peptide 2 was obtained by SPPS onto a Wang resin, one of the most widely used in SPPS since it offers a good loading, compatibility with different reaction conditions and in this case any conflicts with the protecting group present. The linear peptide obtained was fully cyclized, purified and then deprotected from the Fmoc protecting group to obtain a cyclic peptide with a free amine necessary for the final coupling with the previously synthesized cyclic peptide while the benzyl protecting group present was left to minimize the formation of side products.

The same peptide was also synthesized with a Rink Amide resin to obtain a linear peptide with the acid terminal protected by the derivatization in the amide group and it was called peptide 6. This protection is necessary to analyse the peptide in neutral form for the biological assay and make a right comparison with the other neutral peptide.

At the end, to verify the correct position of the amino acid inside the cyclic mimetic, we also synthesized the linear peptide 3, where the amino acids are the same of peptide 1 but placed in a different order.

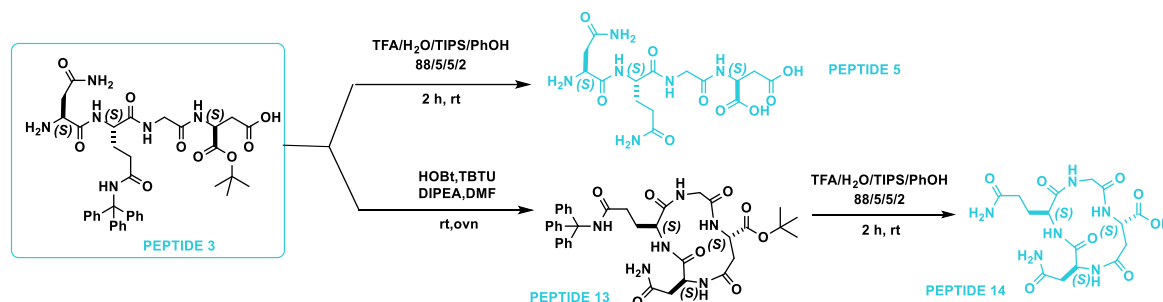


Fig.22 Schematic synthesis from peptide 3 to the final cyclic structure of peptide 14.

The synthesis was performed in the same way and the cyclic derivative peptide 14 was successfully obtained and purified to be ready for the biological tests.

3.5 - Enzymatic assay

After purification, both linear and cyclic peptides were tested *in vitro* to evaluate their inhibition power that is deduced from kinetic measurements of enzymatic reduction rate of pyruvate to lactate with and without peptidic inhibitor. Each measurement was performed under steady state condition, using substrate concentration higher than their standard K_M , thus, a pseudo zero-order enzymatic kinetic is observed. Tuning of incubation time, substrate concentration, TRIS buffer concentration, pH values were also explored to understand their influence on results and design optimal experimental conditions for testing inhibitors.

At the beginning the first two compounds were tested, MSP58 and MSP92. Samples were at first prepared with a concentration 0.9 nM of monomeric LDH-A, 500 μ M of pyruvate, 125 μ M of β -NADH, and 10 μ M or 50 μ M of peptidic inhibitor in DMSO and TRIS buffer 50 mM (pH = 7.5). In both cases unfortunately, the inhibition activity resulted to be very modest with a rate of 13% and 14% in the best case, and so they were considered not active.

We therefore continued the test with the second part of the peptidomimetics starting with peptide 5 and the correspondent cyclic peptide 14 and we performed several attempts to find the best conditions. The samples were prepared in the same condition of the first try but with a concentration

of 80 μM of peptidic inhibitor. This concentration is very high for sensing an inhibition, however it represents a threshold to exclude from further screening those compounds which yield a poor inhibition, even though they are present in a huge excess. After mixing, the cuvette was left incubate at room temperature for 5 minutes.

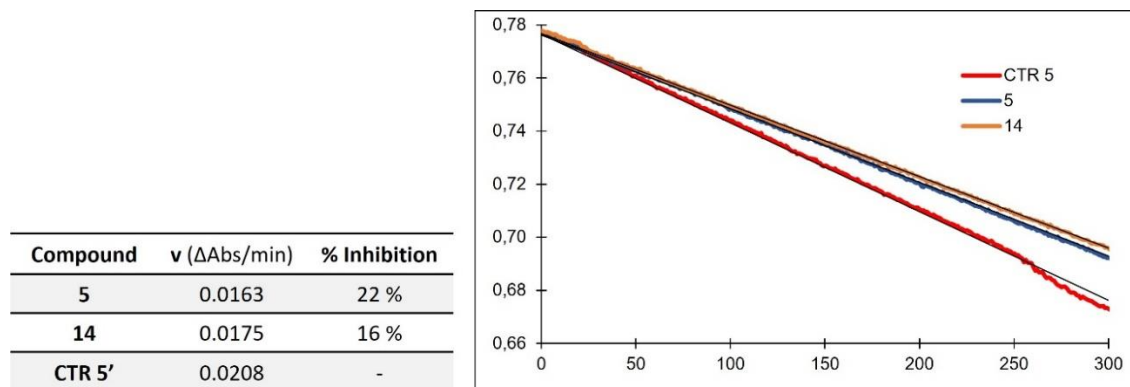


Fig.23 Enzymatic reaction rate ($\Delta\text{Abs}/\text{min}$), % inhibition and related β -NADH absorbance decay, abs vs t (0.9 nM LDHA, 500 μM pyruv., 125 μM β -NADH, 80 μM inhibitor, 50 mM TRIS, incub. T = 5 min.)

This first screening shows that compounds 5 and 14 have a significant inhibition activity while compound 6 resulted to have an inhibition activity minor than 1%. This result suggested that the retropeptide 5 and the related macrolactam 14 are biologically active compound despite their inverted aminoacidic sequence.

After mixing substrates, monomeric enzyme and inhibitor, an incubation period is required to let the protein surface-inhibitor interaction occur. Samples were prepared with the same concentration, but the incubation time was increased from 5 minutes to 20 minutes with no significant effect in the activity. In fact, it appears that an incubation time of five minutes is long enough to ensure a complete interaction between the monomeric unit of the enzyme and the inhibitor and so this time it was chosen to be used for the following tests.

For a better understanding, we also tested different concentrations of the substrate. In fact, a reduced concentration of β -NADH was also tested to evaluate whether the inhibition activity was in part due to the large amount of substrate present. The sample was therefore prepared with a concentration of 0.9 nM of monomeric hLDH-A, 500 μM of pyruvate, 30 μM of β -NADH, 80 μM of peptidic inhibitor in DMSO and 50 mM of TRIS buffer (pH = 7.5). Once again, the reduced molar concentration of β -NADH does not modify the observed inhibition and with 30 μM of β -NADH the reaction rate and the % of inhibition are not significantly different if compared with the results obtained with a concentration of 125 μM .

In biological tests it is very common to use Tri(hydroxymethyl)aminomethane (TRIS) because it has a good buffer power near to physiologic conditions and it offers major compatibility with biological fluids.

respect to other buffers. It is well known that TRIS concentration affects ionic strength of the solution and the aggregation of the enzyme so, to verify how this parameter affect our tests, we changed the concentration from 50 mM to 10 mM while the other components of the sample were used at the same concentration of before.

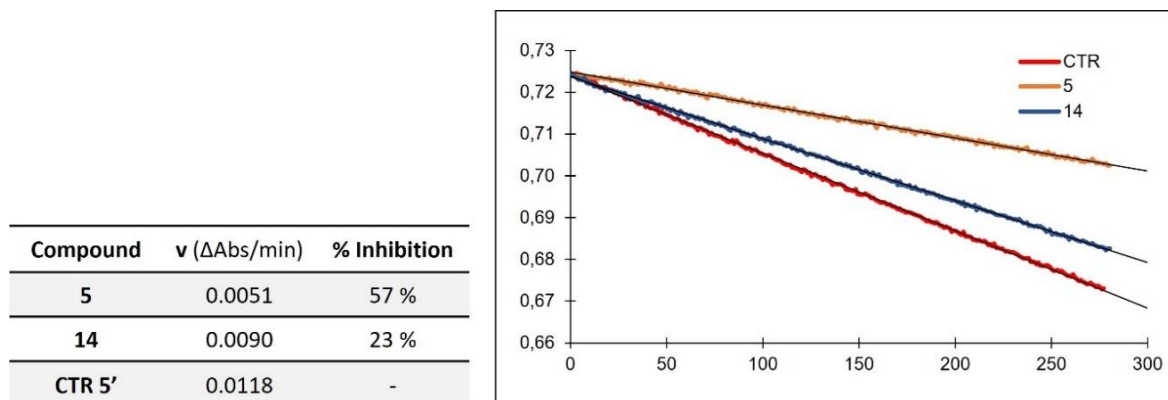


Fig.24 Enzymatic reaction rate (Δ Abs/min), % inhibition and related β -NADH absorbance decay, abs vs t (0.9 nM LDHA, 500 μ M pyruv., 125 μ M β -NADH, 80 μ M inhibitor, 10 mM TRIS, incub. T. = 5min.)

As we can see from the figure, the plotted lines clearly highlight the influence of TRIS concentration on kinetic measurement: 50 mM determinates a higher ionic strength and monomeric subunits of the enzyme may not tolerate this condition and consequently the aggregation occurs to limits protein surface exposition to the medium. On the other hand, a gentle ionic strength maintains dissociated the enzyme, thus, an efficient binding of the inhibitor to the subunit surface occurs and in fact, all the tested compounds present a better % inhibition. After this observation, the concentration 10 mM of TRIS will be used in the next enzymatic assay but since the first two peptides, MSP58 and MSP92, appear to give the worst response, they won't be tested in the following experiments. PH effect was also explored, and the inhibition was evaluated at pH 7.5 and pH 6.5 using the universal buffer TRIS 10 mM/Bis-TRIS 10 mM. At the mild acidic condition, LDH-A subunits association is strongly slowed, thus, in the sample the enzyme exists mainly as monomer. Kinetic measurements at pH 6.5 demonstrate that the monomeric unit is still capable to catalyse reduction of pyruvate into lactate, although a lower efficiency and smaller % of inhibition is observed since no assembly could be achieved and probably a partial denaturation occurred. The inhibition rate for compound 5 resulted to be extremely decreased from 57% to a 13 % while surprisingly, for the compound 14 the trend is reversed, and it passed from an inhibition rate of 25% at pH = 7.5 to a rate of 37% in slightly acidic condition.

All the tests were performed for all the peptidomimetics and compound 8 appeared to be the most promising inhibitor, since it reduces for almost the 80 % the activity of LDH-A preventing its association. Further investigations were carried on evaluating if inhibition was still significative at

lower concentration and the compound was also tested at concentration of 40 μM , resulting in a reduced, but desirable, inhibition activity of 58%.

Starting from this data a very approximated dose-response curve could be traced to estimate the IC50 value that appeared to be around 20 μM . However other test with different peptidic inhibitor concentration must be performed to obtain a more precise dose-response curve.

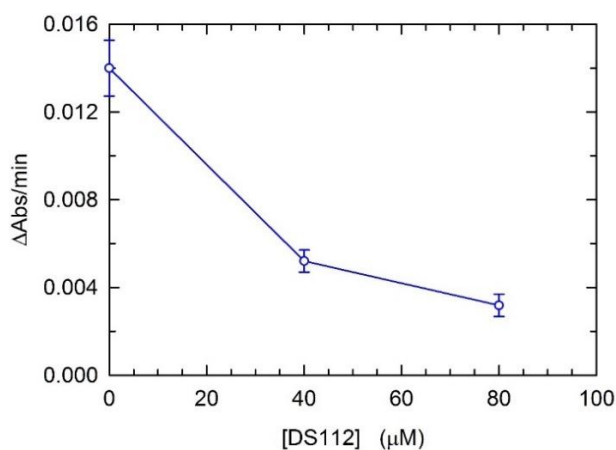


Fig.25 Dose-response curve with related standard deviation for compound 8.

3.6 - Conclusions

After a deep analysis of the LDHA structure, some cyclic peptidomimetics were designed and synthesized in solid phase in search of a new inhibitor. Unfortunately, the first two compounds almost didn't have any inhibitory activity while, among all the other molecule of the second series, compound 8 resulted to have the most promising result. Regarding the second series particularly, compounds 4, 5, 8 and 14 were mimetics for the sequence Gly295-Gly298 and induce a better inhibition while compounds 12 and 6 were mimetics for the sequence Ile299-Val302.

The results obtained confirmed the hypothesis that the β -turn occurring from Ile299-Leu302 has a marginal role in surfaces contact between the subunits. In fact, only macrolactamization of precursor 4 improved inhibition power of the mimetic, since a conformational restrain is achieved and later chain occupies a precise orientation in the space while macrolactamization of compound 6 to yield mimetic 12 resulted in no further improvement of inhibition activity and macrocyclization of compound 5 aggravated inhibition since for compound 14 a higher reaction rate is recorded. This may be caused by the wrong aminoacid sequence of these compounds respect to the one in the subunit and the conformational restrain introduced by macrolactamization. In fact, if in one hand the side chain of Ans and Gln in the reverse order and with a frozen orientation determined an unfavourable interaction with residues on the targeted N-terminal arm of the subunit, on the other hand, the major flexibility of the linear peptide made the side chain freer to interact, even with the

incorrect order. In addition, the better inhibition of compound 8 could also be explained considering that the sequence H-Asn-Gln-Gly-Asp-OH naturally folded as β -turn because it is well known that Asn at the first position and Gly at the third position of the sequence are β -turn inducer. In fact, Asn side chain forms a stable H-bond with residue at position 2, while Gly has high mobility to assure the twist conformation typical of a turn.

3.7 - Experimental procedures

General Information

Chemical reagents, including protected amino acids, were purchased from commercial sources, and used without purification.

Peptide purity was assessed by analytical RP HPLC performed on an 1100 series apparatus Agilent Technologies, Milan, Italy, using an XSelect Peptide CSH C18 column (Waters, Milford, MA, USA), 4.6 mm \times 100 mm, 130 Å, 3.5 μ m. The mobile phase was a mixture of 0.5% HCOOH in H₂O and 0.5% HCOOH in CH₃CN for ionic peptides (method A) or H₂O/CH₃CN for neutral peptides (method B). Alternative to HPLC-MS, purities were assessed by reverse-phase ultra-performance liquid chromatography (RP-UPLC), using a reverse-phase (RP) column mod. Acquity UPLC[®] BEH C18 1.7 μ m (2.1 \times 50 mm); DAD 210 nm; DAD 254 nm; mobile phase: from 2:8 solvent A/solvent B to 7:3 solvent A/solvent B, in 26 min, at a flow rate of 0.3 mL/min, followed by 4 min at the same composition; solvent A = 0.1% HCOOH in H₂O, B = 0.1% HCOOH in CH₃CN.

MS (ESI) analysis was performed using an MS single quadrupole HP 1100 MSD detector (Agilent Technologies, Milan, Italy).

Fmoc-Rink Amide resin (0.5 g, substitution 0.45 mmol/g) was swollen in DMF (5 mL) for 15 min before the use. Fmoc deprotection was carried out by treatment with 20% piperidine/DMF (5 mL) for 20 min; after filtration, the treatment was repeated for further 40 min. The resin was subsequently washed 3 times with DMF, Et₂O, DCM (5 mL each). Fmoc-amino acid (2.5 eq.) carrying orthogonal protecting groups at the side chains and HOBt (2.5 eq.) were dissolved in DMF (3 mL), and after 10 min this mixture was added to the resin at RT. Then, TBTU (2.5 eq.) and DIPEA (4.0 eq.) were also added, and the mixture was shaken for 3 h at RT. The suspension was filtered, and the resin was subsequently washed 3 times with DMF, Et₂O, DCM (5 mL each). Coupling efficacy was monitored by the Kaiser test.

General procedure for solid phase peptide synthesis

For the loading of the first amino acid Clrt resin (0.5 g, substitution 0.45 mmol/g), the amino acid

(1.2eq.) and DIPEA (5eq.) were allowed to stir at room temperature for two hours in DCM (10mL/g). Capping was performed adding MeOH (1mL/g) and letting the reaction swelled for 20 minutes before the washes. The suspension was filtered, and the resin was subsequently washed 3 times with DMF, Et₂O, DCM (5 mL each). Coupling efficacy was monitored by the Kaiser test.

For the Fmoc deprotection 4 mL of a 25 % piperidine in DMF solution were added in the reactor. After 20 minutes of orbital shaking, resin was washed with DMF (1 min x 3 times). Other 4 mL of 25 % piperidine in DMF solution were poured in the reactor and further left stir for 30 minutes. The suspension was filtered, and the resin was subsequently washed 3 times with DMF, Et₂O, DCM (5 mL each). Deprotection efficacy was monitored by the Kaiser test.

N-Fmoc protected amino acid (2.5 eq.) and HOBT (2.5 eq.) were dissolved in 4 mL of DMF and allowed to stir from 5 to 10 minutes, until complete dissolution. The solution was quantitative poured in the reactor, then TBTU (2.5 eq.) and DIPEA (4 eq.) were added. The reactor was vigorously shaken by an orbital shaker from 2 to 3 hours at room temperature, and the coupling was monitored by Kaiser test.

The cleavage of the peptide from the resin was performed with 10 ml of a mixture of 1:1:8 TFE/AcOH/DCM, added to the reactor and allowed to act for 2 hours while stirring at room temperature. The mixture was then collected in a flask and numerous washes were carried out of the resin remaining in the reactor with DCM and Et₂O. Then all the solvent was evaporated, and a shredding was carried out in Et₂O. The precipitate obtained was then analyzed with LC-MS.

General procedure for cyclization

HOBT (3 eq.), TBTU (3 eq.) e DIPEA (6eq.) were dissolved in 15 mL of DMF. Linear peptide was dissolved in 10 mL of DMF and took up in a syringe. The syringe was placed into a syringe pump in order to slowly add dropwise the linear precursor to the coupling reagents solution. Reaction was carefully monitored by analytical HPLC-MS until complete conversion was achieved. DMF was removed by compressed air, the residue was dissolved in EtOAc (10 mL) and washed with HCl 1 M (5 mL) and Na₂CO₃ saturated solution (5 mL). The organic phase was concentrated under reduced pressure and trituration in cold ether afforded the product.

Acetyl-D-alloisoleucine (MSP34)

The amino acid is dissolved in 8mL of THF (1mL/100mg) and a saturated solution of Na₂CO₃ in 1:1 ratio together with a large excess of acetic anhydride (10 eq., 30.5 mmol, 2.8mL). The mixture was then stirred for two hours at room temperature. The solution was acidified with HCl 1M and the

organic solvent was removed before the extraction with DCM/MeOH. The crude product was then dissolved in 5 mL of glacial acetic and acetic anhydride (0.5 eq., 150 μ L) and allowed to stir under reflux for 5 hours. Solvent was removed and Ac-L-Ile: Ac-D-alle 1:1 mixture was then treated with NH₃ 1M and precipitated into ethanol, resulting in only Ac-D-alle crystals.

¹H NMR (DMSO-d₆, 400MHz): δ 7.23 – 7.20 (d, 1H), 4.05 – 4.01 (dd, 1H), 1.79 (s, 3H), 1.29 – 1.26 (m, 1H), 1.02 – 0.98 (m, 1H), 0.85 (s, 3H); **HPLC-MS:** [M+1] = 174, [2M+1] = 347

Fmoc-D-Alleucine (MSP42)

Ac-D-alleNH₄ (165mg; 1,26mmol) was dissolved in 5 mL of HCl 5M. The mixture was stirred for 3 hours at 80°C. The solvent was removed, and the crude product dissolved in 6mL of THF: H₂O (1:1). Na₂CO₃ (1 eq., 1.26 mmol, 134 mg) was added together with Fmoc-Cl (1eq., 1.26 mmol, 326 mg) in the precooled mixture, then the reaction was allowed to reach room temperature and allowed to stir overnight. The day after the solution was slowly acidified to reach pH=3 and the product was recollected pure by filtration. (350 mg, Y=80%); **HPLC-MS:** [M+1] = 353, [2M+Na] = 726

H₂N-Gaba-D-Leu-Asp(tBu)-Ser-D-alle-OH (MSP56)

It was isolated as a white solid as a TFA salt (40 mg, 0.068 mmol). Purity was determined to be 94% by analytical RP HPLC (method A); **HPLC-MS:** [M+1] = 531

H₂N- β Ala-D-Leu-Asp(tBu)-Ser-D-alle-OH (MSP89)

It was isolated as a white solid as a TFA salt (20 mg, 0.04 mmol). Purity was determined to be 96% by analytical RP HPLC (method A); **HPLC-MS:** [M+1] = 519

Cyclization of MSP 56 (MSP 58)

General procedure for cyclization was performed on linear peptide MSP 56 (40 mg, 0.068 mmol). After the extraction, HPLC preparative was performed on the crude product to obtain the pure product MSP 58. To remove tBu protecting group, the product was dissolved in 2mL of a solution of DCM with 25% of TFA and allowed to stir at room temperature for 1 hour. Solvent was removed and the crude mixture triturated with Et₂O to obtain the pure product (3mg); **HPLC-MS:** [M+1] = 514

Cyclization of MSP 89 (MSP 92)

General procedure for cyclization was performed on linear peptide MSP 89 (20 mg, 0.04 mmol). After the extraction, HPLC preparative was performed on the crude product to obtain the pure

product MSP 92. To remove tBu protecting group, the product was dissolved in 2mL of a solution of DCM with 25% of TFA and allowed to stir at room temperature for 1 hour. Solvent was removed and the crude mixture triturated with Et₂O to obtain the pure product (2mg); **HPLC-MS**: [M+1] = 501

H₂N-Gly-Gln(Trt)-Asn-isoAsp(tBu)-OH (peptide1)

General procedure for solid phase peptide synthesis was performed using a ClTrt resin in order to obtain peptide 1 as a white solid (196.7 mg, Y=27 %); **HPLC-MS**: [M+1] = 731, [M+23] = 753.

Fmoc-Lys-Ser-Asp(Obn)-Leu-OH (peptide2)

General procedure for solid phase peptide synthesis was performed using a Wang resin in order to obtain peptide 1 as a white solid (254 mg, Y= 54 %); **HPLC-MS**: [M+1] = 774, [M+23] = 796.

H₂N-Asn-Gln(Trt)-Gly-isoAsp(tBu)-OH (peptide3)

General procedure for solid phase peptide synthesis was performed using a ClTrt resin in order to obtain peptide 1 as a white solid (95 mg, Y= 14 %); **HPLC-MS**: [M+1] = 731, [M+23] = 753.

H₂N-Gly-Gln-Asn-isoAsp(tBu)-OH (peptide4)

Peptide 1 (5.6 mg, 0.0077 mmol) was treated for 2 hours with the cocktail cleavage TFA/water/TIPS/PhOH: 88/5/5/2. The vial was dried under compressed air. Purification by trituration in cold ether afforded the pure product as white crystals (2.8 mg, Y= 84 %); **HPLC-MS**: [M+1] = 433, [M+23] = 455

H₂N-Asn-Gln-Gly-isoAsp(tBu)-OH (peptide5)

Peptide 3 (96 mg, 0.13 mmol) was treated for 2 hours with the cocktail cleavage TFA/water/TIPS/PhOH: 88/5/5/2. The vial was dried under compressed air. Purification by trituration in cold ether afforded the pure product as white crystals (41.2 mg, Y= 73 %); **HPLC-MS**: [M+1] = 433, [M+23] = 455.

Cyclization of peptide 1 (peptide 8)

General procedure for cyclization was performed on linear peptide 1 (86.9 mg, 0.12 mmol). After the extraction, HPLC preparative was performed on the crude product to obtain the pure product peptide 7. Solvent was removed and the crude mixture triturated with Et₂O to obtain the pure product (2mg); **HPLC-MS**: [M+1] = 713.

After the analysis the product 7 was treated for 2 hours with the cocktail cleavage TFA/water/TIPS/PhOH: 88/5/5/2. The vial was dried under compressed air. Purification by trituration in cold ether afforded the pure product 8 as white crystals; **HPLC-MS**: [M+1] = 415

Cyclization of peptide 2 (peptide 10)

General procedure for cyclization was performed on linear peptide 2 (254 mg, 0.33 mmol). After the extraction. Solvent was removed and the crude mixture trituated with Et₂O to obtain the pure product 9 (211mg, Y= 85%); **HPLC-MS**: [M+1] = 756.

After the analysis, the product 9 (12mg, 0.018 mmol) was dissolved in 2mL of a 2.0M solution of DMA in THF and the reaction was allowed to stir for 1 hour at room temperature. Solvent was removed and the crude washed three times with THF/Hexane 2:1 affording peptide 10 as a pure product (5.5 mg, Y= 69%); **HPLC-MS**: [M+1] = 534, [M+23] = 557.

Cyclization of peptide 3 (peptide 14)

General procedure for cyclization was performed on linear peptide 3 (70 mg, 0.096 mmol). After the extraction. Solvent was removed and the crude mixture trituated with Et₂O to obtain the pure product 13 (43.2mg, Y= 63%); **HPLC-MS**: [M+1] = 713.

After the analysis the product 13 (43.2mg, 0.061mmol) was treated for 2 hours with the cocktail cleavage TFA/water/TIPS/PhOH: 88/5/5/2. The vial was dried under compressed air. Purification by trituration in cold ether afforded the pure product as white crystals (24.1 mg, Y=96%); **HPLC-MS**: [M+1] = 415, [M+23] = 437.

Enzymatic assay

Reaction rates were derived spectrophotometrically, following β -NADH absorbance decay over 600 s at the fixed wavelength of 340 nm, since it corresponds to the maxima excitation. Data were analysed by "Kinetic" software, which interpolates experimental point and provides initial reaction rates expressed as Δ Abs/min. Molar reaction rates could be calculated by dividing those values by the molar extinction coefficient of β -NADH, $\epsilon = 6200 \text{ M}^{-1} \text{ cm}^{-1}$.

Samples were prepared from stock solutions of monomeric hLDH-A, pyruvate, β -NADH, inhibitor (diluted in DMSO) and a buffer. After mixing, samples were let incubate to favour association between subunits and inhibitor.

Peptidic inhibitors were diluted in Eppendorf with DMSO to final concentration of 8 mM and cooled to 0°C in ice bath. Stock solutions of pyruvate (100 mM in TRIS 50 mM), monomeric hLDH-A (18 μ M

in TRIS 50 mM), buffer and β -NADH in TRIS 50 mM were also cooled to 0 °C. β -NADH solution concentration was determined by Lambert-Beer equation ($\epsilon = 6200 \text{ M}^{-1} \text{ cm}^{-1}$). TRIS 50 mM pH = 7.5, TRIS 10 mM pH = 7.5, TRIS 10 mM/Bis-TRIS 10 mM pH = 7.5 and TRIS 10 mM/Bis-TRIS 10 mM pH = 6.5 were used as buffer. Pyruvate and enzyme stock solution were further diluted 1: 100 in analysis buffer to the final concentration of 1 mM and 180 nM respectively. Samples were prepared adding by micropipette the appropriate volume to have the final concentration. For each assay a control (CTR) sample was prepared in the same way without adding the peptidic inhibitor. The samples were let incubate at room temperature for variable time, then NADH absorbance decay was monitored spectrophotometrically (Cary Bio 300 Agilent) at a fixed absorption wavelength of 340 nm. All the test performed are reported in the table below.

Table 1 Schematic representation of all the tests performed on the peptidomimetic compounds.

name	conc.	Pyruv.	NADH	LDH-A	Buffer	pH	time	v($\Delta A/m$)	% inh.
MSP58	10 μM	500 μM	125 μM	0.9 nM	50 mM	7.5	10 min	0.0157	7%
MSP58	50 μM	500 μM	125 μM	0.9 nM	50 mM	7.5	10 min	0.0159	13%
MSP92	10 μM	500 μM	125 μM	0.9 nM	50 mM	7.5	10 min	0.0163	9%
MSP92	50 μM	500 μM	125 μM	0.9 nM	50 mM	7.5	10 min	0.0151	14%
P5	80	500	125	0.9	50	7.5	5 min	0.0163	22%
P5	30	500	125	0.9	50	7.5	5 min	0.0165	14%
P5	80	500	125	0.9	10	7.5	5 min	0.0051	57%
P5	80	500	125	0.9	10	6.5	5 min	0.0092	13%
P6	80	500	125	0.9	50	7.5	5 min	0.0192	<1%
P6	80	500	125	0.9	10	7.5	5 min	0.0081	31%
P14	80	500	125	0.9	50	7.5	5 min	0.0175	16%
P14	80	500	125	0.9	50	7.5	20 min	0.0164	19 %
P14	80	500	125	0.9	10	7.5	5 min	0.0090	23%
P14	80	500	125	0.9	10	6.5	5 min	0.0067	37%
P4	80	500	125	0.9	10	7.5	5 min	0.0073	41%
P8	80	500	125	0.9	10	7.5	5 min	0.0032	77%
P8	40	500	125	0.9	10	7.5	5 min	0.0057	58%
P12	80	500	125	0.9	10	7.5	5 min	0.0114	28%

Fig.26 Schematic representation of all the tests performed on the peptidomimetic compounds.

3.8 – Bibliography

- (1) Farhana, A.; Lappin, S. L. *Biochemistry, Lactate Dehydrogenase*; 2022.
- (2) Read, J. A.; Winter, V. J.; Eszes, C. M.; Sessions, R. B.; Brady, R. L. Structural Basis for Altered Activity of M- and H-Isozyme Forms of Human Lactate Dehydrogenase. *Proteins* **2001**, *43* (2), 175–185. [https://doi.org/10.1002/1097-0134\(20010501\)43:2<175::aid-prot1029>3.0.co;2-#](https://doi.org/10.1002/1097-0134(20010501)43:2<175::aid-prot1029>3.0.co;2-#).
- (3) Holmes, R. S.; Goldberg, E. Computational Analyses of Mammalian Lactate Dehydrogenases: Human, Mouse, Opossum and Platypus LDHs. *Comput Biol Chem* **2009**, *33* (5), 379–385. <https://doi.org/10.1016/j.compbiolchem.2009.07.006>.
- (4) Adeva-Andany, M.; López-Ojén, M.; Funcasta-Calderón, R.; Ameneiros-Rodríguez, E.; Donapetry-García, C.; Vila-Altesor, M.; Rodríguez-Seijas, J. Comprehensive Review on Lactate Metabolism in Human Health. *Mitochondrion* **2014**, *17*, 76–100. <https://doi.org/10.1016/j.mito.2014.05.007>.
- (5) SPRIET, L. L.; HOWLETT, R. A.; HEIGENHAUSER, G. J. F. An Enzymatic Approach to Lactate Production in Human Skeletal Muscle during Exercise. *Med Sci Sports Exerc* **2000**, *32* (4), 756–763. <https://doi.org/10.1097/00005768-200004000-00007>.
- (6) Brown, J. M.; Wilson, W. R. Exploiting Tumour Hypoxia in Cancer Treatment. *Nat Rev Cancer* **2004**, *4* (6), 437–447. <https://doi.org/10.1038/nrc1367>.
- (7) Feng, Y.; Xiong, Y.; Qiao, T.; Li, X.; Jia, L.; Han, Y. Lactate Dehydrogenase A: A Key Player in Carcinogenesis and Potential Target in Cancer Therapy. *Cancer Med* **2018**, *7* (12), 6124–6136. <https://doi.org/10.1002/cam4.1820>.
- (8) Fantin, V. R.; St-Pierre, J.; Leder, P. Attenuation of LDH-A Expression Uncovers a Link between Glycolysis, Mitochondrial Physiology, and Tumor Maintenance. *Cancer Cell* **2006**, *9* (6), 425–434. <https://doi.org/10.1016/j.ccr.2006.04.023>.
- (9) Augoff, K.; Hryniewicz-Jankowska, A.; Tabola, R. Lactate Dehydrogenase 5: An Old Friend and a New Hope in the War on Cancer. *Cancer Lett* **2015**, *358* (1), 1–7. <https://doi.org/10.1016/j.canlet.2014.12.035>.
- (10) Fan, T.; Lane, A.; Higashi, R. Stable Isotope Resolved Metabolomics Studies in Ex Vivo Tissue Slices. *Bio Protoc* **2016**, *6* (3). <https://doi.org/10.21769/BioProtoc.1730>.
- (11) Granchi, C.; Bertini, S.; Macchia, M.; Minutolo, F. Inhibitors of Lactate Dehydrogenase Isoforms and Their Therapeutic Potentials. *Curr Med Chem* **2010**, *17* (7), 672–697. <https://doi.org/10.2174/092986710790416263>.
- (12) Yu, Y.; Deck, J. A.; Hunsaker, L. A.; Deck, L. M.; Royer, R. E.; Goldberg, E.; vander Jagt, D. L. Selective Active Site Inhibitors of Human Lactate Dehydrogenases A4, B4, and C4. Abbreviations: LDH, Lactate Dehydrogenase; and LDH-A4, -B4, and -C4, Human Lactate Dehydrogenases A4, B4, and C4. *Biochem Pharmacol* **2001**, *62* (1), 81–89. [https://doi.org/10.1016/S0006-2952\(01\)00636-0](https://doi.org/10.1016/S0006-2952(01)00636-0).
- (13) Shi, Y.; Pinto, B. M. Human Lactate Dehydrogenase A Inhibitors: A Molecular Dynamics Investigation. *PLoS One* **2014**, *9* (1), e86365. <https://doi.org/10.1371/journal.pone.0086365>.
- (14) Granchi, C.; Roy, S.; Giacomelli, C.; Macchia, M.; Tuccinardi, T.; Martinelli, A.; Lanza, M.; Betti, L.; Giannaccini, G.; Lucacchini, A.; Funel, N.; León, L. G.; Giovannetti, E.; Peters, G. J.; Palchaudhuri, R.; Calvaresi, E. C.; Hergenrother, P. J.; Minutolo, F. Discovery of *N*-Hydroxyindole-Based Inhibitors of Human Lactate Dehydrogenase Isoform A (LDH-A) as Starvation Agents against Cancer Cells. *J Med Chem* **2011**, *54* (6), 1599–1612. <https://doi.org/10.1021/jm101007q>.

- (15) Fauber, B. P.; Dragovich, P. S.; Chen, J.; Corson, L. B.; Ding, C. Z.; Eigenbrot, C.; Giannetti, A. M.; Hunsaker, T.; Labadie, S.; Liu, Y.; Liu, Y.; Malek, S.; Peterson, D.; Pitts, K.; Sideris, S.; Ultsch, M.; VanderPorten, E.; Wang, J.; Wei, B.; Yen, I.; Yue, Q. Identification of 2-Amino-5-Aryl-Pyrazines as Inhibitors of Human Lactate Dehydrogenase. *Bioorg Med Chem Lett* **2013**, *23* (20), 5533–5539. <https://doi.org/10.1016/j.bmcl.2013.08.060>.
- (16) Mayer, M.; Berger, A.; Leischner, C.; Renner, O.; Burkard, M.; Böcker, A.; Noor, S.; Weiland, T.; Weiss, T. S.; Busch, C.; Lauer, U. M.; Bischoff, S. C.; Venturelli, S. Preclinical Efficacy and Toxicity Analysis of the Pan-Histone Deacetylase Inhibitor Gossypol for the Therapy of Colorectal Cancer or Hepatocellular Carcinoma. *Pharmaceuticals* **2022**, *15* (4), 438. <https://doi.org/10.3390/ph15040438>.
- (17) vander Jagt, D. L.; Deck, L. M.; Royer, R. E. Gossypol Prototype of Inhibitors Targeted to Dinucleotide Folds. *Curr Med Chem* **2000**, *7* (4), 479–498. <https://doi.org/10.2174/0929867003375119>.
- (18) Conners, R.; Schambach, F.; Read, J.; Cameron, A.; Sessions, R. B.; Vivas, L.; Easton, A.; Croft, S. L.; Brady, R. L. Mapping the Binding Site for Gossypol-like Inhibitors of Plasmodium Falciparum Lactate Dehydrogenase. *Mol Biochem Parasitol* **2005**, *142* (2), 137–148. <https://doi.org/10.1016/j.molbiopara.2005.03.015>.
- (19) Rellinger, E. J.; Craig, B. T.; Alvarez, A. L.; Dusek, H. L.; Kim, K. W.; Qiao, J.; Chung, D. H. FX11 Inhibits Aerobic Glycolysis and Growth of Neuroblastoma Cells. *Surgery* **2017**, *161* (3), 747–752. <https://doi.org/10.1016/j.surg.2016.09.009>.
- (20) Deck, L. M.; Royer, R. E.; Chamblee, B. B.; Hernandez, V. M.; Malone, R. R.; Torres, J. E.; Hunsaker, L. A.; Piper, R. C.; Makler, M. T.; vander Jagt, D. L. Selective Inhibitors of Human Lactate Dehydrogenases and Lactate Dehydrogenase from the Malarial Parasite *Plasmodium falciparum*. *J Med Chem* **1998**, *41* (20), 3879–3887. <https://doi.org/10.1021/jm980334n>.
- (21) Wang, Z.; Wang, D.; Han, S.; Wang, N.; Mo, F.; Loo, T. Y.; Shen, J.; Huang, H.; Chen, J. Bioactivity-Guided Identification and Cell Signaling Technology to Delineate the Lactate Dehydrogenase A Inhibition Effects of Spatholobus Suberectus on Breast Cancer. *PLoS One* **2013**, *8* (2), e56631. <https://doi.org/10.1371/journal.pone.0056631>.
- (22) Manerba, M.; Vettraino, M.; Fiume, L.; Di Stefano, G.; Sartini, A.; Giacomini, E.; Buonfiglio, R.; Roberti, M.; Recanatini, M. Galloflavin (CAS 568-80-9): A Novel Inhibitor of Lactate Dehydrogenase. *Chem Med Chem* **2012**, *7* (2), 311–317. <https://doi.org/10.1002/cmdc.201100471>.
- (23) Granchi, C.; Roy, S.; Mottinelli, M.; Nardini, E.; Campinoti, F.; Tuccinardi, T.; Lanza, M.; Betti, L.; Giannaccini, G.; Lucacchini, A.; Martinelli, A.; Macchia, M.; Minutolo, F. Synthesis of Sulfonamide-Containing N-Hydroxyindole-2-Carboxylates as Inhibitors of Human Lactate Dehydrogenase-Isoform 5. *Bioorg Med Chem Lett* **2011**, *21* (24), 7331–7336. <https://doi.org/10.1016/j.bmcl.2011.10.031>.
- (24) Granchi, C.; Calvaresi, E. C.; Tuccinardi, T.; Paterni, I.; Macchia, M.; Martinelli, A.; Hergenrother, P. J.; Minutolo, F. Assessing the Differential Action on Cancer Cells of LDH-A Inhibitors Based on the N-Hydroxyindole-2-Carboxylate (NHI) and Malonic (Mal) Scaffolds. *Org Biomol Chem* **2013**, *11* (38), 6588. <https://doi.org/10.1039/c3ob40870a>.
- (25) Calvaresi, E. C.; Granchi, C.; Tuccinardi, T.; di Bussolo, V.; Huigens, R. W.; Lee, H. Y.; Palchaudhuri, R.; Macchia, M.; Martinelli, A.; Minutolo, F.; Hergenrother, P. J. Dual Targeting of the Warburg Effect with a Glucose-Conjugated Lactate Dehydrogenase Inhibitor. *Chem Bio Chem* **2013**, *14* (17), 2263–2267. <https://doi.org/10.1002/cbic.201300562>.

- (26) Baker, B. R.; Bramhall, R. R. Irreversible Enzyme Inhibitors. 189. Inhibition of Some Dehydrogenases by Derivatives of 4-Hydroxyquinoline-2- and -3-Carboxylic Acids. *J Med Chem* **1972**, *15* (3), 230–233. <https://doi.org/10.1021/jm00273a005>.
- (27) Baker, B. R.; Bramhall, R. R. Irreversible Enzyme Inhibitors. 190. Inhibition of Some Dehydrogenases by 1-Substituted-1,4-Dihydro-4-Quinolone-3-Carboxylic Acids. *J Med Chem* **1972**, *15* (3), 233–235. <https://doi.org/10.1021/jm00273a006>.
- (28) Baker, B. R.; Bramhall, R. R. Irreversible Enzyme Inhibitors. 191. Hydrophobic Bonding to Some Dehydrogenases by 6-, 7-, or 8-Substituted-4-Hydroxyquinoline-3-Carboxylic Acids. *J Med Chem* **1972**, *15* (3), 235–237. <https://doi.org/10.1021/jm00273a007>.
- (29) Chai, D.; C. M.; D. C.; D. K. J.; S. A. N. Preparation of Substituted Quinoline Derivatives as Lactate Dehydrogenase A Inhibitors. WO2012061557, 2012.
- (30) Xie, H.; Hanai, J.; Ren, J.-G.; Kats, L.; Burgess, K.; Bhargava, P.; Signoretti, S.; Billiard, J.; Duffy, K. J.; Grant, A.; Wang, X.; Lorkiewicz, P. K.; Schatzman, S.; Bousamra, M.; Lane, A. N.; Higashi, R. M.; Fan, T. W. M.; Pandolfi, P. P.; Sukhatme, V. P.; Seth, P. Targeting Lactate Dehydrogenase-A Inhibits Tumorigenesis and Tumor Progression in Mouse Models of Lung Cancer and Impacts Tumor-Initiating Cells. *Cell Metab* **2014**, *19* (5), 795–809. <https://doi.org/10.1016/j.cmet.2014.03.003>.
- (31) Dragovich, P. S.; Fauber, B. P.; Corson, L. B.; Ding, C. Z.; Eigenbrot, C.; Ge, H.; Giannetti, A. M.; Hunsaker, T.; Labadie, S.; Liu, Y.; Malek, S.; Pan, B.; Peterson, D.; Pitts, K.; Purkey, H. E.; Sideris, S.; Ultsch, M.; VanderPorten, E.; Wei, B.; Xu, Q.; Yen, I.; Yue, Q.; Zhang, H.; Zhang, X. Identification of Substituted 2-Thio-6-Oxo-1,6-Dihydropyrimidines as Inhibitors of Human Lactate Dehydrogenase. *Bioorg Med Chem Lett* **2013**, *23* (11), 3186–3194. <https://doi.org/10.1016/j.bmcl.2013.04.001>.
- (32) Fauber, B. P.; Dragovich, P. S.; Chen, J.; Corson, L. B.; Ding, C. Z.; Eigenbrot, C.; Giannetti, A. M.; Hunsaker, T.; Labadie, S.; Liu, Y.; Liu, Y.; Malek, S.; Peterson, D.; Pitts, K.; Sideris, S.; Ultsch, M.; VanderPorten, E.; Wang, J.; Wei, B.; Yen, I.; Yue, Q. Identification of 2-Amino-5-Aryl-Pyrazines as Inhibitors of Human Lactate Dehydrogenase. *Bioorg Med Chem Lett* **2013**, *23* (20), 5533–5539. <https://doi.org/10.1016/j.bmcl.2013.08.060>.
- (33) Dragovich, P. S.; Fauber, B. P.; Boggs, J.; Chen, J.; Corson, L. B.; Ding, C. Z.; Eigenbrot, C.; Ge, H.; Giannetti, A. M.; Hunsaker, T.; Labadie, S.; Li, C.; Liu, Y.; Liu, Y.; Ma, S.; Malek, S.; Peterson, D.; Pitts, K. E.; Purkey, H. E.; Robarge, K.; Salphati, L.; Sideris, S.; Ultsch, M.; VanderPorten, E.; Wang, J.; Wei, B.; Xu, Q.; Yen, I.; Yue, Q.; Zhang, H.; Zhang, X.; Zhou, A. Identification of Substituted 3-Hydroxy-2-Mercaptocyclohex-2-Enones as Potent Inhibitors of Human Lactate Dehydrogenase. *Bioorg Med Chem Lett* **2014**, *24* (16), 3764–3771. <https://doi.org/10.1016/j.bmcl.2014.06.076>.
- (34) Labadie, S.; Dragovich, P. S.; Chen, J.; Fauber, B. P.; Boggs, J.; Corson, L. B.; Ding, C. Z.; Eigenbrot, C.; Ge, H.; Ho, Q.; Lai, K. W.; Ma, S.; Malek, S.; Peterson, D.; Purkey, H. E.; Robarge, K.; Salphati, L.; Sideris, S.; Ultsch, M.; VanderPorten, E.; Wei, B.; Xu, Q.; Yen, I.; Yue, Q.; Zhang, H.; Zhang, X.; Zhou, A. Optimization of 5-(2,6-Dichlorophenyl)-3-Hydroxy-2-Mercaptocyclohex-2-Enones as Potent Inhibitors of Human Lactate Dehydrogenase. *Bioorg Med Chem Lett* **2015**, *25* (1), 75–82. <https://doi.org/10.1016/j.bmcl.2014.11.008>.
- (35) Kotlyar, A. B.; Randazzo, A.; Honbo, N.; Jin, Z.-Q.; Karliner, J. S.; Cecchini, G. Cardioprotective Activity of a Novel and Potent Competitive Inhibitor of Lactate Dehydrogenase. *FEBS Lett* **2010**, *584* (1), 159–165. <https://doi.org/10.1016/j.febslet.2009.11.022>.
- (36) Moorhouse, A. D.; Spiteri, C.; Sharma, P.; Zloh, M.; Moses, J. E. Targeting Glycolysis: A Fragment Based Approach towards Bifunctional Inhibitors of HLDH-5. *Chem. Commun.* **2011**, *47* (1), 230–232. <https://doi.org/10.1039/C0CC01166E>.

- (37) Kohlmann, A.; Zech, S. G.; Li, F.; Zhou, T.; Squillace, R. M.; Commodore, L.; Greenfield, M. T.; Lu, X.; Miller, D. P.; Huang, W.-S.; Qi, J.; Thomas, R. M.; Wang, Y.; Zhang, S.; Dodd, R.; Liu, S.; Xu, R.; Xu, Y.; Miret, J. J.; Rivera, V.; Clackson, T.; Shakespeare, W. C.; Zhu, X.; Dalgarno, D. C. Fragment Growing and Linking Lead to Novel Nanomolar Lactate Dehydrogenase Inhibitors. *J Med Chem* **2013**, *56* (3), 1023–1040. <https://doi.org/10.1021/jm3014844>.
- (38) Janin, J.; Bahadur, R. P.; Chakrabarti, P. Protein–Protein Interaction and Quaternary Structure. *Q Rev Biophys* **2008**, *41* (2), 133–180. <https://doi.org/10.1017/S0033583508004708>.
- (39) Keskin, O.; Gursoy, A.; Ma, B.; Nussinov, R. Principles of Protein–Protein Interactions: What Are the Preferred Ways For Proteins To Interact? *Chem Rev* **2008**, *108* (4), 1225–1244. <https://doi.org/10.1021/cr040409x>.
- (40) Jafary, F.; Ganjalikhany, M. R.; Moradi, A.; Hemati, M.; Jafari, S. Novel Peptide Inhibitors for Lactate Dehydrogenase A (LDHA): A Survey to Inhibit LDHA Activity via Disruption of Protein–Protein Interaction. *Sci Rep* **2019**, *9* (1), 4686. <https://doi.org/10.1038/s41598-019-38854-7>.
- (41) Nadal-Bufi, F.; Mason, J. M.; Chan, L. Y.; Craik, D. J.; Kaas, Q.; Troeira Henriques, S. Designed β -Hairpins Inhibit LDH5 Oligomerization and Enzymatic Activity. *J Med Chem* **2021**, *64* (7), 3767–3779. <https://doi.org/10.1021/acs.jmedchem.0c01898>.
- (42) Thabault, L.; Brisson, L.; Brustenga, C.; Martinez Gache, S. A.; Prévost, J. R. C.; Kozlova, A.; Spillier, Q.; Liberelle, M.; Benyahia, Z.; Messens, J.; Copetti, T.; Sonveaux, P.; Frédérick, R. Interrogating the Lactate Dehydrogenase Tetramerization Site Using (Stapled) Peptides. *J Med Chem* **2020**, *63* (9), 4628–4643. <https://doi.org/10.1021/acs.jmedchem.9b01955>.

CHAPTER 4

Nanoparticles for drug delivery

The fast growth of nanotechnology has made nanoparticles a promising candidate to improve therapeutic approaches. A nanoparticle (NPs) is defined as a microscopic particle with the size between 1 and 100 nm, but sometimes the term is also used to describe larger particles up to 500nm. They have very particular physical and chemical properties as colloidal properties, ultrafast optical effect or electric properties that make them suitable for a wide range of application.¹

Because of their huge variety, they are usually divided into groups based on their composition and consequent properties, shape, and size. It is possible to distinguish between inorganic nanoparticles (metallic, carbon nanotubes, silica) and organic nanoparticles in turn divided into polymeric and lipidic.

Nanoparticles are increasingly used in medical field to build drug delivery systems². In fact, their unique characteristics make them capable of improve the efficacy of the drug by increasing the half-life, the solubility, and the control of the release³. Polymer nanoparticles are the most common drug carriers. The polymers can either be natural or synthesized as long as they result biocompatible, non-toxic and without any leaking impurities. Amphiphilic block or graft copolymers are able, under appropriate conditions, to self-assemble in aqueous media in globular colloidal micelles, macromolecules with higher solubility and stability that mime the phospholipidic bilayer and enhance permeation and retention effects. In fact, they have a core-shell architecture that consents the loading of lipophilic antitumor agents inside the hydrophobic core and the stability in water thanks to the hydrophilic outer shell. Generally, it is common to use PEG for the hydrophilic segment while the hydrophobic portion is composed by materials that easily degrade either by hydrolysis, enzymatic degradation, temperature or pH variation such as PCL (poly (ϵ -caprolactone)), PLA (poly (lactic acid)), PLGA (poly(lactic-co-glycolic acid)).⁴

The capacity of self-assembling is typical of many materials whether they are natural or not and influence their morphology and ordered structures because of a microphase separation. This phenomenon in turn is strongly influenced and governed by three parameters: the overall degree of polymerization that consists in the number of monomer units of a single block compared to the total number of monomer units making up the copolymer; the volume fraction which is the volume of a single block compared to the total volume of the whole copolymer and the Flory-Huggins segment-segment interaction, an empirical and dimensionless parameter χ_{AB} (for a diblock

copolymer) that helps describe the free energy cost per monomer in a situation where two different units want to separate⁵.

In literature three mainly structures are described: spheres, cylinders, and lamellae. The most diffused morphologies are spherical micelles and spherical vesicles, the latter consisting of a lamellar microstructure and generally, it is possible to obtain them if the soluble block is larger than the insoluble block.⁶

4.1 - Silica Nanoparticles

During the years, many of these NPs have been approved for cancer treatments, and many others are facing advanced clinical stage^{7,8}. Among the inorganic NPs, silica ones are also widely used for drug delivery systems because of their several advantages. They are photophysically inert, non-toxic, and easily editable to control the size and the properties of the system demonstrating great versatility.⁹ They can be synthesized using a large variety of approaches.¹⁰ The most employed methods are the Stöber process and the microemulsion protocol. The first one is used for monitored synthesis of monodispersed particles and operates through silica precursors (usually tetraethyl orthosilicate TEOS, $\text{Si}(\text{OC}_2\text{H}_5)_4$) which undergoes hydrolysis and consequent polycondensation, with this method, very particular nanoparticles are obtained, rich in silanol groups easily modified to anchor molecules of different kinds.

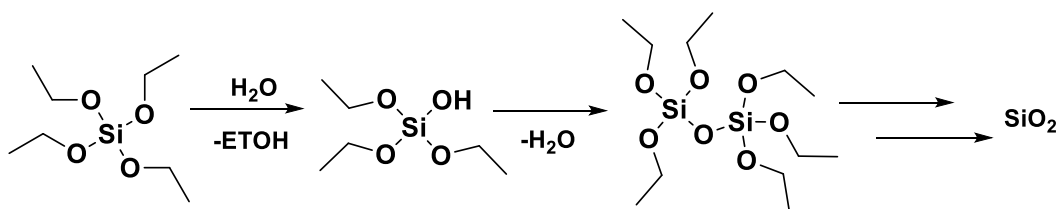


Fig.1 Chemical structure of the core of silica nanoparticles.

The surface modification is desirable to increase the colloidal capacity and avoid the aggregation of the particles with each other. In particular, it is very useful to use hydrophilic polymers such as PEG as a modifying agent, which also increases the circulation time in the blood and the biocompatibility of the compound by forming a protective layer around the nanoparticle. This system can also be used as a cage for the cargo¹¹: instead of being exposed on the surface, the drugs can be encapsulated within the nanoparticle where they are protected from premature degradation.

The microemulsion method instead, involves the formation of oil-in-water micelles or water-in-oil reverse micelles, stabilized by surfactants that act as nanoreactors upon which the size of

nanoparticles depends. Inside the nanoreactors the hydrolysis of the precursor and the condensation reaction take place.¹²

As with the other types of nanoparticles, size is one of the key parameters for governing the cellular uptake and it is governed by the variation of some reaction parameters as the speed of mixing or the rate of TEOS addition. Also, the shape is very important, and the most common ones are spheres and rods. The connection between the size, shape and the physiological behaviour was underlined for the first time by Zhao and collaborators¹³ when they compared the in vivo oral bioavailability of a long rod, a short rod, and a spherical shape of the same mesoporous silica nanoparticles (MSN). The study proved that the long rod nanoparticles had longer in vivo residence time, slower renal clearance, and extended blood circulation. Furthermore, and in line with these results, the small rods resulted to be easily degradable.

While shape and size are important for penetration and distribution, porosity is the essential parameter for the correct loading of the bioactive molecule and optimizing the pore size accordingly with the size of the drug for a controlled release is fundamental to the ultimate effectiveness of the system.¹⁴ Interestingly, the use of capping agents that allow the drug release prompted by specific trigger, is one of the most used strategy to avoid the premature delivery.

Silica nanoparticles have also been considered for imaging and medical diagnosis with the intention of exploiting the luminescence phenomenon. Luminescence is a spontaneous emission highly sensitive and non-invasive but when the detection involves molecular dyes, it can be hampered by some drawbacks such as photodegradation or interference from background signals.¹⁵ These problems represent a major hindrance when the analyte is diluted and a complex matrix is used, like in a biological system.

These systems generally take advantages of Förster resonance energy transfer (FRET) a process to obtain systems where a very high signal/noise ratio is achieved thanks to the reduced interferences from Rayleigh-Tyndall and Raman bands since it is possible to have a large separation between the excitation and the emission maximum.¹⁶ The luminescence emission of the silica NPs depends strictly on the doping dye so there is a large variety of options that can be achieved by choosing the right element for the conjugation. Most of the time luminophores can be attached from the surface and interact with species in solution. This is a highly effective solution to confine the dye inside the silica matrix, where it can be more stable and protected by the environment.¹⁷

Nowadays, researchers tend to focus on the development of hybrid organic – inorganic NPs to improve their properties and before the work of Prodi et al. in 2014¹⁸, nobody was able to achieve

a complete energy transfer in systems based on organic or polymeric nanoparticles. Starting from their previous results obtained with a FRET based nanoparticles¹⁹, they develop a new platform with the introduction of pluronic acid to create a new pluronic-silica nanoparticle doped with various dyes and able to almost complete the energy transfer.

It is also possible to functionalize NPs with proper peptide sequence in order to promote the multivalent target of a receptor or enhance the selectivity. Many protocols have been proposed for this purpose depending on the stability of the systems, the functional groups present and consequent possible interference with the bioconjugation conditions. All these aspects must be controlled to preserve the activation of the systems and its proper functioning.

Biofunctionalization can be achieved by either covalent or non-covalent interactions but the first one, as the conjugation of maleimide to thiols or the azide-alkyne cycloaddition that we will further be described, are preferred to avoid weaknesses of the system such as poor stability and uncontrolled orientation with consequent undefined shape.²⁰

4.2 – Design of Non-Toxic Fluorescent Peptide-Coated Silica/PEG NPs

Apart from connect the peptide to the surface of the nanoparticles, it is also possible to mix, using convergent or divergent strategies, structures of a different nature, like synthetic polymers and natural macromolecules, for a better control of the bioactivity.

The divergent strategy consists in the growth of one polymer on the other while the convergent strategy is based on the coupling of the two moieties. In our work, we couple a polymer with peptides portion using a convergent protocol and we tried to enhance the permeability of the product with the application of Pluronic F127 instead of simple PEG in silica core nanoparticles.

Pluronic® F127 is part of the family of poloxamers, invented in 1973 by Irving Schmolka and protected by patent, and it is a non-ionic triblock copolymer composed of a central hydrophobic chain of poly-propylene oxide (PPO) laminated on both sides with two hydrophilic chains of poly-ethylene oxide (PEG).

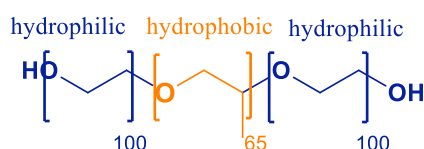


Fig.2 Chemical composition of Pluronic F127.

Since the discovery in 1994 that nanospheres composed by block copolymers exhibit increased bioavailability properties, amphiphilic block copolymers are increasingly used in nanomedicines for

their possible biological activity and their capacity to enhance blood circulation time, turn down liver accumulation and solve drug delivery problems²¹. Being composed by ABA triblock, (as shown in fig.2) they offer a wide possibility of materials that can change their physical and chemical properties managing the molar mass ratio between the blocks.

Pluronic is able to self-assemble in aqueous media, and above the critical micelle concentration, to form core-shell micelles where the PPO create the core, where the poor soluble drugs can be incorporated, and the hydrated PEO is arranged outside, surrounds it as a corona, and protecting the inactivation of the active molecule.

Thanks to the entry of certain formulations into clinical trials²², it has been discovered that drug delivery systems containing Pluronic, can control many important biological responses, including the modification of cellular membrane microviscosity, the inhibition of multidrug resistance, the enhancement of levels of reactive oxygen species (ROS), and many others all of which are very useful aspects to manage in order to make a therapy effective.

As mentioned above, we decided to take advantages of all these great characteristics and coupled to Pluronic some peptide sequences with biological activities chosen from the world of amphibians. As we all know, frogs and toads protect themselves from predators and infections, with skin secretions and depending on the use, those secretions have a huge variety of compounds like polypeptides, alkaloids, and steroids with related large variety of pharmacological application.²³

To control any possible effect of peptide charge in the formation of the micelles, we utilized a model peptide with net 2+ positive charge, derived from the bioactive peptide PTP7²⁴, a neutral peptide, derived from the highly folded 310-helical foldamer Cbz-(Ala-Aib)₂-Ala-Gly-NH₂,²⁵ and finally a peptide with a net 2- negative charge derived from a peptide isolated from frog skin, Pleurain-C2.²⁶ Among them, the positive charge sequence is expected to have higher cell penetration thanks to electrostatic interactions with negatively charged phospholipids.

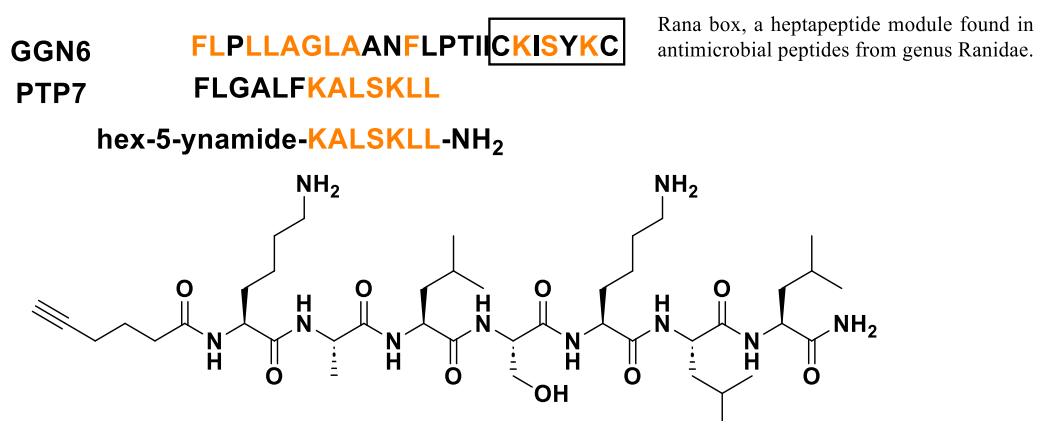


Fig. 3 Structure of PTP7 derived from the larger sequence of GGN6.

PTP7 is a tridecapeptide derived from gaegurin 6, a longer peptide isolated from the skin of *Glandirana Rugosa*, and discovered in 2003 from Lee and collaborators while they were looking for new antimicrobial peptides with anticancer activities.

Among all the peptides isolated from this frog species, PTP7, in addition to showing a fair antimicrobial activity, returned very interesting IC₅₀ values towards the growth of several tumor cell lines. The authors proposed a mechanism of apoptotic cell death based on DNA fragmentation following the treatment of cells with PTP7.

Subsequently it was tested against various antibiotic-resistant bacterial lines and also in this case it showed very interesting results. Unfortunately, one of the major problems in the use of this peptide is the poor stability in vivo, for this reason, considering its great preliminary tests, we choose it for being encapsulated inside a nanoparticle.

Pleurain-C2 is a tridecapeptide isolated from the skin of *Nidirana pleuraden*, and it is part of the family of Anionic Antimicrobial Peptides (AAMPs). This class of molecules has been isolated more recently and it is much less studied than the cationic sequences. For this reason, their mechanism of action has not yet been fully elucidated. However, it is thought that they are involved in exchanges with intracellular targets, like DNA, but anyway interactions with cell membranes are very likely to occur through the formation of salt bridges with the binding sites of the metal cation-ion.

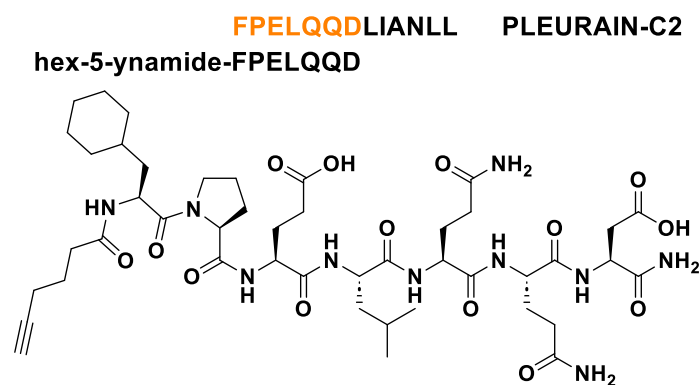


Fig. 4 Structure of the acidic peptide sequence derived from the larger Pleurain-C2 sequence.

The neutral sequence doesn't have biological activity, but it was chosen because of its characteristic to be highly folding.

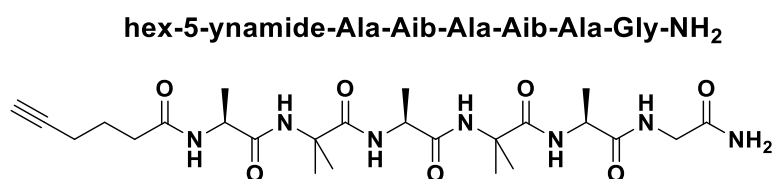


Fig. 5 Neutral peptide sequence chosen for the ability to be highly folding.

All three portions are constructed in such a way that they end with an alkyne so that the peptide sequence can be bound to the polymer, previously functionalised with an azide, through a click reaction copper catalysed. In this way, it is possible to create different kind of nanoparticles, with diverse combinations of positive and negative peptide sequences.

4.3 – Synthesis of Non-Toxic Fluorescent Peptide-Coated Silica/PEG NPs

Considering all the aspects analysed so far, we decided to use the tri-block surfactant copolymer Pluronic F127 (PF127) conjugated with the three chosen model peptidic sequences of similar lengths but different net charge.²⁷

Typically, the functionalization of a nanoparticle takes place by adhering the peptide sequence onto the surface of a preform particle, but this protocol leads to uncertain quantification of coating density and moderate yields. We have therefore thought of anticipating the functionalization by having it take place directly in the polymer before the micellization.

The conjugation was carried out via the CuAAC (copper-catalysed click reaction) and to achieve this, the pluronic was derivatized on both sides with the azide group, while inside the peptide sequences was inserted an alkyne moiety, as already described.

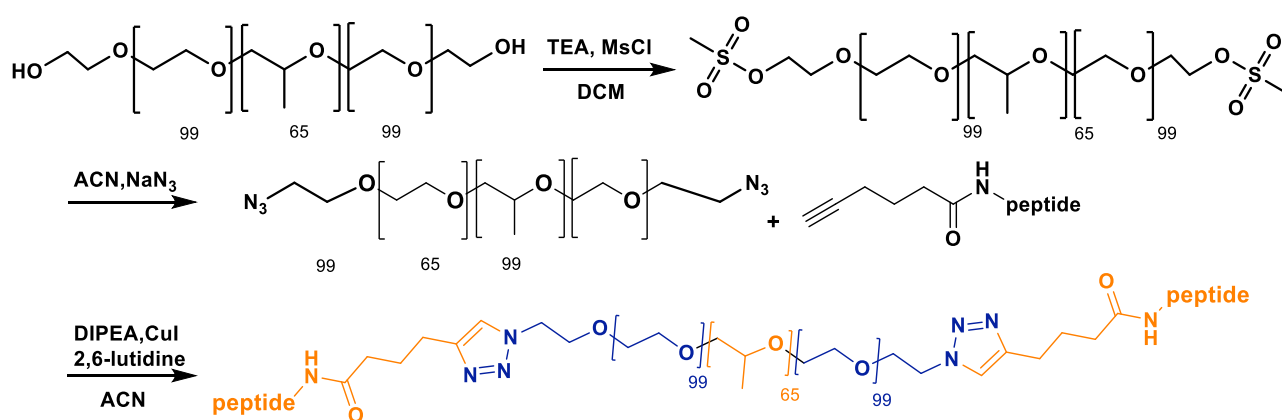


Fig. 6 Generic structure of the chimeric nanoparticles designed.

PF127 was treated with trimethylamine (TEA)/methanesulfonyl chloride (MsCl) and then the resulting dimesylate derivative was reacted with NaN_3 , giving PF127-(N_3)₂. The polymer-diazide was conjugated to each alkyne-peptide (2 eq) by CuAAC chemistry in the presence of 2,6-lutidine, DIPEA, and a catalytic amount of CuI. The resulting polymer-dipeptides were purified by dialysis in 2 kDa cutoff tubes. It was possible to monitor the efficacy of the reactions with the integration of ¹H NMR peaks in the 7 ÷ 9 ppm region. Using the peak of the PPO methyls as reference, the success was estimated to be 80-90%. The reaction outcome was also monitored by FT IR where the accomplishment of the reaction was confirmed by the disappearance of the azide IR signal

recognizable around 2100 cm^{-1} and by the appearance of the characteristic carbonyl peaks in the region $1600 \div 1700\text{ cm}^{-1}$.

As mentioned before, we decided to introduce peptides with different net charge to monitor how this parameter might influence the size and the shape of the nanoparticles. About the charged sequences, we had no clue how they could have arranged, instead, for the presence of 2-aminoisobutyric acid residues (Aib), the neutral peptide was expected to adopt a folded secondary structure. For determining the structure, we decide to perform circular dichroism (CD). The CD spectra of random coil structures, usually show a negative band around 200nm, while for helical arrangement, a positive band appears below 200 nm, supported by two minimal points. Considering that all helical structures exhibit this pattern, the intensity of the bands is used to distinguish between α and 3_{10} helices.²⁸ The peptide structure is highly influenced by the environment and the solvent, in fact in water, the neutral peptide shows a predominant random coil, but in ethanol and in 1-octanol, it adopts a 3_{10} helical conformation.

For the positively charged peptide instead, while a similar trend is detected in ethanol, the addition of 1-octanol produces a significant CD variation, that could indicate a structural adjustment or the adoption of an α helix conformation.

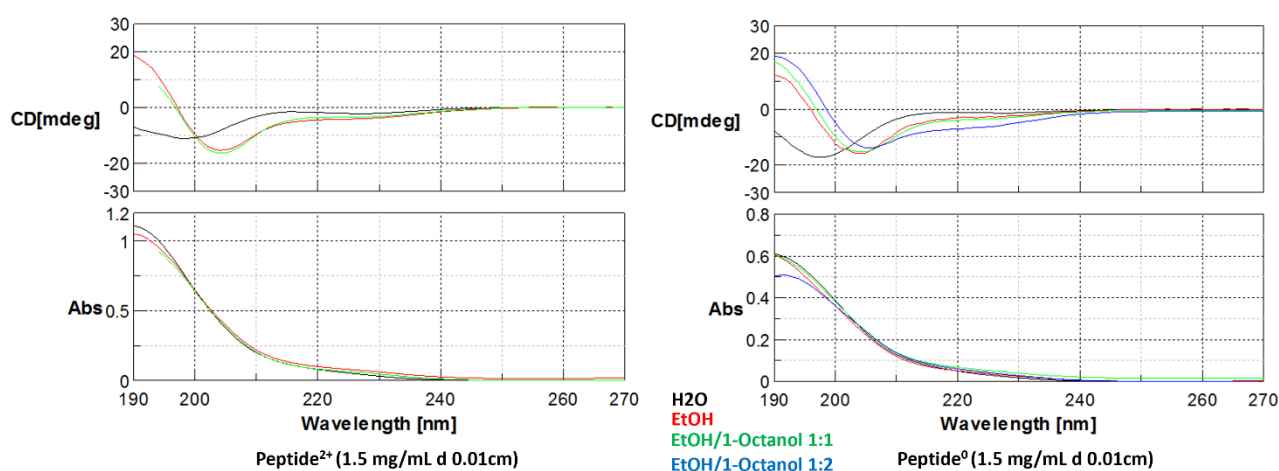


Fig. 7 Circular dichroism results of the positive and the neutral charged peptides.

The platform resulted from the conjugation of the peptide and the polymer was directly used for the preparation of our polymeric micelles. The nanoparticles were prepared by mixing not conjugated pluronic to 10, 20 and 30% of polymer-peptide. The silica core was obtained in acidic conditions with a 9:1 mixture of TEOS and TMS-Cl, following the Stöber method and in the presence of rhodamineB- triethoxysilane (RhB-TES 0.2 % mol/mol) as doping dye. The resulting NPs were purified by water dialysis at room temperature using cellulose tubes with a cut-off > 12kDa. We also prepared mixed NPs by performing the click reaction between the diazide derivative PF127-(N₃)₂ and a 1:1

mixture of peptide²⁺ and peptide²⁻ and NPs formed by 70% of native polymer and 30% of 1:2:1 mixture of the charged peptides conjugated with pluronic (2⁺)₂-PF127/PF127-(2⁻)₂.

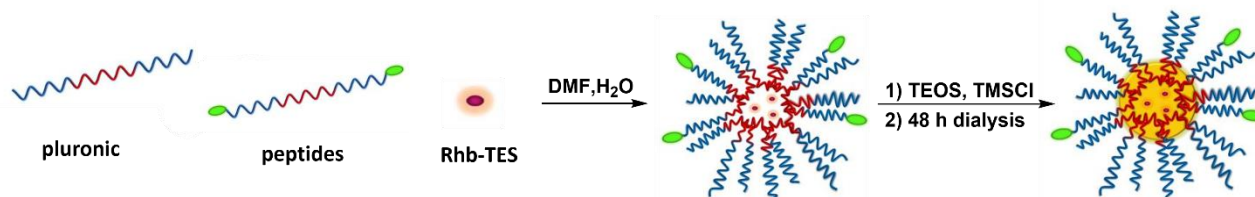


Fig.8 Schematic representation of nanoparticles synthesis. Legend: blue PEG, red PPO, green peptide, yellow silica, purple rhodamine B.

Once the nanoparticles were ready and purified, their hydrodynamic diameter (dh) was analysed by Dynamic Light Scattering (DLS). As expected from the previous work, the bare NPs prepared for comparison just with the commercial pluronic, resulted to be 22 ± 0.5 nm. The presence of an increasing amount of peptide has in parallel led to a higher hydrodynamic radius, finding a value of from 30 ± 1 nm for NP-10%peptide²⁺ and NP-20%peptide²⁺, to 35 ± 1 nm for NP-30%peptide²⁺. For nanoparticles formed through conjugation of the polymer with the neutral peptide, on the other hand, the dh value remains constant even as the amount of conjugated peptide increases.

Once the nanoparticles were ready and purified, their hydrodynamic diameter (dh) was analysed by Dynamic Light Scattering (DLS). As expected from the previous work, the bare NPs prepared for comparison just with the commercial pluronic, resulted to be 22 ± 0.5 nm. The presence of an increasing amount of peptide has in parallel led to a higher hydrodynamic radius, finding a value of from 30 ± 1 nm for NP-10%peptide²⁺ and NP-20%peptide²⁺, to 35 ± 1 nm for NP-30%peptide²⁺. For nanoparticles formed through conjugation of the polymer with the neutral peptide, on the other hand, the dh value remains constant even as the amount of conjugated peptide increases.

The presence of anionic peptide instead, gave a very high value of dh, probably because of the formation of aggregates that, in the case of the minimum amount, do not even allow the analysis because of the quickly gel formation. The hydrodynamic diameters for blend and mixed samples appeared significantly higher if compared with the nanoparticles with just one kind of peptide present.

The Zeta Potential values (ζ) have also been determined for completeness performing the analysis at pH 8 but the results appear to be very similar for all samples.

Probably because of this reason, when the sample were analyzed with the transmission electron microscopy (TEM) to measure the diameter, no major change in size and shape was perceived as we can see from the following figure where the TEM images of the compounds with respectively 10%, 20% and 30% of the cation fragment of PTP7 are represented.

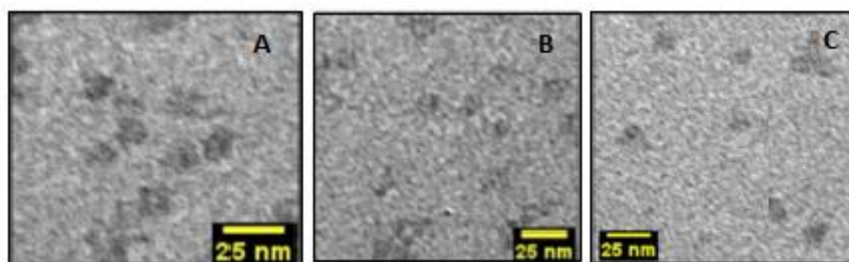


Fig. 9 TEM images of the compounds with 10% of cationic fragment (A), 20% (B) and 30% (C).

Due to lack of time, just the first three compounds have been analyzed with TEM but in the table are briefly reassumed the results of all the compounds synthesized and analyzed.

Table 1 Characterization of peptide–NPs: hydrodynamic diameter (dh) and Polydispersion Index (Pdl) as determined by DLS, Zeta Potential (ζ), core diameter (d_{core}) determined by TEM. ^a Gel-like; ^b 70% native PF127 + 30% of a 1:1 mixture of PF127-peptide²⁺ and PF127-peptide²⁻; ^c 70% native PF127 + 30% of a 1:2:1 mixture of the 3 peptide–polymer block copolymers PF127-(peptide²⁺)₂/peptide²⁺-PF127-peptide²⁻/PF127-(peptide²⁻)₂. Nd = not determined.

	charge	amount (%)	dh (nm)	Pdl	ζ (mv)	d _{core} (nm)
1	0	-	22 ± 0.5	0.14	-4.3 ± 0.1	10 ± 1
2	2+	10	30 ± 0.5	0.17	-5 ± 1	10 ± 2
3	2+	20	30 ± 1	0.25	-3.0 ± 0.5	11 ± 2
4	2+	30	35 ± 1	0.26	-4.5 ± 0.2	13 ± 2
5	0	10	29 ± 1	0.16	-4.2 ± 0.2	10 ± 2
6	0	20	30 ± 0.5	0.10	-3.9 ± 0.4	11 ± 2
7	0	30	31.5 ± 0.5	0.14	-4.9 ± 0.1	12 ± 2
8	2-	10 ^a	nd	nd	nd	nd
9	2-	20	180 ± 20	0.27	nd	nd
10	2-	30	104 ± 10	0.16	nd	nd
11	blend	30 ^b	41 ± 1	0.20	-3.0 ± 0.1	13 ± 2
12	mixed	30 ^c	44 ± 1	0.45	-5.8 ± 0.4	13 ± 2

Biological tests of toxicity and cellular uptake were also performed in collaboration with prof. M Paolillo. The toxicity was evaluated using the cell viability 3-MTS assay, according to the manufacturer's instructions. The cells were treated for 24 and 48 hours with a culture medium of 5 and 10 μ M of NPs, and the decrease of vitality was detected just in the presence of the second concentration. Nevertheless, the toxicity in vivo cannot be ruled out for the nanoparticles composed with anionic peptides. In fact, as they have formed agglomerates, their characteristics have changed, especially regarding the area of exposure, but in vivo, by administering much lower concentrations,

this phenomenon may not occur. Finally, the internalization was observed just for the platform containing the PTP7 portion with the confocal microscopy in A549 cells and the test shows that the nanoparticles are indeed capable of penetrating inside the cells although the precise mechanism has not yet been identified.

4.4 – Experimental procedures

General information

Chemical reagents, including protected amino acids, were purchased from commercial sources, and used without purification.

Peptide purity was assessed by analytical RP HPLC performed on an 1100 series apparatus Agilent Technologies, Milan, Italy, using an XSelect Peptide CSH C18 column (Waters, Milford, MA, USA), 4.6 mm × 100 mm, 130 Å, 3.5 μm. The mobile phase was a mixture of 0.5% HCOOH in H₂O and 0.5% HCOOH in CH₃CN for ionic peptides (method A) or H₂O/CH₃CN for neutral peptides (method B). Alternative to HPLC-MS, purities were assessed by reverse-phase ultra-performance liquid chromatography (RP-UPLC), using a reverse-phase (RP) column mod. Acquity UPLC[®] BEH C18 1.7 μm (2.1 × 50 mm); DAD 210 nm; DAD 254 nm; mobile phase: from 2:8 solvent A/solvent B to 7:3 solvent A/solvent B, in 26 min, at a flow rate of 0.3 mL/min, followed by 4 min at the same composition; solvent A = 0.1% HCOOH in H₂O, B = 0.1% HCOOH in CH₃CN.

MS (ESI) analysis was performed using an MS single quadrupole HP 1100 MSD detector (Agilent Technologies, Milan, Italy).

Fluorescence measurements were performed with an LS-55 Fluorescence Spectrometer (Perkin Elmer, Milan, Italy).

Circular dichroism (CD) measurements were performed at room temperature with a Jasco J-715 spectropolarimeter by using a circular quartz cell of 0.1 mm path length. Reported CD spectra were obtained by taking the average of five scans made at 100 nm/min. Spectral data are expressed in units of millidegree.

Fourier transform IR (FT IR) analysis was performed on an Alpha FT IR spectrophotometer (Bruker, Billerica, MA, USA).

¹H NMR was performed at 400 MHz on a Varian Gemini 400 (Agilent) in 5 mm tubes in CDCl₃ or DMSO-d₆ at RT; chemical shifts are reported as δ values relative to residual CHCl₃ (δH = 7.26 ppm) or to residual DMSO (δH = 2.50 ppm). In general, CDCl₃ was used for the derivatives of PF127 and DMSO-d₆ for the chimeras.

Dynamic Light Scattering (DLS) for the determination of the hydrodynamic diameter distribution of the NPs was carried out employing a Malvern Nano ZS instrument equipped with a 630 nm laser diode. Samples were housed in disposable polystyrene cuvettes of 1 cm optical path length. Samples were prepared diluting 300 μL of NP solution in 900 μL of water and 60 μL of PBS 10x (Phosphate-buffered saline, pH 7.4, 1.37 M NaCl, 27 mM KCl, 100 mM Na_2HPO_4 , 18 mM KH_2PO_4).

Zeta Potential was measured with the same instrument; the samples were prepared by diluting 100 μL of NPs solution, 120 μL of 0.02 M KCl, 120 μL of 0.1 M EPPS (3-[4-(2-Hydroxyethyl)piperazin-1-yl]propane-1-sulfonic acid, pH 8) in 860 μL of water.

Transmission electron microscopy (TEM) was conducted in a Philips CM 100 TEM operating at 80 kV. For the investigations, conventional Formvar-film copper microgrids were dried under vacuum after deposition of a drop of NP solution diluted with water (1:50). The size distribution was obtained by analyzing the images manually using the software ImageJ (Rasband, W.S., ImageJ, U.S. National Institutes of Health, Bethesda, MD, USA, <https://imagej.nih.gov/ij/> accessed on, 1997–2018).

Confocal images were obtained with a C1s confocal laser-scanning microscope equipped with a PlanApo 60X or 40X oil immersion lens (Nikon, Tokyo, Japan).

General procedure for peptide synthesis

Fmoc-Rink Amide resin (0.5 g, substitution 0.45 mmol/g) was swollen in DMF (5 mL) for 15 min before the use. Fmoc deprotection was carried out by treatment with 20% piperidine/DMF (5 mL) for 20 min; after filtration, the treatment was repeated for further 40 min. The resin was subsequently washed 3 times with DMF, Et_2O , DCM (5 mL each). Fmoc-amino acid (2.5 eq.) carrying orthogonal protecting groups at the side chains and HOBt (2.5 eq.) were dissolved in DMF (3 mL), and after 10 min this mixture was added to the resin at RT. Then, TBTU (2.5 eq.) and DIPEA (4.0 eq.) were also added, and the mixture was shaken for 3 h at RT. The suspension was filtered, and the resin was subsequently washed 3 times with DMF, Et_2O , DCM (5 mL each). Coupling efficacy was monitored by the Kaiser test. The final coupling with 5-hexynoic acid was carried out in the presence of HOBt/TBTU/DIPEA under the same conditions as described above. The residues Lys, Ser, Asp, Gln, Glu, were introduced as Fmoc-Lys(Boc)-OH, Fmoc-Ser(tBu)-OH, Fmoc-Asp(tBu)-OH, Fmoc-Gln(Trt)-OH, Fmoc-Glu(tBu)-OH, respectively. The removal of the acid-labile groups at the side chains occurred during the cleavage of the sequences from the resin.

The cleavage of the peptide from the resin was performed by treatment with TFA/TIPS/H₂O/PhOH (88:5:5:2 v/v/v/m, 10 mL) while shaking for 6 h at RT. The mixture was filtered, and the resin was washed in sequence with 1% TFA in Et₂O (5 mL), DCM (5 mL), and MeOH (5 mL). The filtrate and the washes were collected, and the organic solvents were removed under reduced pressure. The resulting residue was suspended in ice-cold Et₂O, and the crude solid that precipitated was collected by centrifugation (70–80% yield, 85–95% pure as determined by RP HPLC).

Hex-5-ynamide-Lys-Ala-Leu-Ser-Lys-Leu-Leu-NH₂ (peptide²⁺)

It was isolated as a beige solid as a 2xTFA salt (385 mg, 78% yield compared to the resin load). Purity was determined to be 94% by analytical RP HPLC (method A), Rt = 1.98 min. **HPLC-MS:** [M+1] = 865.58.

Hex-5-ynamide-Ala-Aib-Ala-Aib-Ala-Gly-NH₂ (peptide⁰)

It was isolated as a pale yellow waxy solid (92 mg, 82% yield compared to the resin load). Purity was determined to be 78% by analytical RP HPLC (method B), Rt = 5.8 min. **HPLC-MS:** [M+1] = 552.8

Hex-5-ynamide-Phe-Pro-Glu-Leu-Gln-Gln-Asp-NH₂ (peptide²⁻)

It was obtained as a beige solid (73 mg, 67% yield compared to the resin load). Purity was determined to be 90% according to analytical RP UPLC, Rt = 3.6 min. **HPLC-MS:** [M+H] = 969.3, [M+Na] = 991.3, [M+2H] = 485.3.

Synthesis of Polymer-(N₃)₂ and Polymer-Peptide Conjugation

Pluronic[®] F127 (6.3 g, 0.5 mmol, 1 eq.) was dried by azeotropic distillation with toluene at reduced pressure. Then, the polymer was solubilized in anhydrous DCM (25 mL) and treated with triethylamine (TEA, 140 μ L, 1 mmol, 2 eq.) and methanesulfonyl chloride (MsCl, 77 μ L, 1 mmol, 2 eq.) under inert atmosphere. The mixture was stirred at 0 °C for 3 h and then at RT overnight. The solvent was evaporated at reduced pressure, the resulting residue was washed with ice-cold Et₂O, and solid was collected by precipitation (>95%).

Sodium azide (122 mg, 1.88 mmol, 4 eq.) was added to a suspension of dimesylate–PF127 (6.026 g, 0.47 mmol, 1.0 eq.) in CH₃CN (25 mL), and the mixture was stirred under reflux for 48 h. Subsequently, the solvent was removed under reduced pressure. The solid so obtained was dispersed in a 5% NaHCO₃ solution saturated with NaCl (20 mL). The mixture was extracted four

times with DCM (4 × 15 mL). The combined organic phases were dried over Na₂SO₄, filtered, and evaporated at reduced pressure, affording a white solid (95%).

PF127-(N₃)₂ (450 mg, 1 eq) was dissolved in dry CH₃CN, and alkyne-peptide (2 eq.), 2,6-lutidine (4 eq), DIPEA (4 eq), and CuI (0.2 eq), were added under an inert atmosphere. The mixture was stirred at RT overnight. Then, the mixture was evaporated at reduced pressure and the solid was dispersed in a 1 M HCl solution saturated with NaCl. The mixture was extracted three times with AcOEt (10 mL). The combined organic layers were dried over Na₂SO₄, filtered, and evaporated at reduced pressure. The resulting solid was washed with ice-cold Et₂O, and the solid was collected by precipitation (90%).

Preparation of the Dye-Loaded NPs

A mixture of pristine PF127 with 10%, 20%, or 30% in weight of polymer-(peptide)₂ was dispersed in 3.2 mL of a solvent mixture composed of DMF (38.7% v/v) in 1 M of AcOH containing 0.85 M NaCl. Then, an 8.67 mg/mL solution of rhodamine B triethoxysilane (RhB-TES) in MeOH (300 μL) was added. The mixture was stirred for 1 h, then TEOS (350 μL) was added. After 3 h under stirring, TMSCl was added (40 μL), and the reaction was stirred for 48 h at RT. The NPs were purified by dialysis in a cellulose dialysis tube (Sigma, MW cutoff >12 kDa, avg. diameter 33 mm) against bi-distilled water at RT. The procedure gave NPs prepared with a content of polymer-peptide of 10, 20, and 30%, in short NP-10%peptide, NP-20%peptide, NP-30%peptide, respectively.

4.5 - Colorectal cancer therapy

Irinotecan is a water-soluble prodrug of the active molecule SN38, and it is used since the late '60s for medical purpose because of its antitumor activity and substantial toxicity. In fact, it can selectively inhibit topoisomerase (TOP1) by trapping the enzyme during cleavage of DNA and consequently provoking cell deaths.²⁹ Nowadays, Irinotecan is one of the most common treatments for advanced colorectal cancer.³⁰ Colorectal cancer is one of the most diagnosed cancers in the world; in fact, it is the third most common cancer diagnosed in the United States, and worldwide, it represents the second leading cause of cancer death. In early stages, the survival rate is quite high, but it decreases rapidly to less than 10% in metastatic stage and sadly, despite the improved screening practises, colorectal cancer is commonly diagnosed in advantages stages when surgery is not sufficient anymore.

SN38, has poor solubility in all human fluids, it can't be used as it is and requires carboxylesterase-2 to be released, an enzyme abundant in liver but not very present in the blood. As a result, just the 1-9% of the injected dose of the drug is converted in the active metabolite³¹ and because of that it is administrated as a prodrug. Additionally, it is important to preserve the active form of SN38; it is well established that after 24h from the administration just the 55% of the SN38 are present in the closed lactone form, the ones active that can easily undergo to conversion to the open inactive carboxylate form that it is also able to bind tight human serum albumin.

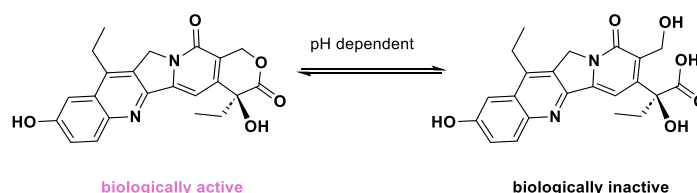


Fig.10 Structure and activity of SN38 in physiological conditions.

In case those problems were not enough challenging, it also must be considered the actual administration of the drug. It is commonly believed that the oral route is the most popular because it is the most convenient for the patient but there are significant additional barriers to be considered, a specific bioavailability and a lot of digestive enzymes ready to degrade the molecules. To solve those problems a number of approaches have been proposed.

Zhao and collaborators³² in 2008, tried to use PEGylation of SN38. In this way, the well know capabilities of PEGlation to enhance solubilization, prolong circulation time and alter distribution of parent drugs with consequent improvement of efficacy, are also transferred to the active portion. In fact, Pegylation is a widely adopted strategy to increase circulating time, because of its ability to

avoid macrophage-mediated uptake and removal from the systemic circulation. It is also helpful to avoid other molecules and non-specific protein binding thanks to steric effects.³³

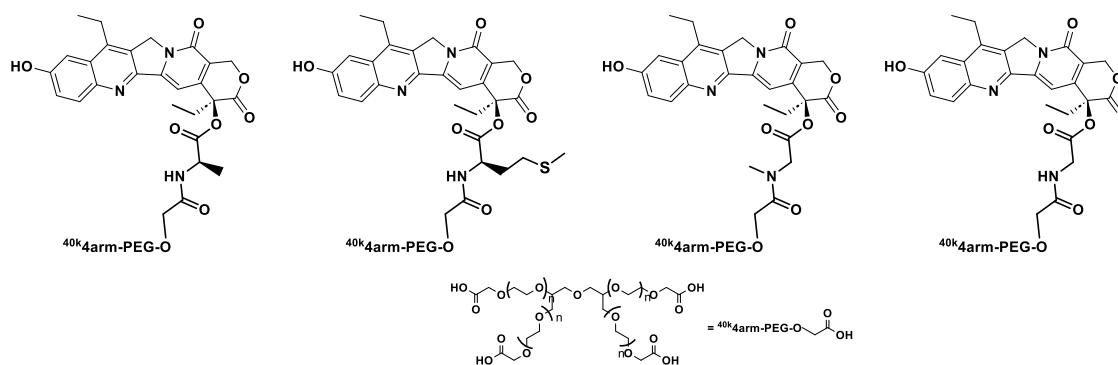


Fig.11 Pegylated compounds for enhancing the permeability and solubilization of SN38.

They previously tried to synthesize a PEG-CPT11 conjugated using a bifunctional linear PEG and then, not being satisfied, they synthesized three different PEG-SN38 conjugates by using different amino acids spacers. In this way, they were able to improve their own results, increase the amount of drug conjugate from 1.7% to 3.7% and consequently, reduce the amount of inactive polymer given to the patient during clinical trials. Further stability studies have demonstrated that PEG conjugates were able under neutral conditions and because the link between the SN38 and the PEG was an ester bond, the release of the drug could happen with hydrolyzation under basic conditions. In particular, SN38 could be released at pH = 7.4 at 37°C with a half-life of about 14h. unfortunately, because of the presence of enzymes like esterases and aminopeptidases, the half-time of the same compound is about 12 minutes in rat plasma suggesting that not just the pH but especially the enzymes play an important role in the drug release.

Apart from PEG, also Hyaluronic acid has gained attraction for its great biocompatibility, biodegradability, and ease of modification. Dinarvard and others³⁴ used this natural carbohydrate polymer in order to take advantage to its ability to interfere with extracellular and intercellular matrix through one of its major receptors called CD44. CD44 was discovered to be over expressed in several types of cancers cells and among them also colon cancer cells thus increasing the interaction of the malignant cells with hyaluronic acid. They easily synthesized an SN38-HA conjugates that, because of the presence of free acid negatively charged, they were able to interact with a positively charged core formed by gold nanoparticles. Gold nanoparticles are becoming increasingly popular in drug delivery because they are biocompatible, easy to prepare and to modify. They can also be used for photothermal therapy because of their unique characteristic of having a surface plasmon resonance (SPR): in fact, an external light can be used for drug released regulation and also for provoking irreversible cell damage. In this case, they were forced to

introduce an external support because SN38-HA conjugates are not able to form self-assembled nanostructure.

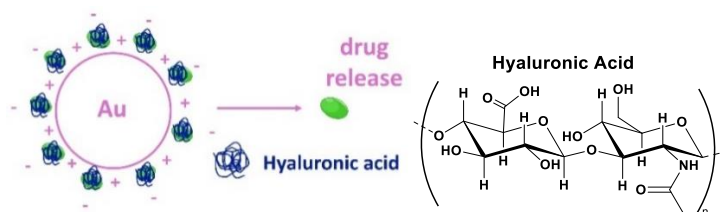


Fig. 12 Schematic representation of SN38-Hyaluronic Acid Nanoparticles.

Recently, also Ebrahimnejad and collaborators used hyaluronic acid but in combination with chitosan to cope with the oral administration problem.³⁵ Chitosan is a natural mucoadhesive polymer which can directly attach the gastrointestinal surface and increase the cellular uptake at the target site. It is furthermore reported for several decades that low molecular weight chitosan is involved in a various of enzymes processes causing chemo-preventing activities and improving solubility in physiological pH. Taking all these aspects into considerations, this research group combined the characteristics of chitosan, hyaluronic acid, and polyethylene glycol in the synthesis of nanoparticles where the SN38 is combined with a non-covalent physical adsorption. In fact, in this project, polar and π interactions between the hydroxyl groups of HA and aromatic rings of SN38, and the hydrogen bond between the oxygen in the carbonyl group of SN38 and the hydroxyl group of HA are exploited with successful results.

Despite the great result, among the nanoparticle-based delivery of SN38, supramolecular polymeric micellar structures stand out. Recently, in 2020, Lavasanifar and collaborators³⁶ synthesized two self-associating SN-38-polymer drug conjugates to solubilize and protect the active portion of irinotecan.

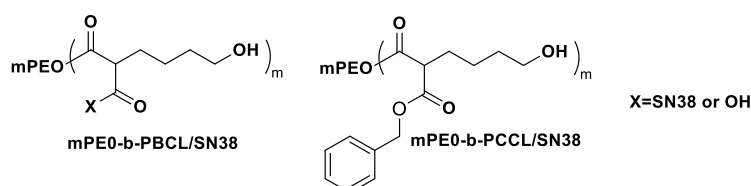


Fig. 13 Chemical structure of SN38-polymer drug conjugates.

The two micellar formulations were composed of either methoxy-poly(ethylene oxide)-block-poly(α -benzyl carboxylate- ϵ -caprolactone) conjugated to SN-38 at the PBCL end (mPEO-b-PBCL/SN-38) or mPEO-block-poly(α -carboxyl- ϵ -caprolactone) attached to SN-38 from the pendent-free carboxyl site (mPEO-b-PCCL/SN-38). In this study, they compared their molecules with another SN38-polymer formulation, NK012, the only one to arrive at phase II of clinical trials for breast and lung cancer. According to their analysis, their molecules seemed to have more advantages because

of the enhancement of stability due to the hydrophobic nature of the chosen polymers. Furthermore, also biodegradability has to be considered and, in this context, a poly(ester) structure is a plus compared to a poly(amino acids) structures.

The same year, also Alibolandi and collaborators have given their solution to the permeability problem with the development of polymersomes loaded with SN38.³⁷ Polymersomes are self-assembled amphiphilic block copolymers³⁸ that have received a lot of attentions in drug delivery approaches because, as artificial vesicles, they are more stable analogues of liposomes and able to encapsulate both hydrophilic and hydrophobic molecules. In particular, this research group developed chimeric nanoscale self-assembled structure with poli- ϵ -caprolactone (PCL), poli-lactic acid (PLA) and poli-(N-2hydroxypropyl) methacrylamide (PHMA) in order to blend their desirable characteristic and generate a novel and more efficient drug carrier. They furthermore improved the structures with the introduction of an aptamer, AS1411, as a targeting ligand on the surface so as to make the platform more selective and specific. They have also been able to verify with in vitro and in vivo tests, the optimal functioning of their molecules, paving the way for a new approach for carrying anticancer drugs.

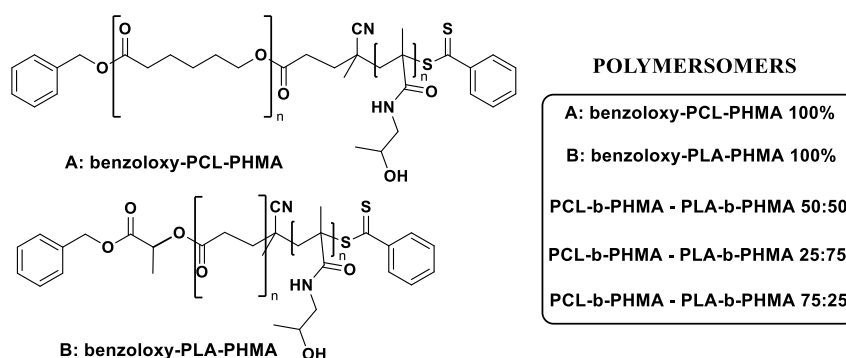


Fig. 14 Chemical structures of polymersomers.

For many years, Gemcitabine was used as a first line therapy but due to the drawbacks and the emergence of chemo-resistance during treatment, combination therapy has become the main tool to tackle cancer. The idea is to increase the efficacy of each drug of the combination for a preservation of the therapeutic activity without addictive toxicity or provoking resistance and reducing administration doses and adverse effect for a better tolerability.³⁹ Folfoxiri is a combination of folinic acid, 5-fluorouracil, oxaliplatin and/or irinotecan and it is currently become the standard treatment.⁴⁰ Despite the great success and the improvements, combination therapy is still suffering of the occurrence of secondary and unwanted responses that make the development of new strategies urgently needed.⁴¹

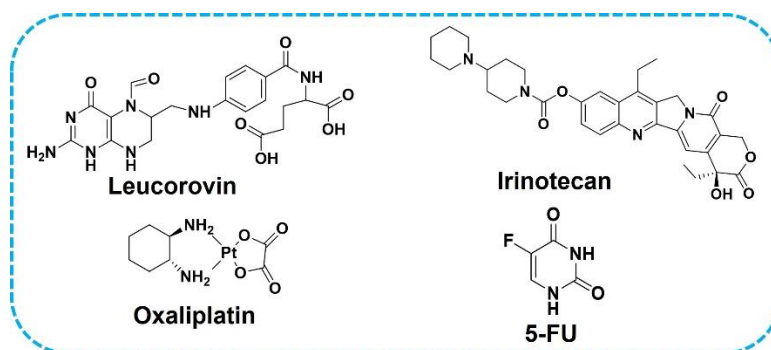


Fig. 15 Chemical structures of the drugs used for the treatment of colorectal cancer.

For this purpose, several formulations have been proposed. Among them, a phase III multicentre clinical trial called NAPOLI-1⁴² and a phase II micellar formulation with PEGylated form of SN38 called NK012⁴³, are currently being tested and they are the most promising since they are demonstrating survival advantages and manageable safety profile.

All these different formulations make it clear that the future of the fight against cancer must be directed towards the implementation of nanotechnology-based therapeutic approaches.⁴⁴ Indeed the unique characteristic of nanocarriers make them perfect for controlling the co-delivery of drugs in a convenient ratio.

4.6 - Development of multivalent delivery systems for combined therapy

Inside the Miriam Royo's research group, I also had the opportunity to work on this topic. This group has specialised over several years⁴⁵ in the development of platforms using labile covalent bonds, such as ester bonds, where the combination of a hydrophobic and hydrophilic moiety brings to the formation of nanoparticles able to facilitate drug administration and release; they connected their ability with the above-mentioned solutions for the advance colorectal therapy and they designed multivalent self-assembled platforms. My duty was not only the improvement of the synthetic pathway for the development of the platforms, but also the upgrade of the SN38-PEG systems with the conjugation of a novel oligomer formulation of 5-fluorouracil, the 5-dFU, and the possible introduction of a targeting moiety in order to be more selective and to try the co-administration of the two drugs observing the clinical trial indications and the correct ratio between the two active agents.

At the beginning, my research group was able to design and develop a small library of compounds with homo and hetero bivalent structures with the aim of testing various lipidic component and find the ideal distance between the hydrophobic drug and the hydrophilic polymer.

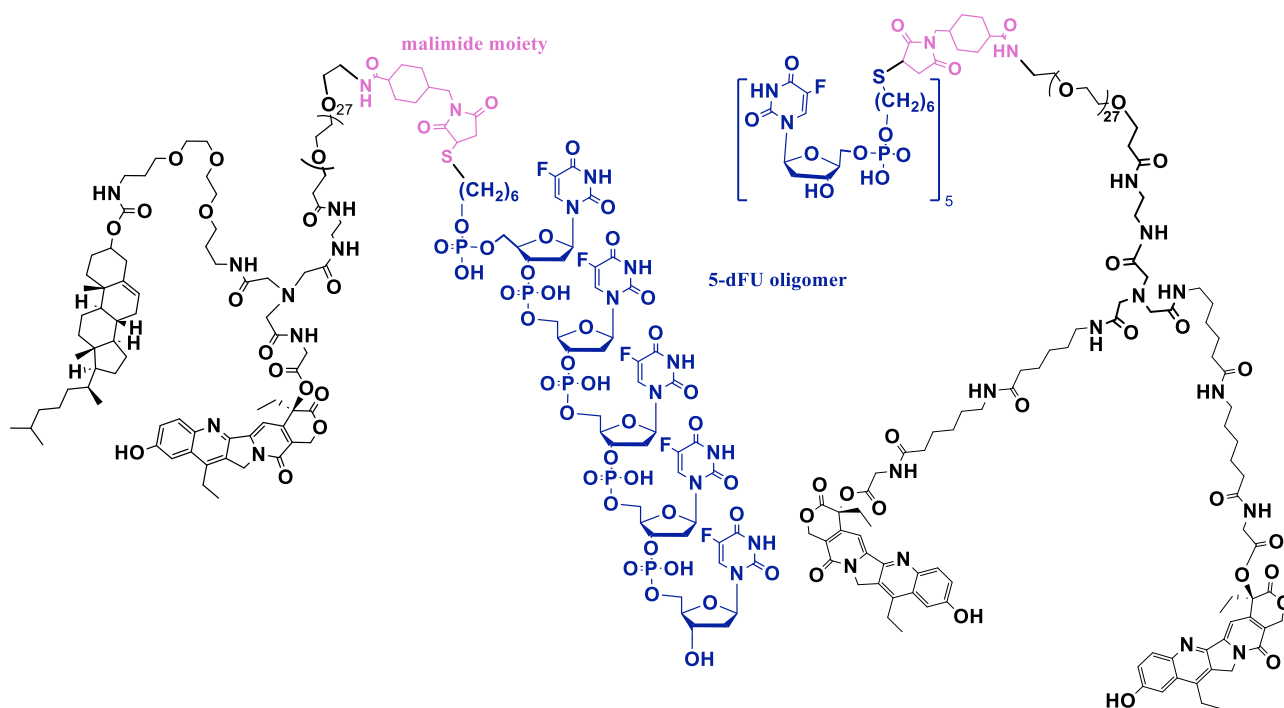


Fig. 16 Chemical structure of the two multivalent platforms for the treatment of colorectal cancer.

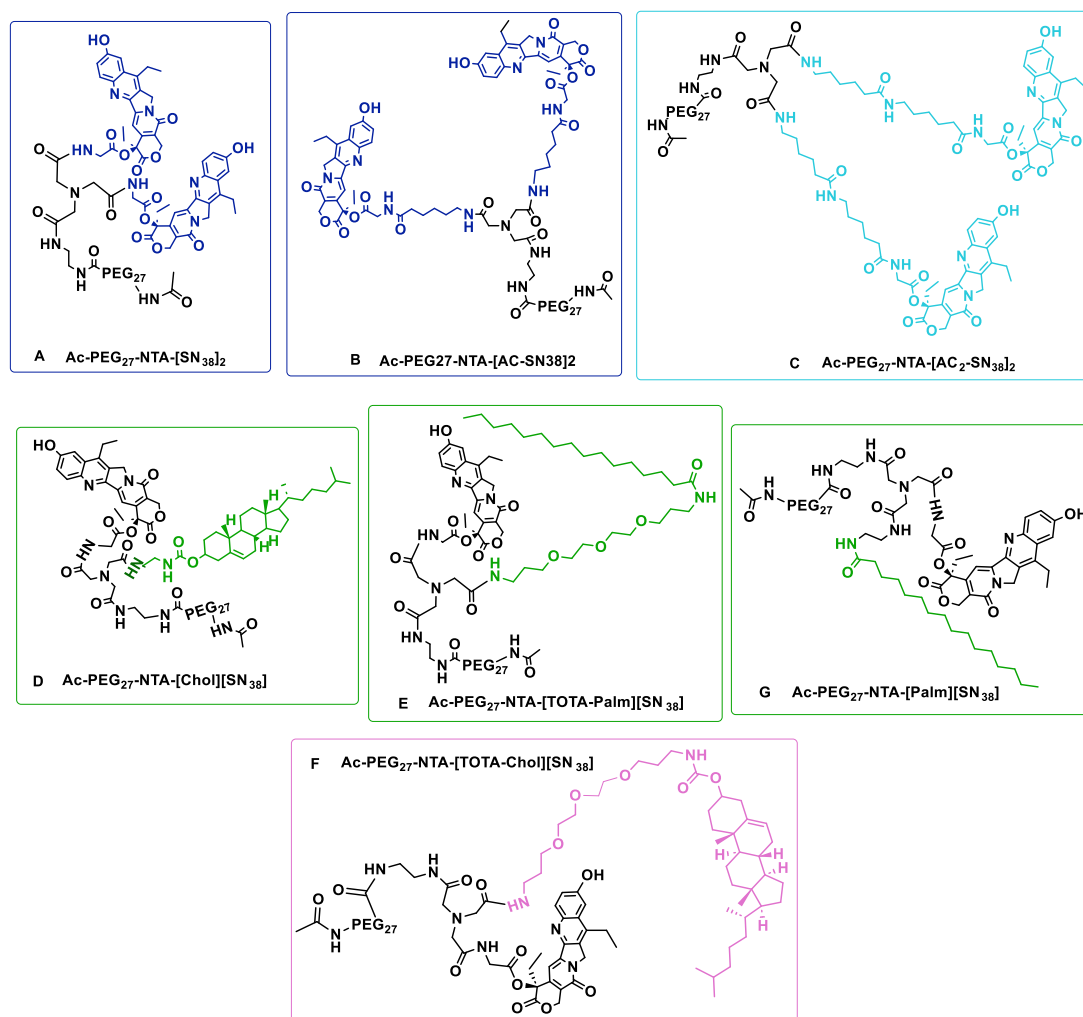


Fig.17 Chemical structure of the compounds of the first library.

The homo platform was designed in order to contain two branches of SN38 while in the other hand, the hetero system carried just one SN38 molecule and a lipidic portion. All the systems were based on a scaffold in which the drug and the polymer portions could be conjugated through a trifunctional platform, the nitrilotriacetic acid. Among the different attempts, both cholesterol and palmitic acids were tested as lipidic portion and also various distance between the drug and the central unit: in particular, starting with the placement of a small molecule as glycine, the distance was gradually increase first with one unit of 6-aminocaproic acid, and then with two unit of it.

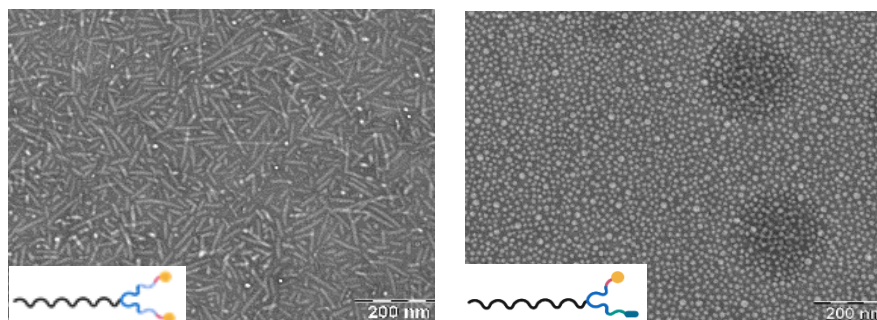
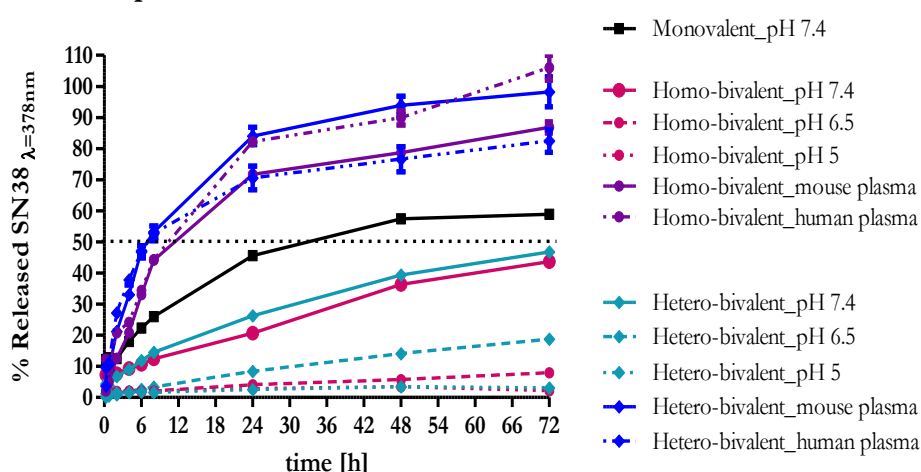


Fig. 18 Transmission electron microscopy images of the hetero and homo compounds selected.

All these compounds were tested for critical micelles concentration and analysed through transmission electron microscopy (TEM) in order to check their ability to form nanostructures in aqueous media and among them, the homo compound C and the hetero compound F containing respectively two units of 6-aminocaproic acid and a total-cholesterol portion, were chosen as the best candidates with the more stable and uniform structures.

SN38 Release Kinetics from PEG-X-SN38 nanosystems upon different conditions_ T=37°C



PEG-X-SN38 Nanosystems Half-life					
	pH 7.4	pH 6.5	pH 5	Mouse Plasma	Human Plasma
Monovalent	32 h	-	-	-	-
Homo-bivalent	> 72 h	> 72 h	> 72 h	11 h	10 h
Hetero-bivalent	> 72 h	> 72 h	> 72 h	6 h	6 h

Fig. 19 Stability tests plot with % of release vs time and related half-life at different pH conditions.

Because of these encouraging results, stability tests were performed in both human and mouse plasma in different pH conditions and the systems appeared to release the drug without quick degradation. These results allowed us to try to be more ambitious and proceed with the combined with the combined therapy.

4.7 - Synthesis of multivalent platforms

Starting with the two selected products, we synthesized the analogues with the amine function of the PEG Boc protected instead of acylated. In fact, the peg acylated compound is necessary for a better understanding of the platform inside the human fluids and it can be used as comparison but the removal of protecting group as final synthetic steps, gives the possibility of the conjugation with the oligomer form of the 5FU. This form, as mentioned before, allows the system to maintain the right ratio between the two drugs and it gives the possibility of an easy modulation with a reduction of the side effects provoked by the separated administration of the two therapies.

We decided to start the synthesis with the protection of the phenol of the SN38 with the tert-butyl diphenyl silyl protecting group. This protection has the characteristic to be very stable in both acid and basic condition, it could be easily removed just in the presence of fluoride salts or at very high temperature and it is necessary for the sake of avoiding side reactions during the following esterification with Boc-glycine. Glycine is placed in order to stabilize the closed lactone form, the ones that preserve the proper action of SN38 and it is placed through an ester link in order to preserve the liability of the link and ensure the easy release of the drug.

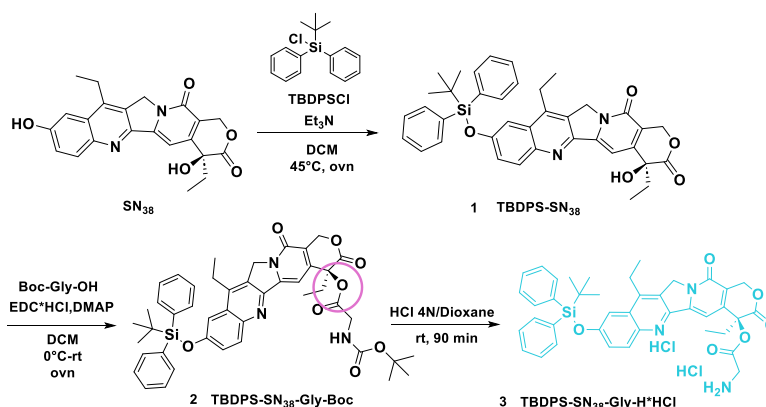


Fig.20 Synthetic pathway for the synthesis of TBDPS-SN₃₈-Gly-H.

As we can see from the figure, the protection of the drug moiety is very easy to obtain despite a purification step is necessary to guarantee the best performance possible for the following coupling with the glycine. The glycine is introduced as Boc-Glycine-OH and classic coupling reagents were used in the presence of DMAP for the correct formation of the desired ester.

4.7.1 - Synthesis of the Homo-bivalent compound

After ensuring the protection of the drug, we started the development of the homo-bivalent platform. At the beginning we complete the synthesis of the SN38 branch with the coupling of two units of boc-6-aminocaproic acid, after, of course, appropriate removal of the protecting group.

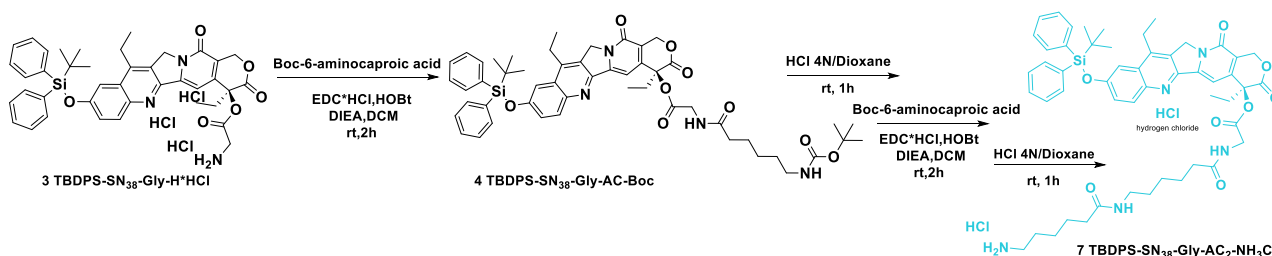


Fig. 21 Chemical scheme for the synthesis of the branch containing the drug.

Once we obtained this branch, we tried different approaches in order to achieve the final product in good yields. Because of the complex nature of the portions necessary to assemble the final molecule and the purification problems caused by the co-presence of a hydrophobic and hydrophilic portion with consequent lowering of the yield, we were forced to try three synthetic routes: the first one starts with the coupling of the N-Boc-Ethylenediamine with the core, the further coupling with the branches and the final coupling with the polyethylene glycol unit.

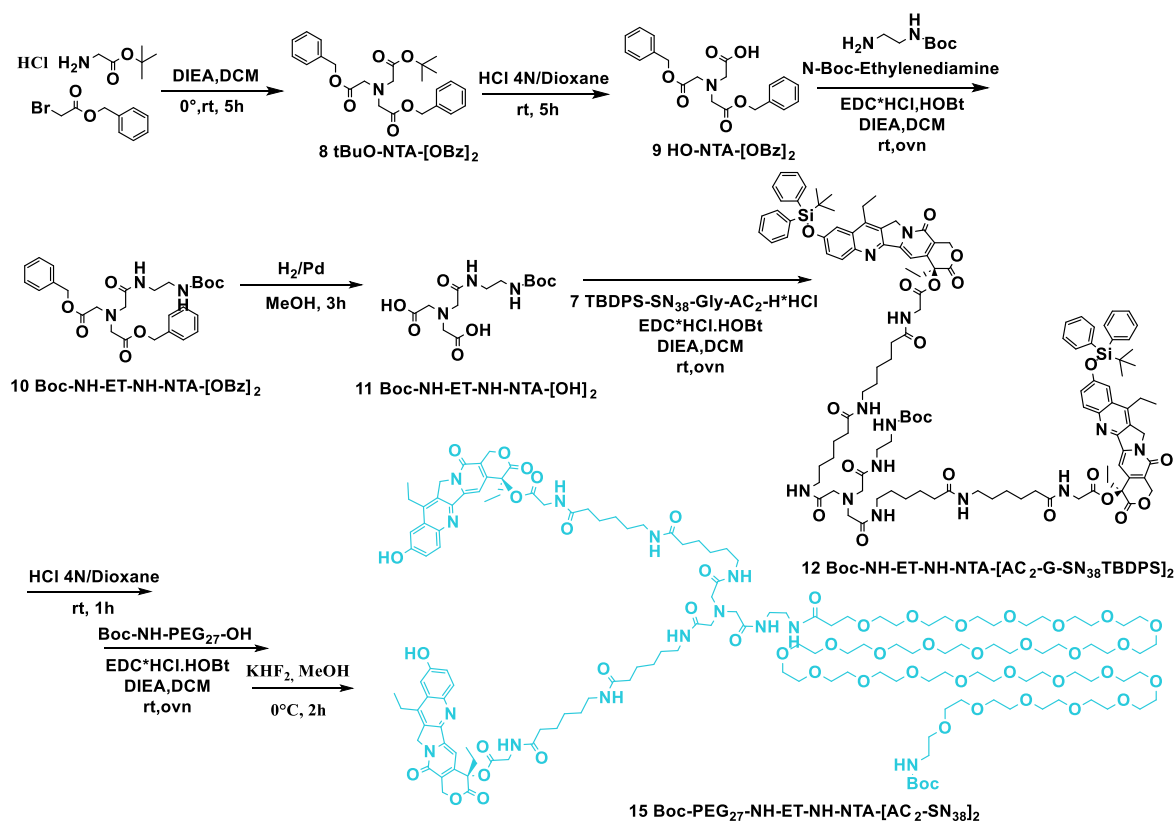


Fig. 22 Chemical scheme for the synthesis of the homo-bivalent platform Boc protected.

The reactivity of all these compounds is known and as expected, the reactions go to completeness without any problems. Nevertheless, it is necessary the purification from the unreacted reagents and the small amount of side products in every single steps as to prevent the formation of unwanted reactions and unfortunately, the purification of the intermediate 10 brings to a substantial loss of product. We have assumed that this was due to the co-presence of the central amine with the two units of SN38, a kind of structure that, although not complex as the final one, begins to have the dual hydrophilic and hydrophobic nature, that make it difficult to handle.

To solve this problem, we change the synthetic pathway to carrying out the purification of the SN38 branches with the core before the introduction of the diamine. Unfortunately, we discovered that in the purification conditions, the TBDPS is not stable, and it is easily removed, despite from the literature it is supposed to be quite steady in both acidic and basic environment, during the purification in direct phase with silica column using DCM/MeOH as solvents. Therefore, because part of the product got stuck inside the column, we decided to proceed through a third route.

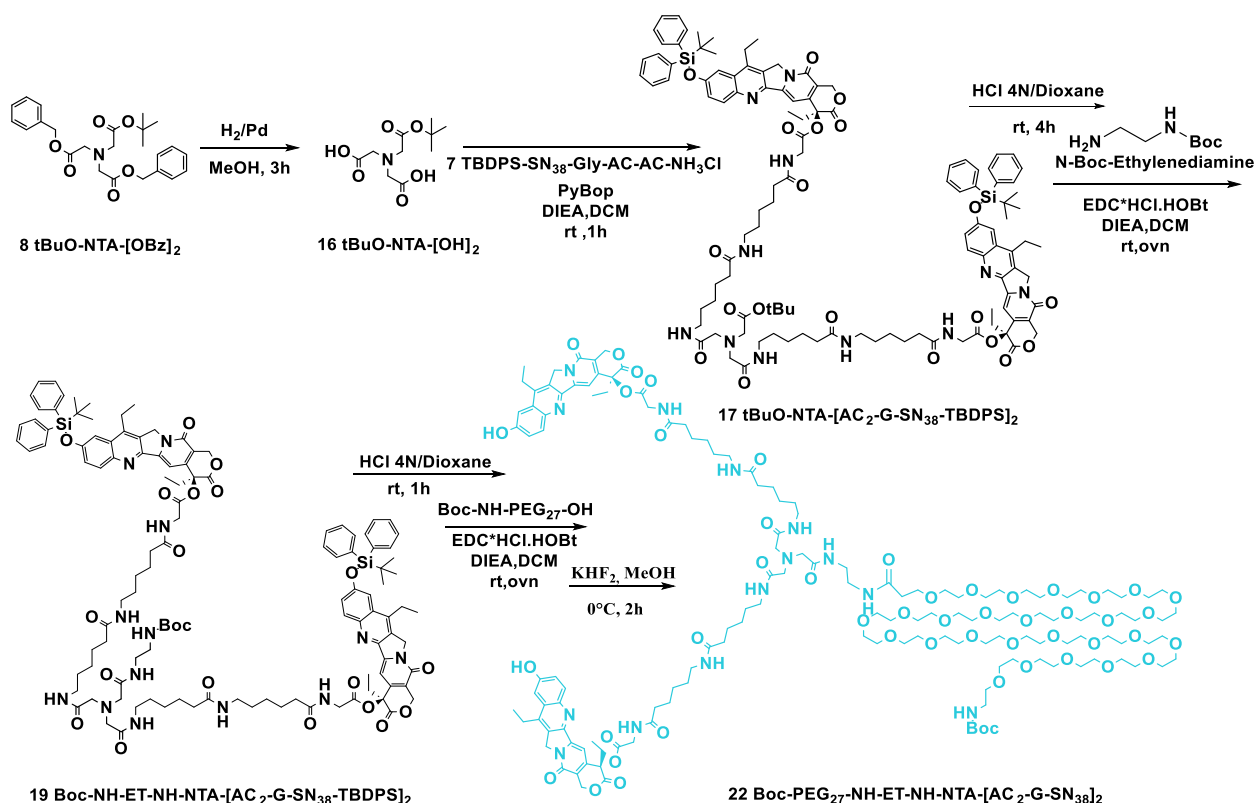


Fig. 23 Second synthetic pathway for the synthesis of the homo-bivalent platform.

To avoid this problem, we designed a different pathway that involved starting from the same core but proceeding with the coupling between the Boc-PEG-Ethylenediamine moiety and the central unit. In this way, the coupling of the branches with the core is the last one and not the first one like the other routes. Even if the inversion of the synthetic steps could be seen useless for the final

attainment, it is instead essential to obtain a better manageability. In fact, it is important to remember that one of the main characteristics of these kind of molecules, must remain the liability of the bond, and some little modifications during the assembling can preserve this characteristic while improve the stability.

In this route, the purification of the two portions with different nature, compound 16 and 7, take place separately and ensure a better result even if not optimal and trouble-free. The yield of the final product is still not very high but sufficient for proceeding with the conjugation with the drug.

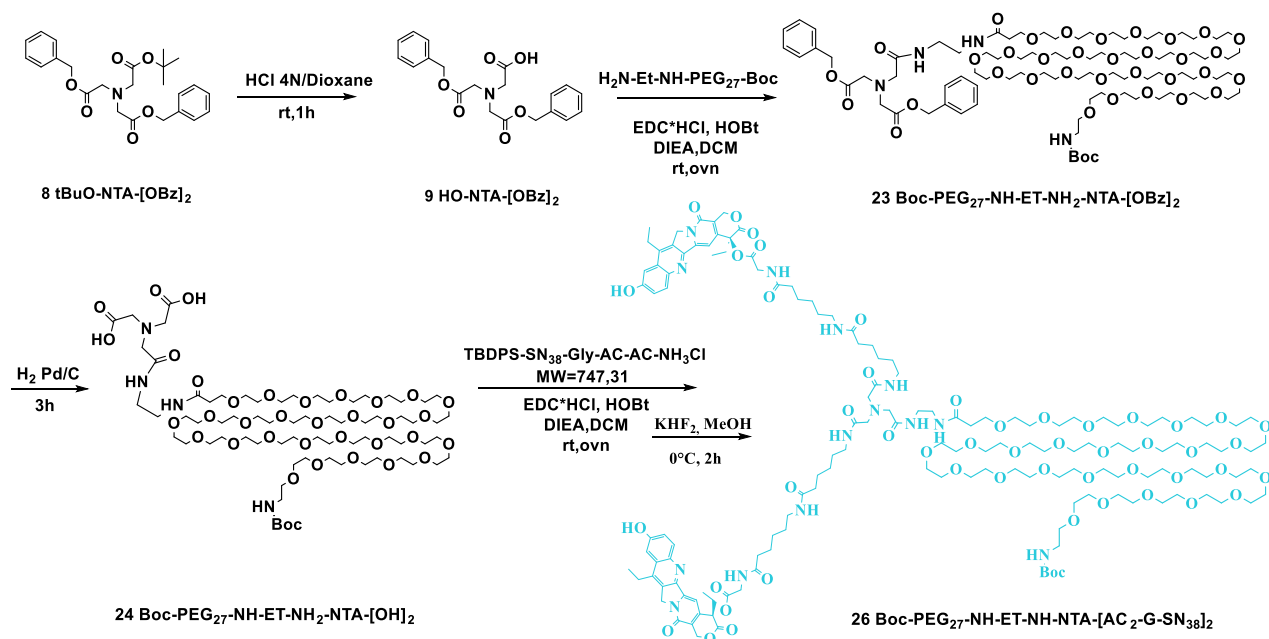


Fig. 24 Third synthetic alternative for the synthesis of the homo-bivalent platform.

4.7.2 - Synthesis of the Hetero-bivalent compound

The nature of this second platform is as complex as the homo-bivalent compound and the synthesis present similar purification problems.

At the beginning, we tried to obtain the differentiation between the two branches thanks to the activation of the core with a cyclic anhydride successfully opened by TBDPS-SN38-glycine. The successive coupling with a TOTA-cholesterol molecule needed to be purify (compound 28 before the tert-butyl deprotection) and unfortunately, this operation causes a significant decrease in the yield probably because of the deprotection of TBDPS. Despite that, the coupling with N-Boc-Ethylenediamine was possible and produced the main moiety that at this point was ready for the final coupling with PEG₂₇.

To avoid the purification problem encountered in the previous synthesis we tried a different approach where the purification step could occur in a different place of the synthesis.

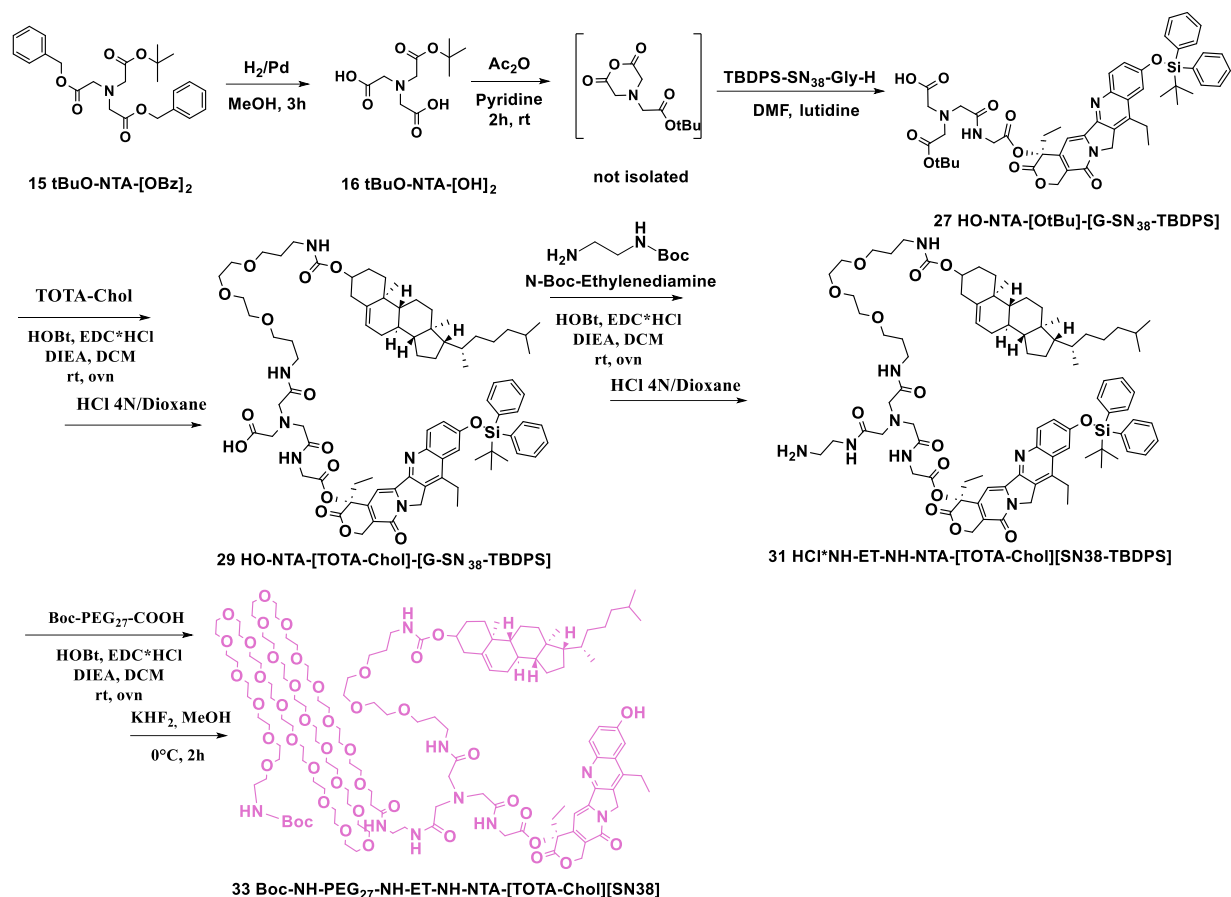


Fig. 25 Synthetic steps for the synthesis of the hetero-bivalent platform.

This second synthetic pathway involved the opening of the cyclic anhydride by mean of the Tota-Chol instead of the SN38. The reaction was a succession again and we were able to couple the diamine and to purify the product without any problems. We nimbly proceeded with the synthesis and having only some difficulties in the product isolation after the methyl ester hydrolysis, we were able to achieve the final product.

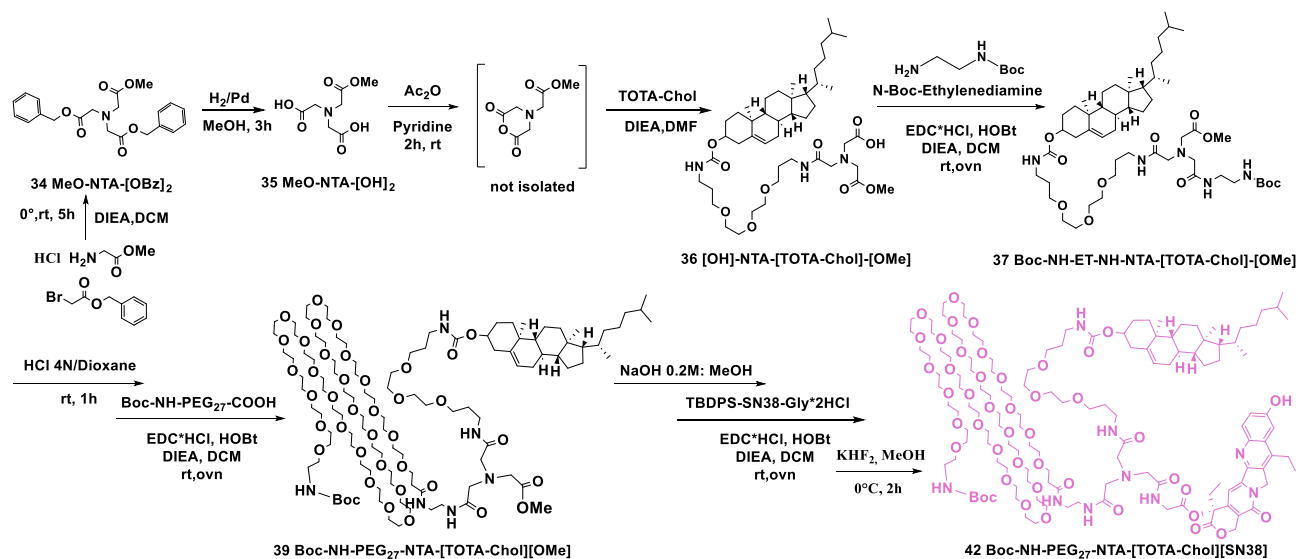


Fig. 26 Alternative synthetic pathway for the synthesis of the hetero-bivalent compound.

Once both platforms were obtained, we proceeded with the removal of the Boc protective group from the terminal portion of the PEG. Once the amine was released, it was reacted with Succinimidyl-trans-4-(N-maleimidymethyl)cyclohexane-1-carboxylate (SMCC) in the presence of DIEA. In this way, the maleimide intermediate was synthesised for both systems and it was ready for the final conjugation with 5-FdU, which was carried out in collaboration with the group of Anna Aviño and Ramón Eritja. The success of the reaction was monitored with MALDI, and further trials are awaited to have sufficient quantities and to start in vitro tests.

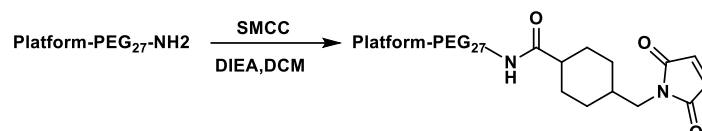


Fig.27 Introduction of the maleimide moiety for the final conjugation with 5FdU.

4.8 – Conclusion

The development of nanoparticles has become one of the most used approaches for the improvement of the therapies and the better administration of the drug. In fact, most of the drugs fail the clinical trials because of the poor permeability, solubility, or selectivity and all these aspects can be improved with the use of a self-assembled structure able to protect the active form without compromising its easy release.

There is a large variety of nanoparticles that can be designed and among them we decided to focus our attention in two different projects for the synthesis of silica core nanoparticles and multivalent platform. Both have the characteristic to be designed to help the active moiety to cross the cell membranes improving the permeability and the solubility, at the moment they don't possess the portion necessary for the selection release, but further development of this aspect has already been scheduled after the biological results.

In the first project, we selected toxic peptides sequence with different total charged to deeply investigate if this characteristic is fundamental for the shape of the nanoparticles. Different percentages of the peptides were used to functionalize with click chemistry pluronic acid and obtain a self-assembled structure. We were able to demonstrate that these structures are very useful to enhance the stability and to modulate the size even if the charge doesn't seem to affect the shape. In the second project a hetero and a homo-bivalent platforms were created to improve the therapeutic activity of two of the most used drugs, the SN38 and the 5FdU, for advanced colorectal cancer. A previous screening was useful to identify the structures most capable of forming nanoparticles. All the systems are based on a scaffold to which the hydrophobic SN38 and a

hydrophilic polyethylene glycol (PEG) are conjugated through a trifunctional platform. When the platforms were completed, the Boc protection of the PEG was removed to introduce a maleimide moiety used to conjugate an oligomer of Floxuridine (5FdU), an antimetabolite tumor drug with similar 5FU mechanism of action.

Once the synthesis of all the conjugates will be completed and characterized, their self-assembly ability will be evaluated together with their stability in physiological conditions.

4.9 – Experimental procedure

General Information

Reagents and solvents were purchased from commercial sources and were used without further purification. Flash chromatography on silica was carried out on a Teledyne Isco Combiflash Rf instrument using Redisep Rf silica columns. ¹H-NMR (400 MHz) and ¹³C-NMR (101 MHz) spectroscopies were performed on a Varian Mercury 400 MHz instrument. Chemical shifts (δ) are expressed in ppm and referenced to the appropriate NMR solvent peak(s). The following abbreviations are used to indicate multiplicity: s: singlet, d: doublet, t: triplet, m: multiplet.

Analytical RP-HPLC and mass spectra were performed on a Waters Alliance 2795 with an automated injector and a photodiode array detector Waters 2996 coupled to an electrospray ion source (ESI-MS) Micromass ZQ mass detector, using an XSelect C18 reversed-phase analytical column (4.6 mm \times 50 mm, 3.5 μ m) or a C4 (4.6 mm \times 250 mm, 5 μ m) and MassLynx 4.1 software was used to manage the data. The instrument was operated in the positive ESI (+) ion mode. Additionally, analytical RP-HPLC was also performed on a Waters Alliance 2795 with an automated injector and a photodiode array detector Waters 2998, using an XBridge BEH C18 reversed-phase analytical column (4.6 mm \times 100 mm, 3.5 μ m) and Empower 2.0 software. Analyses were carried out with several elution systems : a linear gradient 5–100%, or 30-100%, or 50-100%, or a 60-100%, or a 80-100% of CH₃CN (0.036% trifluoroacetic acid (TFA)) in H₂O (0.045% TFA) over 4.5 min at a flow rate of 0.6 mL/min. Semipreparative RP-HPLC purification was performed on a Waters system with a 2545 binary gradient module, a 2767 manager collector, and a 2489 UV detector, coupled to an electrospray ion source (ESI-MS) Micromass ZQ mass detector and MassLynx 4.1 software.

General synthesis

The general procedure is as follows: a mixture of the molecule with free acid (0.3 mmol) and 1-Hydroxybenzotriazole hydrate (HOBt \cdot H₂O) (1.2 eq., 0.36 mmol) was stirred in 10mL of 3:1

DCM/DMF at rt, and after 10 minutes, the free amino counterpart (1 eq., 0.3 mmol), N-Ethyl-N'-(3-dimethylaminopropyl) carbodiimide hydrochloride (EDC*HCl) (1.2 eq., 0.36 mmol) and N,N-Diisopropylethylamine (DIEA) were added to the mixture and the reaction was allowed to stir at room temperature overnight under nitrogen atmosphere. The crude mixture was extracted with 0.5% w/v citric acid (2x10 mL), saturated NaHCO₃ (2x 10mL) and brine (1x 10mL). The organic phase was dried over MgSO₄, filtered, and evaporated under vacuum.

Boc and tertbutyl deprotection were accomplished by stirring the crude peptides in a solution of HCL 4N in dioxane at room temperature. The solvent is removed under vacuum and the product is dried in the stove at 39°C for three hours. Benzyl ester deprotection was accomplished by stirring the crude peptides in a mixture of MeOH with 10% of Pd/C overnight under hydrogen atmosphere at a pressure of 1atm. The catalyst was removed by filtration through celite and washed with methanol and DCM. The product was recollected and concentrated under vacuum.

TBDPS-SN38 (1):

Triethylamine (4.5 eq., 11.48 mmol, 1.161 g) and tert-Butyl(chloro)diphenylsilane (4 eq., 10.2 mmol, 2.8 g) were added to a suspension of SN38 (1eq., 2.55 mmol, 1g) in 50 mL di DCM anhydrous. The reaction was allowed to stir overnight at 45°C under reflux. After cooling to room temperature, the mixture was extracted with 0.5% w/v citric acid (2x50 mL), saturated NaHCO₃ (2x 50mL) and brine (1x 50mL). The organic phase was dried over MgSO₄, filtered, and evaporated under vacuum. The residue was purified in flash chromatography on silica using CH₂Cl₂ and MeOH as solvents and compound 1 was obtained (1.51 g, 2.4 mmol, Y= 96%).

¹H NMR (400MHz, CDCl₃, 298K): δ 7.95 (s, 1H), 7.67 – 7.69 (m, 4H), 7.50 – 7.52 (d,1H), 7.37 – 7.33 (m, 6H), 7.04 (s,1H), 5.74 – 5.70 (d,2H), 5.10 (s,2H), 3.57 – 3.51 (q, 2H), 1.96 – 1.90 (m, 2H), 1.11 (s,9H), 0.91 – 0.94 (t,3H), 0.82 – 0.86 (t,3H); **HPLC-MS** (ESI): [M+1] = 631

TBDPS-SN38-Gly-Boc (2):

N-(tert-butoxycarbonyl) glycine (Boc-Gly-OH) (1.4 eq., 3.10 mmol, 544.31 mg), N-Ethyl-N'-(3-dimethylaminopropyl) carbodiimide hydrochloride (EDC*HCl) (1.4 eq.; 3.10 mmol, 594.3 mg) and 4-Dimethylaminopyridine (DMAP) (0.4 eq., 0.88 mmol, 108.5 mg) were added at 0°C to a solution of compound 1 in 30 mL DCM. The reaction was allowed to reach room temperature and was stirred overnight. The crude mixture was extracted with 0.5% w/v citric acid (2x30 mL), saturated NaHCO₃

(2x 30mL) and brine (1x 30mL). The organic phase was dried over MgSO₄, filtered, and concentrated under vacuum to yield compound 2 as a yellow solid (1.41 g, 1.8 mmol, Y=81%).

¹H NMR (400MHz, CDCl₃, 298K): δ 8.06 - 8.04 (dd, 1H), 7.50 – 7.45 (m, 5H), 7.46 – 7.44 (d, 1H), 7.40 (s,1H), 7.37 – 7.33 (m, 6H), 7.08 (s,1H), 5.74 – 5.70 (d, 2H), 5.10 (s, 2H), 3.70 (s, 2H), 2.67 – 2.61 (q, 2H), 1.84 – 1.90 (m, 2H), 1.42 (s,9H), 1.17 (t,3H), 0.98 (s,9H), 0.87- 0.91 (t,3H);

HPLC-MS (ESI): [M+1] = 788

After characterization, the product is deprotected following the general Boc deprotection procedure to obtain product **3 (TBDPS-SN38-Gly-H*HCl)**.

TBDPS-SN38-Gly-AC-Boc (4):

By performing the general procedure over product 3, product 4 is obtain as a yellow solid (266.8 mg, 0.33 mmol, Y=90%).

¹H NMR (400MHz, CDCl₃, 298K): δ 9.56 – 9.54 (dd,1H), 8.06 – 8.04 (dd, 1H), 7.50-7.45 (m,5H), 7.44 – 7.42 (d,1H), 7,40 (s, 1H), 7.37-7.33 (m, 6H), 7.09 (s, 1H), 6.74 – 6.70 (d, 2H), 5.10 (s, 2H), 4.22 (s, 2H), 3.57 – 3.51 (q, 2H), 3.20 – 3.17 (q, 2H), 2.15 – 2.13 (t, 2H), 1.96 – 1.90 (q, 2H), 1.50 – 1.46 (m, 2H), 1.42 (s, 9H), 1.33-1.28 (m,4H), 1.42 (s,9H), 1.18 (s,3H), 0.98 (s,9H); **HPLC-MS (ESI): [M+1] = 902**

After characterization, the product is deprotected following the general Boc deprotection procedure to obtain product **5 (TBDPS-SN38-Gly-AC-H*HCl)**.

TBDPS-SN38-Gly-AC₂-Boc (6):

By performing the general procedure over product 5, product 6 is obtain as a yellow solid (157.6 mg, 0.155 mmol, Y=82%).

¹H NMR (400MHz, CDCl₃, 298K): δ 9.56 – 9.54 (dd,1H), 8.06 – 8.04 (dd, 1H), 7.70 – 7.72 (dd, 1H), 7.50-7.45 (m,5H), 7.44 – 7.42 (d,1H), 7,40 (s, 1H), 7.37-7.33 (m, 6H), 7.09 (s, 1H), 6.74 – 6.70 (d, 2H), 5.10 (s, 2H), 4.22 (s, 2H), 3.57 – 3.51 (q, 2H), 3.20 – 3.17 (q, 2H), 3.01 – 2.98 (q, 2H), 2.15 – 2.13 (t, 4H), 1.96 – 1.90 (q, 2H), 1.50 – 1.46 (m, 4H), 1.42 (s, 9H), 1.33-1.28 (m, 8H), 1.42 (s,9H), 1.18 (s,3H), 0.98 (s,9H); **HPLC-MS (ESI): [M+1] = 1015**

After characterization, the product is deprotected following the general Boc deprotection procedure to obtain product **7 (TBDPS-SN38-Gly-AC₂-H*HCl)**.

tBuO-NTA-[OBz]₂ (8):

To a solution of glycine tert-butyl ester hydrochloride (6.08 mmol, 1.05 g) in ACN (30 mL) were

added benzyl bromoacetate (2.3 eq., 13.9 mmol, 2.3 mL) and DIEA (5 eq., 30.4 mmol, 5.3 mL) at 0 °C and the reaction was allowed to stir at room temperature for 5 hours. Saturated NaHCO₃ (10 mL) was poured inside the reaction flask and the crude product was extracted with DCM (2x25 mL). The organic phase was dried over MgSO₄, filtered, and evaporated under vacuum. The residue was purified in flash chromatography on silica using EtOAc and Hexane as solvents and compound 8 was obtained as a transparent oil (2.35 g, 5.49 mmol, Y= 90%).

¹H NMR (400MHz, CDCl₃, 298K): δ 7.36–7.33 (m, 10H), 5.14 (s, 4H), 3.72 (s, 4H), 3.58 (s, 3H), 1.44 (s, 9H); HPLC-MS (ESI): [M+1] = 429

After characterization, the product is deprotected following the general tBu deprotection procedure to obtain product **9 (HO-NTA-[OBz]₂)**.

Boc-NH-Et-NH-NTA-[OBz]₂ (10):

By performing the general procedure over product 8 with N-Boc-Ethylenediamine, the crude of 10 is obtained. The residue was purified in flash chromatography on silica using CH₂Cl₂ and MeOH as solvents and compound 9 was obtained (680.6 mg, 1.33 mmol, Y= 61%).

¹H NMR (400MHz, CDCl₃, 298K): δ 7.40 – 7.33 (m, 10H), 5.32 (s, 4H), 3.66 – 3.62 (t, 2H), 3.42 – 3.38 (t, 2H), 3.32 (s, 4H), 3.29 (s, 2H), 1.42 (s, 9H); HPLC-MS (ESI): [M+1] = 514

After characterization, the product is deprotected following the general Benzyl deprotection procedure to obtain product **11 (Boc-NH-Et-NH-NTA-[OH]₂)**.

Boc-NH-Et-NH-NTA-[AC2-G-SN38TBDPS]₂ (12):

By performing the general procedure over product 7 with Boc-NH-Et-NH-NTA-[OH]₂, the crude of 12 is obtained. The residue was purified in flash chromatography on silica using CH₂Cl₂ and MeOH as solvents and compound 12 was obtained (65.4 mg, 0.03 mmol, Y= 35 %).

¹H NMR (400MHz, DMSO-d₆, 298K): δ 8.92 – 8.85 (dd, 2H), 8.65 – 8.53 (dd, 2H), 8.44 – 8.35 (t, 2H), 8.22 – 8.06 (m, 8H), 7.86 – 7.70 (m, 12H), 7.61 – 7.45 (m, 16H), 7.19 – 7.16 (d, 2H), 7.09 (s, 2H), 5.54 (s, 4H), 5.25 (s, 4H), 4.26 – 3.69 (m, 6H), 3.18 – 3.09 (m, 6H), 3.05 – 2.88 (m, 8H), 2.27 – 2.11 (m, 8H), 1.64 – 1.23 (m, 33H), 1-19 (s, 18H), 0.96 – 0.91 (t, 6H), 0.90 – 0.80 (t, 6H);

HPLC-MS (ESI): [M+1] = 2126

After characterization, the product is deprotected following the general Boc deprotection procedure to obtain product **13 (HCl*NH-Et-NH-NTA-[AC2-G-SN38TBDPS]₂)**.

Boc-PEG₂₇-NH-Et-NH-NTA-[AC2-SN38-TBDPS]₂ (14):

By performing the general procedure over product 12 with Boc-NH-PEG₂₇-COOH, the crude of 14 is obtained. The residue was purified with precipitation using Et₂O and Hexane as solvents three times and compound 13 was obtained as a yellow oil (42.6 mg, 0.012 mmol, Y= 80%).

HPLC-MS (ESI): [M+1] = 3431

Boc-PEG₂₇-NH-Et-NH-NTA-[AC2-SN38]₂ (15):

KHF₂ (2eq., 0.025mmol, 2mg) and compound 14 (0.012mmol, 42.6 mg) were dissolved in 2mL of MeOH at 0°C and allowed to stir for 1 hour. DCM was added and the product was extracted with brine. The residue was purified with preparative HPLC using ACN and Water as solvents and compound 15 was obtained as a white solid (11.05 mg, 0.004 mmol, Y= 32 %).

HPLC-MS (ESI): [M/2+1] = 910, [M/3+1] = 607

tBuO-NTA-[OH]₂ (16):

Compound 16 is obtained by following the general benzyl deprotection procedure over compound 8. The product was recollected as a transparent oil after concentration under vacuum (1.01 mmol, 250.6 mg, Y= 87.4%). **HPLC-MS (ESI):** [M+1] = 248.

tBuO-NTA-[AC2-G-SN38-TBDPS]₂ (17):

By performing the general procedure over product 7 with tBuO-NTA-[OH]₂ (compound 16), the crude 17 is obtained. The residue was purified in flash chromatography on silica using CH₂Cl₂ and MeOH as solvents and compound 17 was obtained (81.5 mg, 0.04 mmol, Y= 25 %).

¹H NMR (400MHz, DMSO-d₆, 298K): δ 8.92 – 8.85 (dd, 2H), 8.65 – 8.53 (dd, 2H), 8.44 – 8.35 (t, 2H), 8.22 – 8.06 (m, 8H), 7.86 – 7.70 (m, 12H), 7.61 – 7.45 (m, 16H), 7.19 – 7.16 (d, 2H), 7.09 (s, 2H), 5.54 (s, 4H), 5.25 (s, 4H), 4.26 – 3.69 (m, 4H), 3.39 (s,4H), 3.09 (s,2H), 3.05 – 2.88 (m, 8H), 2.27 – 2.11 (m, 8H), 1.96 – 1.92 (m, 4H), 1.42 (s, 9H). 1.28 – 1.23 (m, 16H), 1-19 (s, 18H), 0.96 – 0.91 (t, 6H), 0.90 – 0.80 (t, 6H); **HPLC-MS (ESI):** [M+1] = 2040

After characterization, the product is deprotected following the general tBu deprotection procedure to obtain product **18 (HO-NTA-[AC2-G-SN38-TBDPS]₂)**.

Boc-NH-Et-NH-NTA-[AC2-G-SN38-TBDPS]₂ (19):

By performing the general procedure over product 18 with Boc-NH-Et-NH₂, product 19 is obtained

(41.24 mg, 0.019 mmol, Y= 97 %). **¹H NMR** and **HPLC-MS** see compound 12 After characterization, the product is deprotected following the general tBu deprotection procedure to obtain product **20(HCl*NH₂-Et-NH-NTA-[AC2-G-SN38TBDPS]₂)**.

Boc-PEG₂₇-NH-Et-NH-NTA-[AC2-SN38-TBDPS]₂ (21): see compound 14.

Boc-PEG₂₇-NH-ET-NH-NTA-[AC2-SN38]₂ (22): see compound 15.

Boc-PEG₂₇-NH-Et-NH-NTA-[OBz]₂ (23):

By performing the general procedure over product 9 with H₂N-Et-NH-PEG₂₇-Boc, the crude of 23 is obtained. The residue was purified with preparative HPLC using ACN and Water as solvents and compound 23 was obtained as a transparent oil (218.18 mg, 0.12 mmol, Y= 75 %).

HPLC-MS (ESI): [M/2+1] = 910, [M/3+1] = 607

After characterization, the product is deprotected following the general benzyl deprotection procedure to obtain product **24 (Boc-PEG₂₇-NH-Et-NH-NTA-[OH]₂)**.

Boc-PEG₂₇-NH-Et-NH-NTA-[AC2-SN38-TBDPS]₂ (25): see compound 21 and 14.

Boc-PEG₂₇-NH-Et-NH-NTA-[AC2-G-SN38]₂ (26): see compound 22 and 15.

HO-NTA-[OtBu]-[G-SN38-TBDPS] (27):

Compound 16 (1.3eq., 0.24 mmol, 60mg) is allowed to stir under nitrogen atmosphere overnight at room temperature in the presence of pyridine (300μl) and acetic anhydride (300μl). The day after the solvent was evaporated under nitrogen atmosphere and the crude mixture was dissolved in anhydrous DMF. Compound 3 (0.2mmol, 149.35 mg) and 2,6-lutidine (1.5 eq., 0.3mmol, 35μl) were added at 0°C and the reaction was allowed to stir 1 hour. Solvent was removed and the crude mixture was extracted with 0.5% w/v citric acid (2x10 mL), saturated NaHCO₃ (2x 10mL) and brine (1x 10mL). The organic phase was dried over MgSO₄, filtered, and concentrated to give the pure product (151.7 mg, 0.17 mmol, Y= 83 %).

¹H NMR (400MHz, DMSO-d₆, 298K): δ 12.4(s,1H), 9.04-9.02 (m,1H), 7.65 (d,1H), 7.59-7.56 (m,4H), 7.4 (s, 1H), 7.36 (s, 1H), 7.35 – 7.32 (m,6H), 7.08 (s,1H), 4.76 (s,2H), 4.22 (s,2H), 4.16 (dd, 2H), 3.49 – 3.46 (q, 2H), 3.32 (s, 4H), 3.30 (s, 2H), 1.96 – 1.93 (q, 2H), 1.42 (s, 9H), 1.18 – 1.16 (t, 3H), 0.98 (s,

9H), 0.89- 0.87 (t, 3H); **HPLC-MS** (ESI): [M+1] = 919.5, [M/2+1] = 459.6

tBuO-NTA-[TOTA-Chol]-[G-SN38-TBDPS] (28):

By performing the general procedure over product 27 with TotaChol, the crude 28 is obtained. The residue was purified in flash chromatography on silica using CH₂Cl₂ and MeOH as solvents and compound 28 was obtained (75.8 mg, 0.05 mmol, Y= 33 %).

¹H NMR (400MHz, DMSO-d₆, 298K): δ 9.04-9.02 (m,1H), 8.01- 7.89 (d,1H), 7.65 (d,1H), 7.59-7.56 (m,4H), 7.4 (s, 1H), 7.36 (s, 1H), 7.35 – 7.32 (m,6H), 7.08 (s,1H), 6.76 (m, 1H), 5.29 (dd,1H), 4.76 (s,2H), 4.60 – 4.56 (q,1H), 4.22 (s,2H), 4.16 (dd, 2H), 3.5 (s, 8H), 3.49 – 3.46 (q, 2H), 3.39 – 3.35 (dd,4H), 3.32 (s, 4H), 3.30 (s, 2H), 3.13 – 3.09 (m, 4H), 2.19 – 2.14 (m, 3H), 1.96 – 1.93 (q, 2H), 1.62 – 1.58 (m, 15H), 1.42 (s, 9H), 1.27 – 1.21 (m, 16H), 1.18 – 1.16 (t, 3H), 0.98 (s, 9H), 0.94 – 0.90 (m, 6H), 0.89- 0.87 (t, 3H); **HPLC-MS** (ESI): [M+1] = 1534, [M/2+1]= 767.

After characterization, the product is deprotected following the general tBu deprotection procedure to obtain product **29 (HO-NTA-[TOTA-Chol]-[G-SN38-TBDPS])**.

Boc-NH-Et-NH-NTA-[TOTA-Chol][SN38-TBDPS] (30):

By performing the general procedure over product 29 with Boc-NH-Et-NH₂ product 30 is obtained without further purification. (58 mg, 0.035 mmol, Y= 72 %).

¹H NMR (400MHz, DMSO-d₆, 298K): δ 9.04-9.02 (m,1H), 8.01- 7.89 (d,1H), 7.83 – 7.85 (d, 2H), 7.65 (d,1H), 7.59-7.56 (m,4H), 7.4 (s, 1H), 7.36 (s, 1H), 7.35 – 7.32 (m,6H), 7.08 (s,1H), 6.76 (m, 1H), 5.29 (dd,1H), 4.76 (s,2H), 4.60 – 4.56 (q,1H), 4.22 (s,2H), 4.16 (dd, 2H), 3.5 (s, 8H), 3.49 – 3.46 (m, 6H), 3.39 – 3.35 (dd,4H), 3.32 (s, 4H), 3.30 (s, 2H), 3.13 – 3.09 (m, 4H), 2.19 – 2.14 (m, 3H), 1.96 – 1.93 (q, 2H), 1.62 – 1.58 (m, 15H), 1.42 (s, 9H), 1.27 – 1.21 (m, 16H), 1.18 – 1.16 (t, 3H), 0.98 (s, 9H), 0.94 – 0.90 (m, 6H), 0.89- 0.87 (t, 3H); **HPLC-MS** (ESI): [M+1] = 1618.

After characterization, the product is deprotected following the general Boc deprotection procedure to obtain product **31 (HCl*NH₂-Et-NH-NTA-[TOTA-Chol][SN38-TBDPS])**.

Boc-NH-PEG27-NH-ET-NH-NTA-[TOTA-Chol][SN38-TBDPS] (32):

By performing the general procedure over product 31 with Boc-NH-PEG₂₇-COOH, the crude of 32 is obtained. The residue was purified in flash chromatography on silica using CH₂Cl₂ and MeOH as solvents and compound 32 was obtained (76.72 mg, 0.026 mmol, Y= 75 %).

HPLC-MS (ESI): [M/2+1] = 1462.5, [M/3+1] = 975, [M/4+1] = 731

Boc-NH-PEG27-NH-ET-NH-NTA-[TOTA-Chol][SN38] (33):

KHF₂ (2eq., 0.052 mmol, 4 mg) and compound 32 (0.026mmol, 76.72 mg) were dissolved in 2mL of MeOH at 0°C and allowed to stir for 1 hour. DCM was added and the product was extracted with brine. The organic phase was dried over MgSO₄, filtered, and concentrated to give the pure product. (68.34 mg, 0.025 mmol, Y= 98 %). **HPLC-MS** (ESI): [M/2+1] = 1343, [M/3+1] = 895

Dibenzyl 2,2'-((2-methoxy-2-oxoethyl)azanediyl)diacetate (MeO-NTA-[OBz]₂) (34) :

To a solution of glycine methylester hydrochloride (5.6 mmol, 500 mg) in ACN (20 mL) were added benzyl bromoacetate (2.3 eq., 12.9 mmol, 2 mL) and DIEA (5eq., 28 mmol, 4.8 mL) at 0 °C and the reaction was allowed to stir at room temperature for 5 hours. Saturated NaHCO₃ (10 mL) was poured inside the reaction flask and the crude product was extracted with DCM (2x25 mL). The organic phase was dried over MgSO₄, filtered, and evaporated under vacuum. The residue was purified in flash chromatography on silica using EtOAc and Hexane as solvents and compound 34 was obtained as a white solid (1.9 g, 5.15 mmol, Y= 92%).

¹H NMR (400MHz, CDCl₃, 298K): δ 7.36–7.33 (m, 10H), 5.25 (s, 4H), 3.8 (s,3H), 3.72 (s, 4H), 3.58 (s, 2H); **HPLC-MS** (ESI): [M+1] = 386

After characterization, the product is deprotected following the general benzyl deprotection procedure to obtain product **35 (MeO-NTA-[OH]₂)**.

[OH]-NTA-[TOTA-Chol]-[OMe] (36):

Compound 35 (1.3eq., 0.65 mmol, 133.36 mg) is allowed to stir under nitrogen atmosphere overnight at room temperature in the presence of pyridine (300μl) and acetic anhydride (300μl). The day after the solvent was evaporated under nitrogen atmosphere and the crude mixture was dissolved in anhydrous DMF. TotaChol (0.5mmol, 334.7 mg) and DIEA (1.5 eq., 0.65mmol, 113.2 μl) were added at 0°C and the reaction was allowed to stir 1 hour. Solvent was removed and the crude mixture was extracted with 0.5% w/v citric acid (2x10 mL), saturated NaHCO₃ (2x 10mL) and brine (1x 10mL). The organic phase was dried over MgSO₄, filtered, and concentrated to give the pure product (307.6 mg, 0.375 mmol, Y= 75 %).

¹H NMR (400MHz, DMSO-d₆, 298K): δ 12.6 (s,1H), 8.01 – 7.89 (d,1H), 6.76 – 6.73 (d,1H), 5.29 – 5.27 (dd,1H), 4.60 – (4.56 (q, 1H), 3.7 (s,3H), 3.5 (s,8H), 3.35 – 3.30 (m, 10H), 3.13 – 3.09 (m, 4H), 2.19 – 2.14 (m, 4H), 1.62 – 1.58 (m, 15H), 1.21 – 1.19 (m,6H), 1.01 (s, 3H), 0.94-0.91 (m,6H), 0.88 – 0.84 (m,6H) ; **HPLC-MS** (ESI): [M+1] = 821.

Boc-NH-Et-NH-NTA-[TOTA-Chol]-[OMe] (37):

By performing the general procedure over product 36 with Boc-NH-Et-NH₂, the crude of 37 is obtained. The residue was purified in flash chromatography on silica using CH₂Cl₂ and MeOH as solvents and compound 37 was obtained (162.4 mg, 0.18 mmol, Y= 48 %).

¹H NMR (400MHz, DMSO-d₆, 298K): δ 8.01- 7.89 (d,1H), 7.83 – 7.81 (d, 1H), 6.76 – 6.73 (d,2H), 5.29 – 5.27 (dd,1H), 4.60 – (4.56 (q, 1H), 3.7 (s,3H), 3.68 – 3.65 (m, 4H), 3.5 (s,8H), 3.35 – 3.30 (m, 10H), 3.13 – 3.09 (m, 4H), 2.19 – 2.14 (m, 4H), 1.62 – 1.58 (m, 15H), 1.42 (s, 9H), 1.21 – 1.19 (m,6H), 1.01 (s, 3H), 0.94-0.91 (m,6H), 0.88 – 0.84 (m,6H) ; HPLC-MS (ESI): [M+1] = 963.

After characterization, the product is deprotected following the general Boc deprotection procedure to obtain product **38 (HCl*NH₂-Et-NH-NTA-[TOTA-Chol]-[OMe])**.

Boc-NH-PEG₂₇-NTA-[TOTA-Chol][OMe] (39):

By performing the general procedure over product 38 with Boc-NH-PEG₂₇-COOH, the crude of 39 is obtained. The residue was purified with precipitation with Et₂O and Exane and the pure product was obtained as a white solid (197.2 mg, 0.09 mmol, Y= 58 %).

HPLC-MS (ESI): [M/3+1] = 756.7, [M/4+1] = 567.9

Boc-NH-PEG₂₇-NTA-[TOTA-Chol][OH] (40):

Compound 39 was dissolved in 5 mL of a solution 1:1 of NaOH 0.2M and MeOH. The reaction was allowed to stir for 3 hours then MeOH was removed, the solution was acidified at pH= 4 at 0°C and the product was extracted with DCM (3x5mL). The organic phase was dried over MgSO₄, filtered, and concentrated to obtain the pure product as a white solid (62.8 mg, 0.03 mmol, Y= 31 %).

HPLC-MS (ESI): [M/2+1] = 1126.3, [M/3+1] = 751.8

Boc-NH-PEG₂₇-NTA-[TOTA-Chol][SN38-TBDPS] (41): see compound 32

Boc-NH-PEG₂₇-NTA-[TOTA-Chol][SN38] (42): see compound 33

[MAL]-NH-PEG₂₇-NTA-[TOTA-Chol][SN38]

Compound 42 is deprotected following the Boc deprotection procedure. The product (0.006 mmol, 18.4 mg) is dissolved in 2mL of DCM. SMCC (1.1 eq, 0.007 mmol, 2.3 mg) and DIEA (1.5 eq, 0.009 mmol, 2 μL) were added and the reaction was allowed to stir at room temperature overnight. Th

solvent is removed, and the crude is concentrated under vacuum. The residue was purified with precipitation with Et₂O and Exane and the pure product was obtained as a white solid (18.4 mg, Y= quant.). The same procedure was performed over compound 26 in order to obtain the two maleimide derivative platforms.

4.10 - Bibliography

- (1) Vert, M.; Doi, Y.; Hellwich, K.-H.; Hess, M.; Hodge, P.; Kubisa, P.; Rinaudo, M.; Schué, F. Terminology for Biorelated Polymers and Applications (IUPAC Recommendations 2012). *Pure Appl Chem* **2012**, *84* (2), 377–410. <https://doi.org/10.1351/PAC-REC-10-12-04>.
- (2) Aghebati-Maleki, A.; Dolati, S.; Ahmadi, M.; Baghbanzhadeh, A.; Asadi, M.; Fotouhi, A.; Yousefi, M.; Aghebati-Maleki, L. Nanoparticles and Cancer Therapy: Perspectives for Application of Nanoparticles in the Treatment of Cancers. *J Cell Physiol.* Wiley-Liss Inc. March 1, 2020, pp 1962–1972. <https://doi.org/10.1002/jcp.29126>.
- (3) Lombardo, D.; Kiselev, M. A.; Caccamo, M. T. Smart Nanoparticles for Drug Delivery Application: Development of Versatile Nanocarrier Platforms in Biotechnology and Nanomedicine. *J Nanomater* **2019**, *2019*. <https://doi.org/10.1155/2019/3702518>.
- (4) Manavitehrani, I.; Fathi, A.; Badr, H.; Daly, S.; Negahi Shirazi, A.; Dehghani, F. Biomedical Applications of Biodegradable Polyesters. *Polymers (Basel)* **2016**, *8* (1), 20. <https://doi.org/10.3390/polym8010020>.
- (5) Fredrickson, G. H.; Bates, F. S. Design of Bicontinuous Polymeric Microemulsions. *J Polym Sci B Polym Phys* **1997**, *35* (17), 2775–2786. [https://doi.org/10.1002/\(SICI\)1099-0488\(199712\)35:17<2775::AID-POLB2>3.0.CO;2-Q](https://doi.org/10.1002/(SICI)1099-0488(199712)35:17<2775::AID-POLB2>3.0.CO;2-Q).
- (6) Fuks, G.; Mayap Talom, R.; Gauffre, F. Biohybrid Block Copolymers: Towards Functional Micelles and Vesicles. *Chem Soc Rev* **2011**, *40* (5), 2475. <https://doi.org/10.1039/c0cs00085j>.
- (7) Zhao, J.; Santino, F.; Giacomini, D.; Gentilucci, L. Integrin-Targeting Peptides for the Design of Functional Cell-Responsive Biomaterials. *Biomedicines*. MDPI AG September 1, 2020. <https://doi.org/10.3390/biomedicines8090307>.
- (8) Bobo, D.; Robinson, K. J.; Islam, J.; Thurecht, K. J.; Corrie, S. R. Nanoparticle-Based Medicines: A Review of FDA-Approved Materials and Clinical Trials to Date. *Pharma Res.* Springer New York LLC October 1, 2016, pp 2373–2387. <https://doi.org/10.1007/s11095-016-1958-5>.
- (9) Jafari, S.; Derakhshankhah, H.; Alaei, L.; Fattahi, A.; Varnamkhasti, B. S.; Saboury, A. A. Mesoporous Silica Nanoparticles for Therapeutic/Diagnostic Applications. *Biomed Pharmacother* **2019**, *109*, 1100–1111. <https://doi.org/10.1016/j.biopha.2018.10.167>.
- (10) DelSecco, B.; Ravotto, L.; Esipova, T. v.; Vinogradov, S. A.; Genovese, D.; Zaccheroni, N.; Rampazzo, E.; Prodi, L. Optimized Synthesis of Luminescent Silica Nanoparticles by a Direct Micelle-Assisted Method. *Photochem Photobiol Sci* **2019**, *18* (9), 2142–2149. <https://doi.org/10.1039/c9pp00047j>.
- (11) Cui, Y.; Dong, H.; Cai, X.; Wang, D.; Li, Y. Mesoporous Silica Nanoparticles Capped with Disulfide-Linked PEG Gatekeepers for Glutathione-Mediated Controlled Release. *ACS Appl Mater Interf* **2012**, *4* (6), 3177–3183. <https://doi.org/10.1021/am3005225>.
- (12) Selvarajan, V.; Obuobi, S.; Ee, P. L. R. Silica Nanoparticles—A Versatile Tool for the Treatment of Bacterial Infections. *Front Chem.* Frontiers Media S.A. July 15, 2020. <https://doi.org/10.3389/fchem.2020.00602>.
- (13) Zhao, Y.; Wang, Y.; Ran, F.; Cui, Y.; Liu, C.; Zhao, Q.; Gao, Y.; Wang, D.; Wang, S. A Comparison between Sphere and Rod Nanoparticles Regarding Their in Vivo Biological Behavior and Pharmacokinetics. *Sci Rep* **2017**, *7* (1). <https://doi.org/10.1038/s41598-017-03834-2>.
- (14) Li, J.; Shen, S.; Kong, F.; Jiang, T.; Tang, C.; Yin, C. Effects of Pore Size on *in Vitro* and *in Vivo* Anticancer Efficacies of Mesoporous Silica Nanoparticles. *RSC Adv* **2018**, *8* (43), 24633–24640. <https://doi.org/10.1039/C8RA03914C>.
- (15) Pokharel, M.; Park, K. Light Mediated Drug Delivery Systems: A Review. *J Drug Target* **2022**, *30* (4), 368–380. <https://doi.org/10.1080/1061186X.2021.2005610>.

- (16) Genovese, D.; Rampazzo, E.; Bonacchi, S.; Montalti, M.; Zaccheroni, N.; Prodi, L. Energy Transfer Processes in Dye-Doped Nanostructures Yield Cooperative and Versatile Fluorescent Probes. *Nanoscale* **2014**, *6* (6), 3022–3036. <https://doi.org/10.1039/C3NR05599J>.
- (17) Bonacchi, S.; Genovese, D.; Juris, R.; Montalti, M.; Prodi, L.; Rampazzo, E.; Sgarzi, M.; Zaccheroni, N. Luminescent Chemosensors Based on Silica Nanoparticles; 2010; pp 93–138. https://doi.org/10.1007/128_2010_104.
- (18) Rampazzo, E.; Bonacchi, S.; Genovese, D.; Juris, R.; Montalti, M.; Paterlini, V.; Zaccheroni, N.; Dumas-Verdes, C.; Clavier, G.; Méallet-Renault, R.; Prodi, L. Pluronic-Silica (PluS) Nanoparticles Doped with Multiple Dyes Featuring Complete Energy Transfer. *J Phys Chem C* **2014**, *118* (17), 9261–9267. <https://doi.org/10.1021/jp501345f>.
- (19) Genovese, D.; Bonacchi, S.; Juris, R.; Montalti, M.; Prodi, L.; Rampazzo, E.; Zaccheroni, N. Prevention of Self-Quenching in Fluorescent Silica Nanoparticles by Efficient Energy Transfer. *Angew Chem Int Ed* **2013**, *52* (23), 5965–5968. <https://doi.org/10.1002/anie.201301155>.
- (20) Spicer, C. D.; Pashuck, E. T.; Stevens, M. M. Achieving Controlled Biomolecule–Biomaterial Conjugation. *Chem Rev* **2018**, *118* (16), 7702–7743. <https://doi.org/10.1021/acs.chemrev.8b00253>.
- (21) Gref, R.; Minamitake, Y.; Peracchia, M. T.; Trubetskoy, V.; Torchilin, V.; Langer, R. Biodegradable Long-Circulating Polymeric Nanospheres. *Science (1979)* **1994**, *263* (5153), 1600–1603. <https://doi.org/10.1126/science.8128245>.
- (22) Pitto-Barry, A.; Barry, N. P. E. Pluronic® Block-Copolymers in Medicine: From Chemical and Biological Versatility to Rationalisation and Clinical Advances. *Polymer Chem. Royal Society of Chemistry* May 21, 2014, pp 3291–3297. <https://doi.org/10.1039/c4py00039k>.
- (23) Clarke, B. T. The natural history of amphibian skin secretions, their normal functioning and potential medical applications. *Biol Rev Camb Philos Soc* **1997**, *72* (3), S0006323197005045. <https://doi.org/10.1017/S0006323197005045>.
- (24) Kim, S.; Kim, S. S.; Bang, Y.-J.; Kim, S.-J.; Lee, B. J. In Vitro Activities of Native and Designed Peptide Antibiotics against Drug Sensitive and Resistant Tumor Cell Lines. *Peptides (N.Y.)* **2003**, *24* (7), 945–953. [https://doi.org/10.1016/S0196-9781\(03\)00194-3](https://doi.org/10.1016/S0196-9781(03)00194-3).
- (25) Marafon, G.; Crisma, M.; Moretto, A. Intrinsically Photoswitchable α/β Peptides toward Two-State Foldamers. *Angew Chem Int Ed* **2018**, *57* (32), 10217–10220. <https://doi.org/10.1002/anie.201806035>.
- (26) Wang, X.; Song, Y.; Li, J.; Liu, H.; Xu, X.; Lai, R.; Zhang, K. A New Family of Antimicrobial Peptides from Skin Secretions of *Rana Pleuraden*. *Peptides (N.Y.)* **2007**, *28* (10), 2069–2074. <https://doi.org/10.1016/j.peptides.2007.07.020>.
- (27) Santino, F.; Stavole, P.; He, T.; Pieraccini, S.; Paolillo, M.; Prodi, L.; Rampazzo, E.; Gentilucci, L. Preparation of Non-Toxic Fluorescent Peptide-Coated Silica/PEG Nanoparticles from Peptide-Block Copolymer Conjugates. *Micro* **2022**, *2* (2), 240–256. <https://doi.org/10.3390/micro2020016>.
- (28) Pengo, P.; Pasquato, L.; Moro, S.; Brigo, A.; Fogolari, F.; Broxterman, Q. B.; Kaptein, B.; Scrimin, P. Quantitative Correlation of Solvent Polarity with the α -310-Helix Equilibrium: A Heptapeptide Behaves as a Solvent-Driven Molecular Spring. *Angew Chem Int Ed* **2003**, *42* (29), 3388–3392. <https://doi.org/10.1002/anie.200351015>.
- (29) Pommier, Y. Topoisomerase I Inhibitors: Camptothecins and Beyond. *Nat Rev Cancer* **2006**, *6* (10), 789–802. <https://doi.org/10.1038/nrc1977>.
- (30) Meyerhardt, J. A.; Mayer, R. J. Systemic Therapy for Colorectal Cancer. *N Eng J Med* **2005**, *352* (5), 476–487. <https://doi.org/10.1056/NEJMra040958>.

- (31) Zhang, H.; Wang, J.; Mao, W.; Huang, J.; Wu, X.; Shen, Y.; Sui, M. Novel SN38 Conjugate-Forming Nanoparticles as Anticancer Prodrug: In Vitro and in Vivo Studies. *J Control Release* **2013**, *166* (2), 147–158. <https://doi.org/10.1016/j.jconrel.2012.12.019>.
- (32) Zhao, H.; Rubio, B.; Sapra, P.; Wu, D.; Reddy, P.; Sai, P.; Martinez, A.; Gao, Y.; Lozanguiez, Y.; Longley, C.; Greenberger, L. M.; Horak, I. D. Novel Prodrugs of SN38 Using Multiarm Poly(Ethylene Glycol) Linkers. *Bioconjug Chem* **2008**, *19* (4), 849–859. <https://doi.org/10.1021/bc700333s>.
- (33) Suk, J. S.; Xu, Q.; Kim, N.; Hanes, J.; Ensign, L. M. PEGylation as a Strategy for Improving Nanoparticle-Based Drug and Gene Delivery. *Adv Drug Deliv Rev* **2016**, *99*, 28–51. <https://doi.org/10.1016/j.addr.2015.09.012>.
- (34) Hosseinzadeh, H.; Atyabi, F.; Varnamkhandi, B. S.; Hosseinzadeh, R.; Ostad, S. N.; Ghahremani, M. H.; Dinarvand, R. SN38 Conjugated Hyaluronic Acid Gold Nanoparticles as a Novel System against Metastatic Colon Cancer Cells. *Int J Pharm* **2017**, *526* (1–2), 339–352. <https://doi.org/10.1016/j.ijpharm.2017.04.060>.
- (35) Sharifi, F.; Jahangiri, M.; Ebrahimnejad, P. Synthesis of Novel Polymeric Nanoparticles (Methoxy-Polyethylene Glycol-Chitosan/Hyaluronic Acid) Containing 7-Ethyl-10-Hydroxycamptothecin for Colon Cancer Therapy: In Vitro, Ex Vivo and in Vivo Investigation. *Artif Cells Nanomed Biotechnol* **2021**, *49* (1), 367–380. <https://doi.org/10.1080/21691401.2021.1907393>.
- (36) Sadat, S. M. A.; Vakili, M. R.; Paiva, I. M.; Weinfeld, M.; Lavasanifar, A. Development of Self-Associating Sn-38-Conjugated Poly(Ethylene Oxide)-Poly(Ester) Micelles for Colorectal Cancer Therapy. *Pharmaceutics* **2020**, *12* (11), 1–22. <https://doi.org/10.3390/pharmaceutics12111033>.
- (37) Taghavi, S.; Abnous, K.; Babaei, M.; Taghdisi, S. M.; Ramezani, M.; Alibolandi, M. Synthesis of Chimeric Polymersomes Based on PLA-b-PPMA and PCL-b-PPMA for Nucleoline Guided Delivery of SN38. *Nanomedicine* **2020**, *28*. <https://doi.org/10.1016/j.nano.2020.102227>.
- (38) Singh, K.; Biharee, A.; Vyas, A.; Thareja, S.; Jain, A. K. Recent Advancement of Polymersomes as Drug Delivery Carrier. *Curr Pharm Des* **2022**, *28* (20), 1621–1631. <https://doi.org/10.2174/1381612828666220412103552>.
- (39) Lei, F.; Xi, X.; Batra, S. K.; Bronich, T. K. Combination Therapies and Drug Delivery Platforms in Combating Pancreatic Cancer. *J Pharm Exp Ther*. **2019**, pp 682–694. <https://doi.org/10.1124/jpet.118.255786>.
- (40) Suker, M.; Beumer, B. R.; Sadot, E.; Marthey, L.; Faris, J. E.; Mellon, E. A.; El-Rayes, B. F.; Wang-Gillam, A.; Lacy, J.; Hosein, P. J.; Moorcraft, S. Y.; Conroy, T.; Hohla, F.; Allen, P.; Taieb, J.; Hong, T. S.; Shridhar, R.; Chau, I.; van Eijck, C. H.; Koerkamp, B. G. FOLFIRINOX for Locally Advanced Pancreatic Cancer: A Systematic Review and Patient-Level Meta-Analysis. *Lancet Oncol* **2016**, *17* (6), 801–810. [https://doi.org/10.1016/S1470-2045\(16\)00172-8](https://doi.org/10.1016/S1470-2045(16)00172-8).
- (41) Zoetemelk, M.; Ramzy, G. M.; Rausch, M.; Nowak-Sliwinska, P. Drug-Drug Interactions of Irinotecan, 5-Fluorouracil, Folinic Acid and Oxaliplatin and Its Activity in Colorectal Carcinoma Treatment. *Molecules* **2020**, *25* (11). <https://doi.org/10.3390/molecules25112614>.
- (42) Wang-Gillam, A.; Li, C.-P.; Bodoky, G.; Dean, A.; Shan, Y.-S.; Jameson, G.; Macarulla, T.; Lee, K.-H.; Cunningham, D.; Blanc, J. F.; Hubner, R. A.; Chiu, C.-F.; Schwartzmann, G.; Siveke, J. T.; Braitheh, F.; Moyo, V.; Belanger, B.; Dhindsa, N.; Bayever, E.; von Hoff, D. D.; Chen, L.-T.; Adoo, C.; Anderson, T.; Asselah, J.; Azambuja, A.; Bampton, C.; Barrios, C. H.; Bekaii-Saab, T.; Bohuslav, M.; Chang, D.; Chen, J.-S.; Chen, Y.-C.; Choi, H. J.; Chung, I. J.; Chung, V.; Csomzi, T.; Cubillo, A.; DeMarco, L.; de Wit, M.; Dragovich, T.; Edenfield, W.; Fein, L. E.; Franke, F.; Fuchs, M.; Gonzales-Cruz, V.; Gozza, A.; Fernando, R. H.; Iaffaioli, R.; Jakesova, J.; Kahan, Z.; Karimi, M.; Kim, J. S.; Korbenfeld, E.; Lang, I.; Lee, F.-C.; Lee, K.-D.; Lipton, L.; Ma, W. W.; Mangel, L.; Mena, R.; Palmer, D.; Pant, S.; Park, J. O.; Piacentini, P.; Pelzer, U.; Plazas, J. G.; Prasad, C.; Rau, K.-M.; Raoul, J.-L.; Richards, D.; Ross, P.; Schlittler, L.; Smakal, M.; Stahalova, V.; Sternberg, C.; Seufferlein, T.; Tebbutt, N.; Vinholes, J. J.; Wadlow, R.; Wenczl, M.; Wong, M. Nanoliposomal Irinotecan with Fluorouracil and Folinic Acid in Metastatic Pancreatic Cancer after Previous Gemcitabine-Based Therapy (NAPOLI-1): A Global, Randomised, Open-Label, Phase 3 Trial. *The Lancet* **2016**, *387* (10018), 545–557. [https://doi.org/10.1016/S0140-6736\(15\)00986-1](https://doi.org/10.1016/S0140-6736(15)00986-1).

- (43) Hamaguchi, T.; Tsuji, A.; Yamaguchi, K.; Takeda, K.; Uetake, H.; Esaki, T.; Amagai, K.; Sakai, D.; Baba, H.; Kimura, M.; Matsumura, Y.; Tsukamoto, T. A Phase II Study of NK012, a Polymeric Micelle Formulation of SN-38, in Unresectable, Metastatic or Recurrent Colorectal Cancer Patients. *Cancer Chemother Pharmacol* **2018**, *82* (6), 1021–1029. <https://doi.org/10.1007/s00280-018-3693-6>.
- (44) Lei, F.; Xi, X.; Rachagani, S.; Seshacharyulu, P.; Talmon, G. A.; Ponnusamy, M. P.; Batra, S. K.; Bronich, T. K. Nanoscale Platform for Delivery of Active IRINOX to Combat Pancreatic Cancer. *J Control Release* **2021**, *330*, 1229–1243. <https://doi.org/10.1016/j.jconrel.2020.11.029>.
- (45) Pulido, D.; Albericio, F.; Royo, M. Controlling Multivalency and Multimodality: Up to Pentamodal Dendritic Platforms Based on Diethylenetriaminepentaacetic Acid Cores. *Org Lett* **2014**, *16* (5), 1318–1321. <https://doi.org/10.1021/ol500022n>.

Final Remarks

During these three years I focused my research on the design and synthesis of peptides for the application in various therapeutic studies where these kinds of drugs are helping overcoming challenges of modern medicine approaches. Despite the considerable benefits they could bring, they also suffer from significant problems that very often make them unsuitable for hospital administration even though they are very effective. In particular, a peptide sequence suffers from problems of permeability inside the cell membranes, stability in the human fluids for the presence of several kind of enzymes and selectivity, because it can be recognized as substrate in different places. In the three chapters described, focusing on a particular topic, I applied different medicinal chemistry techniques to modify the native structures and obtain peptidomimetics with the aim of solving the above-mentioned problems and making the molecules potentially suitable for the therapies studied.

In the first chapter, I focused my research in the development of κ opioid receptor ligands, with the design and synthesis of several molecules where the sequence of endomorphine-1, a MOR selective endogenous agonist, has been modified with the introduction of trans configuration inductor moieties in the place of the proline. In this way the sequences are forced to maintain a linear structure and, we hope, switched their selectivity from MOR to KOR with a partial agonist profile, according to the precursor molecule from which they derived.

In the second chapter, the peptide sequences are designed to inhibit the action of lactate dehydrogenase, an enzyme involved in the fast growing of tumour cells. To improve their permeability, we have chosen to close the sequences in big rings and create a macro cycle more stable and more likely to cross cell membranes.

For the synthesis of nanoparticles, covered in the last chapter, we focused our attention on two different techniques. While in the first one we conjugated Pluronic acid through click chemistry with toxic peptide sequences, to create a self-assemble structures with a silica core able to enter inside the cells, in the second project, carried out thanks to the collaboration with Miriam Royo at the Institut de Química Avançada de Catalunya, in Barcelona, we developed of a small library of multivalent drug delivery systems with hetero- and homo-bivalent structured molecules, designed in order to test their ability to form nanostructures in aqueous media. All these systems are based on a scaffold to which the hydrophobic SN38 and a hydrophilic polyethylene glycol are conjugated through a trifunctional platform to improve the SN38 permeability, solubility and stability and conjugated it with the 5FdU, the second drug widely used for Advanced Colorectal Cance

Ringraziamenti

Nessuno mi aveva detto che sarebbe stato facile, ma nemmeno così difficile.

È stato chiaro fin dall'inizio, con lo scoppio della pandemia solo dopo pochi mesi. È stato un percorso fortemente desiderato, ma non per questo privo di incertezze e difficoltà, e se sono stata in grado di superare questi momenti lo devo alle persone che mi sono state vicine e che desidero ringraziare. Prima fra tutti, la mia grande famiglia, i miei adorati cugini, i miei nonni anche se non ci sono più, mio padre e i miei fratelli, a cui dedico il lavoro di questi tre anni, Michela, per essere diventata in breve tempo una meravigliosa sorella maggiore e un importante punto di riferimento. Grazie per non aver sempre capito la mia lontananza ma per avermi sempre supportato, per tutti i treni non presi, per le volte in cui non potevo essere presente e per le volte in cui tornavo sconvolgendo il vostro precario equilibrio. Grazie per la pazienza, per le volte in cui una vostra chiamata o un vostro pensiero mi hanno dato la forza per andare avanti, per superare i fallimenti e per ricominciare.

E se la famiglia ti capita, gli amici te li sceglie e i miei formano una bellissima famiglia.

Grazie quindi prima di tutto a Giulia, per essere stata lì al mio fianco, dall'inizio alla fine ma anche un po' oltre. Grazie per le birre sia nelle brutte che nelle belle giornate, per le passeggiate e per le lunghe chiamate. E poi ancora per i sorrisi, per i pianti, per i consigli, per i viaggi, per tutto.

Grazie a Claudia, per accettare tutte le mie fughe ed aspettare sempre il mio ritorno. Grazie per aver capito, per aver condiviso, per essere sempre rimasta fondamentale. Per aver gioito e pianto con me, grazie per tutto il piccolo grande amore di ogni giorno.

Grazie a Maria, più vecchia di me di sole due settimane ma infinitamente più saggia. Grazie per sostenermi da sempre, per ascoltarmi, per essere il mio rifugio e la mia roccia.

Grazie a Gloria, per essere un uragano. Per avermi sostenuto con dolcezza ed energia, per essermi venuta incontro, per essere stata presente, per capirmi.

Grazie a Carolina, per la sua forza, per i suoi sorrisi. Grazie per essere sempre dalla mia parte, per trovare sempre il tempo, per essere sempre sorridente, per rimanere sempre vicino.

Grazie a Silvia, per la sua timida e forte presenza. Compagna di squadra, di gioie, ma soprattutto di sventure, grazie per non avermi fatto mai mollare niente.

Grazie anche a Filippo e a tutta la squadra di nuoto. Per essere stati di fondamentale sostegno nelle giornate difficili e per avermi permesso di coltivare la mia passione.

Grazie alla famiglia di Barcellona. Ad Anca prima di tutti, il mio prezioso regalo del 2022, a Fede ed Ivan, a Maca e Ginevra e tutto il meraviglioso gruppo di Miriam. Per avermi fatto sentire sempre a casa, accolta e capita. Grazie per l'aiuto, per le risate, per gli abbracci.

Grazie a Carolina P, per essere lontana ma vicina sempre, a Manfredi, per la spensieratezza, a Francesca, per aver illuminato il bunker con una ventata di allegria. Grazie a Paolone, Paolino, Tommi, Giulia, Marti, Giulio, Lello, Ciccio, Franca, Gian, Pot, Alexia, Chiara e tutto il piano di Organica, per aver condiviso con me ogni giorno la frustrazione e le soddisfazioni. Grazie per i consigli, per i caffè, per le risate. Grazie al mio gruppo di ricerca, al prof. Gentilucci, ai miei studenti, in particolare Pasquale e Michele, per avermi permesso di imparare così tanto. Grazie ad Elena, anche se non è un chimico ma in fondo vorrebbe. Grazie a Gabriele, per l'arrampicata e l'affetto.

Grazie agli amici di Roma, a Giulia, Miles, Pippo e Cap per essere sempre lì, da sempre.

Nessuno aveva detto che sarebbe stato facile ma ce l'abbiamo fatta. Dragons can be killed.